

BOILING HEAT TRANSFER AROUND A
CYLINDER AND IN TUBE BUNDLES

BOILING HEAT TRANSFER AROUND A
HORIZONTAL CYLINDER AND IN TUBE BUNDLES

by
JULES THIBAUT, B.ENG.

A Thesis
Submitted to the School of Graduate Studies
in Partial Fulfilment of the Requirements
for the Degree
Doctor of Philosophy

McMaster University

March 1978

JULES THIBAUT 1978

DOCTOR OF PHILOSOPHY (1978)
(Chemical Engineering)

McMASTER UNIVERSITY
Hamilton, Ontario

TITLE: Boiling Heat Transfer Around a Horizontal Cylinder
and in Tube Bundles

AUTHOR: Jules Thibault

o B.Eng. (Royal Military College of Canada)

SUPERVISOR: Dr. T.W. Hoffman

NUMBER OF PAGES: (xxii), 324

ABSTRACT

From the analysis of a postulated loss-of-coolant and loss-of-emergency cooling accident in a typical horizontal pressure tube nuclear reactor, the need was established for a systematic investigation on the boiling heat transfer coefficient, to be expected on a 12.7 cm diameter cylinder and a bundle of these cylinders under saturated and subcooled conditions. To accomplish this, a three-part experimental program was instigated.

In the first part, a successful technique based on a quenching (transient) procedure and the use of a heat flux meter was developed to measure directly the local boiling heat flux density around a large horizontal cylinder (12.7 cm diameter) as a function of wall temperature under saturated and subcooled conditions. These experiments were complemented by pertinent theoretical analyses. Although the surface averaged critical heat flux densities are shown to be predicted very well by known correlations, these experiments and analyses do reveal that there is considerable variation of the local critical heat flux density (CHF) around the cylinder. It was shown by high speed motion pictures (1000 frames/s) and from quenching experiments on partially insulated cylinders that this variation results from the interaction of the upflowing liquid-vapour boundary layer with the boiling phenomena. These results for the partially insulated surface and for steam injection underneath a single copper cylinder are also presented.

In the second portion of the experimental program, a five row

by three column array of instrumented copper cylinders was quenched to determine the interaction effect on the boiling curve of the vapour-liquid mixture rising from tubes located below. This bundle was investigated under saturated and subcooled conditions. Results show that there is a significant critical heat flux increase over the lower part of the cylinder and no appreciable effect over the other parts. The critical heat flux increase is relatively independent of the amount of upflowing vapour.

In the third part of the program, a steam-heated tube, 2.67 cm outer diameter, was used to study the steady-state boiling characteristics of heptane on single horizontal tubes. The average boiling heat flux for each of these steam-heated tubes in a four row by three column array was determined and compared with that observed when each was used alone. The results show a substantial increase in the critical heat flux value and essentially no increase in the nucleate boiling regime on any tube when the lower tubes were boiling. When all tubes were at their critical heat flux, the average CHF in the bundle was about 20% higher than the one obtained in a single tube experiment.

It is recommended to initiate a study to calculate the pressure drop in a horizontal boiler. It is suggested that the apparent decrease in the overall average critical heat flux for a bundle of tubes, which has been reported in the literature for horizontal reboiler systems, may not be caused by vapour blanketing but may result from insufficient liquid being drawn into the bundle, by natural convection or the thermosiphon effect, to satisfy that required to generate the vapour if all

tubes are operating at the critical heat flux. Some recommendations
for future work relating to this problem are presented.

ACKNOWLEDGMENTS

I wish to express my sincere thanks and appreciation to all those who have contributed their time and talents during this investigation. In particular I am indebted to :

My research supervisor, Dr. T.W. Hoffman, for numerous discussions and his patient guidance throughout the study. I would not have learned as much from the thesis research without his suggestions and criticisms.

Bob Dunn and Joe Newton for their craftsmanship in building equipment and for their many valuable suggestions to improve the equipment efficiency.

Atomic Energy of Canada Limited for their financial assistance over the four years of this project. Especially to Dr. Jim Bridges for his valuable cooperation throughout this investigation.

The people of Canada, through the generous N.R.C. Sciences 1967 Scholarships which I have received while at McMaster.

To Miss Heather Ridge for careful proofreading of this thesis.

Enfinement, j'offre ma plus sincère appréciation à mon épouse, Jocelyne, qui m'a assisté dans l'acquisition et l'analyse des données expérimentales et dans la rédaction de cette thèse. Je tiens à la remercier aussi pour avoir dactylographié les nombreux rapports qui ont été écrits tout au long de ce projet. Sans aucun doute, elle mérite d'être coauteur. C'est à elle que je dédie cette thèse.

TABLE OF CONTENTS

	Page	
NOMENCLATURE	xii	
LIST OF FIGURES	xv	
LIST OF TABLES	xx	
CHAPTER 1	INTRODUCTION	1
CHAPTER 2	LITERATURE REVIEW	5
2.1	Boiling Heat Transfer	5
2.1.1	Introduction	5
2.1.2	The Various Boiling Regimes	7
2.1.3	Nucleate Boiling	10
2.1.4	Critical Heat Flux	17
2.1.5	Transition Boiling	27
2.1.6	Film Boiling	29
2.1.7	Boiling Heat Transfer in a Tube Bundle	30
2.2	Quenching Boiling Curves	34
2.2.1	Calorimeter Method	35
2.2.2	Heat Flux Meter Technique	37
2.2.3	Quenching vs Steady-State	40
CHAPTER 3	DESCRIPTION OF EQUIPMENT AND EXPERIMENTAL PROCEDURE	43
3.1	Apparatus for Unsteady-State Experiments	43
3.1.1	Instrumented Copper Cylinder	43
3.1.2	Heat Flux Meter	46

3.1.3	Steam Injection System	48
3.1.4	Experimental Procedure	50
3.2	Apparatus for Steady-State Calibration of a Heat Flux Meter	51
3.2.1	Description of the Experimental System	52
3.2.2	Experimental Procedure	55
3.3	Apparatus for Unsteady-State Experiments in Tube Bundles	56
3.3.1	Description of the Experimental System	56
3.3.2	Experimental Procedure	60
3.4	Apparatus for Steady-State Experiments in Tube Bundle	62
3.4.1	Description of the Experimental System	62
3.4.2	Choice of a Boiling Liquid	66
3.4.3	Experimental Procedure	67
CHAPTER 4	HEAT FLUX METER CHARACTERISTICS AND ANALYSIS	70
4.1	Experimental System	70
4.2	Factors Affecting the Design of the Heat Flux Meter	72
4.3	Experimental Procedure	73
4.4	Calibration of the Heat Flux Meter	74
4.4.1	Unsteady-State Calibration	76
4.4.2	Steady-State Calibration	78
4.4.3	Boiling Curve Prediction	81
4.5	Conclusion	85
CHAPTER 5	RESULTS OBTAINED ON A SINGLE COPPER CYLINDER	86
5.1	Boiling Curves	87

	5.1.1	Boiling Curves Reproducibility	87
	5.1.2	Angular Variation	87
	5.1.3	Influence of Subcooling	89
5.2		The Critical Heat Flux Density	92
	5.2.1	Calibration Factor	92
	5.2.2	Critical Heat Flux Density Under Saturated Conditions	93
	5.2.3	Effect of Length of Cylinder	94
	5.2.4	Angular Variation of Critical Heat Flux Density	98
	5.2.5	Effect of Subcooling	104
	5.2.6	Surface Temperature at the Critical Heat Flux	106
	5.2.7	Effect of Partially Insulating the Cylindrical Surface	110
	5.2.8	Effect of Vapour Injection Underneath a Single Copper Cylinder	114
	5.2.9	Boiling Curves With a Plated Cylinder	121
5.3		Closing Remarks	125
CHAPTER 6		RESULTS OBTAINED WITH THE ARRAY OF CYLINDERS	127
	6.1	Introduction	127
	6.2	Discussion of the Results	129
	6.2.1	Saturation ($\phi = 180^\circ$)	131
	6.2.2	20°C Subcooling ($\phi = 180^\circ$)	132
	6.2.3	Steam Injection System	134
6.3		General Discussion and Conclusion	136
CHAPTER 7		RESULTS OBTAINED WITH THE STEADY-STATE STEAM-HEATED TUBE BUNDLE	139

7.1	Introduction	139
7.2	Single Tube Experiments	140
7.2.1	Pool Boiling Curve on a Copper Tube	140
7.2.2	Pool Boiling Curve on a Chrome-Plated Tube	144
7.2.3	Critical Heat Flux Density	148
7.2.4	Influence of the Liquid Level	149
7.3	Multiple Tube Experiments	149
7.3.1	Pool Boiling Curves for Individual Rows	149
7.3.2	Downward Bundle Effect	151
7.3.3	Influence of Tube 1 on Tube 2	155
7.3.4	Influence of Tube(s) 1 and/or 2 on Tube 3	
7.3.5	Influence of Tube(s) 1, 2 and/or 3 on Tube 4	151
7.4	Summary and General Discussion of the Results	151
7.5	Conclusion	155
CHAPTER 8	SUMMARY AND CONCLUSIONS	157
8.1	Introduction	157
8.2	Single Horizontal Cylinders	168
8.3	Steady-State Calibration Experiments	172
8.4	Unsteady-State Bundle Experiments	174
8.5	Steady-State Bundle Experiments	174
CHAPTER 9	RECOMMENDATIONS FOR FUTURE WORK	175
REFERENCES		180
APPENDIX A	TABLES OF PROPERTIES USED IN THIS STUDY	190
APPENDIX B	EXPERIMENTAL RESULTS OBTAINED WITH THE STEAM-HEATED SYSTEM	191

APPENDIX C	EXPERIMENTAL RESULTS OBTAINED WITH SINGLE COPPER CYLINDERS	196
APPENDIX D	EXPERIMENTAL RESULTS OBTAINED WITH THE MULTIPLE CYLINDER ARRAY	213
APPENDIX E	DEVELOPMENT OF THE HEAT FLUX METER-PROBLEMS ENCOUNTERED	215
APPENDIX F	DATA ACQUISITION AND ANALYSIS OF RAW DATA	225
APPENDIX G	STEADY-STATE TEMPERATURE DISTRIBUTION IN A TILTED HEAT FLUX METER	231
APPENDIX H	UNSTEADY-STATE CALIBRATION PROCEDURE	242
APPENDIX I	THEORETICAL ANALYSIS OF A HEAT FLUX METER	252
APPENDIX J	STEADY-STATE CALIBRATION	269
APPENDIX K	COOLING AND BOILING CURVES PREDICTION	280
APPENDIX L	CORRECTION OF SUBCOOLING LEVEL AT THE CRITICAL HEAT FLUX	302
APPENDIX M	CALCULATION OF SONIC ORIFICE VAPOUR FLOW RATE	306
APPENDIX Y	MAIN MINICOMPUTER PROGRAMS USED IN THIS STUDY	310
APPENDIX Z	MAIN FORTRAN PROGRAMS USED IN THIS STUDY	318

NOMENCLATURE

A	Area, cm ²
C	Heat flux meter characteristic (Equation 2.16)
CF	Calibration Factor
C _P	Specific heat at constant pressure, J/g ^o C
C _s	Constant in Equation 2.2
C _V	Specific heat at constant volume, J/g ^o C
D	Diameter, cm
ΔE	e.m.f. difference on heat flux meter, mV
g	Acceleration of gravity, 980 cm/s ²
K	Zuber's constant (Equation 2.3)
k	Thermal conductivity, W/cm ^o C
L	Length, cm
M _w	Molecular weight, g/mole
P	Pressure, kPa or psi
ΔP	Pressure difference, kPa or psi
$Pr = \frac{C_P \mu}{k}$	Prandtl number
Q	Heat content, J
(q/A)	Heat flux density, W/cm ² or kW/m ²
R	Radius, cm
R _o	Heat flux meter radius, cm
r	Radial coordinate, cm
T	Temperature, ^o C

ΔT	Temperature difference, $^{\circ}\text{C}$
t	Time, s
t_d	Heat flux meter thickness, cm
V	Volume, cm^3
W	Mass flowrate, g/s
x, y	Cartesian coordinate, cm
z	Axial coordinate, cm
$\alpha = \frac{k}{\rho C_p}$	Thermal diffusivity, cm^2/s
$\gamma = \frac{C_p}{C_v}$	Isentropic exponent
λ	Latent heat of vaporization, J/g
λ_d	Most susceptible Taylor unstable wavelength, cm
μ	Dynamic viscosity, g/cm s
ρ	Density, g/cm^3
σ	Surface tension, dyne/cm
τ	Bubble parameter in Zuber's equation (Equation 2.9), s
ϕ	Angle in cylindrical coordinate system, radian

Subscripts

app.	Apparent
C	Critical
d	Disk
f	Final
f	Fluid
g	Gas

i Initial
l Liquid
max Maximum
min Minimum
sat Saturation
sub Subcooling
T Total
v Vapour

LIST OF FIGURES

Figure		Page
2.1	Pool Boiling Heat Transfer Under Saturated Conditions	9
2.2	Regimes in Pool Boiling Heat Transfer	9
2.3	Typical Bundle Boiling Coefficient	32
2.4	Typical Tube Bundle Boiling Data	32
3.1	Apparatus For Quenching Experiments	45
3.2	Steam Injection System	49
3.3	Heater Configuration	53
3.4	Boiling Chamber Assembly	53
3.5	Apparatus for Steady-State Calibration of a Heat Flux Meter	53
3.6	Apparatus for Multiple Cylinder Quenching Experiments	58
3.7	Quenching Bath System	59
3.8	Bundle Heating System	59
3.9	Apparatus for Steady-State Tube Bundle Experiments	64
3.10	Boiling Chamber Assembly	64
3.11	Graph for Heat Flux Density Evaluation	68
4.1	Typical Response of a Heat Flux Meter	75
4.2	Temperature Distribution on a Heat Flux Meter and its Vicinity	79
4.3	Comparison of Predicted and Experimental Boiling and Cooling Curves	84

5.1	Reproducibility of Experimental Boiling Curves	88
5.2	Typical Local Boiling Curves Under Saturated and Subcooled Conditions for Various Points Around the Cylinder	90
5.3	Typical Boiling Curves Showing the Effect of Subcooling	91
5.4	Variation of Local CHF Around a Cylinder for Different Subcoolings (Heat Fluxes are Divided by the Overall CHF Average Obtained for a Given Subcooling).	100
5.5	Influence of Subcooling on CHF	105
5.6	Histogram of Wall Temperature at CHF	107
5.7	Variation of Local CHF Around a Cylinder Obtained with Steam Injection	119
5.8	Influence of Steam Injection on Boiling Curves	120
5.9	Boiling Curves of a Plated Cylinder	123
6.1	Boiling Curves for a 3-Row Bundle	133
7.1	Typical Boiling Curves for an Unplated Copper Tube Showing the Effect of Fouling	142
7.2	Boiling Curve for Tube 1 Obtained with Single Tube Experiment	146
7.3	Boiling Curve for Tube 2 Obtained with Single Tube Experiment	146
7.4	Boiling Curve for Tube 3 Obtained with Single Tube Experiment	146

7.5	Boiling Curve for Tube 4 Obtained with Single Tube Experiment	146
7.6	Boiling Curve for Tube 1 Obtained with Single Row Experiment	152
7.7	Boiling Curve for Tube 2 Obtained with Single Row Experiment	152
7.8	Boiling Curve for Tube 3 Obtained with Single Row Experiment	152
7.9	Boiling Curve for Tube 4 Obtained with Single Row Experiment	152
7.10	Boiling Curve for Tube 1 Obtained with Single Row Experiment when Above Tube(s) are Undergoing Boiling	154
7.11	Boiling Curve for Tube 2 Obtained with Single Row Experiment when Above Tube(s) are Undergoing Boiling	154
7.12	Boiling Curve of Tube 2 when Tube 1 is Active	156
7.13	Boiling Curve of Tube 3 when Tube 1 is Active	156
7.14	Boiling Curve of Tube 3 when Tube 2 is Active	156
7.15	Boiling Curve of Tube 3 when Tubes 1 and 2 are Active	156
7.16	Boiling Curve of Tube 4 when Tube 1 is Active	159
7.17	Boiling Curve of Tube 4 when Tube 2 is Active	159
7.18	Boiling Curve of Tube 4 when Tube 3 is Active	159
7.19	Boiling Curve of Tube 4 when Tubes 1 and 2 are Active	159
7.20	Boiling Curve of Tube 4 when Tubes 1 and 3 are Active	160

7.21	Boiling Curve of Tube 4 when Tubes 2 and 3 are Active	160
7.22	Boiling Curve of Tube 4 when Tubes 1, 2 and 3 are Active	160
E.1	Heat Flux Meter with a Copper Wire	217
E.2	Photograph Showing the Bottom Section of the Plug Insert	223
E.3	Photograph Showing the Location of the Edge Thermocouple	223
F.1	Data Acquisition System	227
F.2	Transmitter Response to a Step Change	227
F.3	Transmitter Response to a Step Change	227
G.1	System of Equations for a Tilted Heat Flux Meter	234
G.2	Temperature Distribution of a Uniform Heat Flux Meter	237
G.3	Temperature Distribution of a Uniform Heat Flux Meter	237
G.4	Temperature Distribution of a Tilted Heat Flux Meter	238
G.5	Temperature Distribution of a Tilted Heat Flux Meter	238
I.1	System of Equations for a Heat Flux Meter	256
I.2	Temperature Distribution on a Heat Flux Meter and its Vicinity	258
I.3	Boiling Curves Used in this Study	261
I.4	Predicted Boiling Curve	265
I.5	Predicted Boiling Curve	266
J.1	Plot of the Steady-State Calibration Factor Versus Heat Flux at the Surface	275

K.1	Cylindrical Coordinate System	283
K.2	Boiling and Cooling Curves Prediction(2-D System)	289
K.3	Boiling and Cooling Curves Prediction(3-D System)	297
K.4	Boiling and Cooling Curves Prediction(3-D System)	298
K.5	Boiling and Cooling Curves Prediction(3-D System)	299

LIST OF TABLES

Table		Page
5.1	Critical Heat Flux Values Under Saturated Conditions	95
5.2	Critical Heat Flux Under Subcooled Conditions	99
5.3	Influence of Subcooling on Critical Heat Flux Density	105
5.4	Summary of Equations Used in Table 5.3	105
5.5	Probability Density Function of the Temperature at Critical Heat Flux	108
5.6	Difference Between Temperature at Which the Critical Heat Flux Occurs for a Given Cylinder Under Saturated and Subcooled Conditions	108
5.7	Average % Increase of Critical Heat Flux With 60° Active Boiling Area	112
5.8	Average % Increase of Critical Heat Flux With 30° Active Boiling Area	112
5.9	Effect of Steam Injection on the Overall Critical Heat Flux	116
5.10	Effect of Steam Injection on the Critical Heat Flux at 180° and 150°	116
5.11	Effect of Steam Injection on the CHF of a Partially Insulated Copper Cylinder	116
5.12	Vapour Volumetric Flow Rate Corresponding to Upstream Pressure	117

6.1	Average % Increase of CHF in Multiple Cylinder Array	130
7.1	Critical Heat Flux Density Obtained During Individual Calibration in a Single Tube Experiment	142
7.2	Influence of Liquid Level on the Critical Heat Flux	150
7.3	Critical Heat Flux Values During Individual Calibration in the Bundle	153
7.4	Average Percentage Increase of the Critical Heat Flux Density Within the Tube Bundle	162
G.1	Summary of the Results Obtained With a Numerical Method for a Uniform and a Tilted Heat Flux Meter	235
H.1	Calibration Factors	246
H.2	Influence of the Temperature Difference Offset on the Calibration Factor	248
H.3	Standard Deviation of the Calibration Factor and Overall Critical Heat Flux	251
I.1	Influence of Steepness in Boiling Curves on the Steady-State Calibration Factor	261
I.2	Boiling Curve Equations	261
I.3	Definition of Variables Used in this Analysis	264
I.4	Heat Flux Meter Analysis	265
I.5	Heat Flux Meter Analysis	266
J.1	Steady-State Calibration Results for Block 14	271
J.2	Evaluation of the Calibration Factor for Block 14 With Steady-State Experiments	275

J.3	Critical Heat Flux Values Obtained With Block 14 During Temperature Runaway	275
J.4	Steady-State Calibration Results for Block 15	277
J.5	Evaluation of the Calibration Factor for Block 15 With Steady-State Experiments	277
K.1	Influence of Transite	301
L.1	Heat Balance up to Critical Heat Flux	305
M.1	Vapour Volumetric Flow Rate Corresponding to Upstream Pressure	309

CHAPTER 1

INTRODUCTION

In a horizontal pressure tube nuclear reactor, the nuclear fuel bundles are housed in pressure tubes, each 11.15 cm O.D. by 0.4 to 0.5 cm wall thickness and the pressurized heavy water coolant flows inside these tubes coaxially with the nuclear fuel bundles. Each pressure tube is housed in a calandria tube (13.175 cm O.D. by 0.14 to 0.16 cm wall thickness), with the annulus between the tubes being maintained by spacers located at appropriate axial locations. This annular gap (0.87 cm) contains a dry gas to provide sufficient insulation between the hot pressure tube and the cool heavy water moderator surrounding the calandria tube. A typical reactor may contain 300 to 500 calandria tubes arranged on a square pitch with a pitch-to-diameter ratio of about 2.18.

Construction and operation of such a nuclear reactor in Canada require licenses from the Atomic Energy Control Board. To obtain these licenses, the applicant must submit detailed accident analyses to the Board. One of the accidents to be analysed is a loss-of-coolant accident with coincident failure of the emergency core cooling system. This postulated accident involves heat transfer to the moderator system as

a major heat removal mechanism. Thus a need arises to understand and be able to predict boiling heat transfer behaviour on the outer surface of a calandria tube within an array of similar tubes.

The problem, then, is to provide design data relating to the boiling curve and particularly the maximum heat flux to be expected on a 13.2 cm O.D. tube which has part of its surface heated to some high temperature and which is immersed in stagnant water in some given subcooled state. This tube is located somewhere within a matrix of similar tubes possibly experiencing the same phenomena.

The specific objectives of this study relate to the designer's needs and may be summarized as follows:

- (i) To provide boiling curves for a single 12.7 cm O.D. horizontal cylinder located in water at various levels of subcooling up to at least 30°C, higher if possible (the 12.7 cm diameter was dictated by the closest commercially available diameter for a copper cylinder). This boiling curve should include the critical heat flux density as well as the nucleate and transition boiling regimes near the maximum heat flux.
- (ii) To provide boiling curves similar to (i) for horizontal cylinders with only part of the periphery being heated.
- (iii) To provide boiling curves for horizontal cylinders located in a matrix of cylinders (initially with a square pitch having a pitch-to-diameter ratio of 2.18) all of which are undergoing similar boiling phenomena.

To provide this information, an experimental program has been devised which has three elements:

- (i) The unsteady-state quenching of a hot copper cylinder, equipped with a heat flux meter, in saturated or subcooled water under pool boiling conditions.
- (ii) The quenching of a bundle of copper cylinders equipped with heat flux meters in a saturated or a subcooled pool of water.
- (iii) Steady-state pool boiling of heptane from a steam-heated 2.67 cm outside diameter tube and a bundle of these tubes.

This thesis reports the experimental results for each of these phases, -Chapter 5 for the single cylinder quenching, Chapter 6 for the quenching of an array of cylinders, and Chapter 7 for the steady-state experiments.

CHAPTER 2

LITERATURE REVIEW

The objective of this chapter is to review, in sufficient depth, the salient theoretical and phenomenological aspects of the boiling phenomena so that the uninformed reader may comfortably read this thesis. The major emphasis is on the critical heat flux aspect of boiling heat transfer.

2.1 Boiling Heat Transfer

2.1.1 Introduction

Boiling heat transfer, as considered here, is based on the change of phase from liquid to vapour at the heating surface. The applications of such boiling heat transfer are numerous, not only in vaporizers but also in situations where it is desired to remove heat from a surface at a high rate with low wall superheat. Developments in nuclear reactors and rockets, where extremely high heat fluxes are transferred through a comparatively small area, have stimulated intensive research into boiling heat transfer.

If a temperature gradient or difference exists, heat will be caused to flow. This temperature gradient or difference is a manifestation of the thermal resistance to heat flow and this resistance is usually expressed as a conductance or by a heat transfer coefficient. The larger the heat transfer coefficient the smaller the resistance.

This heat transfer coefficient will depend on the mechanism of heat transfer (forced or natural convection, boiling etc.). In boiling heat transfer, it is shown that the heat transfer coefficient also depends upon the temperature difference between the heat transfer surface and the liquid. This variation is usually shown by a plot of heat flux density versus the temperature difference between the heat transfer surface and the liquid. It is this variation which is being determined in boiling experiments and the plot is called a boiling curve.

There are two basic types of boiling: pool boiling and flow boiling. Pool boiling is when the system consists of a heating surface such as a flat plate or a wire, submerged in a pool of liquid without external agitation. Flow boiling, also referred to as forced convection boiling, takes place in a flowing stream where the boiling surface may itself be a portion of the flow passage. A further subdivision of boiling is saturation and subcooled boiling where the liquid bulk temperature is at or below the saturation temperature respectively. Subcooled boiling is also known as local boiling.

Although boiling has been widely employed in evaporators, boilers and other process equipment for years, basic knowledge on this heat transfer phenomena is still lacking in many details. The main difficulties arise because boiling is a complex phenomena involving the interaction of fluid motion, heat transfer, surface and interfacial phenomena and evaporation. Moreover, unless extreme care is taken boiling is not reproducible. Pool boiling heat transfer is the prime interest in this project and will be covered in much greater detail in the sections to follow.

2.1.2 The Various Boiling Regimes (N4, R6, R9, W3, Y1)

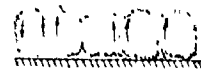
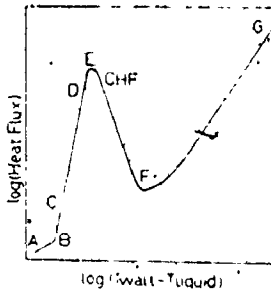
To acquire a physical understanding of the different phenomena which are characteristic of the various boiling regimes, consider the traditional electrically heated horizontal wire or flat plate submerged in a pool of liquid at saturation temperature. Figure 2-1 illustrates the typical dependence between the heat flux density, q/A , and the temperature difference between the heating surface and the liquid.

This curve is typical of all boiling curves encountered in boiling heat transfer. Its exact shape and location is determined by a variety of factors such as the nature of the heating surface, pressure, gravity, etc. which are discussed later. Part of the difference in behaviour is related to the behaviour of the vapour near the heat transfer surface. Figure 2.1 also illustrates what would be observed with high speed photography in the region near the heated surface for each of the boiling regimes.

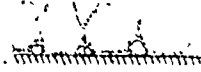
As the temperature of the heating surface is raised above the saturation temperature, the liquid near the heater reaches a temperature slightly in excess of saturation. This superheated liquid is less dense and therefore tends to rise to the free surface, where vaporization takes place. Although there is evaporation at the free surface, this mechanism, represented by region AB, is called the natural convection regime insofar as the conditions at the heating surface are concerned. At point B, the boiling process enters into the region of nucleate boiling which is characterized by the generation of vapour bubbles at favoured spots or nucleating sites on the heating surface. The nucleate

boiling region will be discussed in greater detail in section 2.1.3.

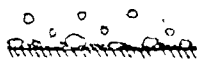
An increase in excess temperature produces a steep rise of the heat flux up to point E, due to an increase in the number of nucleation sites; this creates more and more vapour in the vicinity of the heated surface. Eventually point E is reached where the nucleate boiling mechanism cannot accommodate a further increase in heat transfer rate. At this point, a decrease in heat flux results as the wall temperature is raised because of partial vapour blanketing of the heat transfer surface. Point E marks the upper limit of nucleate boiling and is termed the critical heat flux. The vapour blanket which forms at this point is very unstable. It collapses and reforms rapidly under the action of circulation currents. This occurs in the region EF which is termed the transition boiling regime. This region is characterized by rapid changes between nucleate boiling and film boiling on the heating surface. As the temperature of the heating surface is increased, the surface tends to have a greater proportion of it covered by the vapour film. At point F, the onset of film boiling, the surface is entirely covered by a stable vapour film and hence the liquid is separated from the heating surface by it. The relatively low thermal conductivity of the vapour film results in much lower heat transfer rates in film boiling than those encountered in nucleate boiling. In the film boiling regime, the heat transfer takes place by conduction through the vapour film. As the excess temperature is increased, the heat flux increases by conduction (since the temperature difference across the vapour film increases); moreover, at higher temperatures radiant heat transfer plays



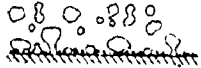
AB Natural Convection



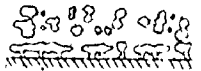
B Onset of nucleate boiling



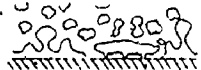
C Nucleate boiling (low heat flux)



D Nucleate boiling (high heat flux)



E Critical heat flux



EF Transition boiling



FG Film boiling

FIGURE 21 - POOL BOILING HEAT TRANSFER UNDER SATURATED CONDITIONS (CG)

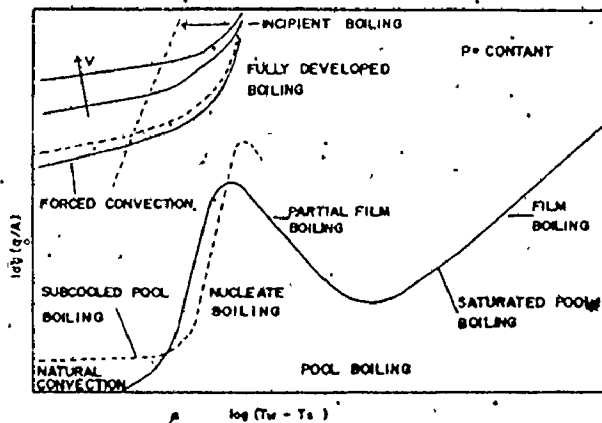


FIGURE 22 - REGIMES IN BOILING HEAT TRANSFER (R9)

an increasingly significant role.

The preceding discussion was based on the assumption that the temperature of the heating surface could be maintained at some desired value. The characteristic boiling curve (Fig. 2.1) is readily obtained when the heat source is a condensing vapour, unless the system itself is unstable as will be discussed later. However, in many cases, it is the heat generation rate and not the surface temperature which is controlled. Nuclear reactors and electrically heated wires are examples of such systems. When an attempt is made to increase the heat flux beyond a value corresponding to point E in Figure 2.1, the boiling process cannot remove heat as fast as it is generated unless the temperature of the heating surface rises to some very high value above that at point G. For most systems, this excess temperature is so high that the heater may melt. For this reason, point E is often referred to as the "burnout heat flux". This name is somewhat misleading since, depending on the fluid and the material of the heater, physical destruction does not necessarily occur.

2.1.3 Nucleate Boiling

Introduction

Nucleate boiling is a process where a liquid undergoes a change to the vapour phase at preferred nucleation sites on a heating surface. The heating surface temperature must be in excess of the saturation temperature of the liquid under ebullition. The very high heat fluxes obtainable with relatively low temperature differences makes the nucleate boiling regime of great engineering importance.

There exists today no completely satisfactory method of predicting nucleate boiling heat flux. The process of nucleate boiling changes from the first bubble generation to the critical heat flux. Therefore, some authors have found it necessary to separate the nucleate boiling regime into several regions in order to correlate heat flux as a function of wall superheat: Gaertner(G2) using high speed photography of boiling on a horizontal surface at atmospheric pressure, observed that, as the surface temperature increased, the vapour structure passed through three, and possibly four distinct regions. These are discrete bubbles, vapour columns and vapour mushrooms, and vapour patches. These four regions were discussed by Darnedde(D1) and Rao(R2). Hsu(H5) and Moissis and Berenson(M5) separated the nucleate boiling regimes into two regions: region of isolated bubbles and region of merging bubbles. The vapour structure at the surface would progress from isolated bubbles to vapour columns in a continuous fashion. They suggested that the average heat transfer coefficient should be determined by an appropriate weighting of the two processes.

Bubble Dynamics

In the natural convection regime, the liquid near the heating surface must be slightly superheated to account for heat transfer. As the wall temperature is increased, a particular wall temperature for a given heater surface is reached where bubbles begin to form on the heat transfer surface. Therefore, the first requirement to produce a bubble is a superheated liquid film next to the heating surface. The amount of superheat depends upon wall surface condition, heat flux, pressure etc.

Liquid superheats of about 5°C are usually required to form isolated bubbles although homogeneous nucleation theories suggest a value about an order of magnitude higher. It can be shown that the liquid must be superheated in the region of a bubble because of the need for a higher pressure (vapour pressure) in the inside of a bubble in order for it to exist. This excess pressure may be determined from a force balance which leads to the expression:

$$\Delta P = P_v - P_f = \frac{2\sigma}{r} \quad (2.1)$$

where P_v is the vapour pressure of the liquid corresponding to a given temperature and P_f is the pressure at the given point in the liquid. In order for the bubble to grow, the superheat must be even higher than this equilibrium value.

The roughness of the heating surface has a major influence on the liquid superheat required for nucleation since the conditions of the surface determines the size of the cavities or nucleating sites on the surface of the heater. These cavities or crevices serve to capture vapour or inert gas. Increasing roughness increases the radius of the cavities on the surface which in turn requires less excess pressure and therefore less superheat. Berenson(86) boiled pentane on copper surfaces at atmospheric pressure and his data lend support to the points concerning wall superheat and surface roughness. For example, by conditioning each heating surface with a different grade of emery paper, he observed a much steeper nucleate boiling curve for a rougher surface and that a given heat flux could be supported at a lower wall-to-liquid temperature

difference. Zuber(Z3) reports that an extremely highly polished heater could sustain a superheat up to 30°C without nucleation. However the curve would overshoot when nucleate boiling did start; this led to a hysteresis in the boiling curve. Many authors, dating from the early experiments of Corty and Foust(C10) have noticed this phenomena. The first nucleation triggers the adjacent sites and therefore the heater cools down.

The bubble rises when the buoyant force is large enough to separate the bubble from the heating surface. Actually, detachment occurs when the buoyant and hydrodynamic forces, tending to pull the bubble away from the surface, overcome surface tension and inertia forces which tends to maintain it in that position. The shape of bubbles leaving the surface varies in a complex way depending on the circumstances of their formation. If the viscosity of the liquid is high, the bubble will be more flat. When the liquid is not viscous, the surface tension will be the prime downward force and the bubble will be more spherical(R10). Rallis and Jawurek(R1) observed that when a bubble departs, it carries away a hot layer of liquid and continues to grow after departure until it reaches the free surface of the liquid. Katto and Kikuchi(K1) came to the same conclusion by studying bubble dynamics with high speed photography.

Mechanisms of Nucleate Boiling

There has been a multitude of mechanisms suggested for nucleate boiling. Zuber(Z3) in a boiling heat transfer review found that available correlations could be in error by as much as 13,000%. Chaudhri and

McDougall(C3) did a study on surface ageing and concluded that no correlation known today can be used over the entire nucleate boiling regime even though a surface factor is included. This demonstrates the complexity of boiling heat transfer. Two different approaches have been taken in studying nucleate pool boiling. The first one is to use high speed photography to study bubble behaviour and thereby suggest models to correlate data. The second approach is concerned with the overall effect of nucleate boiling and attempts to obtain empirical correlations of the boiling phenomena by considering it as a process by which heat is transmitted.

There is a sharp change in slope of the boiling curve at the onset of nucleate boiling. Heat fluxes for nucleate boiling at a given wall-to-fluid temperature difference are much higher than for a single phase fluid. Therefore the first obvious mechanism to be proposed for nucleate boiling was that heat was removed as the latent heat of vaporization. This model is commonly called the latent heat transport model. However, in 1951, Rohsenow and Clark(R7) presented measurements on sub-cooled boiling heat transfer and concluded that only a few percent of the heat flux could be accounted for by the latent heat content at the surface. Rather, the major portion of heat transfer could be accounted for by the high degree of turbulence produced by bubble motion in the vicinity of the heated surface. Forster and Grief(F4) proposed the vapour-liquid exchange model as being the best model to explain their data. This model is a slight variation of the Rohsenow and Clark description. Moore and Mesler(M6) observed with a high response thermocouple that the surface temperature in nucleate boiling periodically

dropped 20° to 30° F, in about 2 milliseconds and then recovered relatively slowly. They suggested that the evaporation of a microlayer of liquid under the growing bubble could account for this rapid heat extraction. Such microlayers have been since observed by light diffraction methods by Cooper and Lloyd(C9) and more recently by Voutsinos and Judd(V2). These observations confirmed that it is a significant heat transfer mechanism under some conditions particularly at low pressures. Harl and Griffith(H1, H2) found that when a bubble left the surface it carries with it the thermal boundary layer surrounding the bubble. Zuber(Z2), Bankoff(B2) and Rallis and Jawurek(R1) have proposed similar models by which heat transfer in nucleate boiling regime is accounted for by both natural convection and latent heat transport. Natural convection is most important at low heat flux values. Latent heat transport is significant at all levels of heat flux but becomes more important as the burnout heat flux is approached. In the light of this model, it is not surprising that Rohsenow and Clark(R7) concluded that only a few percent of the heat flux could be accounted for by the latent heat content at the surface as they dealt with subcooled pool boiling.

Judd and Merte(J2) identified six principal nucleate boiling models in the literature. Through a series of experiments done at various degrees of subcooling and acceleration, they tested their data against all these six models. All the models investigated predicted decreasing values of the heat flux ratio (predicted over measured heat fluxes) as subcooling and acceleration increased. This suggests that the

mechanisms upon which the models are based are not adequate. The authors suggest that mass transfer through the bubbles resulting from the evaporation of a microlayer at the base of the bubble and the subsequent condensation of the vapour at the liquid-vapour interface is a most likely prospect.

It is almost impossible to correlate nucleate boiling heat transfer because it varies with different types of liquids, surface conditions etc. Moreover, surface conditions (cleanliness, ageing etc.) are arbitrary and impossible to put in quantitative form. However, one of the most popular correlations for nucleate pool boiling is that presented by Rohsenow(R6):

$$\frac{C_{pf} \Delta T}{\lambda Pr_f^{1.7}} = C_{sf} \left[\frac{(q/A)}{\mu_f \lambda} \sqrt{\frac{\sigma}{g(\rho_f - \rho_g)}} \right]^{0.33} \quad (2.2)$$

The constant C_{sf} is an empirically determined quantity which is dependent upon the way in which the liquid wets the heating surface. In a recent paper, Fand and Ho(F1) provided a critical evaluation of Rohsenow and Clark's correlation and indicated that the coefficient C_{sf} is not a constant but a function of pressure. Nevertheless, they showed that the correlation is fairly accurate in the range between 4 and 115 psia. The main advantage in this correlation is that C_{sf} can be determined for a particular fluid-surface combination in a unique test at one pressure and results can be used at all pressures(K4).

However, if the surface characteristics change, the value of C_{sf} will also change and it is impossible to predict this coefficient a priori.

2.1.4 Critical Heat Flux

Introduction

The heat flux in the nucleate boiling region cannot be increased without bounds. There is a point where the heating surface cannot accommodate any further increase in heat flux and a vapour film is formed thus adding a resistance to heat flow. This point is the critical heat flux. The terms critical heat flux, burnout heat flux, boiling crisis and limiting heat flux in nucleate boiling are used interchangeably. With recent developments of nuclear reactors, there is a pressing need for methods to predict the magnitude of the critical heat flux and the surface temperature at which it occurs. As nuclear reactors are constant power input systems, the critical heat flux cannot be exceeded for safe operation. Critical heat flux is very important in this work and will be discussed in detail.

Mechanism and Prediction

The reason for the maximum in the boiling curve may be found by examining the heat transfer mechanism during boiling. As in the "flooding" phenomenon, the discontinuous phase (vapour) and the continuous phase (liquid) compete for the free volume (24). Rohsenow (R6) describes three models explaining the condition at critical heat flux and they are briefly summarized here:

(i) At the critical heat flux, the maximum number of bubbles occurs which is determined by a critical bubble packing; exceeding this maximum leads to vapour blanketing.

(ii) The updraught of vapour flow inhibits the downflow of liquid required to replace it.

(iii) Vapour columns merge and this coalescence produces a vapour blanket.

Although these three different mechanisms explain how the critical heat flux may arise, the final result is the same: for efficient heat transfer, the liquid must get to the surface. Therefore, the critical heat flux is characterized by a limiting vapour volumetric flow rate from the surface. All analyses have led to essentially the same equation for the critical heat flux from a horizontal flat plate, viz.:

$$(q/A)_c = K \rho_g \lambda \left[\frac{\sigma g (\rho_f - \rho_g)}{\rho_g^2} \right]^{0.25} \quad (2.3)$$

where $\frac{(q/A)_c}{\rho_g \lambda}$ is a measure of the average velocity of the vapour leaving the heating surface.

Kutateladze(K5) postulated that the crisis in the boiling process is a purely hydrodynamic phenomenon: the destruction of stability of two-phase flow existing close to the heating surface. Applying similarity considerations to the equations of motion and energy, he identified important dimensionless groups and then using experimental data he proposed a value of 0.16 for the coefficient K. Zuber(Z1, Z4), by applying a Helmholtz instability analysis to the upward-flowing vapour columns, arrived at exactly the same equation. In this analysis, he

considered the critical size and spacing of the vapour jets leaving the surface; a K value of $\pi/24$ was derived from this hydrodynamic instability analysis. Berenson(86) found that the level of critical heat flux was relatively independent of the surface roughness. The above equation is only a function of coolant properties and is therefore in agreement with Berenson's findings.

However, Rogers(R5) through a careful analysis of the level of critical heat flux for the different roughnesses of Berenson's data found an increase of approximately 10%. Few authors have tried to correlate the critical heat flux considering surface roughness. Chang(C2), by considering the surface conditions derived an equation for a flat plate which is identical to the equation derived by Kutateladze and Zuber with a K value of 0.13. Gaertner(G1,G2) considered also the effect of surface roughness and obtained the following value for K:

$$K = \frac{\sqrt{2}}{4} \pi D^2 \frac{n}{A} \quad (2.4)$$

Rogers(R5) assumed that the correlating variables were correct and found that the available data suggested a value of 0.124 as the best K value. There are many other models which have been proposed in the literature for a horizontal flat plate: Rohsenow and Griffith(R8), Lienhard and Shrock(L5), Lienhard and Watanabe(L6), Moissis and Berenson(M5) are some. For a more detailed description of the various models the reader is referred to references G3, L2, R6 and R9.

It has been claimed and disputed many times that hydrodynamic instability is the cause of burnout in pool boiling heat transfer.

The fact that the question still persists is not surprising in view of the confusion that has arisen over the number of physical models that have been proposed, and the effect of certain parameters on the maximum heat flux, such as geometry, orientation and surface conditions, which few of the models, if any, are able to account for. Nevertheless, the great success already achieved in treating this very complex problem by analysis based on the hydrodynamic instability theory is truly amazing.

Cobb and Park(C7), attempting to eliminate the different factors affecting CHF such as surface variables have derived a correlation which predicts CHF value for liquids which follow the theory of corresponding state. However the correlation requires one burnout heat flux to be known. This could be very useful in predicting high pressure heat fluxes from atmospheric data. The authors claim that their equation can fit the data to an accuracy of better than 7%.

Lienhard et al.(L4) carried out critical heat flux experiments on flat plates and found that Zuber's formula should have a K-value of 0.15 (about 14% higher than suggested by Zuber). He found that the predicting equation was good as long as the dimensions of the plate are at least 3 Taylor wavelengths on a side. This Taylor wavelength or most susceptible wavelength in a horizontal liquid-vapour interface was defined by the following equation:

$$\lambda_d = 2\pi \sqrt{\frac{3\sigma}{g(\rho_l - \rho_g)}} \quad (2.5)$$

They found that for smaller heaters, the hydrodynamic theory requires a wide variation in heat flux owing to discontinuities in the number of escaping jets. Data for smaller plates bear out this predicted variation with a critical heat flux range between 40% and 235% of the Zuber's predicted value. Hence, it is not surprising to find that the value of K has been suggested as ranging from 0.095 to 0.20(12); in most cases, this variation can be attributed to the heater dimensions employed. For a large plate, however, predictions are quite good if a K value of 0.15 is used.

Forced Convection

Forced convection refers to a flow of liquid relative to a heating surface caused by an external source. This is the most common type of heat transfer in engineering applications. Pool boiling with external agitation is a type of forced convection. Pramuk and Westwater (P6) studied the effects of agitation in pool-boiling heat transfer. They found that the superheat at which the critical heat flux occurs increased with an increase of the degree of agitation. On the other hand, the critical heat flux was increased by 25% and an increase of up to 100% was observed at other heat fluxes. They concluded that the agitation increased the frequency with which bubbles left the surface but the number of active sites remained essentially constant. This provides an explanation for the observations relating to the critical heat flux behaviour under forced convection conditions.

Figures 2.2 shows typical curves obtained with boiling heat transfer in forced convection as compared with pool boiling. In single

phase heat transfer the heat flux increases with increasing flow velocity. Since above incipient boiling it was observed that the effects of forced convection seem to be superimposed on pool nucleate boiling, Bergles and Rohsenow(87) suggested that the superposition could be applied, viz.:

$$(q/A)_{TOTAL} = (q/A)_{BOILING} + (q/A)_{CONVECTION} \quad (2.6)$$

They suggested that the boiling heat flux could be calculated from the Rohsenow pool boiling correlation and the convective flux from the normal single phase correlations. Moreover, the critical heat flux could be predicted from Equation 2.3 with the superimposed convective heat flux. It has been since found that this procedure, although providing a good first approximation, oversimplifies the actual convection boiling phenomena since interactions between the two heat transfer phenomena do occur(86).

Subcooling

Subcooled boiling heat transfer is obtained when boiling takes place in a bulk of liquid which is below the saturation temperature of the boiling liquid at the system pressure. The dotted line in Figure 2:2 represents a typical curve obtained with subcooled pool boiling. A bubble generated at the heating surface rarely leaves the liquid bulk, but collapses as a result of condensation in the colder liquid. The effect of subcooling is to rapidly reduce the vapour volume near the heated surface.

Most of the correlations derived to date show a significant increase in the CHF value as the degree of subcooling of the liquid is increased. The most common correlations are:

Ivey and Morris(I2)

$$\frac{(q/A)_{c,SUB}}{(q/A)_{c,SAT}} = 1 + 0.1 \left[\frac{\rho_v}{\rho_f} \right]^{0.25} \left[\frac{C_p \rho_f}{\lambda \rho_v} \right] \Delta T_{SUB} \quad (2.7)$$

Kutateladze(K5)

$$\frac{(q/A)_{c,SUB}}{(q/A)_{c,SAT}} = 1 + \left[\frac{\rho_f}{\rho_v} \right]^{0.923} \left[\frac{C_p}{25 \lambda} \right] \Delta T_{SUB} \quad (2.8)$$

Zuber(Z4) has extended his hydrodynamic theory to derive

$$\frac{(q/A)_{c,SUB}}{(q/A)_{c,SAT}} = 1 + \frac{2k(T_s - T_f)}{\sqrt{\pi \dot{a} \tau}} \frac{24}{\pi} \frac{1}{\lambda \rho_v} \left[\frac{\rho_v^2}{\sigma g (\rho_f - \rho_v)} \right]^{0.25} \quad (2.9)$$

where

$$\tau = \frac{\pi}{3} \sqrt{2\pi} \left[\frac{\sigma}{g (\rho_f - \rho_v)} \right]^{0.5} \left[\frac{\rho_v^2}{\sigma g (\rho_f - \rho_v)} \right]^{0.25} \quad (2.10)$$

Ponter and Haigh(P5) performed experiments on a 0.6 cm diameter stainless steel tube and found through a regression analysis that the critical heat fluxes in the subcooled pool boiling of water at pressures in the region of 760 and 100 torr and with liquid subcooling up to 60°C are correlated by the expression

$$\frac{(q/A)_{c,SUB}}{(q/A)_{c,SAT}} = 1.06 + 1.015 \frac{\Delta T_{SUB}}{P^{0.474}} \quad (2.11)$$

with a standard deviation of 0.106. At 760 torr the data were best fitted through the following equation:

$$\frac{(q/A)_{c,SUB}}{(q/A)_{c,SAT}} = 1.014 + 0.04458 \Delta T_{SUB} \quad (2.12)$$

Heater Geometry

The geometry of the heater has no appreciable effect on the nucleating mechanism since the influence of the bubble motion on the fluid conditions is limited locally (M2, M3). However, the orientation of the heating surface has an influence because the bubble has to move up through the liquid. Moreover, since its detachment from the heating surface is affected by the buoyancy, the surface and interfacial tension forces, the orientation of the gravity vector relative to its direction of growth will affect its detachment frequency and hence the boiling heat flux. Githinji and Sabersky (G6) studied the effect of orientation on heat flux by using a flat strip heating element insulated on one side. They found that for a constant temperature difference the vertical position yielded the highest heat flux, the facing-up position was second and the facing-down position yielded a very low heat flux. A cylinder has all orientations and Rosta (R11) suggested that the local critical heat flux of the lower part of a large cylinder could approach that of a downward-facing surface.

Lienhard (B1, L3, S5) derived an analytical correlation for critical heat flux by taking into account the geometry and size of the heater. He suggests that the overall CHF of a large horizontal cylinder

should be about 0.9 the critical heat flux value predicted by Zuber's equation. This prediction has a variance of about $\pm 10\%$. Earlier, Bernath(B10), McAdams(M3) and Breen and Westwater(B12) came to a similar conclusion. However, all experiments to date have been performed with very small diameter cylinders (smaller than 2.5 cm in diameter). Power or other heat source limitations precluded the use of larger diameter cylinders in steady-state experiments. In this project, this limitation is overcome by employing a fast response heat flux meter and unsteady-state quenching experiments. The only assumption is that the heat flux is determined by local conditions only and is independent of previous history.

All these predictions only provide information concerning the overall or average critical heat flux for a surface; they provide no information concerning the local variation over a surface such as around a large diameter cylinder where the surface orientation varies relative to the gravity vector. As early as 1958, Lance and Myers(L1) found that the nucleate boiling heat transfer coefficient varies substantially with angular position on 3 cm and 5 cm copper tubes. The greatest variation on a tube was such that the maximum coefficient was 120% greater than the minimum. The variation in local boiling coefficients was found to decrease as the heat flux was increased. Stolz et al.(S4) used a sophisticated calorimeter method in their quenching experiments involving a 5 cm diameter sphere. They showed that there was an appreciable variation of critical heat flux around a sphere, being highest at the top and smallest at the bottom. The differences, however, were not always detectable in the cooling curves, since detection required both an

accurate temperature determination and a sensitive evaluation procedure(P4). Since it is well known that artificial agitation causes a significant increase in boiling coefficients, it appears likely that the liquid-vapour mixture rising from the lower portion of a horizontal tube should have an effect on the heat transfer characteristics of the upper portion of the same tube or cylinder. Since the magnitude of this flow will be affected by the size and geometry of the heating surface, some effect is expected on the local value of the boiling heat transfer rate.

Factors Affecting Critical Heat Flux

As mentioned earlier, an increase of about 10% was found in Berenson(B6)'s data due to surface roughness. However the 10% increase in CHF was obtained by considering two extreme surface finishes; therefore for an average surface finish it can be concluded that the critical heat flux is independent of surface conditions. This is very important in this study because a copper surface was used instead of a Zircaloy-2 surface of the calandria tube. Although the critical heat flux will be essentially the same, the wall superheat at which it occurs will still depend on surface.

The level of liquid immersion has little effect on the critical heat flux value beyond a certain depth(S4). Results show that a liquid level of 2 cm to 13 cm above the heating surface do not affect the boiling curve(N2).

Farber and Scoriah(F2) found an increase in the critical heat flux when the pressure was increased from atmospheric pressure to 100

psig. Kutateladze(K5) presents the critical heat flux data for various liquids as a function of pressure. For low or near-critical pressures, the value of the critical heat flux tends to zero while it goes through a maximum at a pressure corresponding to approximately 0.35 times the critical pressure.

Costello and Frea(C11) claimed that tests run with distilled water showed CHF values of 130 W/cm^2 on a 0.5 mm diameter stainless steel semicylinders whereas a value of 202 W/cm^2 using tap water was determined. However, these tests were testing the influence of materials deposited on the surface and the high value was only obtained after a long boiling time in the tap water. A part of this experimental project uses tap water; however, because of the relatively small time of quenching there should not be a major effect.

2.1.5 Transition Boiling

Beyond the inflection point of the boiling curve (critical heat flux), there is a decrease in heat flux as the wall superheat is increased. The surface is partially blanketed by an unstable vapour film. It is the region of transition from nucleate boiling (through an intermediate stage in which nucleate boiling coexists with unstable accumulations of vapour bubbles) to film boiling. This vapour film has been shown to form and collapse periodically. For this reason the term "unstable film boiling" is often used to describe it (C12).

Using high speed photography, Westwater and Santagelo(W4) showed that there is no contact between the heating surface and the boiling liquid in the transition regime. They concluded that when a vapour burst was formed, the liquid rushed toward the heating surface

but a miniature explosion of vapour occurred before contact was made. However, Berenson(86) could show experimentally that the transition regime is a combination of nucleate boiling and film boiling, both processes being unstable. He found that the transition region was a function of surface conditions and that the film boiling was not. He also concluded that the variation of average heat flux with wall superheat is dependent on the fraction of time with which each boiling regime exists at a particular position on the heating surface. Bankoff and Mehra(83) proposed a quenching theory for transition boiling which is in agreement with Berenson's findings. This model is based on the heat removal which occurs when the liquid contacts the surface and cools it.

As the excess temperature is increased the heat flux decreases due to a greater portion of the surface being active on the average, in the film boiling regime. Finally a point is reached where the surface is completely covered by a vapour film. At this point, this film is stable and a minimum in the boiling curve is observed. This is referred to as the Leidenfrost point or simply as the point of minimum heat flux.

Zuber(21) carried out a hydrodynamic stability analysis on the vapour film and from it developed the following relationship for the minimum heat flux:

$$(q/A)_{\min} = C P_g \lambda \left[\frac{\sigma g (\rho_l - \rho_v)}{(\rho_l + \rho_v)^2} \right]^{0.25} \quad (2.13)$$

This is generally considered valid for large heaters. The coefficient, C was determined empirically as 0.13 by Zuber(21) and 0.09 by Berenson(85). Many other equations have been proposed based on the same hypothesis by Berenson(85) and Lienhard(L5, L7). Chang in a discussion of Bernath's work(89) remarked that

$$\frac{(q/A)_{\max}}{(q/A)_{\min}} = 5.75 \pm 20\% \quad (2.14)$$

For water, benzene, methanol and cyclohexane.

Transition boiling is difficult to achieve with an electrical heating system unless a sophisticated feedback control system is employed. Even if a high-enthalpy condensing vapour, such as steam, is used as a heat source, Hesse(H3) indicates through an analysis involving relative thermal capacities, that operating in this transition boiling regime may not always be possible. He derived a criterion that has to be met for an evaporator to allow it to be operated in transition boiling. The wall through which the heat flows must have sufficient heat capacity and resistance such that it does not respond to rapid variations in heat flux that occur in transition boiling. Therefore, unstable transition boiling can be expected to occur on a very thin wall tube unless other precautions are taken:

2.1.6 Film Boiling

Film boiling is the regime of boiling during which the liquid and the heating surface are always separated by a stable film of vapour.

This film of vapour becomes the principal thermal resistance for heat flow. A good literature review for film boiling from a horizontal surface can be found in references(B5) and (H4) and from a cylinder in reference(N1).

There are two heat transport processes in film boiling: convective-conductive and radiative. In the first process, heat is transferred by conduction across the vapour film to the liquid where it is absorbed as latent heat. Vapour is removed from this interface by the vapour bubbles releasing periodically in a regular fashion from the oscillating film of vapour. Bubbles produced are much larger than those in nucleate boiling. In the case of cylinders, the vapour flows to the top of the cylinder where the vapour bubbles are formed. The film thickness increases toward the top of the cylinder and an oscillating film is produced over the upper surface.

The contribution of the radiation mechanism will only become important when the surface temperature is very high. The film boiling process is independent of the surface material, cleanliness and roughness as long as the height of roughness is less than the film thickness(B6). However, when radiation becomes significant the heat flux can depend on surface conditions(B12).

2.1.7 Boiling Heat Transfer in a Tube Bundle

Most of the research in pool boiling heat transfer has been done with only one tube and very little is known of the effect of vapour generated by a multitube bundle on the boiling heat transfer rate of any

tube within the bundle. However, there is considerable evidence that the heat transfer coefficient expected in a tube bundle may be appreciably reduced by the vapour generation from boiling on the lower tubes. A good literature review which pertains to this problem is given by Rogers(R5).

Only a few references have mentioned the bundle effect in pool boiling heat transfer. McAdams(M2) compared the performance of a small sixty tube evaporator (p/d ratio = 2) with results obtained on a single tube and no appreciable difference was noticed. Kern(K2) suggested that a maximum heat flux of 3.8 W/cm^2 to be used as a rule-of-thumb in designing a multitube evaporator to account for vapour blanketing regardless of the boiling liquid used. However, Palen and Taborek(P1) report heat flux as high as 7.9 W/cm^2 . Molek(M1) proposed a new correlation to predict the effective heat flux to nucleate boiling liquids and presents an example in his paper where he predicts an average heat flux of 3.4 W/cm^2 for water due to fouling. It, in fact, predicts the rule-of-thumb of Kern.

Palen and Taborek(P2) present a review of the current methods usually employed in industry to predict boiling heat transfer coefficients in a tube bundle. They then proposed a new correlation based on a statistical analysis of considerable data from existing industrial reboiler systems to predict the bundle effect. They have taken into consideration the effects of tube layout geometry such as pitch-to-diameter ratio, distance between tubes, projected tube area and tube overlap; the specific volume enclosed by one typical tube layout pattern and finally the number of tubes in vertical tube rows. They have also taken into consideration the effects of vapour accumulation and the vapour removal mass velocity to obtain a rather complex relationship(P2).

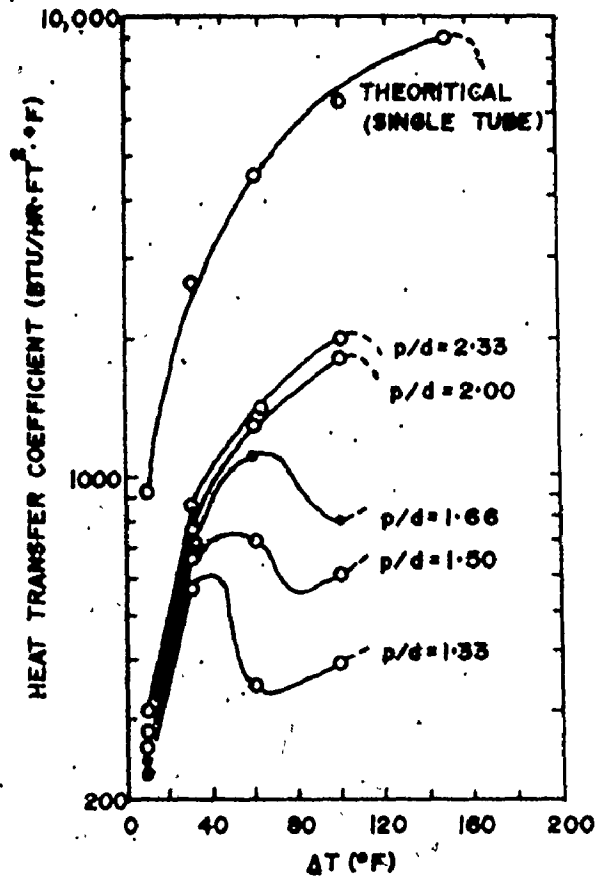


FIGURE 2-3 - TYPICAL BUNDLE BOILING COEFFICIENT (P2)

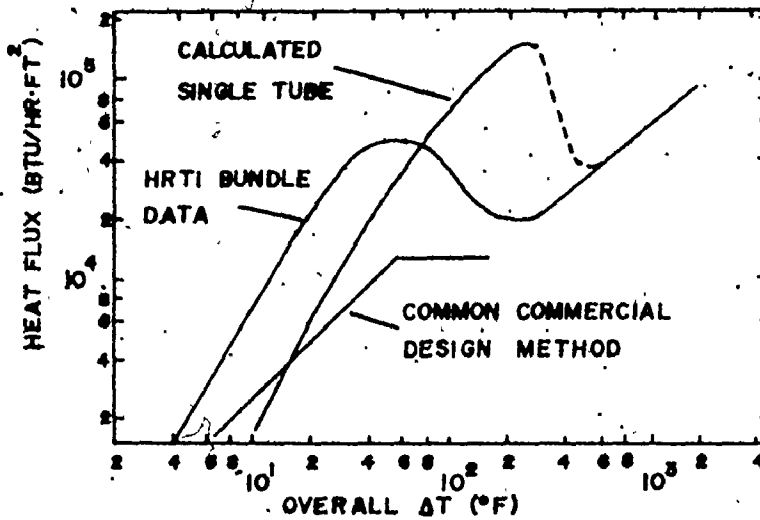


FIGURE 2-4 - TYPICAL TUBE BUNDLE BOILING DATA (P3)

A typical prediction of this equation is given in Figure 2-3 for different pitch-to-diameter ratio. The average boiling heat transfer coefficient for a multitude bundle is lower than a single tube and becomes worse as the pitch-to-diameter is decreased. This decrease is attributed to the availability of liquid in the bundle. A decrease in the spacing between tubes increases the vapour retention and restricts the liquid flow.

Palen and Small(P1) presented a correlation to predict the critical heat flux from a multitube bundle. They found that the vapour blanketing is a function of tube spacing, bundle diameter and rate of vapour generation. Their correlation is said to be accurate to within 30% but does not account for fouling effects.

A recent study of Palen et al.(P3) presented a good review of pool boiling in horizontal multitube evaporators. Typical tube bundle boiling is presented on Figure 2-4. The critical heat flux for a bundle is considerably less than for single tubes. However, a higher heat flux is observed for a tube bundle than that obtained with a single tube at the same wall superheat in the nucleate boiling regime. They suggested that this arises because of the greater turbulence generated by the boiling in the bundle. They also found that the tube layout was not significant although the pitch-to-diameter ratio has a great influence. They reported that the rising bubbles from the lower tubes can generate turbulence which in turn can increase the heat flux at the upper tubes over that expected for a single one if there are only a few rows (4 to 6) in the bundle.

Robinson and Katz(R4) studied the bundle effect in an array of tubes under low nucleate boiling conditions. They observed a significant increase in the non-bubbling regime but found no effect at higher heat fluxes.

Rogers(R5) used Palen and Small's method to predict the critical heat flux to be expected in a multitube bundle of geometry typical of the horizontal calandria in a CANDU nuclear reactor. This analysis suggested that the critical heat flux could be as low as 28% of that obtained for a single tube.

2.2 Quenching Boiling Curves

Because of the power or steam requirements (heat source), most research on boiling under steady-state conditions is restricted to using relatively small test specimens. For this reason, more recently, researchers have been using a quenching technique to study pool boiling heat transfer. Quenching offers the advantage that there are usually no serious limitations as to heat source requirements or size of the heat transfer surface undergoing boiling. Quenching has been studied for a long time by metallurgists. They control hardness by regulating the temperature history of the quenched piece.

The basic idea in a quenching experiment is to heat the object to be quenched to a desired temperature and then follow the temperature history of the object as it is being quenched. By a proper thermal analysis of the test object, a boiling curve may be obtained. Usually this involves starting at sufficiently high temperature to operate initially in the

film boiling regime and as the object cools, pass through each of the boiling regimes in turn, including the critical heat flux. It is important to note that these quenching experiments involve studying boiling under unsteady-state conditions. Whether boiling under this transient condition is the same as that observed under steady-state conditions has led to considerable controversy in the literature, as will be discussed later.

In the sections to follow, the methods of obtaining boiling curves from quenching data will be described. The calorimeter method will be described first; this is followed by the heat flux meter technique. Finally, the applicability of the quenched boiling curves generated from quenching experiments to those obtained from steady-state experiments or vice versa will be discussed.

2.2.1 Calorimeter Method

All the quenching boiling curves obtained so far employed a single or a few internal thermocouples to follow the temperature history of the quenched piece. Most of the researchers used only one internal thermocouple and usually assumed the system to be thermally lumped, that is at a uniform temperature throughout. This involves making the tacit assumptions that the Biot number ($Bi = hR/k$) is small and that the process is quasi-static. Kreith(K4) suggests that as long as the Biot number is less than 0.1 that the system can be lumped. Bergles and Thompson(BB) suggest that Bi at the critical heat flux density should not be much more than 0.4 for accuracy. The heat flux can be calculated from an appropriate heat balance using the curve of

the temperature as a function of time.

$$(q/A) = -\left(\frac{V}{A}\right) \rho C_p \left(\frac{dT}{dt}\right) \quad (2-15)$$

However, when the heat flux is high enough to cause an appreciable temperature gradient in the specimen, the boiling curve may not represent the actual phenomena. In this case, many thermocouples should be inserted at appropriate locations inside the specimen.

Bradfield(B11) used the quenching technique with a single thermocouple located at the centre of a chrome-plated sphere. He assumed his system to be thermally lumped. In this case, this assumption was valid, because his experiments were performed in the film boiling region where relatively small heat fluxes are encountered. Stolz et al.(S3, S4) introduced many thermocouples inside a sphere for a better representation of the temperature time history. A calculation method termed the "inverse heat conduction problem" was used to solve for the heat transfer at the surface(S3). In this method, the calculation of the transient surface heat flux and the surface temperature can be obtained by matching (called inverting) a temperature history measured at some location inside the quenched specimen. Stolz et al. reported that they obtained good reproducibility. Many authors have dealt with the transient problem in more sophisticated ways(B4, C4, C5, I1, S2) by using different forms of the inverse problem. Burggraaf(B15) in a general paper dealing with the theory and application of the inverse problem derived an exact solution of it. However the word "exact" is not necessarily true, because this method makes use of inexact temperature

measurements. The limitation is not in the method but rather in the accuracy of the available cooling curves.

The main advantage of the calorimeter method is that it is simple and easy to use. It is a very useful technique when relative short test times are available such as in the dropping tower used by Merte and Clark(M4) to study boiling under reduced gravity conditions. On the other hand, this method cannot account for angular variation in heat flux around a test specimen unless many internal thermocouples are used. Stolz et al.(S4) claim to be able to measure variations in heat flux by this method; for example, they report that critical heat flux on the top of a sphere is higher than that on the bottom.

2.2.2 Heat Flux Meter Technique

A heat flux meter, as implied by its name, gives a direct measurement of the heat flux out of a surface after proper calibration. A heat flux meter based on a design originally suggested by Gardon(G4, G5) has been successfully used by Dervedde(D1) and Rao(R2) to measure instantaneous boiling heat fluxes. Yamanis(Y2) used these meters to measure the instantaneous heat flux in a scraped-surface heat exchanger. The same type of heat flux meter was successfully used by Northover and Hitchcock(N3) in radiation experiments.

The heat flux meter forms an integral part of the heat transfer surface. It consists of a thin metal disk machined into a copper heat transfer surface; one face of the disk is involved with the heat transfer process; the other face is insulated. There are three constantan wires soldered into the disk, one located at its centre and the other

two at the edge of the disk. This allows the simultaneous measurement of the surface temperature by one of the edge thermocouples; the other two provide a measure of the temperature difference between the edge and the centre. When heat flows out of the surface, the thermal resistance of the disk gives rise to a temperature difference between the centre and the edge of the disk. This temperature difference is proportional to the magnitude of the heat flux density at the surface. A point on the boiling curve can be obtained by measuring the surface temperature simultaneously with the centre-to-edge thermocouple which provides the appropriate average heat flux density.

Assuming a uniform heat flux over the disk surface and negligible temperature gradients over the disk thickness (radial heat flow only), Darnedde(01) derived an equation expressing the average heat flux density over the disk in terms of the e.m.f. generated by the pair of copper-constantan thermocouples, viz.:

$$(q/A) = \frac{4 k_0 t_d}{R_0^2} \frac{\Delta E}{C} \quad (2.16)$$

where C is a function of the thermal conductivity variation with temperature and the temperature e.m.f. characteristics of the couple. With a copper disk and reasonable dimensions for the heat flux meter (0.48 cm diameter and 0.05 cm thick), the thermal gradients in the z-direction can be shown to be very small. The coefficient, C, depends on temperature. Darnedde used the edge temperature to calculate the variable C because it is not a strong function of temperature. On the other hand, at high heat fluxes the centre-to-edge temperature difference may be

significant. Moreover, since the heat flux in boiling is dependent upon the wall temperature, the heat flux should vary over the disk surface. If the variation of heat flux with temperature is linear over this range, then an average value will not introduce appreciable error. The appropriate wall temperature should, however, be the average temperature of the disk, not the edge thermocouple as used by Darnedde and Rao. The question of how large a surface area is required to obtain reliable average boiling heat fluxes still needs to be resolved. Certainly the boiling curves obtained by Darnedde and Rao for the boiling of thin liquid films compared favourably with other pool boiling data. Northover and Hitchcock(N3) use Equation 2.16 along with the meter's average temperature in their radiation studies. Some additional analyses of other effects associated with these heat flux meters will be presented later in Section 4.4.2.

In this project, this heat flux meter was used in transient boiling heat transfer. It has many advantages over the transient calorimeter method. The heat flux meter can measure directly the heat flux out of a surface but more specifically it can measure the local heat flux and thus easily determine angular variations. Yamanis(Y2) obtained an unsteady state solution of the heat flux meter and thus determined the time constant of 7 msec for a meter of similar dimensions as used in this work (0.397 cm diameter by .0254 cm thick). Hence with relatively slow cooling of the test specimen, the meter should follow the heat flux variations quite well.

2.2.3 Quenching vs Steady-State

Considerable controversy exists in the literature concerning the uncertainty of the applicability of the boiling curves obtained under steady-state conditions to those associated with transient behaviour and vice-versa. Some authors say that they are equivalent and others argue they are not the same.

Bradfield(811) and Merte and Clark(M4) used transient boiling curves assuming that there is no difference with those obtained at steady-state. After reviewing the literature, Bergles and Thompson(88) observed that in general quenching experiments produced lower critical heat fluxes at higher wall superheat when compared to steady-state experimental data. Moreover, the minimum heat flux was also shifted to higher temperature. They did their own experiments and came to the conclusion that there is a significant difference between boiling curves obtained at steady-state and those obtained with quenching. A careful examination of their experimental procedure and results suggests that extremely heavy oxidation of the boiling surface prevailed. This probably explains the lowering of the critical heat flux and the shift of wall superheat to higher temperatures that they observed. More recently Veres and Florschuetz(V1) argued that the difference between the steady and unsteady-state results that were observed by Bergles and Thompson arose because they failed to use the same heaters in both transient and steady-state tests. But the heaters for the two situations differed little in shape and in initial surface condition. On the other hand, Veres and Florschuetz did obtain similar critical heat flux results

under steady-state and unsteady-state conditions when they quenched the same heaters as long as the heaters were kept fairly clean during the quench. They did observe that if the heavy oxide layers which formed during the preheat period were allowed to remain on their specimen during the quenching experiment, deviation from the steady-state observations resulted. The data of Tachibana et al.(T2) suggest that for very rapid cooling the critical heat flux value will be higher from quenched data than from steady-state measurements. For relatively slow cooling they are equal.

More recent studies provide more detailed considerations on the validity of quenching data. Johnson(J1) studied transient boiling in water with exponential heat inputs on thin metallic ribbons. His results showed that for cooling periods greater than 5 msec the transient nucleate boiling is a good representation of steady-state data. Tachibana and Enya(T3) concluded that boiling heat transfer rate measured under rapid cooling conditions was in very good agreement with that obtained at steady-state. They observed better agreement in the nucleate boiling regime than that at minimum heat flux. They used a cylinder less than 2.5 cm O.D. in very rapid cooling and found good agreement with steady-state data. In this project a 12.7 cm O.D. cylinder was used which has more than 25 times the thermal capacity of their small cylinder; therefore, the cylinder was submitted to a relatively slow cooling rate.

In conclusion, this chapter has shown that the present state of the art is not sufficient to provide the data pertinent to the present

problem. Therefore, the data must be obtained through an experimental investigation.

CHAPTER 3


DESCRIPTION OF EQUIPMENT AND EXPERIMENTAL PROCEDURE

This chapter covers the description of the various equipment used throughout this investigation. It is divided into four main parts: The first section deals with the description of the apparatus used in quenching a single horizontal cylinder. The second section deals with the description of the apparatus used for the steady-state calibration of a heat flux meter. This is followed by a third section which presents a description of the equipment used to obtain unsteady-state measurements in an array of tubes. Finally, the fourth section describes the apparatus used for steady-state experiments in tube bundles. Each section contains the actual experimental procedure used for each specific study.

3.1 Apparatus for Unsteady-State Experiments

3.1.1 Instrumented Copper Cylinder

It was desired to establish local boiling curves for a long tube, 13 cm in diameter, at various conditions as described in the introduction. To accomplish this, a quenching technique was used in which a copper cylinder, 12.7 cm in diameter by 7.62 cm long, was heated to a high temperature and quenched in a pool of stagnant water at the desired level of subcooling. A quenching technique was used because to do a corresponding steady-state experiment would require an



enormous amount of energy because of the relatively large boiling surface involved.

A diagrammatic sketch of the copper cylinder assembly is presented in Figure 3.1. To simulate a long calandria tube the ends of the cylinder were insulated with transite disks. The transite disks were 2.5 cm thick and 15.2 cm in diameter; the inner face of the transite disk was machined to a depth of 0.63 cm over the inner 13.0 cm diameter. This recess accommodated the ends of the copper cylinder; the two transite disks therefore served as a holder for the copper cylinder as well as to insulate it electrically from the metal frame and thermally from the surrounding liquid. The cylinder was instrumented with a heat flux meter which provided a direct measurement, upon proper calibration, of the local heat flux density at the surface.

A copper surface was used in this study, instead of a zirconium alloy surface as in the calandria tube, because of the need for a high thermal conductivity material to ensure that the surface of the cylinder remained near the average temperature of the cylinder during the transient. Since, Berenson(86) found that the surface texture and material has little effect on the critical heat flux density, it is expected that the results obtained in this study should be applicable to the calandria tube. Copper was also chosen so that it would be compatible with the heat flux meter which is described in the next section: First a thermocouple of known temperature e.m.f. characteristics was required and secondly the material of the cylinder has to be the same as one of the connecting wires. For convenience this should be a conventional thermocouple.

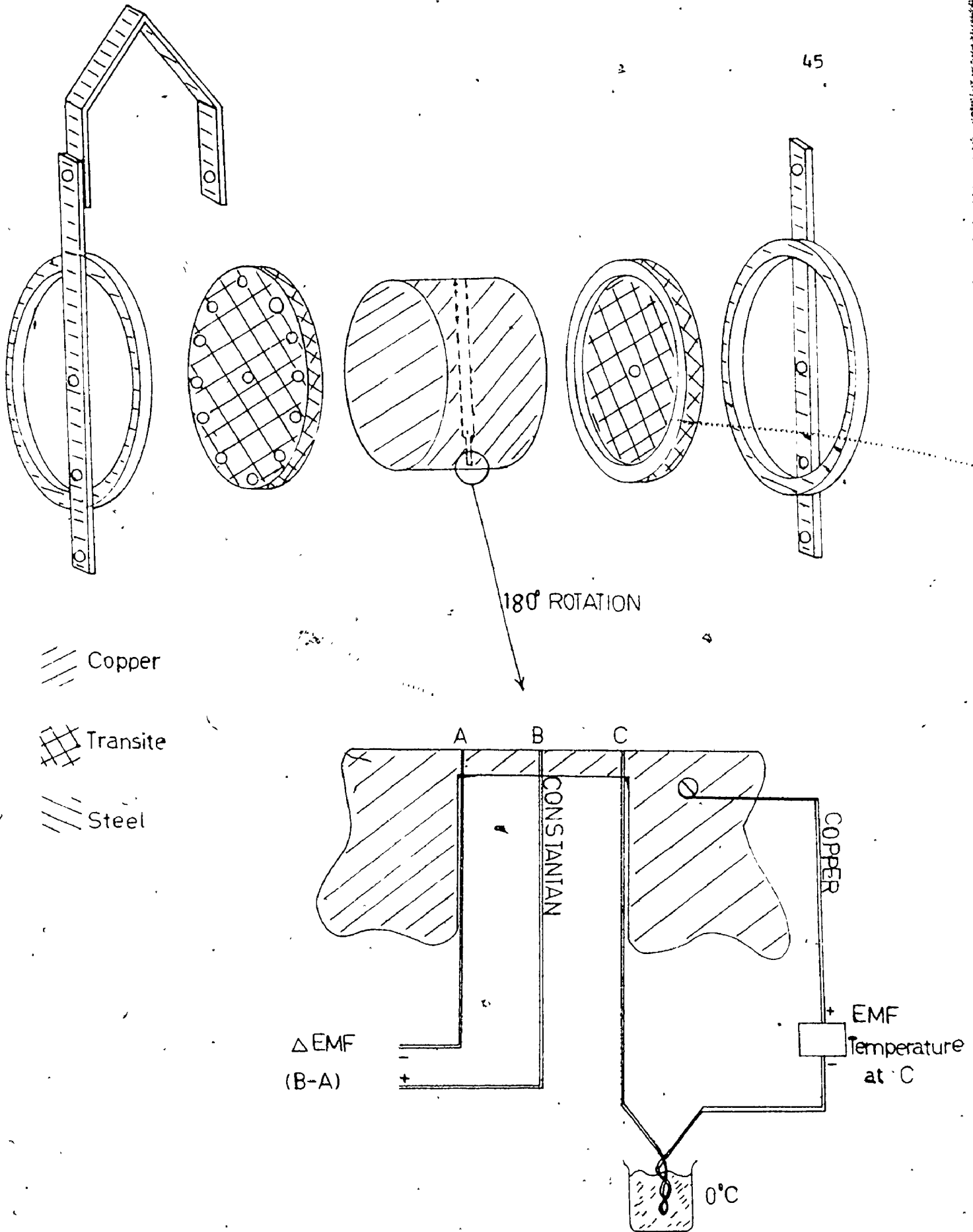


FIGURE 3-1 - APPARATUS FOR QUENCHING EXPERIMENTS



3.1.2 Heat Flux Meter

This experimental project relied heavily on the performance of a heat flux meter which was an integral part of the boiling surface. The details of the heat flux meter are shown at the bottom of Figure 3.1. Many problems were encountered in the construction of the heat flux meter. Appendix E gives a brief description of these problems. Only the description of the final design and fabrication procedure is given here.

The experimental program employed a disk-type heat flux meter which formed an integral part of the copper cylinder. A heat flux meter was first constructed in a small cylindrical plug, 1.27 cm diameter by 2.54 cm long by drilling a 0.476 cm hole from one flat face to within 0.635 mm of the other flat surface; the bottom of the hole was made flat with a special drill. Thus a thin circular disk was formed on one face of this cylinder. Using a high speed drill, three 0.279 mm holes were drilled, two on the edge and one at the centre of the thin circular disk. Three .254 mm constantan wires were silver soldered with an acetylene torch. Sulfuric acid was used to remove the oxide layer which formed during the soldering operation. A 1.27 cm hole was drilled in the large copper test cylinder in order to accept the copper plug. The dimension of the plug was between 0.002 to .005 cm larger than the hole in the copper cylinder. The plug was press-fitted into the hole using pressures greater than 40 MPa on an Instron testing machine. The cylinder and the plug were then machined together in a lathe to provide a cylinder of known diameter. Usually a thickness of 0.127 mm was removed

thus leaving a nominal thickness of 0.508 mm for the heat flux meter. The final step was to polish the entire circumferential surface with 4/0 emery paper.

This press-fitting procedure ensured a good thermal contact between the plug, which contained the heat flux meter, and the rest of the cylinder. In fact, the interfacial joint between the plug and the cylinder was hardly discernable even under low magnification. This method of construction did, however, produce a number of practical difficulties, chief among which was the unknown exact dimension of the thickness of the disk. In addition, some distortion of the plug could result during the press-fitting operation and this could mean that the axis of the plug was not coincident with the axis of the hole. Then, under this condition, when the cylinder and the plug were machined, the disk could end up with non-parallel faces. The effect of this is analyzed and discussed in detail in Appendix E.

The copper cylinder was placed between the transite disks to almost eliminate the heat transfer on the end flat faces. With these insulated ends and the length used, it is expected that the region in the vicinity of the heat flux meter was undergoing the same boiling phenomena as would be experienced by a long calandria tube. The angular location of the heat flux meter could be changed easily to one of seven different angles by holding pins located in twelve holes in the transite end plates. RTV 899 Silicone Rubber (Dow Corning Corporation) was used to join the transite disks and the copper cylinder. It also provided an extra resistance to heat losses on the ends. A steel frame firmly held the assembly as well as providing an easy way to handle the copper

block. The thermocouples were connected as shown on Figure 3.1 to simultaneously provide the temperature difference between the centre and the edge of the disk and also the temperature of the block. The hole from which the thermocouple wires protruded was filled with RTV. A layer of RTV was also put on the bare wires near the cylinder surface. Shielded thermocouple lead wires transmitted the voltage signal from the thermocouples to transmitters which in turn converted the voltage signals to milliampere signals which were transmitted directly through an 11-pair shielded cable to the A/D input terminal on a Data General Minicomputer where the signals produced voltages in the 0-10 V range. Appendix F describes the system used for data acquisition and analysis.

3.1.3 Steam Injection System

One part of this experimental project dealt with the effect of live steam injection underneath a single copper cylinder or the tube bundle undergoing quenching. The objective of this study was to study the influence of vapour (steam) impinging on the underside of the cylinder and the flow of steam over the cylinder on the boiling heat transfer coefficients. A diagram of the experimental system is shown in Figure 3.2. Steam from the 100 psig laboratory supply line was throttled by a control valve to maintain any desired pressure upstream of a sonic orifice (0.635 cm diameter). The steam flow rate was calculated from the following equation(813):

$$W = A \sqrt{\frac{\gamma M_w}{R} \cdot \left[\frac{2}{\gamma+1} \right]^{\frac{\gamma+1}{\gamma-1}} \frac{P_0}{\sqrt{T_0}}} \quad (3.1)$$

for $P_{upstream} \geq 0.5 P_{downstream}$

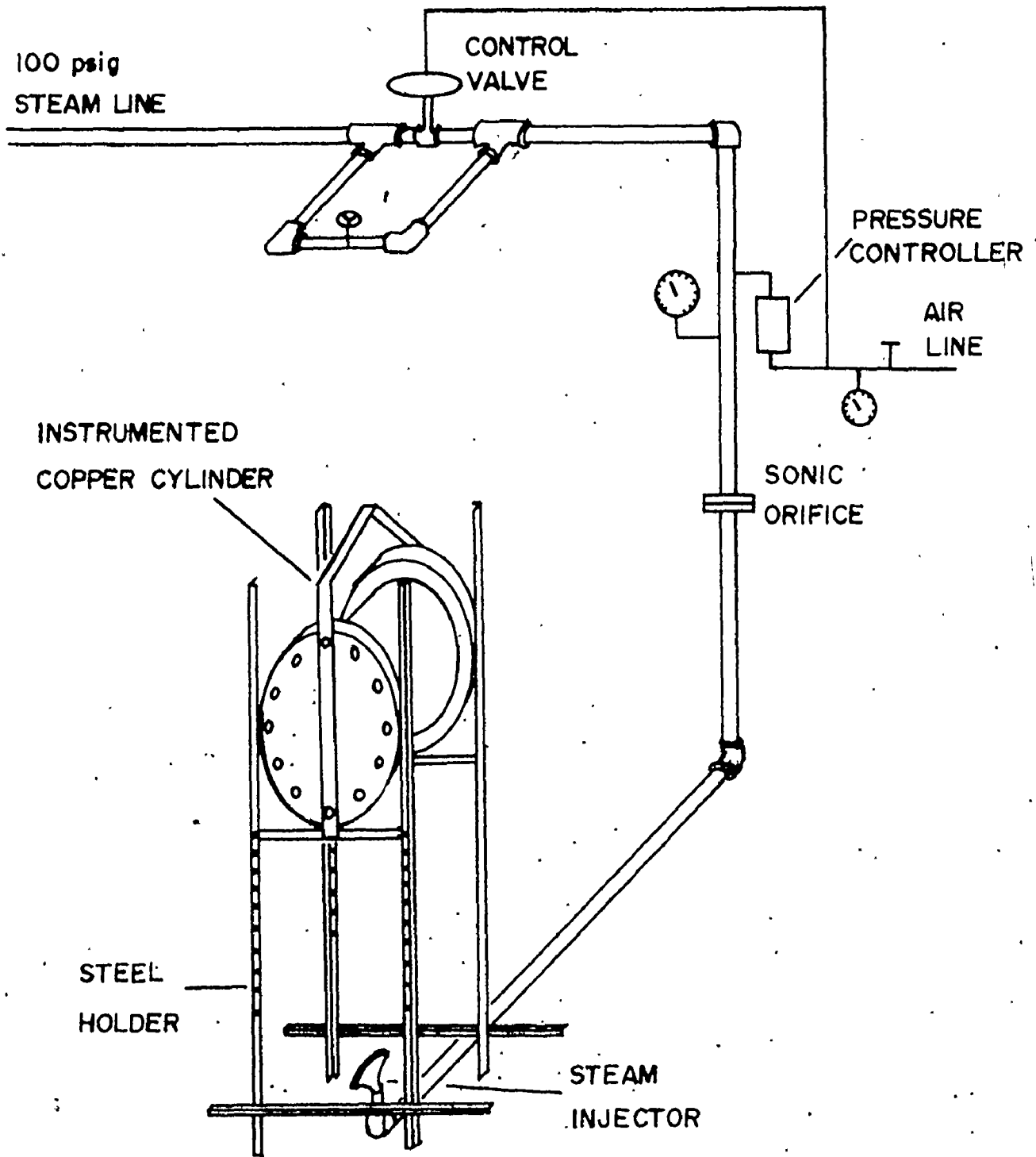


FIGURE 3-2 - STEAM INJECTION SYSTEM

The orifice coefficient was determined experimentally to be very near unity.

The steam was uniformly distributed over the length of the cylinder by employing an expansion piece which has an opening rectangular cross-section, 10 cm long by 0.5 cm wide. The distance between the steam sparger and the cylinder was adjustable from 0 cm to 32 cm. The whole system was contained in a 140 liter plastic tank filled with water.

3.1.4 Experimental Procedure

The copper cylinder was heated in an electrically-heated oven to a temperature varying between 200°C to 300°C , depending on the level of subcooling. A flow of nitrogen was admitted to the oven continuously to minimize oxidation of the copper. The copper cylinder was removed and quenched in the tank of water at the desired level of subcooling (up to 30°C). Readings of the block temperature and the disk temperature difference were recorded continuously by the minicomputer. The relatively large mass of copper meant that it cooled relatively slowly and thus it was expected to represent steady-state boiling. In a typical experiment under saturated conditions, the temperature of the copper cylinder dropped from 215°C to 155°C in about 30 sec., from 155°C to 115°C in about 13 sec. and finally from 115°C to 104°C in about 40 sec.; these time periods correspond to the transition boiling regime, the region of critical heat flux and nucleate boiling regime respectively. It is implicitly assumed that the heat transfer coefficient at the disk surface at one particular time is the same as that which would be

obtained at the same surface temperature in a steady-state situation. During quenching the boiling curve was obtained from the transition regime through to the nucleate boiling regime and included the critical heat flux. One boiling curve was obtained from each quenching experiment. The angular location of the heat flux meter was changed in a random fashion after carrying out two duplicate experiments at the same angle. The boiling curves were determined at seven different angles uniformly distributed from top to bottom of the cylinder (30° between each point).

At each experiment, the copper block was exposed to air during the period required to transfer the cylinder from the electrical furnace to the quenching bath. Unfortunately, this led to some oxidation of the copper surface. Excessive oxidation was found to lower the boiling curve; hence it was necessary to polish the cylinder lightly with 4/0 grit emery paper and to carefully clean the surface before each two or three runs to remove the small amount of oxide formed. This procedure, in accordance with the results of Veres and Florschuetz(V1), should give data that are equivalent to steady-state results. In an attempt to alleviate this oxidation problem, the surface of the copper cylinder was chrome-plated and nickel-plated (thickness of about 0.0005 cm or less). This treatment led to other problems which are discussed later.

The distilled water in the tank was changed after every five or six experiments.

3.2 Apparatus for Steady-State Calibration of a Heat Flux Meter

To verify the pseudo-steady-state assumption imposed on the heat

flux meter used in a transient experiment and also to find if the critical heat flux obtained from unsteady-state experiments was the same as the one which would be obtained from steady-state experiment, a steady-state experiment was designed. It also served as an independent check of the calibration procedure for the heat flux meter.

3.2.1 Description of the Experimental System

A 12.7 cm in diameter cylinder, which had been calibrated using the unsteady-state method, was drilled with fourteen holes (1.267 cm diameter by 6.35 cm long) according to the specifications shown on Figure 3.3. Fourteen "Firerod" cartridge heaters (1.260 cm diameter) were placed inside the holes and provided the energy requirement for the boiling process. Each heater has 500 watt capacity at 220 V. The power input to each set of five heaters was controlled by a powerstat transformer. Four copper-constantan thermocouples were inserted in the block to record the temperatures at different locations in the cylinder. Only the active area subtended by an angle of 76° and 5.1 cm wide was used in this experiment because of the power limitation. The heat flux meter was located at the centre of this boiling heat transfer area.

A set of boiling chambers, as shown on Figure 3.5, made of copper plate, was constructed to feed the water to the surface undergoing boiling and to collect the vapour emanating from the surface and transmit it to a condenser. The system was designed with two boiling chambers. The outside boiling insulated the inner chamber from heat loss and prevented condensation on the walls of the inside chamber. This design was also chosen to eliminate the edge effect on the boiling

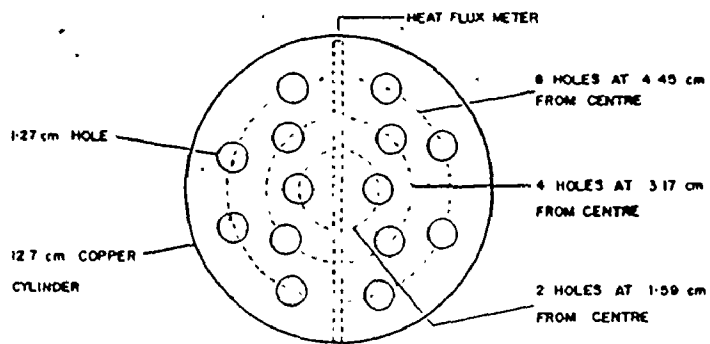


FIGURE 3-3 - HEATERS CONFIGURATION

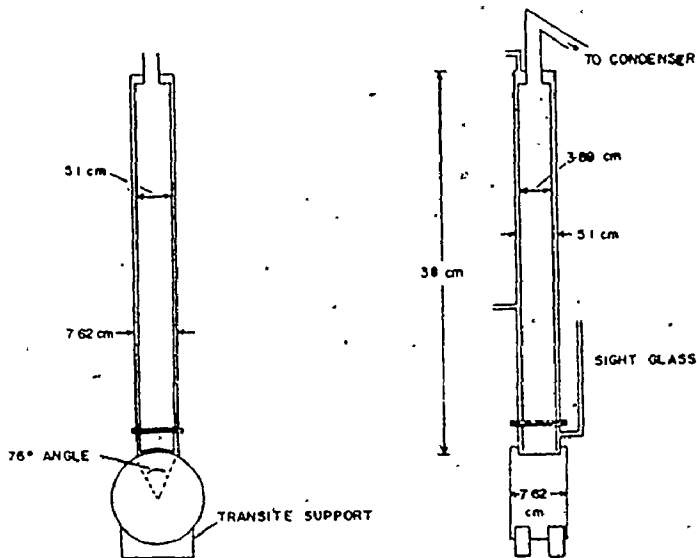


FIGURE 3-4 - BOILING CHAMBER ASSEMBLY

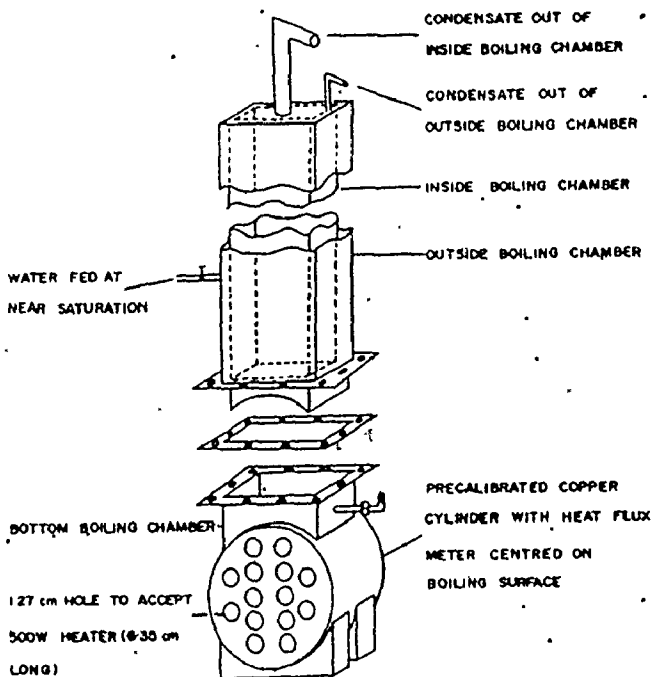


FIGURE 3-5 - APPARATUS FOR STEADY-STATE CALIBRATION OF A HEAT FLUX METER

process and have a more accurate reading of the prevailing average heat flux on the surface. The outside chamber was made up of two sections joined together with flanges and sealed with a neoprene gasket. The bottom section of the outside boiling chamber was 5.1 cm wide by 7.62 cm long by 1.3 cm high as measured from the top of the cylinder. It followed the curvature of the copper cylinder and was attached to it with RTV Silicone Rubber (Selastic 899 Dow Corning) which also prevented water leakage from the system. This design allowed relatively easy cleaning of the heating surface prior to each experiment. For relative dimensions of the system the reader is referred to Figure 3.4. The inside boiling chamber was separated from the outside chambers by an all around gap of 0.65 cm. At the bottom end, it followed the contour of the cylinder at a distance of 0.32 cm from it. At the top, it was joined to a 2.5 cm copper tube which was in turn connected to the condensing system.

The water was fed at near saturation to the outside chamber and allowed to flow to the internal chamber by a series of holes at the bottom of the inside chamber and through the circular gap between the top of the cylinder and the inside boiling chamber. The water level was maintained at a height of 15 cm to 18 cm during operation as indicated by a sight glass; the water flow was manually controlled. The water used was double distilled and deionized.

The system was equipped with two sets of condensing system, one for the inside chamber and one for the outside chamber. The whole system was well insulated with fiberglass insulation to minimize heat losses.

3.2.2 Experimental Procedure

The boiling surface of the copper cylinder was first polished with 4/0 grit emery paper and cleaned with acetone. The apparatus was then assembled and insulated. Deionized double distilled water was used as the boiling liquid. The water was heated and fed to the system at almost its boiling point. During the operation, the liquid level was maintained at about 15 to 18 cm above the cylinder.

The electrical power was set at a desired value and when steady-state was achieved the condensate was collected over known time interval for both the inside and the outside boiling chambers. The heat flux meter temperature and the temperature difference on the disk were recorded over the same time period. The experiment was repeated for a number of different power inputs to cover the nucleate boiling portion of the boiling curve, including very close to the critical heat flux.

It was quite common, when operating at high heat flux densities, for the temperature of the cylinder to rise to quite high values. In those cases, the power was immediately turned off and the cylinder was allowed to cool to a temperature lower than the temperature at which CHF occurred; the experiment was then continued at a slightly lower power input.

The heat flux meter response and the rate of condensate provided a steady-state calibration factor at every point on the boiling curve.

3.3 Apparatus for Unsteady-State Experiments in Tube Bundles

3.3.1 Description of the Experimental System

One of the main objectives of this research project is to provide the boiling curves on a 12.7 cm in diameter tube which is located somewhere in a bank of similar tubes undergoing the same boiling phenomena. To accomplish this, a steel frame, as shown on Figure 3.6, was built to support up to 15 copper cylinders (similar to those described earlier) on a pitch-to-diameter ratio of 2.18. The centre column was composed of copper cylinders, each instrumented with a heat flux meter which was calibrated individually by means of a set of unsteady-state experiments. The bundle could be moved quickly up and down by a pneumatic hoist. Lateral movement of the hoist was effected by a wheeled carriage which moved on a I-beam which was fixed in the ceiling of the laboratory. This allowed the bundle to be removed from a special oven, which was specially constructed for this experiment, to a quenching tank. This rectangular aluminum quenching tank was 91 cm long by 61 cm wide by 152 cm deep; it has a maximum capacity of about 850 litres. A viewing window, 32 cm wide over almost the full height of the tank, was mounted on the front of the tank and it allowed observation of the boiling phenomena during the quench. The complete tank (except the viewing window) was well-insulated with about 7 cm of fiberglass insulation. An aluminum frame was built and installed in the centre of the quenching bath to guide the bundle and position it in the middle of the tank. It also inhibited any movement and oscillation of the bundle during boiling.

Figure 3.7 shows the quenching bath system. The water was pumped from the bottom of the tank to the tube side of a shell and tube heat exchanger and returned at the top of the water tank. Steam was introduced on the shell side. The temperature of the water at the exit of the exchanger was controlled by a pneumatic controller-steam control valve system on the exchanger.

The tank was filled with fresh tap water before each experiment and discharged to the drain immediately after. Initially, distilled water was used but the capacity of the distilled water supply was insufficient to allow fresh water to be used for each experiment. In any event, it was not possible to detect any difference between tap and distilled water.

An electrical furnace was constructed to heat up the copper cylinder bundle. This oven and its auxiliary equipment are shown on Figure 3.8. The floor of the furnace was made up of specially hard insulating firebricks to support the weight of the bundle. The four vertical walls of the furnace were made up of soft refractory firebricks (Kaiser M-28). The top of the furnace was closed with a hinged lid which was made of fiberglass wool insulation in an aluminum sheath casing which had the dimension of the outside of the furnace. This lid was opened manually with a rope and a pulley. The outside of the furnace was enclosed in an aluminum box; the gap between the aluminum box and the brick walls was filled with spin silica wool insulation. A steel frame was built which contained rings to accept the transite end pieces which were glued to the ends of the copper cylinder. This frame was held in another steel frame in the oven to ensure that the

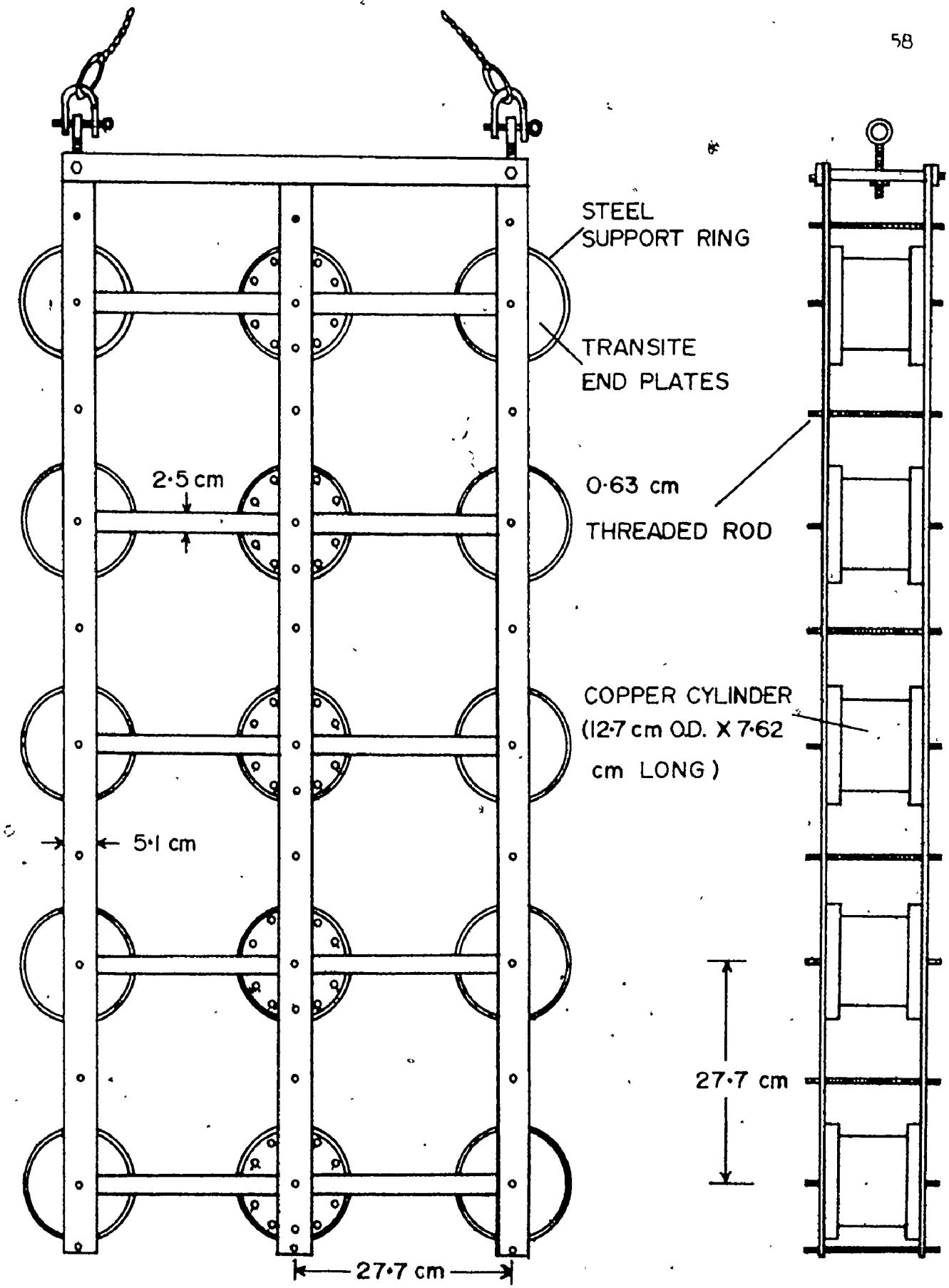


FIGURE 3-6- APPARATUS FOR MULTIPLE CYLINDERS QUENCHING EXPERIMENTS

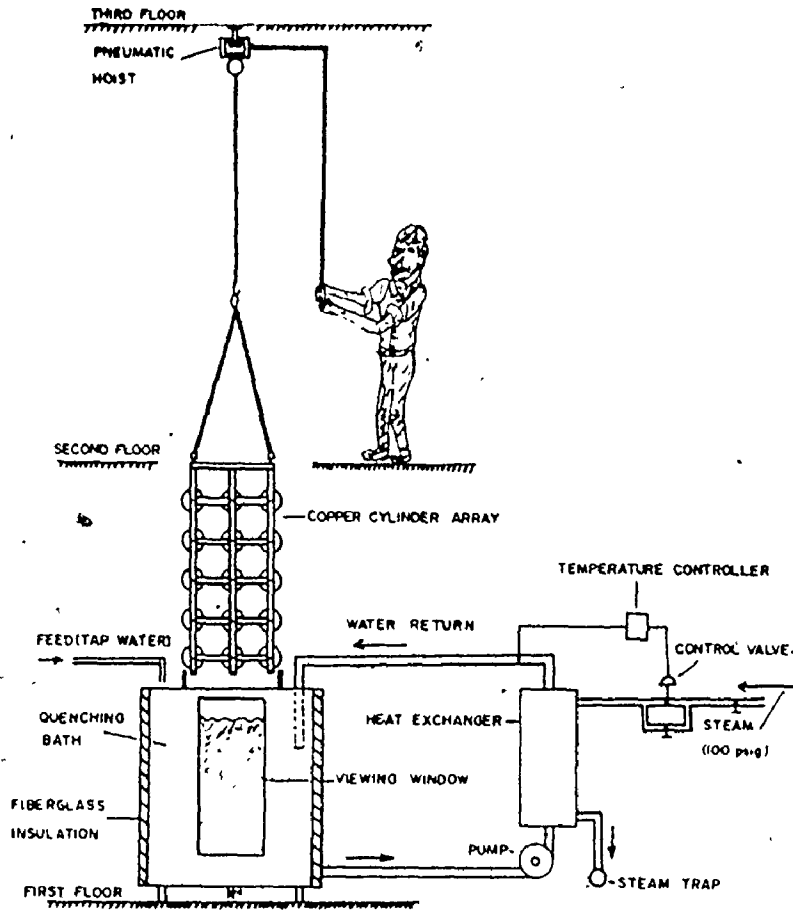


FIGURE 37- QUENCHING BATH SYSTEM

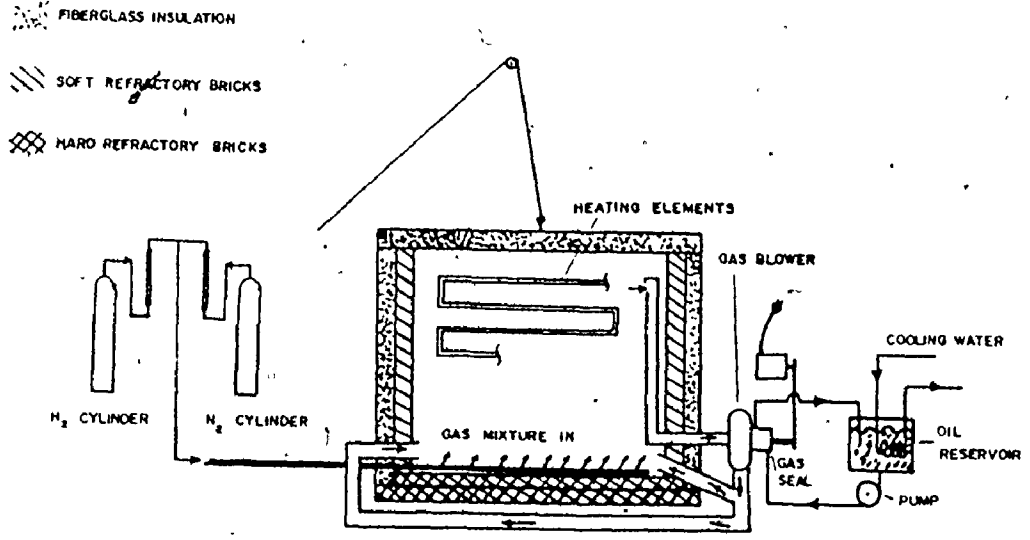


FIGURE 38- BUNDLE HEATING SYSTEM

copper bundle was held in a prescribed position in order to keep the bundle from touching the heating elements.

The heat was provided in the furnace by nichrome heating strips which were anchored to the inside brick walls. Grooves were cut into the brick wall to accept these heating strips and stainless steel wire held them in place. Power was supplied to the system from an A.C. welder at about 25 kw. With this power, the heating period was about two hours.

The furnace was also equipped with a blower which circulated the gas within the furnace in an effort to distribute the heat evenly through the oven. The gas was withdrawn from the top of the furnace and returned at the bottom through a T-junction to both sides of the furnace. This return flow could be distributed unevenly if required by adjusting two dampers in the return lines. The blower drive shaft was equipped with an oil-cooled seal to prevent any air from being sucked into it. The cooling oil was pumped from a water-cooled reservoir.

Oxygen was removed from the furnace by a constant nitrogen purge containing about 2% hydrogen. Residual oxygen was removed by reaction with hydrogen; the red hot nichrome heaters were assumed to effectively catalyze the hydrogen-oxygen reaction. The gas mixture was introduced at the top or bottom and distributed through two large pipes drilled with 0.3 cm holes.

3.3.2 Experimental Procedure

The procedure used here was essentially the same as the one

used for a single tube experiment. Before every experiment the 15 copper cylinders were polished with a 4/0 grit emery paper and cleaned with a soft cloth saturated with acetone. Before they were placed in the oven, all the thermocouples connections were verified with an ohmmeter, to detect any improper connections.

The copper cylinder array was then transferred to the oven, the lid closed and the oven was purged with a high flow of nitrogen gas for about 5-10 minutes before the power was turned on. The nitrogen-hydrogen purge stream was maintained at 92.5 and 1.85 liters/min. respectively (rotameter settings of 38 and 9) during the heating period (550 A, 25 kW power rate). The gas blower was then turned on along with its associated oil cooling system and oil-water exchange system. During the heating period, the gas flows were periodically checked while other functions were accomplished: calibration of the thermocouple transmitters, washing of the quenching bath system and periodic recordings of the temperature distribution in the array.

Forty five minutes before the experiment, the quenching bath was filled with tap water and heated to the desired temperature. It required approximately 20 minutes to fill the tank with water and about the same period to bring it to the desired temperature. Ten minutes prior to the experiment, the computer program used for data acquisition was loaded in the minicomputer and initiated. The number of heat flux meters and the number of individual temperatures which were to be read or fed to the computer were required to be supplied at the initiation of the program. Just before the array was quenched, the power to the oven, the fan and the steam supply to the heat exchanger were turned off.

The bundle was then removed from the oven and transferred to its position in the track above the quench tank (ca. 20-30 seconds) and then lowered quickly (ca. 4-5 seconds). The responses from the thermocouples were recorded continuously (averaged over 0.1 second or 1 second intervals depending upon the cooling rate) in the minicomputer. These responses were then converted to engineering units and outputted to a teletype, a line printer or to a disk file. The actual cooling rate depended on the initial temperature of the cylinders in the array and the degree of subcooling of the quench water, but usually it required less than 60 seconds to complete the cooling when the water was saturated at the outset.

3.4 Apparatus for Steady-State Experiments in Tube Bundle

The purpose of this experimental part was to acquire some knowledge concerning the steady-state boiling heat transfer performance to be expected on a 2.67 cm O.D. tube located in a bundle of similar tubes submitted to the same experimental conditions. This information should add some additional evidence and information of the boiling heat transfer results obtained from the quenching experiments.

This section describes the apparatus used in this study, discusses the choice of a boiling liquid and finally outlines the experimental procedure used in this study.

3.4.1 Description of the Experimental System

The system was designed to obtain a boiling curve which would cover all the boiling regimes, from the nucleate boiling regime,

including the critical heat flux to the low film boiling regime. Electrical heating was rejected because it is definitely not suited for work in the transition boiling regime. Instead, a steam-heated, horizontal, thick-walled copper tube was used as the heating surface. This type of heat source had the advantage that the tube wall temperature can be controlled to any specified value by controlling the pressure of the condensing steam. This meant that boiling heat fluxes in all regimes, including the transition regime could be measured; the apparatus also allows the critical heat flux to be well defined.

The experimental system is shown in Figure 3.9. It consisted of a boiling and a condensing system with the condensate returning to the boiling chamber. The boiling chamber was rectangular (91.4 cm high by 30.5 cm wide by 30.5 cm deep) and made of carbon steel; it was equipped with liquid level sight glass along with two 7.5 cm diameter viewing ports. The entire boiling chamber was insulated with 5 cm thick fiberglass mats. Two rectangular blank flanges were drilled with twelve 2.57 cm diameter holes (4 rows of 3 holes) on a square pitch with a pitch-to-diameter ratio being the same as that in the CANDU reactor. These flanges were bolted to the front and back walls of the chamber and covered the large rectangular hole in each of these faces, as shown in Figure 3.9. Four small flanges were also constructed; two with a single hole and the other two with twelve holes (see Figure 3.10). A flange system was used to make this equipment as modular as possible. This construction allowed the testing of a single tube or a bundle of the same tubes; hence, the boiling characteristics of each tube in the bundle could be tested and evaluated and then compared with

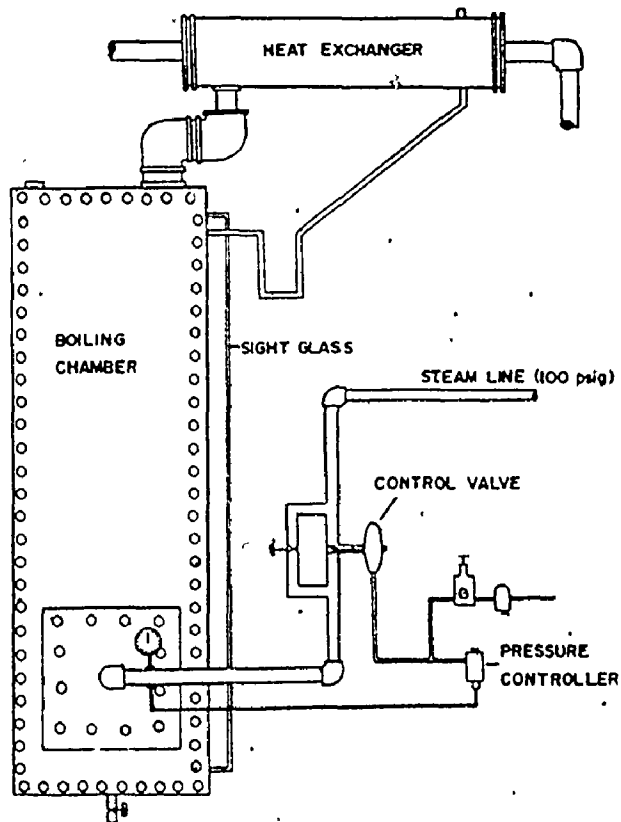


FIGURE 3-9 - APPARATUS FOR STEADY-STATE TUBE BUNDLE EXPERIMENTS

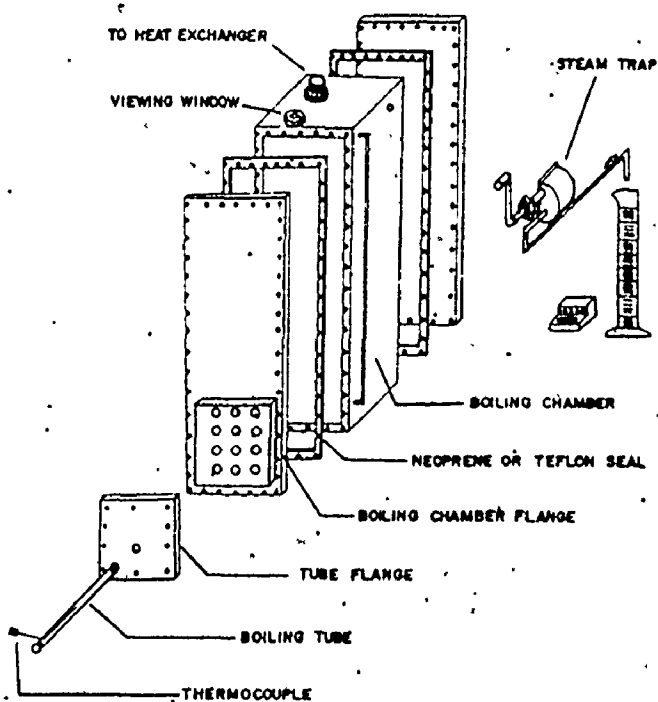


FIGURE 3-10 - BOILING CHAMBER ASSEMBLY

the observed characteristics in the bundle. The pitch-to-diameter ratio was varied by simply changing the flanges and not the whole boiling vessel.

Heavy walled copper pipes ($\frac{3}{4}$ in., schedule 80) were chosen to minimize temperature differences around the circumference of the tube and alleviate the problems associated with the widely fluctuating heat fluxes in the transition boiling regime which have been alluded to by Hesse(H3). Preliminary tests with an unplated copper pipe showed deterioration of the boiling surface due to excessive oxidation and contamination. The copper pipe was then chrome-plated to minimize fouling. A pneumatic control valve in the steam line, regulated by a pressure controller, kept the heating system at a constant pressure and therefore, at constant outside wall temperature. A copper-constantan thermocouple was inserted in a groove milled half way along the copper pipe. The thermocouple was insulated with RTV 899 Silicone Rubber (Dow Corning Corporation). The condensing steam was removed from the system through a float-type steam trap and subsequently cooled to avoid flashing prior its collection. When twelve tubes were tested, the steam pressure of each row was controlled individually from the others. The condensate for a row was collected with two steam traps; one for the centre tube and the other for the two outside tubes.

The vaporized heptane from the boiling chamber was condensed in a set of two parallel heat exchangers and returned to the boiling chamber. The areas for the two heat exchangers were 1.8 m^2 and 1.2 m^2 .

3.4.2. Choice of a Boiling Liquid

The liquid must be chosen such that it is possible to obtain a boiling curve which would include the nucleate boiling regime, the critical heat flux value, the transition boiling regime and, possibly, a portion of the film boiling regime. Therefore, the boiling point of the liquid must be high enough to permit operation in the nucleate boiling region with a steam pressure greater than atmospheric. On the other hand, to obtain the critical heat flux and the transition boiling regime, the boiling temperature must be low enough to be attainable within the limits of the steam supply pressure. Moreover, the critical heat flux must be low enough that sufficient steam is available to supply the heat required. As the average wall superheat at the critical heat flux is about 30°C , an ideal boiling point would be in the range of 85°C to 110°C .

There are therefore, three limitations imposed by the system: Steam pressure, maximum steam flow rate and the capacity of the condensing system. The steam pressure determines the wall temperature and was implicitly considered in the boiling point consideration. The steam flow rate is a measure of the heat supplied to the boiling liquid; therefore, the critical heat flux value of the boiling liquid must not exceed the steam supply capacity. The maximum steam flow rate available is about 160 kg/hr so that the critical heat flux value must be smaller than about 30 W/cm^2 if a bundle of twelve tubes is to be used. A stainless steel condenser having an area of 1.8 m^2 was available and its capacity depends on the vapour to be condensed; hence only after a

liquid was chosen could the condenser performance be evaluated. Another aspect to be considered in choosing a suitable liquid was the safety aspects both with respect to flammability and toxicity.

Of the liquids considered, heptane satisfied the criteria the best. It was then determined that the condenser could probably just operate satisfactorily under the conditions envisaged. It is worthwhile to mention at this point that it was necessary to add another condensing system in parallel with the original one even though calculation of the area required indicated that the system was more than adequate for the condensing duty involved.

3.4.3 Experimental Procedure

Heptane was introduced in the boiling chamber. The level of liquid was maintained at approximately 6 cm above the top copper tube. The steam pressure was first adjusted to about 200 kPa to bring the heptane to its boiling point. When the system achieved steady-state, the steam pressure was changed. At each setting, the volume of condensate over a given collection time interval, the steam pressure and the wall temperature were recorded for each centre tube. The first three measurements provided an average heat flux on each tube surface. This value coupled with the surface temperature gave a point on the boiling curve. As a convenience, Figure 3.11 was used to calculate heat flux values quickly. This immediate drawing of a rough boiling curve gave a good indication of what the new pressure setting should be to fill in the appropriate values on the curve. More points were taken in the region of the critical heat flux as it is the most

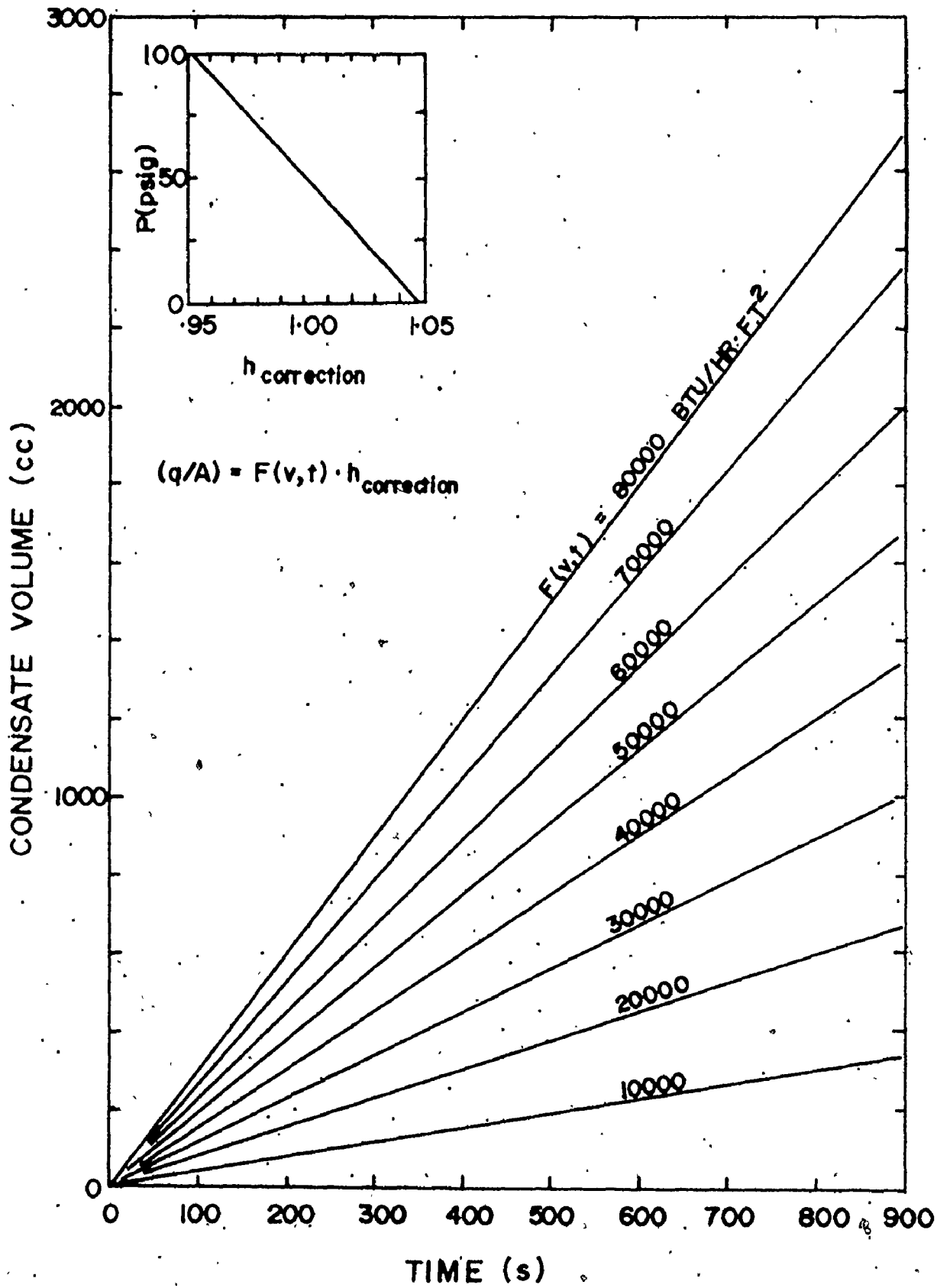


FIGURE 3-11 - GRAPH FOR HEAT FLUX

important aspect of this study. When four rows of tubes were used, the pressure setting on each row was set individually to provide a uniform wall temperature throughout the bundle.

At the initial stage of this experimental program, the boiling liquid was distilled after each run to remove any impurities that arose during the boiling process. It was found that after several hours of boiling, the heptane took on a faint yellowish colour (probably from the neoprene o-rings used as seals) and upon vaporization left this residue on the surface of the tube. The surface of the copper tube was also cleaned with acetone prior to each set of experiments to remove any fouling. This problem disappeared during the final stages of this experimental program because the neoprene o-rings and seals were replaced with teflon cord (GORE-TEX Teflon Joint Sealant, Anchor Packing Co. Ltd.).

After each experiment, the data were analysed on a computer and the boiling curves were drawn. Reproducibility was tested many times with a given tube and was found to be very good.

In this chapter, the description of the various equipments and the experimental method were presented. In the next chapters, the results obtained with each of these apparatus will be presented and discussed.

CHAPTER 4

HEAT FLUX METER CHARACTERISTICS AND ANALYSIS

To determine the boiling heat flux density around large horizontal cylinders, a need was established for a local heat flux meter which would respond essentially instantaneously to the local heat flux which existed at the point in question. Such a meter has been constructed by modifying one which was originally suggested by Gardon(G4). This modified meter was used effectively previously by Dornedde(D1) and Rao(R2) in their experimental studies on the boiling of turbulently flowing liquid films. Since that time, fabrication and calibration techniques have been perfected and its performance has been studied in detail. This is reported in this chapter.

4.1 Experimental System

The experiment involved quenching a 12.7 cm diameter by 7.62 long copper cylinder, which had been previously heated to about 250°C, into a tank of water which had been heated to a desired subcooled or saturated boiling condition. The response from a heat flux meter which was fabricated at a particular point in the cylinder was then transmitted to and stored in a minicomputer at specific time intervals and a boiling curve was obtained.

Copper cylinders were used to provide a cylinder with a high thermal conductivity in order to minimize thermal gradients within the

cylinder, thus ensuring that the boiling heat flux at the surface was not limited by conduction within it. Anomalous behavior was observed if an appreciable oxide layer was allowed to accumulate on the surface. Indeed, this experience and that with chrome-plated cylinders suggests that much of the controversy relating to the differences observed between steady-state and unsteady-state boiling heat transfer can be traced to the surface thermal resistance offered by either oxide layers or electroplated surfaces or the internal conduction problem. In this project, the cylinders were heated in a nitrogen atmosphere and any thin oxide layer that resulted from continued use was removed by light cleaning with fine (4/0) emery paper.

The cylinder was equipped with a heat flux meter of the Gardon type. This heat flux meter required that a thin disk of suitable metal be built into the heat transfer surface. In the original design (G4), the disk was made of constantan; one copper wire was soldered into the centre of the disk and one was attached to the copper body onto which the foil was mounted.

By a simple one-dimensional conduction analysis on the disk, assuming an insulated inner (lower) face of the disk and radial heat flow only, the average heat flux density over the outer face of the disk can be related to the centre-to-edge temperature difference, ΔT , by:

$$(q/A) = \frac{4 k t_d \Delta T}{R_o^2} \quad (4-1)$$

where t_d and R_o are the thickness and radius of the disk, respectively.

This original design was modified for use in high heat flux density situations as exist under boiling conditions by making the heat flux meter an integral part of the cylinder. The detailed construction of the heat flux meter is contained in Chapter 3 and a description of the problem encountered in its construction are outlined in Appendix E.

4.2 Factors Affecting the Design of the Heat Flux Meter

To use this heat flux meter in this unsteady-state boiling application, it must be designed with the following factors in mind:

(i) The heat flux meter must have a very fast response time.

Gardon(G4) has shown how the time constant of these meters varies with the dimensions and the thermal diffusivity of the meter material.

Dernedde(D1) has shown that with reasonable dimensions, the time constants for copper heat flux meters are of the order of several milliseconds.

(ii) The radius of the disk must be of sufficient size to be representative of the average heat flux conditions existing under the conditions of the experiment. In this case, this means that it must contain sufficient nucleation sites to be representative of the average boiling behaviour existing for the wall temperature condition. It is not known a priori how many nucleation sites are required.

(iii) Since the boiling heat flux density is a strong function of the wall temperature, the temperature variation from the edge to the centre of the disk must be relatively small, even at the critical heat flux condition. In this project, the temperature difference between

edge and centre was designed to be no more than 10°C at the critical heat flux condition. This means that it is necessary to measure relatively small EMF's quite accurately since heat flux varies 100-fold during a quenching experiment.

(iv) The choice of material is also extremely important, not only for the need of a metal with a high thermal conductivity but also that the body should be made from the same material as one of the connecting wires. For convenience this should be a conventional thermocouple material. In this project, the disk and the body were made of copper and the three connecting wires on the disk were made of constantan.

In the present use of the heat flux meter, the material of the disk was fixed by the need for a cylinder which would not have the heat flux around its boundary limited by internal conduction, hence the use of copper. Previous experience(D1) indicated that a disk diameter of 0.397 cm (exact radius fixed by available drill sizes) gave results which represented boiling heat transfer quite well. The disk thickness was thus fixed by the need to keep the edge-to-centre temperature difference within the defined limits. In these experiments it was nominally 0.051 cm.

4.3 Experimental Procedure

The instrumented copper cylinder was heated in an electrical oven to a temperature between 200°C and 300°C depending upon the level of subcooling of the quenching bath. The response of the heat flux meter during quenching was recorded using a minicomputer; the signals were read at a rate of 100 values per second and averaged over a

specified time interval depending on the level of heat flux at the surface. Typical curves obtained with this averaging procedure are presented in Figure 4.1. For more details concerning the experimental procedure the reader is referred to Chapter 3.

One boiling curve was obtained from each quenching experiment. The angular location of the heat flux meter was changed in a random fashion after carrying out at least two replicate experiments at the same angle. In this series of experiments, boiling curves were determined with the meter located at seven different azimuthal angles (0, 30, 60, 90, 120, 150 and 180^o). Reproducibility of the data was good (about 10-15%) as long as the oxidation of the cylinder was slight. This oxidation problem was alleviated by using moderate preheat temperatures and the nitrogen environment in the oven and periodic clearing of the boiling surface.

4.4 , Calibration of the Heat Flux Meter

Although, in theory, the heat flux meter can provide a direct measure of the instantaneous heat flux density for any given average wall temperature, in practice, each meter requires calibration to compensate for uncertainties which arise in fabrication, such as:

(1) The heat flux meter may not be constructed according to specifications, that is, the thickness and radius may differ from specification and/or the thermocouples may not be located exactly at the desired points nor recording the expected temperature. For instance, a few of the heat flux meters were sectioned by machining. This problem is fully discussed in Appendix E (photographs are also shown). In

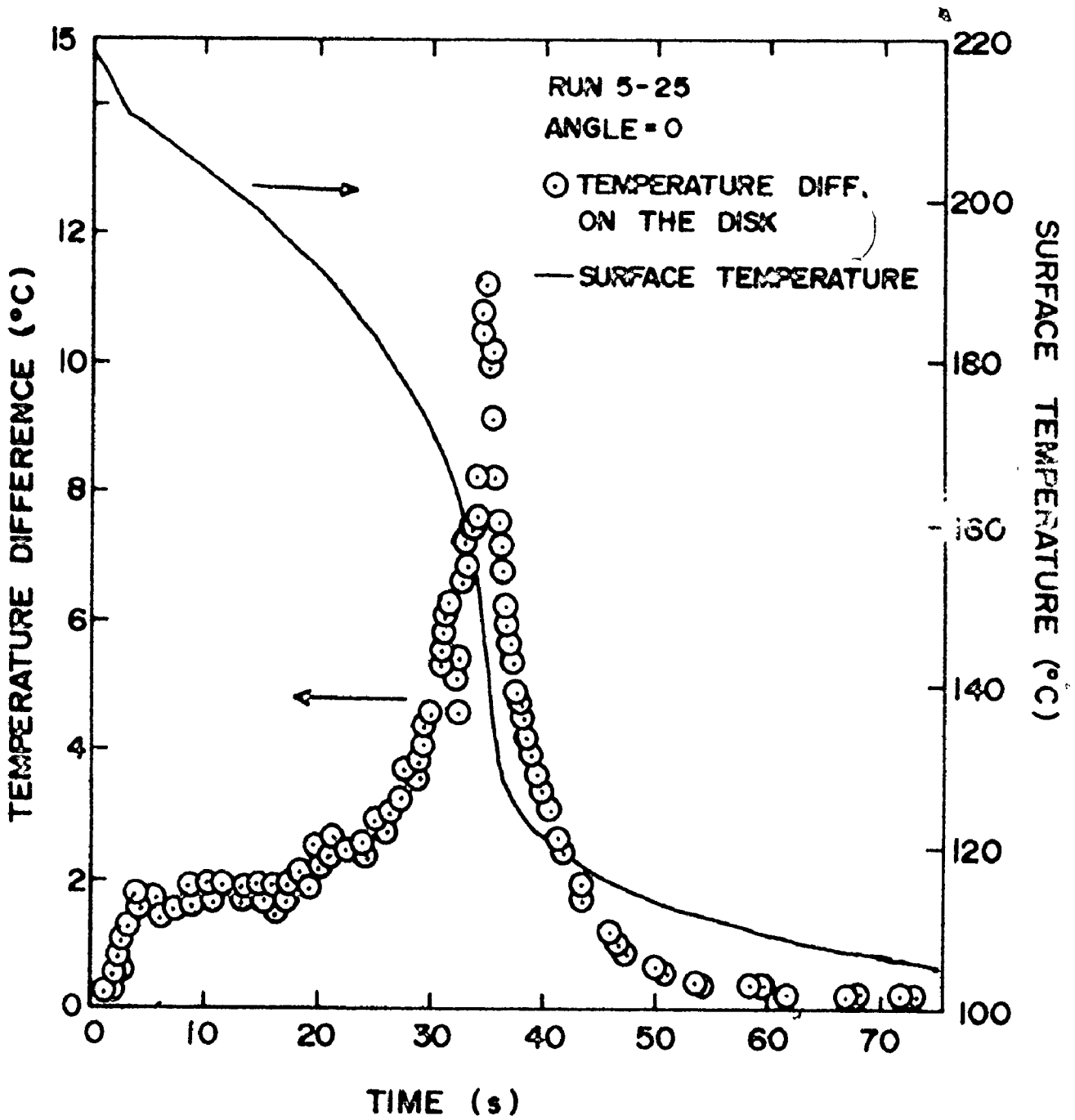


FIGURE 4-1 - TYPICAL RESPONSE OF A HEAT FLUX METER

summary, it was discovered with one that the silver solder ran down the wire and made a junction somewhat below the disk on the wall of the hole.

(ii) When the copper plug containing the heat flux meter was press-fitted into the cylinder, it is possible that the axis of the plug was not exactly parallel to the axis of the hole. The subsequent machining operation would then produce a disk of non-uniform thickness. It was shown by a conduction analysis employing an implicit finite difference method (Appendix G) that a tilt of only a few degrees could induce quite different edge-to-centre temperature differences depending upon which side thermocouple was used. Such differences were observed experimentally. Experiments did show, however, that although the calibration factors were different, the final calibrated heat flux results were the same regardless of which actual temperature differences used. For more details concerning this numerical method, the reader is referred to Appendix G.

Because these defects can be introduced during fabrication it is imperative to calibrate each heat flux meter. Two separate ways were used to obtain a calibration factor; another indirect method was also used to check it. These are discussed in turn.

4.4.1 Unsteady-State Calibration

A calibration factor (CF) of a heat flux meter can be obtained by comparing the total enthalpy loss from the cylinder, over the duration of the experiment, with that obtained by integrating the measured (apparent) local heat flux density over the total heat transfer area

and over the quenching time, viz.:

$$Q = \rho C_p V (T_i - T_f) = \int_0^t \int_A (CF) \cdot (q/A)_{app} dA dt \quad (4.2)$$

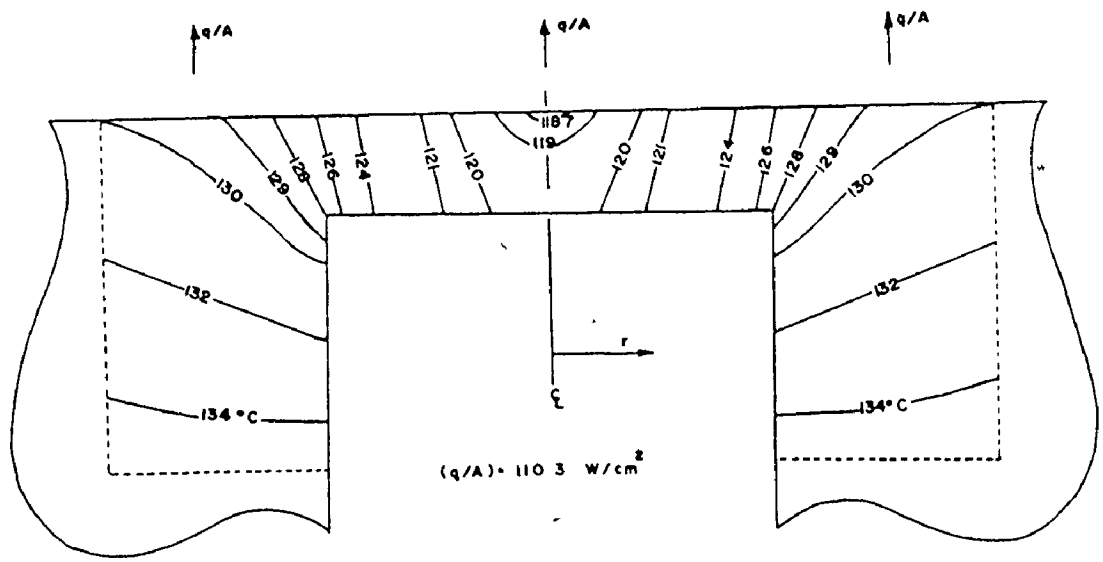
The apparent heat flux density is calculated by Equation 4.1, assuming a uniform average heat flux density over the disk. The integral is evaluated numerically by assuming the calibration factor is constant (independent of heat flux) and the measured instantaneous heat flux density at any angle is symmetric, uniform over the length and pertains over an angle of $\pm 15^\circ$ from the point in question. Because it was practically impossible to start all experiments for each angle at the same time, a direct integration of the heat flux density was impossible. Instead a discrete summation over the seven angles used was performed. A complete description of the unsteady-state calibration is presented in Appendix H along with a variance analysis of the calibration factor. This calibration procedure, although producing different calibration factors for different meters, did provide excellent reproducibility of the boiling heat flux densities from one test cylinder to another (within $\pm 10\%$ in most cases). The calibration factor was essentially the same whether it was evaluated under saturated or sub-cooled conditions. The average variance of the calibration factor evaluated by this method using only one experiment at each of the seven angular locations was about 3%; if two experiments were used the variance on the calibration factor was roughly 0.4%.

4.4.2 Steady-State Calibration

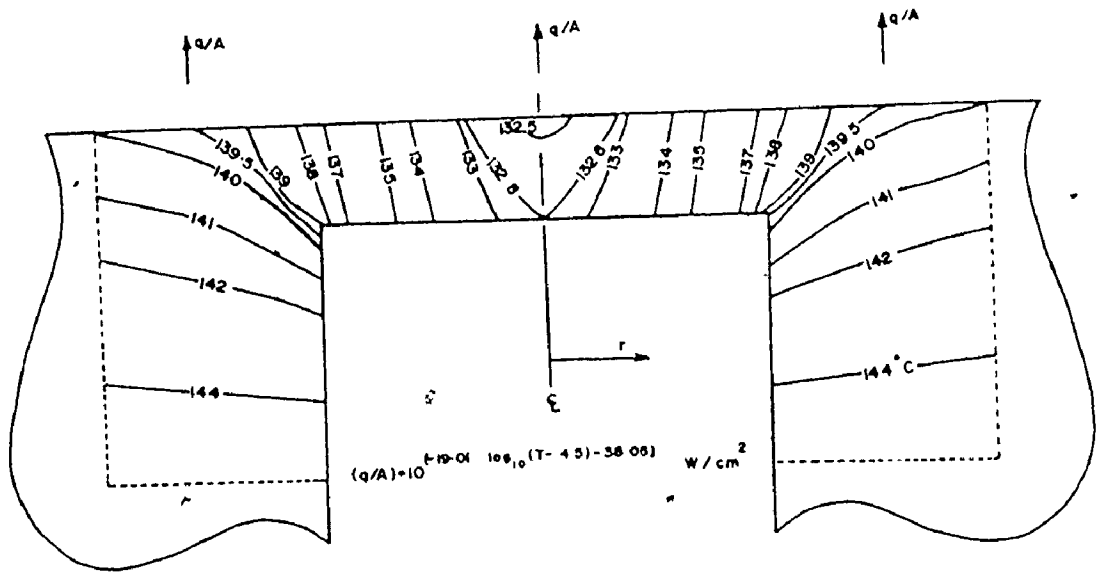
As a check on this procedure, the steady-state experiment, as outlined in Chapter 3, was designed to determine the calibration factor for a particular meter directly. After the calibration factor had been determined by the indirect unsteady-state method, the cylinder with its meter was used in a steady-state boiling experiment. The copper cylinder was drilled to allow the insertion of fourteen, 500 W, 230 V cylindrical heaters which were used as a heat source. A complete description of the experimental system was presented in Chapter 3.

The condensate collection rate gave a direct measurement of the average heat flux density on the boiling surface. The directly measured heat flux density could be compared to that indicated by the heat flux meter and a calibration factor determined.

Unfortunately it was found by direct observation of the boiling phenomena that the heat flux density in the immediate vicinity of the heat flux meter was considerably lower than that which occurred over the rest of the surface. A conduction analysis of the temperature field in and around the heat flux meter was performed by solving the Laplace equation in a finite difference form. The heat flux density variation with local surface temperature as determined with the calibration factor from the unsteady-state method was taken into consideration in the solution. Appendix I contains a description of the method of solution used to obtain the temperature distribution within a heat flux meter and its vicinity. Figure 4.2 shows typical temperature distributions obtained with this analysis. This study indicates that the temperature on and



(a) UNIFORM SURFACE HEAT FLUX



(b) VARIABLE SURFACE HEAT FLUX

FIGURE 4-2- TEMPERATURE DISTRIBUTION ON A HEAT FLUX METER AND ITS VICINITY

in the immediate vicinity of the disk is lower than that at some distance from the meter; hence the average heat flux density over the meter is considerably different from that over the main surface and the calibration method failed. A temperature depression around the heat flux meter may also occur because of some thermal contact resistance between the plug and the cylinder. On the other hand, this effect becomes less severe as the average heat flux density over the surface becomes less and should disappear at zero heat flux. Therefore, the apparent calibration factor at each measured heat flux was extrapolated to zero heat flux. This extrapolated calibration factor was then compared with that obtained by the unsteady-state method and excellent agreement was found. Appendix J presents the results obtained with Block 14 and 15. In both cases the calibration factor was the one which was expected.

It should be emphasized at this point that the effect observed during these steady-state experiments will in no way invalidate the use of the heat flux meter during the quenching experiments since the area surrounding the heat flux meter will register a lower average temperature just before the rest of the cylinder. Each local area will still exhibit the boiling phenomena corresponding to the local temperature condition. Since the surface temperature will be different over the meter and its immediate surroundings, some unknown averaging of the heat flux density by the meter will occur. This will be particularly important at the critical heat flux condition. The conduction analysis referred to Appendix I suggests that the heat flux registered by the meter corresponded to the average temperature of the disk (average

between the edge and the centre temperature).

These steady-state experiments also provided some valuable information. The copper cylinder was submitted to a deliberate temperature runaway, that is the cylinder went through the critical heat flux to low heat flux densities of the transition regime. The response of the heat flux meter was measured with the minicomputer. The power input was turned off as soon as the cylinder passed through CHF and the cylinder then slowly cooled down by going relatively slowly through the CHF. The response of the heat flux meter was also recorded with the minicomputer. Results of this study are presented in Appendix J. These results show that the transient CHF obtained with this method is the same as the one which was obtained in the single unsteady-state experiment. The CHF is the same whether it is approached from the nucleate regime or the transition regime, therefore showing no hysteresis in the boiling curve. Moreover, the CHF occurred at the same temperature. The cooling from the transition regime to the nucleate boiling regime, following a temperature runaway, was extremely slow and nevertheless has the same CHF value as in the unsteady-state experiment where the cylinder cooled much faster. This tends to prove that the critical heat flux value obtained in this study is the same as the one which would be obtained in a steady-state experiment as it is independent of the cooling rate of the cylinder, at least over the range of cooling rates observed.

4.4.3 Boiling Curve Prediction

Because of the assumptions and uncertainties inherent in obtaining the calibration factor for the heat flux meter, independent

checks of the calibration factor were sought. An attempt to evaluate the calibration factor directly from an independent steady-state experiment, as seen in the last section, was not as successful as expected, although it did suggest that the calibration factor was reasonable.

Another check of the results from the indirectly calibrated meter was achieved by carrying out an unsteady-state conduction analysis on the cylinder to predict the cooling curves for particular points on the surface of the cylinder assuming the measured boiling curves for specific areas of the cylinder as the boundary condition. This analysis along with the results obtained are presented in Appendix K.

At the outset, this conduction analysis was simplified by assuming a uniform heat flux density over the entire circumference at any instant (neglecting angular variations); thus only a 2-dimensional analysis was required (r and z directions only). An ADI (alternating direction implicit) finite difference method was used. The assumption of uniform heat flux was known to be invalid since severe variations in heat flux density were observed. Nevertheless, the results of this analysis were very encouraging and demonstrated that it was worthwhile improving the accuracy of the prediction. Moreover, another numerical method based on the superposition principle was reported by Archambault and Chevrier(A1). It was shown that this method was faster and as accurate as the ADI method as long as the boundary conditions were properly formulated(T4). This method therefore allowed the relatively easy extension of the heat conduction analysis to the three-dimensional case thereby relaxing the assumption of uniform heat flux density around the circumference. Since it accounts for the variation in the boiling

heat flux density around the cylinder and involves three-dimensional heat conduction, the predictions from this method are better than those from the two-dimensional analysis. The details of this analysis are outlined in Appendix K. A typical set of graphs obtained with this analysis are presented in Figure 4.3. The agreement of the predicted and experimental cooling curves is very good and this lends credence to the heat flux meter calibration.

This conduction analysis was also used to predict the boiling curves for each point on the surface. The three-dimensional analysis based on the superposition principle was used. In this case, however, a boiling curve was assumed for the surface mesh points and the surface temperature at each point was calculated after a specified time step (the experimental time between measured temperatures). If the predicted temperature differed by more than 0.05°C from that measured, a new boiling heat flux density was assumed for that point and the calculation repeated. This procedure was continued through the entire quenching time. It was observed that small errors in the surface temperature measurement led to appreciable variations in the heat flux density, particularly at high heat flux densities; thus some smoothing of the experimental cooling curves was required to minimize this variation. This was achieved by using a cubic spline data smoothing procedure(R3). The resulting boiling curves for all the seven angular locations and for different conditions are contained in Appendix K. A typical set of boiling curves obtained with this procedure is presented on Figure 4.3. The boiling curves generated by this procedure compare very well with those obtained by the indirectly calibrated heat flux meter, thus

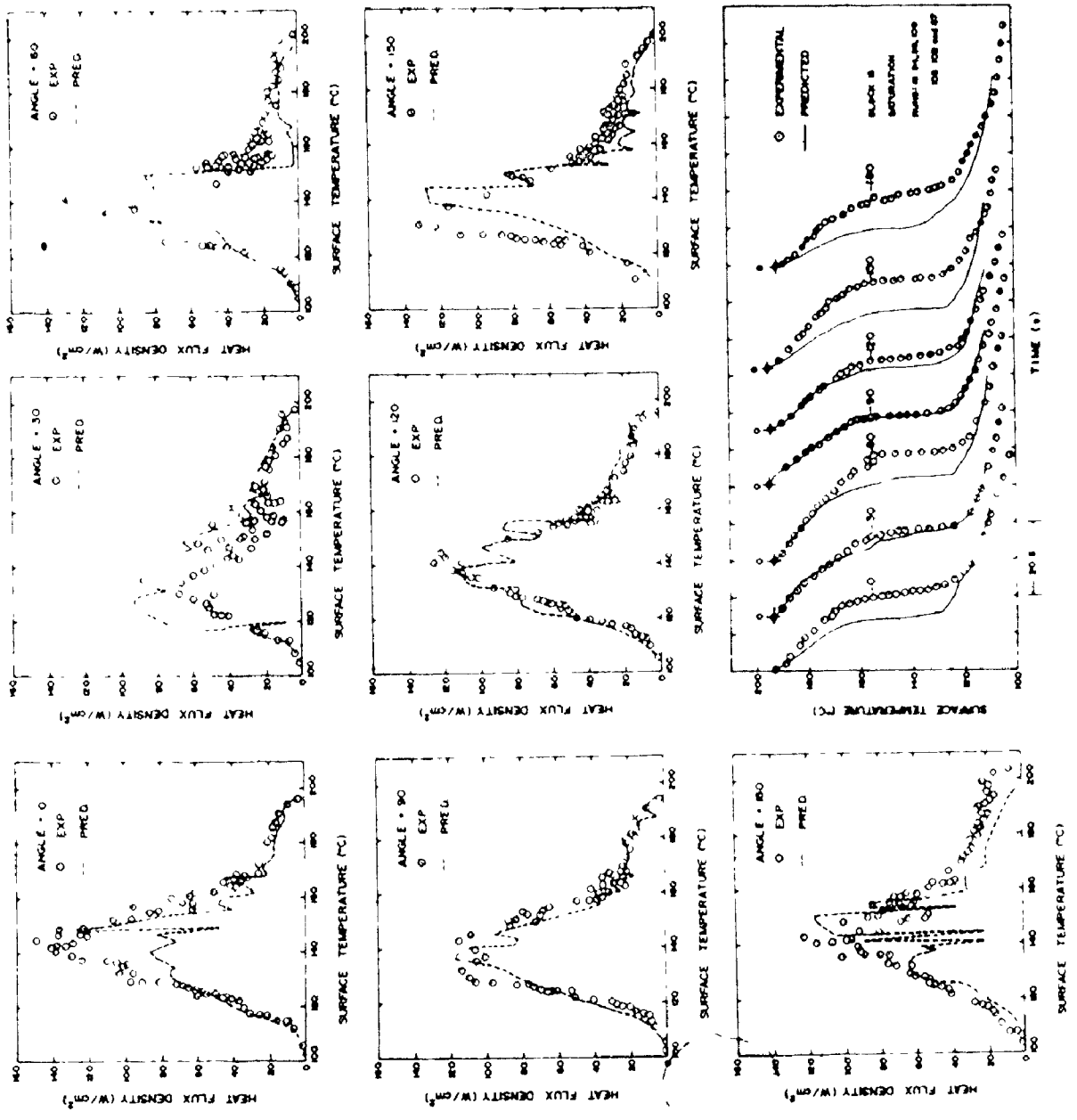


FIGURE 4.3 - COMPARISON OF THE EXPERIMENTAL HEAT FLUX DENSITY AND COOLING CURVES

suggesting again that the meter calibration procedure is reasonable and that reliable heat transfer rates can be measured in this way.

4.5 Conclusion

The use of a modified Gardon-type heat flux meter(G4) for measuring the local boiling heat flux density around a large diameter horizontal cylinder which was quenched from a high temperature in saturated or subcooled water was described. The calibration procedure was provided along with a detailed conduction analysis of the temperature field in and around the meter. Since this experimental program relied heavily on the performance of the heat flux meter, it was the object of this chapter to build confidence in its ability to provide good pool boiling heat transfer data. It can be concluded that the heat flux meter can be used effectively to provide reproducible measurements of the entire boiling curve during quenching experiments.

CHAPTER 5

RESULTS OBTAINED ON A SINGLE COPPER CYLINDER

The objective of this experimental program was to study the boiling heat transfer performance to be expected on a 12.7 cm diameter tube located in a matrix of similar tubes undergoing similar boiling conditions. Improved understanding and additional data are required for safety analysis studies for CANDU nuclear reactors. A 12.7 cm copper cylinder, equipped with a heat flux meter, is used to obtain the pool boiling heat transfer curve as a function of subcooling and location on the circumference. This technique offers the advantage that the actual size of the calandria tube is used to obtain the boiling curve. Furthermore the boiling is carried out in water, the medium in which the boiling information is required, and therefore modelling of the boiling process is not required to extrapolate from one fluid system to another. The problem, however, still remains as to the temperature at which a particular heat flux occurs, since this depends on the material and its surface condition. Fortunately, in this case, this information is not critical; only the level of the heat flux is.

This particular series of experiments achieves two goals. It first provides the characteristic pool boiling data for any particular single cylinder and then also a method to calibrate each individual meter in a given copper cylinder before it is placed in the bundle.

The experimental system used in this portion is described in

Chapter 3 along with the experimental procedure. In summary, the copper cylinder was heated in an electric furnace to a temperature varying between 200 and 300°C depending on the level of subcooling of the quenching bath. It was then quenched in a stagnant pool of distilled water which had been preheated to the desired temperature. The response of the heat flux meter was recorded by a minicomputer and in the final analysis, a boiling curve was obtained for each experiment.

This chapter reports all the results of the experiments performed with single copper cylinders. The main emphasis is placed on the critical heat flux (CHF) of the boiling curve where it is determined as a function of angular location, level of subcooling, amount of the boiling surface participating in the active boiling and the influence of vapour injection underneath a single copper cylinder. Each aspect will be discussed in turn.

5.1 Boiling Curves

5.1.1 Boiling Curves Reproducibility

Graphs of Figure 5.1 have been plotted to show the reproducibility obtained throughout this experimental program for different conditions tested: Angular location, subcooling and cylinder length for various cylinders investigated. The reproducibility in most cases is very good.

5.1.2 Angular Variation

Boiling curves under saturated and subcooled conditions at

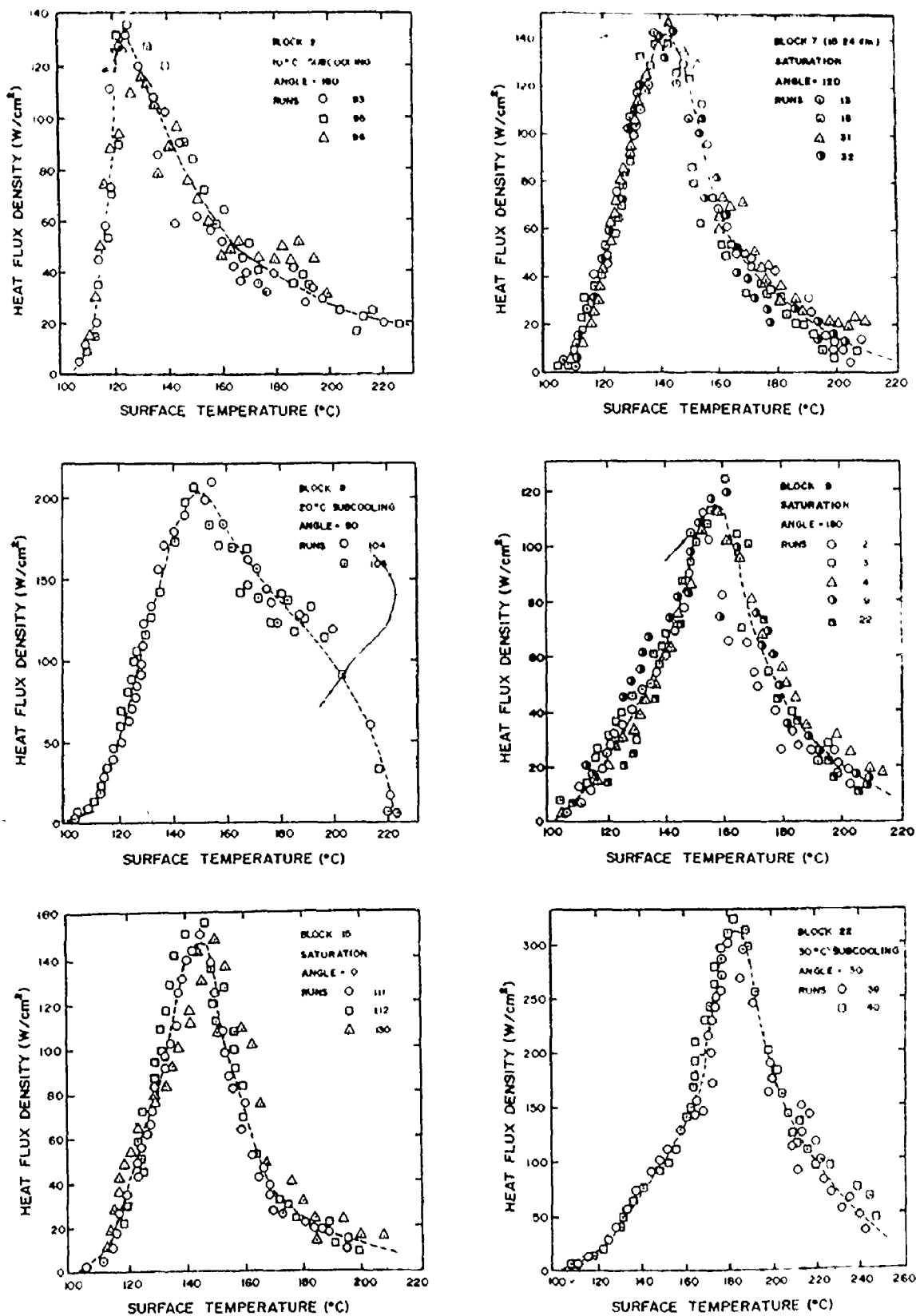


FIGURE 5.1 - REPRODUCIBILITY OF EXPERIMENTAL BOILING CURVES.

different locations around the cylinder are presented on Figure 5.2 for various copper cylinders. There is a definite heat flux density variation as a function of angular location. There is a substantial difference in the transition regime, especially at an angle of 30° . The greatest difference occurs at the CHF point. In the nucleate boiling regime, the angular heat flux density variation disappears and the majority of the boiling curves lie on the same line. The point of highest variation will be considered separately when the critical heat flux values are analysed. Some explanation will be provided for the extremely low CHF encountered at 30° angle.

5.1.3 Influence of Subcooling

The effect of the quenching bath subcooling on boiling curves for various copper cylinders at various angular locations is depicted on Figure 5.3. It is interesting to note that under the largest subcooling the boiling curve shifts to higher temperatures. Larger levels of subcooling are difficult to attain because the cylinder must be heated initially to temperatures where the oxidation of the copper becomes severe. The shift of the temperature at which CHF occurs with higher subcooling will be considered in Section 5.2.6.

The results are similar to what is usually observed, namely that the nucleate boiling curves are essentially the same at any wall temperature for different levels of subcooling, that the nucleate boiling regime extends to larger wall temperatures, and that the CHF is usually higher as the level of subcooling is increased.

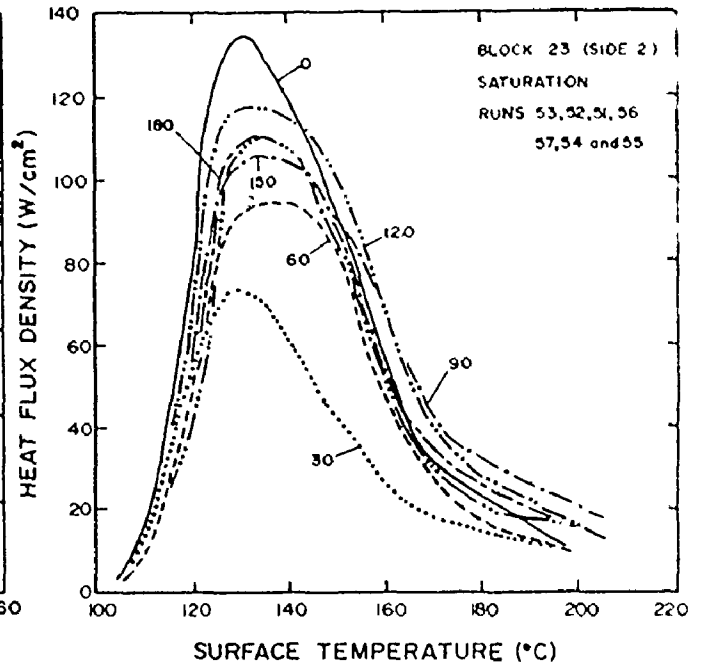
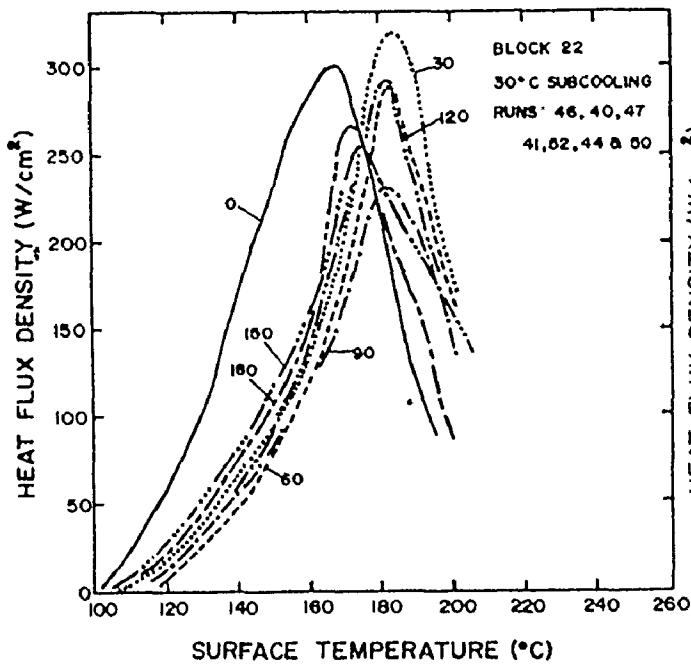
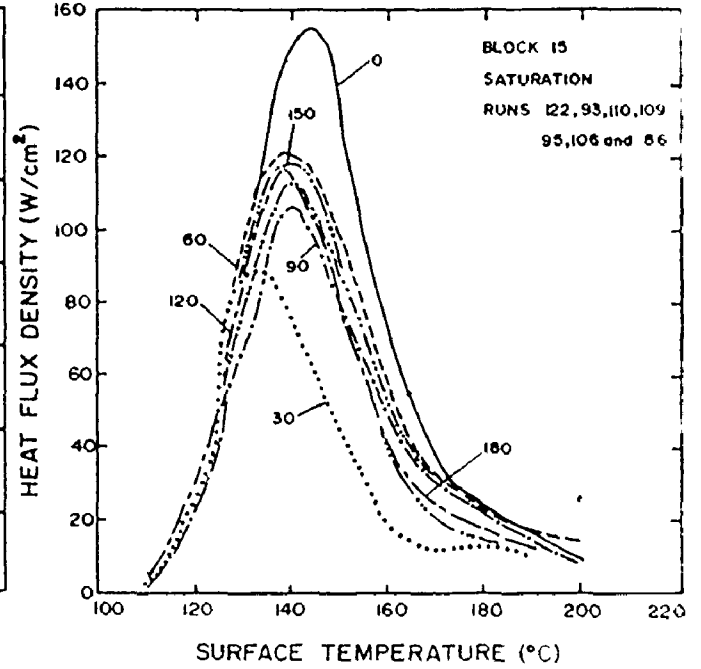
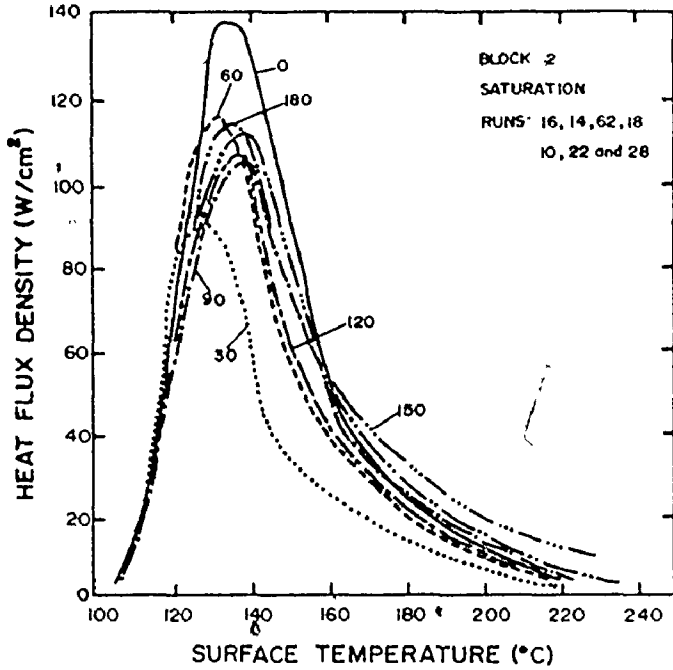


FIGURE 5.2 - TYPICAL LOCAL BOILING CURVES UNDER SATURATED AND SUBCOOLED CONDITIONS FOR VARIOUS POINTS AROUND THE CYLINDER.

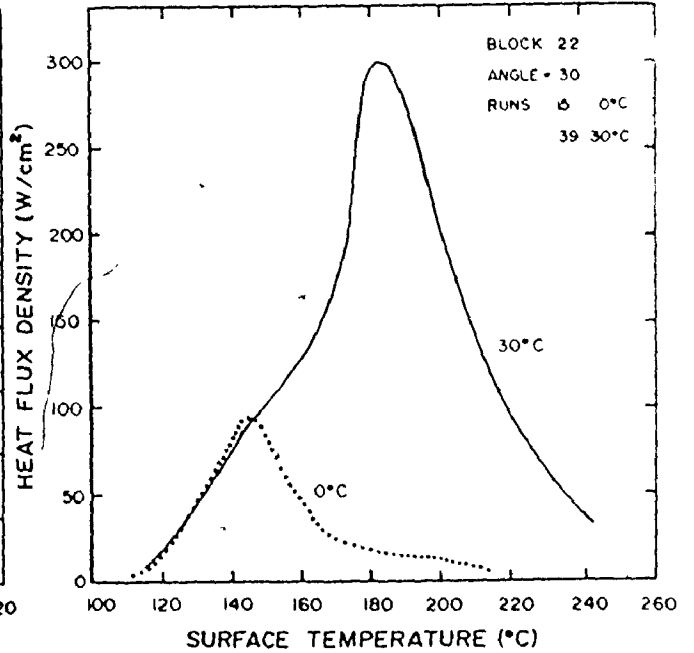
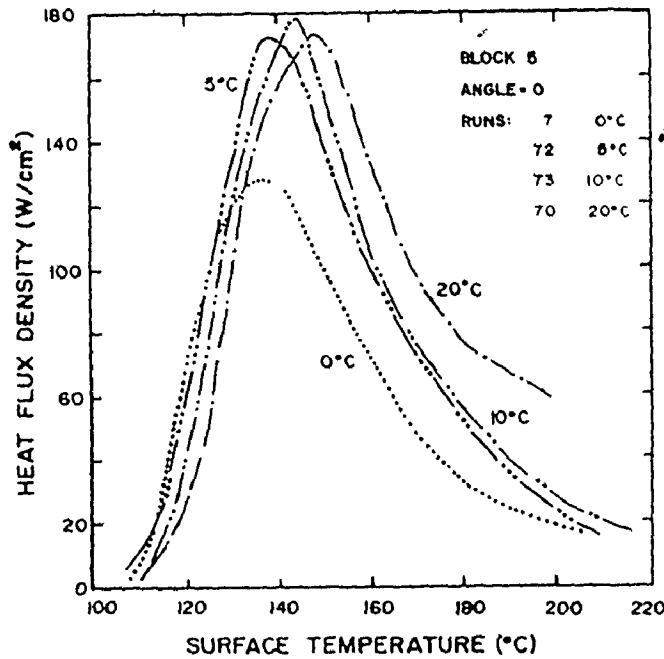
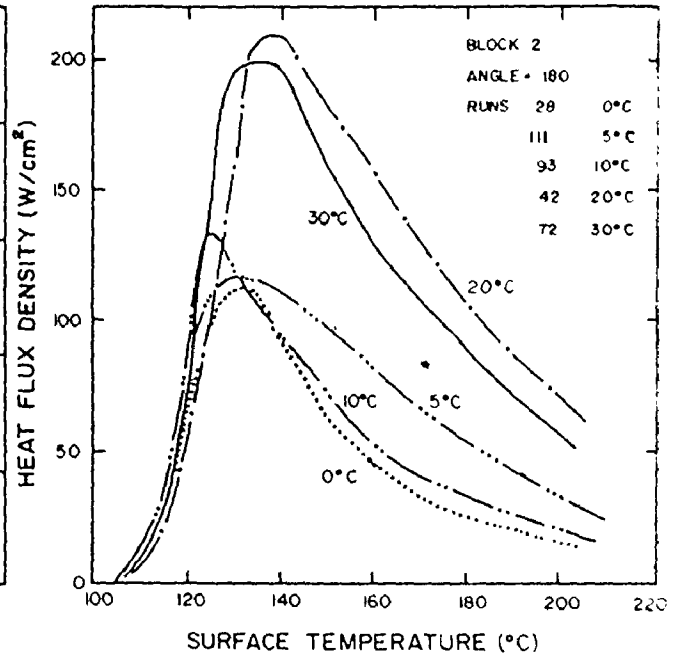
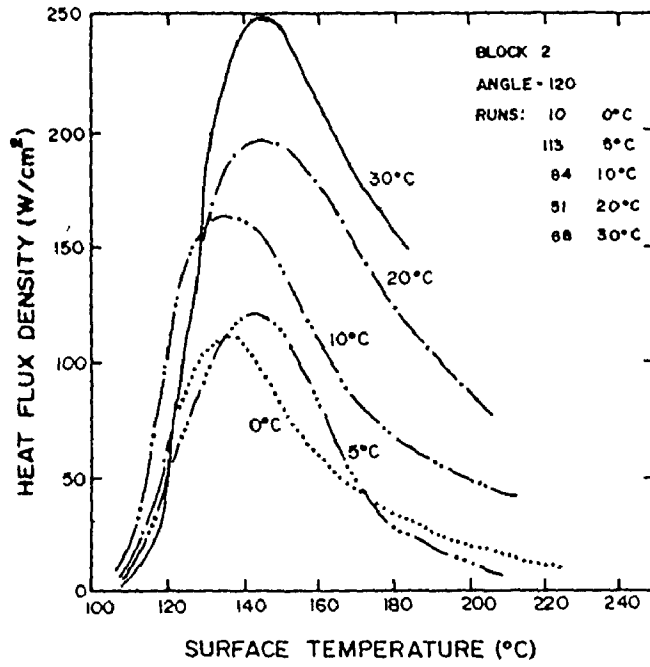


FIGURE 5.3 - TYPICAL BOILING CURVES SHOWING THE EFFECT OF SUBCOOLING.

5.2 The Critical Heat Flux Density

A great number of experiments were performed with single copper cylinders and this section will attempt to extract and explain the pertinent results obtained throughout this investigation. The complete set of data for this section is contained in Appendix C along with the calibration factors for each cylinder which was used.

5.2.1 Calibration Factor

Because of a number of factors, a calibration factor of a heat flux meter is required, as detailed in Chapter 4. In essence, this indirect procedure involves comparing the total enthalpy loss from the cylinder, over the duration of the experiment, with that obtained by integrating the apparent local heat flux density over the total heat transfer area and over the quenching time of the experiment. This procedure was briefly described in Chapter 4. The set of equations used in this procedure is derived in Appendix H; this appendix also indicates a sensitivity analysis of the effect of errors in the measurement of the initial temperature offset (zero reading adjustment) on the calibration factor. It is shown that the calibration factor is very sensitive to the choice of the offset used to zero the base line of the temperature difference curve and this effect can significantly affect the calibrated critical heat flux densities. In fact, most of the variation in the absolute values of the critical heat flux densities from one cylinder to the next can be attributed to this source of error. On the other hand, this same analysis shows that the uncalibrated

data is insensitive to the accuracy of the offset measurement. Therefore, the results are presented as a ratio of critical heat flux densities. This procedure should provide a more accurate indication of the trends which were observed for subcooling since it removes the main source of error, which is the uncertainty associated with the baseline offset and the attendant effect on the calibration factor. The critical heat flux density obtained under saturated conditions with the cylinder being uninsulated was chosen to be the reference point. This procedure allows a better comparison of similar tests on different cylinders. The problem of providing an accurate value for the reference critical heat flux density still remains. However, an average value of the sixteen sets of critical heat fluxes obtained under saturated conditions on a 7.62 cm long cylinder must surely provide a good estimate of the reference CHF. Moreover, the results obtained with the steady-state calibration (Appendix J) and the boiling curve prediction (Appendix K) suggest that the critical heat fluxes obtained through the unsteady-state calibration procedure are reasonable.

5.2.2 Critical Heat Flux Density Under Saturated Conditions

Since each of the heat flux meters in each of the cylinders was required to be calibrated and its performance characterized before it was inserted in the central column of the array, considerable information was accumulated concerning the boiling phenomena around single cylinders. In all, in excess of 1000 successful quenching experiments were performed. This allows the reproducibility of the experimental system to be evaluated as well as providing very good estimates of the

distribution of heat flux density around a large diameter horizontal cylinder under saturated and subcooled conditions.

All the information on the local values of the critical heat flux density as a function of angle for boiling under saturated conditions around a 7.62 cm cylinder is summarized in Table 5.1. In most cases, the reported values are the average for two or more separate experiments. Apart from the behaviour of a few cylinders, the values of the local critical heat flux density at any angle are remarkably close to the average of the local values at the point in question for all cylinders, even though, the calibration factors show wide variation from cylinder to cylinder.

5.2.3 Effect of Length of Cylinder

Since the object of this experimental investigation was to provide information on the boiling phenomena around very long cylinders, it was important to determine if the observed boiling heat flux densities were affected in any way by the use of relatively short copper cylinders. It must be remembered that the short length was required in studying the boiling phenomena in an array of cylinders under subcooled conditions. In that experiment, if long cylinders were used, the sub-cooling would change significantly during the quenching time unless an unreasonably large volume of water was used. The effect of length was nevertheless investigated using three different cylinders which were twice the length of the usual test cylinder. The critical heat flux results from these experiments indicated an average CHF value of about 20% higher than for the short one. The full results are shown in

TABLE 5.1

PITEL HEAT CONDUCT

UNDER SATURATED CONDITIONS (U/cm²)

7.62 CM (3 IN) VENTS

WALL	T ₁ T ₂	BLOCK 4		BLOCK 8		BLOCK 9		BLOCK 11		BLOCK 12		BLOCK 13		BLOCK 14		BLOCK 15		BLOCK 16		BLOCK 17		AVERAGE
		INSIDE	OUTSIDE	INSIDE	OUTSIDE	INSIDE	OUTSIDE	INSIDE	OUTSIDE	INSIDE	OUTSIDE	INSIDE	OUTSIDE	INSIDE	OUTSIDE	INSIDE	OUTSIDE	INSIDE	OUTSIDE	INSIDE	OUTSIDE	
0	121.1	122.2	146.9	143.5	139.4	116.4	136.4	156.2	115.1	150.1	151.4	143.0	108.6	151.2	115.1	135.2	139.1					139.1
30	113.3	125.8	146.0	149.5	126.4	91.2	85.1	92.4	117.2	86.8	83.2	146.9	88.1	109.1	111.6	111.6	111.6	111.6	111.6	111.6	111.6	111.6
60	107.8	113.5	143.1	146.6	116.3	110.3	100.2	121.8	82.1	107.1	121.6	122.4	93.9	110.4	129.9	102.4	112.8					112.8
90	97.1	106.9	109.2	132.4	129.1	103.4	110.1	120.1	88.1	126.3	111.1	118.4	95.0	141.8	147.3	111.5	113.2					113.2
120	105.1	96.0	121.5	130.4	106.2	119.0	116.5	118.4	97.4	122.5	119.3	116.3	99.3	131.4	141.5	119.9	115.1					115.1
150	81.1	91.2	131.1	110.1	115.5	92.8	116.3	112.4	72.3	130.1	127.3	125.1	102.1	145.6	153.1	108.2	112.1					112.1
180	94	107.2	93.0	106.0	116.9	85.9	91.1	91.2	83.1	127.4	127.5	123.9	92.6	125.5	129.0	110.4	125.9					125.9
OVER.	99.5	99.9	110.1	109.4	117.3	103.1	105.2	113.3	88.5	118.1	117.2	117.8	96.5	133.6	135.0	106.5	110.7					110.7
U.F.	526	705	1242	1786	1008	779	613	1246	528	736	704	664	1353	871	706	532						

11.43 CM (4.5 IN) VENTS

WALL	T ₁ T ₂	BLOCK 15 (INSIDE)	BLOCK 15 (OUT)	AVERAGE
0	132.0	146.1	155.2	144.9
30	124.6	81.5	75.0	81.1
60	116.0	111.2	99.4	108.9
90	109.4	113.5	123.5	109.8
120	104.9	129.8	126.3	121.0
150	111.4	125.0	115.2	113.1
180	107.5	111.4	110.3	109.4
OVER.	112.7	115.7	112.4	113.6

15.24 CM (6 IN) VENTS

WALL	BLOCK 17	BLOCK 18	BLOCK 15	AVERAGE
0	141.6	139.4	147.4	143.0
30	77.8	121.4	112.9	97.4
60	139.4	130.6	133.8	122.1
90	122.2	137.6	141.1	135.3
120	143.0	154.9	126.7	143.5
150	136.0	155.0	136.2	143.1
180	125.5	111.1	111.3	112.7
OVER.	122.3	141.9	134.1	132.8

Table 5.1.

Some other experiments were also performed to discriminate among any other confounding effects:

- (i) By conducting the quenching experiment in a larger test tank, it was determined that this increase in CHF did not result from fluid mechanical effects arising because of cylinder-to-tank dimensions (Cylinder 8, runs 28 to 32).
- (ii) A possible cause of this effect may be that the insulating transite end pieces, which protrude about 0.6 cm above the copper cylinder, may impede the liquid-vapour flow over the central active 6.35 cm length. Two tests were conducted with the 15.24 cm cylinder (Cylinder 15). One test involved insulating the outer extremities of the cylindrical surface with 0.25 mm thick teflon sheet; this left a central active length of 10.16 cm for one test condition and a 6.35 cm length for the other (Runs 20 to 42 and 47 to 62 respectively). Since the same heat flux meter was used in these experiments, a direct comparison is possible and the confounding effect of different calibration factors is removed. Table 5.1 summarizes the CHF results of Cylinder 15 and it can be seen that the results for the 6.35 cm length, although slightly higher, are still within the observed variation from cylinder to cylinder of the smaller length. The results for the cylinder of intermediate length are the same as for the smallest length. As a further test of the experimental apparatus, the effect of the protuberance of the transite end pieces was investigated by placing two separate transite rings, of the same height as the end pieces, around the teflon insulated, 15.24 cm cylinder for the two active lengths

investigated (Runs 43 to 46 and 63 to 67 respectively). Since essentially no change in CHF was observed, it may be concluded that the transite end pieces do not inhibit or affect the liquid-vapour around the cylinder.

(iii) To further test the length effect, the two long cylinders were cut to 11.43 cm and then, after testing, to 7.62 cm lengths and quenching experiments under saturated conditions were performed with them (active boiling lengths of 10.16 cm and 6.35 cm respectively). The results are presented in Table 5.1. Again the CHF values are essentially the same as for the other cylinders with these active lengths.

It can be concluded therefore that the critical heat flux density for the longest cylinder is approximately 20% higher than that for the shorter ones. This effect is unexplained, but may be related to the increased natural convective flow generated by the longer cylinder (greater total fluid flow movement in the tank giving rise to a greater convective effect). In addition, it is possible that a situation similar to the results on flat plates discussed by Lienhard(L4) prevails; in this case, the length of the cylinder would greatly influenced the number of escaping vapour jets that the cylinder can accomodate and in turn the critical heat flux value. The effect of thermal capacity or rate of cooling and axial temperature gradients within the cylinder must be ruled out because of the observations made with the partially insulated cylinder.

It was, however, experimentally impractical to use a 15.24 cm long cylinder in the bundle since these cylinders take substantially longer to heat up and would have such a high thermal capacity that the

water under subcooled conditions would have its temperature raised substantially.

5.2.4 Angular Variation of Critical Heat Flux Density

The twelve holes which were uniformly distributed on the transite end plates permitted tests to be performed with the heat flux meter located at seven different angles. Usually two runs were made with the heat flux meter located at a particular angle and then it was changed randomly to cover all the circumference. The results are contained in Appendix C and summarized in Tables 5.1 and 5.2 for saturation and subcooled conditions respectively. The results summarized in these two tables do show a definite variation of CHF around the cylinder which has heretofore not been reported. Figure 5.4 was drawn to illustrate this variation in CHF relative to the average CHF for the cylinder for the five subcooled conditions investigated. The angular variation of CHF for saturation and subcooled conditions will be discussed in turn.

Saturation Condition

As depicted in Figure 5.4, the critical heat flux at saturation boiling shows a variation with angular position with the maximum occurring at the top of the cylinder (0°) and the minimum occurring at an angle of 30° from the top of the cylinder. Although the CHF at the top is usually more than 50% greater than that at 30° , the CHF at other angles, although somewhat lower than that at the top, is approximately the same and roughly equal to the overall average CHF. Under saturated conditions this observed phenomena is similar for all cylinders (except

TABLE 5.2
 CRITICAL HEAT FLUX DENSITIES
 UNDER SUBCOOLED CONDITIONS (W/CM^2)
 (7.62 CM LONG CYLINDERS)

<u>5°C SUBCOOLING</u>				<u>10°C SUBCOOLING</u>			
<u>ANGLE</u>	<u>BLOCK 2</u>	<u>BLOCK 5</u>	<u>AVERAGE</u>	<u>ANGLE</u>	<u>BLOCK 2</u>	<u>BLOCK 5</u>	<u>AVERAGE</u>
0	129.0	166.4	147.7	0	167.0	169.9	168.5
30	95.6	94.3	95.0	30	139.0	154.4	146.7
60	116.8	126.9	121.8	60	117.3	154.4	135.9
90	126.9	120.6	123.8	90	139.7	146.6	143.1
120	110.0	117.7	113.8	120	145.9	131.8	138.9
150	136.3	117.0	126.7	150	153.0	111.4	132.2
180	115.5	114.9	115.2	180	124.6	127.9	126.1
AVER.	116.0	119.6	116.8	AVER.	140.1	141.2	140.6
	(18.6%) ^a	(19.7%)	(19.2%)		(40.8%)	(41.4%)	(41.1%)

<u>20°C SUBCOOLING</u>						<u>40°C SUBCOOLING</u>			
<u>ANGLE</u>	<u>BLOCK 2</u>	<u>BLOCK 5</u>	<u>BLOCK 8</u>	<u>BLOCK 15</u>	<u>AVERAGE</u>	<u>ANGLE</u>	<u>BLOCK 2</u>	<u>BLOCK 22</u>	<u>AVERAGE</u>
0	176.5	160.5	108.3	194.0	161.8	0	—	295.4	295.4
30	193.9	155.5	213.3	210.2	193.2	30	—	311.5	311.5
60	162.4	177.7	196.1	206.8	191.3	60	—	324.1	324.1
90	166.5	192.5	213.6	197.9	197.6	90	—	242.5	242.5
120	172.4	160.7	166.9	219.5	165.4	120	223.1	292.6	257.8
150	196.5	191.8	196.7	239.9	206.2	150	—	278.7	278.7
180	204.8	187.5	172.6	202.3	191.8	180	205.7	253.1	229.7
AVER.	187.1	176.0	191.5	212.4	191.8	AVER.	217.3	287.3	279.4
	(88.7%)	(76.2%)	(75.1%)	(81.7%)	(80.7%)		(118.4%)	(115.7%)	(115.0%)

^a As suggested in Section 5.2.1, the % increase in Q_{cr} due to subcooling is compared with the results obtained with the same block at saturation.

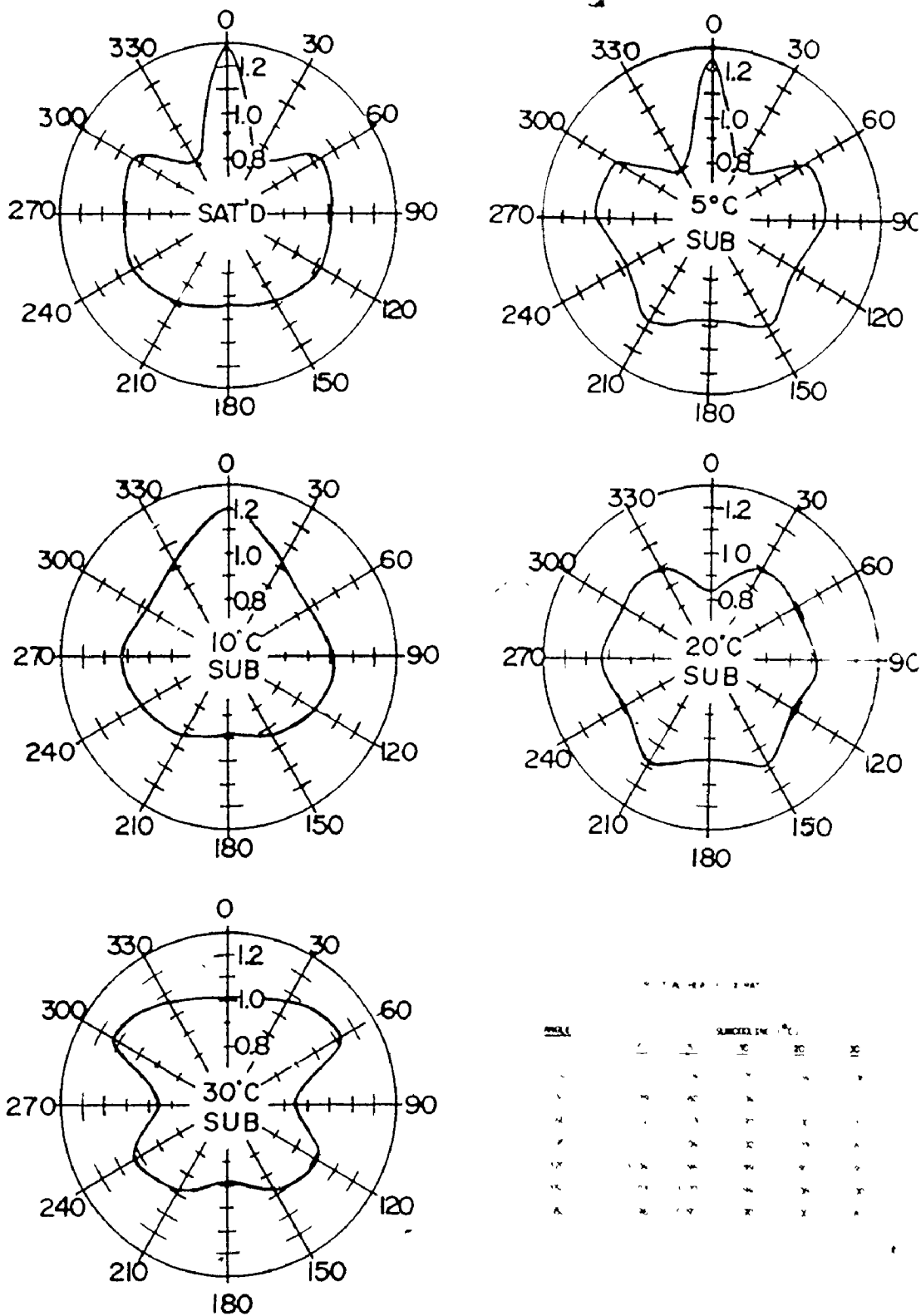


FIGURE 5.4 - VARIATION OF LOCAL CHF AROUND A CYLINDER FOR DIFFERENT SUBCOOLING.

for cylinder 14 which seems to be anomalous); furthermore, as shown in Table 5.1, it is independent of the length of the cylinder.

It was suspected that this variation around the cylinder resulted from the variation in the time at which the local surface temperature went through the critical heat flux. If the critical heat flux occurred first at the top and then at other points around the cylinder, the cooling effect could be transmitted to other parts of the cylinder and, consequently, the local temperature, at say 30° , would pass through the critical heat flux too quickly to allow the local surface temperature to remain at a high value for the required time to establish the conditions appropriate for boiling conditions at the critical heat flux. The following points are presented to show that this hypothesis cannot be substantiated:

- (i) A graphical representation of the total boiling curve for this point shows continuity in the data points near the CHF.
- (ii) Many experiments were performed with a cylinder (Cylinder 6) equipped with five heat flux meters and in all cases the critical heat flux occurred essentially at the same time for all points. (Results for Cylinder 6 are not presented here because, during the recording of data by the computer, there was interaction amongst heat flux meters which were located on the same cylinder. It was possible nevertheless to determine the time at which each CHF occurred).
- (iii) High-speed motion pictures (ca. 1000 frames/sec.) were taken of the vapour flow occurring over the entire cylinder during quenching. This involved photographing a cylinder in the direction of the flat face with a Fastax camera, the ends of the cylinder being insulated

with high temperature RTV silicone adhesive. These pictures suggest that the pulsating upflowing vapour separated in an intermittent fashion at about 30° . Hence it seems reasonable to assume that the minimum value arose from external hydrodynamic effects rather than the internal conduction effects.

(iv) When the cylinder was partially insulated (as will be described later) so that the active heat transfer area was subtended by an angle of 60° (or less) from the centre, the heat flux density at 30° was higher than that measured for the uninsulated cylinder, although the area at the top of the cylinder was participating in the boiling phenomena. That is, to say, that when the point at 30° is not influenced by the vapour flow from below, the critical heat flux density is essentially the same as for other points on the cylinder.

(v) Under subcooled conditions, where the vapour generation is suppressed, a minimum in CHF did not occur, although the critical heat flux density at the top was even higher than that observed under saturated conditions.

It can be concluded, therefore, that the variation in CHF around the cylinder is directly related to the fluid mechanical behaviour of the liquid-vapour around the cylinder. In fact Figure 5.2 shows that the boiling curve at 30° is considerably lower than the others not only at the CHF but also in the transition regime; the effect disappears in the nucleate boiling regime. The maximum effect though, is at the CHF at which point the greatest amount of upward vapour flow occurs.

Subcooled Conditions

The wide variation in local CHF around the cylinder with different subcoolings was not expected. The maximum occurred at the top for subcooling from 0 to 10°C; the minimum at 30° angle for saturated boiling disappeared when the liquid was subcooled 10°C or more. As subcooling was increased, the maximum at the top disappeared. As already noted, high speed motion pictures revealed intermittent separation of the upflowing vapour-liquid boundary layer at the 30° location for saturated boiling. It is probable that, under these conditions, the upflowing fluids enhanced the critical heat flux at the top. Motion picture studies under subcooled conditions did not reveal any obvious fluid mechanical effect since the vapour bubbles collapsed in the near vicinity of the wall and hence did not provide flow visualization of the upward liquid flow. No doubt the local subcooling decreases as the upward flowing liquid proceeds around the cylinder. This and other interactive effects of the natural convective flow and the forming and collapsing of vapour bubbles should play a primary role in affecting local CHF. These phenomena would probably be revealed using interferometric photographic techniques.

However, the variation of CHF with angle is much less pronounced at subcooling greater than 10°C, thus, tending to reinforce the belief that the variation results from the bulk vapour flow, since it is almost absent at these subcoolings.

5.2.5 Effect of Subcooling

Subcooled boiling is an important aspect in the safety analysis of CANDU nuclear reactors because the heavy water contained in the calandria is maintained at a high degree of subcooling. Therefore it is necessary to establish the boiling curve to be expected on a calandria tube surrounded by a subcooled liquid.

Five different temperatures of the quenching bath were used: 100°C, 95°C, 90°C, 80°C and 70°C. The complete data are contained in Appendix C and summarized in Tables 5.1 and 5.2. The effect of subcooling on the whole boiling curve and on the angular variation of the critical heat flux density has already been considered. In this section, we consider the average heat flux density for the entire cylinder, that is the integrated average value. The percentage increase of this average value with degree of subcooling is also indicated in Table 5.2 for each cylinder.

The important points to be noted are:

- (i) As expected, substantial increases in CHF occur as the level of subcooling increases. As shown in Table 5.3, the percentage increase is predicted quite well by the equation presented by Ponter and Haigh(P5), (Equation 2.12). This equation was based on boiling water on a 5.8 mm stainless steel tube; Ponter and Haigh reported a standard deviation of about 0.1. Note that the level of subcooling was corrected to include the enthalpy addition to the water from the cylinder up to the time when CHF occurred. This level of subcooling is about 90% of the initial subcooling (see Appendix L). This correction is believed

TABLE 5.3

INFLUENCE OF SUBCOOLING ON CRITICAL HEAT FLUX DENSITY

SUBCOOLING		$(q/A)_{SUB,CRIT}/(q/A)_{SAT,CRIT} \times 100$				
INITIAL (°C)	AT CHF (°C)	EXPERIMENTAL (%)	EQ. 2-7 (%)	EQ. 2-8 (%)	EQ. 2-9 (%)	EQ. 2-12 (%)
5	4.5	19.2	21.3	30.5	23.1	21.5
10	9.0	41.1	42.5	61.1	47.0	41.8
20	18.0	80.2	85.1	127.1	91.9	81.7
30	27.0	116.8	127.7	183.2	140.9	121.8

TABLE 5.4

SUMMARY OF EQUATIONS USED IN TABLE 5.3

AUTHOR	EQUATION NUMBER	$(q/A)_{SUB,CRIT}/(q/A)_{SAT,CRIT} =$
Ivey and Morris	2.7	$1 + 0.0473 \Delta T_{sub}$
Kutateladze	2.8	$1 + 0.0678 \Delta T_{sub}$
Zuber et al.	2.9	$1 + 0.0522 \Delta T_{sub}$
Ponter and Haight	2.12	$1.014 + 0.04458 \Delta T_{sub}$
Present Work	5.1	$1.076 + 0.04363 \Delta T_{sub}$

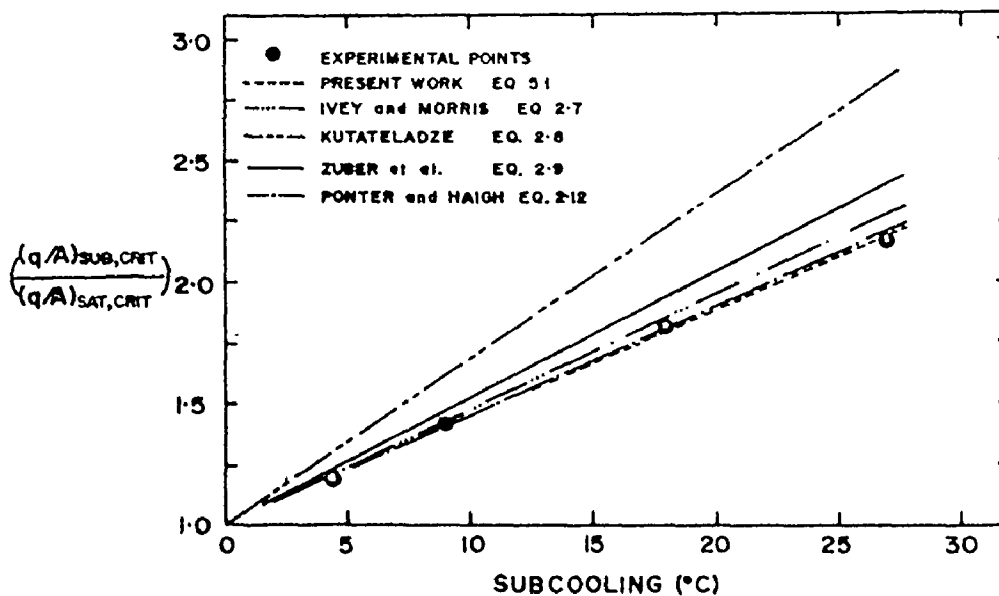


FIGURE 5.5 - INFLUENCE OF SUBCOOLING ON CHF

to be on the conservative side. The results are close to those predicted by the correlations contained in the references shown in Table 5.3 and Figure 5.5. Table 5.4 summarizes the equations used to compare the experimental data obtained in this study. The physical properties contained in Appendix A were used throughout.

A linear least squares fit of the experimental data produced the following equation:

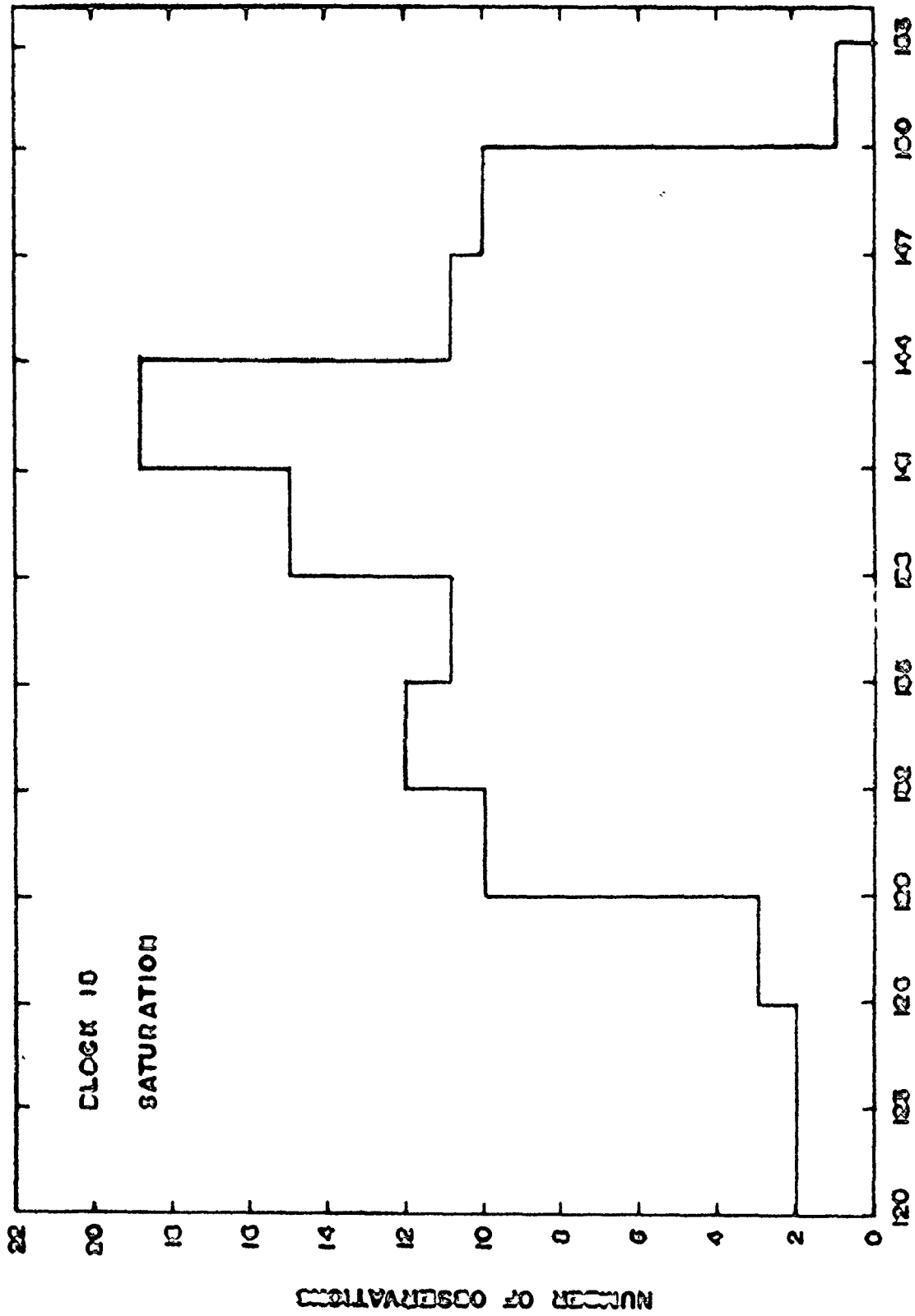
$$\frac{(q/A)_{c,sub}}{(q/A)_{c,sat}} = 1.0 + 0.0437 \Delta T_{sub} \quad (51)$$

with a standard deviation of .03.

5.2.6 Surface Temperature at the Critical Heat Flux

It is of interest to look at the surface temperature at which the critical heat flux density occurred for each quenching experiment and construct a histogram to indicate the extent of the variation in this temperature. The probability density function plot for one copper cylinder is shown in Figure 5.6. It will be noted that there was considerable variation. This is to be expected, however, for the following reasons:

- (i) The temperature at which the critical heat flux occurs is known to be a function of condition of the surface and the state of oxidation of surface. Although the cylinders undergo the same surface treatment prior to each experiment (rubbed lightly in the circumferential direction with 4/0 emery paper to remove any oxidation products), there is



WALL TEMPERATURE AT CMF (°C)
 FIGURE 5.0 - HISTOGRAM OF WALL TEMPERATURE AT CMF

TABLE 5.5

PROBABILITY DENSITY FUNCTION OF THE
TEMPERATURE AT CRITICAL HEAT FLUX (°C)

BLOCK NUMBER	CODE NUMBER*	SUBCOOLING (°C)	ANGULAR LOCATION						OVERALL			
			0°	30°	60°	90°	120°	150°	180°	TEMP.	STD. DEV.	NO. OBS.
2	0	0	126.9	125.4	124.1	133.0	129.0	126.6	121.9	127.2	6.7	50
2	0	5	141.5	126.8	141.7	111.4	137.5	134.0	138.9	135.3	9.1	21
2	0	10	141.7	138.9	125.6	139.5	137.0	141.9	125.0	136.3	10.0	18
2	0	20	142.5	145.9	144.5	145.0	144.5	135.0	139.5	142.6	5.7	14
2	0	30	—	—	—	—	140.6	—	131.7	137.5	11.5	4
5	0	0	138.1	122.9	137.6	134.7	132.9	139.2	131.4	133.6	6.7	25
5	0	0	139.9	129.6	139.4	142.5	133.4	134.0	147.0	137.1	7.1	14
5	0	5	136.9	137.8	136.6	137.5	139.5	138.3	149.6	138.8	7.8	9
5	0	10	144.4	135.1	135.1	140.2	145.8	137.4	136.1	138.8	4.9	10
5	0	20	148.4	156.8	150.9	151.9	151.3	151.4	144.9	151.5	5.5	9
7	3	0	146.1	130.9	138.4	143.2	141.1	140.6	134.8	139.0	6.1	27
8	3	0	134.6	127.6	128.9	137.6	133.5	136.5	131.0	132.5	5.8	26
8	6	0	136.6	133.3	137.2	138.8	135.9	138.9	130.9	136.3	5.5	11
8	0	0	136.6	132.7	126.7	138.0	131.7	138.3	131.8	133.6	7.1	18
8	0	20	133.3	144.6	156.5	152.3	141.7	150.7	141.8	147.2	8.3	15
9	0	0	166.4	151.2	161.3	162.8	159.1	155.0	157.0	158.5	5.4	25
11	0	0	156.1	143.8	147.3	147.3	150.8	145.9	141.7	147.3	5.3	15
12	0	0	121.1	128.4	127.2	121.0	127.8	123.4	119.5	124.7	5.0	19
13	0	0	119.5	122.8	123.4	127.4	122.3	130.5	124.9	124.8	4.5	25
14	0	0	115.9	113.6	115.8	116.3	114.7	133.9	118.4	118.5	6.1	24
15	3	0	138.1	128.0	136.5	127.3	133.5	135.7	137.9	137.0	8.7	16
15	4	0	140.4	134.4	141.1	139.7	137.1	138.7	144.1	138.0	7.7	17
15	5	0	139.6	134.8	140.0	136.7	134.4	140.4	137.8	137.5	5.1	17
15	6	0	144.8	137.5	141.0	142.9	144.5	139.5	147.0	141.9	5.1	17
15	0	0	143.1	131.1	134.1	146.5	142.2	132.1	140.0	138.1	7.7	17
15	0	20	144.2	146.5	152.5	155.1	153.4	150.6	148.1	150.7	5.3	17
17	0	0	138.9	147.8	144.5	139.7	138.7	131.3	145.4	140.6	5.6	14
20	0	0	130.4	127.9	128.3	132.6	131.4	132.9	130.0	130.9	3.9	17
22	0	0	149.7	140.0	141.5	146.2	146.6	146.2	149.8	145.0	5.0	21
22	0	30	170.2	181.1	184.9	179.1	179.3	170.5	173.4	177.6	7.4	15
23	0	0	145.8	135.6	146.0	146.9	147.7	145.1	140.4	144.1	6.7	20
23	0	0	128.3	127.9	145.0	127.7	127.1	139.1	134.1	133.0	11.0	7

*Code numbers are given in Appendix C

*Side number 2 of the heat flux meter.

TABLE 5.6

DIFFERENCE BETWEEN TEMPERATURE AT WHICH THE
CRITICAL HEAT FLUX OCCURS FOR A GIVEN CYLINDER
UNDER SATURATED AND SUBCOOLED CONDITIONS

SUBCOOLING (°C)	CYLINDER	TEMPERATURE DIFFERENCE (°C)	AVERAGE (°C)
5	2	8.1	6.6
	5	5.2	
10	2	9.1	7.2
	5	5.2	
20	2	15.4	14.9
	5	17.9	
	8	13.1	
	15	13.2	
30	22	32.6	32.6

no doubt that some variation existed in both the surface finish and the oxidation state from experiment to experiment.

(ii) There was a difficulty in determining the exact temperature at which the critical heat flux occurred since there was considerable fluctuation in temperature and heat flux before and during the critical heat flux. Moreover, the heat flux density versus temperature plot did not exhibit a sharp maximum. In fact, the surface temperature was chosen as the one which occurred at experimentally measured maximum heat flux density (as determined by a search conducted by the computer); hence it was not obtained from a smoothed boiling curve. Consequently, this temperature may exhibit a wider variation than might have actually occurred because the fluctuation in heat flux may have given rise to a false maximum.

(iii) As suggested by Figure 5.2, the boiling curve at 30° angle under saturated conditions showed a very low heat flux density in the transition regime and the CHF at this location usually occurred at an abnormally low temperature (temperatures where other parts of the cylinder were exhibiting nucleate boiling). Table 5.5 indicates this low temperature tendency for most of the copper cylinders investigated. Therefore the low temperature data in Figure 5.6 arise mainly from this source.

The mean surface temperature at CHF and its standard deviation for each cylinder are also reported in Table 5.5. It is noted that the variation from cylinder to cylinder is fairly high although the standard deviations are consistent from cylinder to cylinder. At least some of this variation can be explained by the effects discussed in Appendix E, namely the actual location of any particular edge thermocouple and what

temperature was actually recorded by it. Apart from the low temperature at 30° angle under saturation conditions, there does not seem to be any other effect of angle on the mean temperature at which CHF occurs.

The wall temperature when the critical heat flux occurred under subcooled conditions can be obtained in a similar way from each experiment. Table 5.6 reports the results of this analysis as the increase in this average temperature as the degree of subcooling was increased. These results show a direct comparison of the increase in average wall temperature, at CHF conditions, for each cylinder as the level of subcooling was increased. Four separate subcooled values (four different cylinders) are available for 20°C subcooling and each value shows an approximate increase of about 15°C .

5.2.7 Effect of Partially Insulating the Cylindrical Surface

In the postulated accident sequences in a nuclear reactor only part of the calandria tube periphery may be in active boiling. Therefore, to assess this effect of only a partially active surface, a part of the test cylinder was insulated with a thin teflon sheet, 0.05 mm thick. The teflon sheet was glued onto the surface to leave a bare area over the length of the cylinder and subtended by an azimuthal angle of 30° or 60° ($1/12$ or $1/6$ of total area, respectively).

Experiments were performed with these partially insulated

cylinders to investigate the effect of subcooling. The complete set of data is presented in Appendix C. Tables 5.7 and 5.8 summarize all the results obtained with these experiments for a 60° and 30° subtended angle respectively. These tables express the average percentage increase in the critical heat flux for the partially insulated cylinder over that observed for the bare one. The most important observations are noted as follows:

(a) Under Saturated Conditions

The critical heat flux was essentially the same for the partially insulated as for the bare cylinder except at the 30° and 90° angular locations. The largest increase occurred at 30° where the average increase was about 45 to 50%; very little difference was observed between the two cylinders which had different fractions of their areas insulated. As indicated earlier, this effect has been attributed to the hydrodynamic effect of the vapour-liquid flow around the cylinder. High-speed motion pictures showed periodic detachment of the upward flowing vapour layer at about an angle of 30° . When the surface was partially insulated, this large vapour flow did not exist and the boiling phenomena was therefore more like any other position on the cylinder. This observation suggests that the periodic detachment of the vapour layer and the associated liquid-vapour movement affected the vapour packing on the surface or the liquid movement to the surface and hence caused a lower critical heat flux.

The relatively large increase in heat flux at the 90° location is thought to be similarly caused by the different (smaller) vapour flow

TABLE 5

AVERAGE % INCREASE OF TAIL WEIGHT IN X
WITH 10° ACTIVE MILLING AREA

SATURATION			20° SUBMITTING				20° SUBMITTING		
ANGLE	BLOOD 1	BLOOD 5	AVERAGE	BLOOD 2	BLOOD 4	BLOOD 8	BLOOD 16	AVERAGE	BLOOD 1
30	+38.7	+44.0	+41.4	+24.6	+26.4	+28.8 ^a	+31.8	+31.4	+29.4
60	—	+31.1	+22.8	—	+19.6	+21.8	+24.6	+22.0	+21.4
90	+46.7	+39.1	+42.9	+28.8	+24.1	+27.3	+31.6	+28.2	+27.8
120	—	—	+10.1	—	—	+17.3	+20.8	+19.0	+18.4
150	—	+7.5	+12.6	—	+11.5	+14.8	+17.8	+16.0	+15.4
180	+12.0	+9.9	+10.9	+11.1	+11.1	+12.1	+13.1	+12.1	+11.1
AVER.	+17.5	+20.9	+19.6	+24.6	+24.6	+27.8	+31.6	+28.2	+27.8

10° SUBMITTING			20° SUBMITTING				20° SUBMITTING		
ANGLE	BLOOD 2	BLOOD 4	AVERAGE	BLOOD 2	BLOOD 4	BLOOD 8	BLOOD 16	AVERAGE	BLOOD 1
30	+10.6	+24.7	+17.4	+24.6	+26.4	+28.8 ^a	+31.8	+31.4	+29.4
60	—	+10.5	+10.5	—	+19.6	+21.8	+24.6	+22.0	+21.4
90	+37.9	+19.2	+28.5	+28.8	+24.1	+27.3	+31.6	+28.2	+27.8
120	—	—	—	—	—	+17.3	+20.8	+19.0	+18.4
150	—	+42.1	+42.1	—	+11.5	+14.8	+17.8	+16.0	+15.4
180	+26.2	+26.9	+26.5	+11.1	+11.1	+12.1	+13.1	+12.1	+11.1
AVER.	+17.0	+21.9	+20.3	+24.6	+24.6	+27.8	+31.6	+28.2	+27.8

^aThis number was not considered in the average.

TABLE 6

AVERAGE % INCREASE OF TAIL WEIGHT IN X
WITH 10° ACTIVE MILLING AREA

SATURATION			20° SUBMITTING				
ANGLE	BLOOD 8	BLOOD 15	AVERAGE	ANGLE	BLOOD 1	BLOOD 15	AVERAGE
30	+16.5	+11.4	+14.0	30	+15.8 ^a	+15.1	+15.4
60	+41.8	+41.4	+41.6	60	+19.2	+21.8	+20.5
90	+32.4	+30.1	+31.2	90	+43.5	+41.1	+42.3
120	+14.1	+26.5	+20.3	120	+15.2	+19.8	+17.5
150	+11.6	+11.6	+11.6	150	+19.4	+24.0	+21.7
180	+18.3	+2.0	+10.5	180	+23.7	+11.1	+17.4
190	+1.0	+1.5	+1.2	190	+19.3	+1.2	+10.2
AVER.	+20.5	+15.6	+18.1	AVER.	+21.1	+20.0	+20.5

^aThis number is not used to calculate the average % increase.

at that location with the partially-insulated cylinder. High-speed motion pictures again revealed some vapour detachment at this point when the whole cylinder was active.

(b) Under Subcooled Conditions

Under subcooled conditions the critical heat flux at the top of the cylinder was less for the partially insulated cylinder. When the whole cylinder actively participates in the boiling process under subcooled conditions, a considerable natural convective flow of liquid from bottom to top develops. When the cylinder is partially insulated, this flow will not be nearly as large. Consequently, the heat flux is expected to be less for this latter case.

It is interesting to note that the limited data for the 60° (subtended angle) active boiling area, the percentage increase in the average CHF does not seem to be a function of subcooling, being about 10% for all conditions. On the other hand, decreasing the active area produced a more substantial increase in the overall average CHF.

It is further noted that the critical heat flux at the bottom of the cylinder was observed to be essentially the same for the bare and the partially insulated cylinders. Boiling behaviour at this location is probably the most important relative to the practical problem of a postulated accident.

In summary, the critical heat flux at any point on a cylinder, whose surface is partially insulated, is never less on the active boiling area than that which would be observed for a cylinder undergoing boiling over the entire area. At some angular locations, the heat flux

density is considerably higher for the partially insulated cylinder. The lower CHF observed at some locations on the bare fully active surface is attributable to the interaction of the upflowing vapour with the boiling phenomena.

5.2.8 Effect of Vapour Injection Underneath a Single Copper Cylinder

The data on the boiling heat flux density at local points on cylinders in a multiple-tube array (as will be discussed in Chapter 6) provide valuable information on the effect on local boiling heat transfer of vapour flowing from below and impinging on the underside of the cylinder. Although that experimental system was useful in demonstrating the effect and defining the problem, unfortunately it was very difficult to control the amount of vapour rising through the array at any instant in time. Moreover, the vapour flow changed continuously. In addition, considerable effort and time was required to do one experiment and then the information obtained during any particular experiment was only applicable to one point on any particular cylinder in the array. Once it was established that there was an increase in heat transfer rate and not a decrease, as would be expected if there was an impediment by the tubes to vapour flow (a form of vapour blanketing), it was decided to attempt to quantify this effect better and alleviate some of the other difficulties by designing a new experiment. The details of the experimental system have been presented in Chapter 3. In summary, the normal quenching of a single instrumented cylinder was carried out but in addition steam was injected continuously from a sparger at a known flowrate. The sparger-to-cylinder distance could also be varied.

The three different vapour flowrates used are shown in Table 5.12. In addition, three different sparger-to-cylinder distances were used: 6 cm, 19 cm and 32 cm. At the 19 cm distance, boiling curves at only the 180^o location were investigated for the three different steam flowrates. For the other two cylinder-to-sparger distances, boiling curves were established for every location on the cylinder with the three different steam flowrates.

Cylinders 22 and 23 were used in this set of experiments. Table 5.9 summarizes the essential results, namely the average percentage increase in CHF for the experimental conditions indicated. The complete data set is contained in Appendix C.

The results indicate that the overall, surface averaged critical heat flux from the cylinder increased relatively little (ca. 27% maximum) as the sparger-to-cylinder distance increased. It is interesting to note that this average CHF was essentially independent of steam flowrate although this flowrate increased about threefold. Obviously at each sparger distance there must be an effect of vapour velocity because an increase was observed. Unfortunately the experimental system would not allow use of lower steam velocities (because a minimum critical pressure ratio was required across the sonic orifice) to allow this threshold velocity to be determined. On the other hand, a decrease in average CHF should be observed at very high steam velocities when vapour blanketing should occur. Again the limitations of the experimental system did not allow higher steam velocities to be employed (considerable water was blown out of the tank at the highest flowrates).

The effect of sparger-to-cylinder distance was not expected.

TABLE 5.9

EFFECT OF STEAM INJECTION ON THE
DU WALL CRITICAL HEAT FLUX
(% INCREASE)

DISTANCE BETWEEN SPARGER AND CYLINDER (CM)	SONIC ORIFICE UPSTREAM PRESSURE (PSIG)		
	20	40	60
	6	10	13
19	—	—	—
32	27	21	26

TABLE 5.10

EFFECT OF STEAM INJECTION ON THE
CRITICAL HEAT FLUX AT 180° AND 150°
(% INCREASE)

DISTANCE BETWEEN SPARGER AND CYLINDER (CM)	180° SONIC ORIFICE UPSTREAM PRESSURE (PSIG)			150° SONIC ORIFICE UPSTREAM PRESSURE (PSIG)		
	20	40	60	20	40	60
	6	-1.7	32	27	-13	56
19	51	68	118	—	—	—
32	53	69	64	47	52	70

TABLE 5.11

EFFECT OF STEAM INJECTION ON THE CHF OF
A PARTIALLY INSULATED COPPER CYLINDER

BLOCK 22

Orifice Upstream Pressure = 40 psia

ANGLE	CRITICAL HEAT FLUX (W/cm ²)		% INCREASE
	NO STEAM	WITH STEAM	
0	161.2	203.5	+26.2
30	109.1	106.0	- 2.1
40	130.4	129.6	- 0.6
90	141.8	152.0	+ 7.2
120	131.4	149.8	+21.2
150	144.6	200.6	+37.8
180	125.5	212.3	+69.1
OVER.	133.6	159.4	+18.6

TABLE 5.12

VAPOUR VOLUMETRIC FLOW RATE
CORRESPONDING TO UPSTREAM PRESSURE

<u>UPSTREAM PRESSURE</u> (psig)	<u>STEAM TEMP.</u> (°K)	<u>MASS FLOW RATE</u> (g/8)	<u>FRACTION OF CHF AT SAT.</u>
100	443	39.3	3.17
60	434	25.9	2.09
40	429	19.1	1.54
20	426	12.2	.98

Certainly the steam bubbles will require time to accelerate to their terminal rise velocity. Also, the vapour will cause liquid to flow with it. The effect shown then is really an effect of the rising vapour-liquid velocity at the point when it impinges on the cylinder. This higher velocity produces a greater forced-convection effect and probably increased turbulence in the boundary layer surrounding the cylinder.

At the same time, this forced convection effect was observed to change the distribution of heat flux around the cylinder. Figure 5.7 shows the polar plot, for some of the experiments, of the percentage change in local CHF resulting from steam injection under the cylinder*. In general, it was observed that the local critical heat fluxes over the lower portion of the cylinder (where the upflowing vapour first impinges) are much higher than over the rest of the cylinder. To illustrate this effect two boiling curves, one with and the other without steam injection, (at 180° location) are presented in Figure 5.8. This is important in the practical situation envisaged for if a loss-of-coolant accident should occur, the pressure tubes in a CANDU nuclear reactor would probably sag under the weight of the fuel bundles and then contact the calandria tube at the bottom.

* It must be noted that the variance in the CHF was much greater for the experiments with vapour flow. Part of this can be attributed to the phenomena occurring and part to the fact that only one or two experiments were performed at each angle.

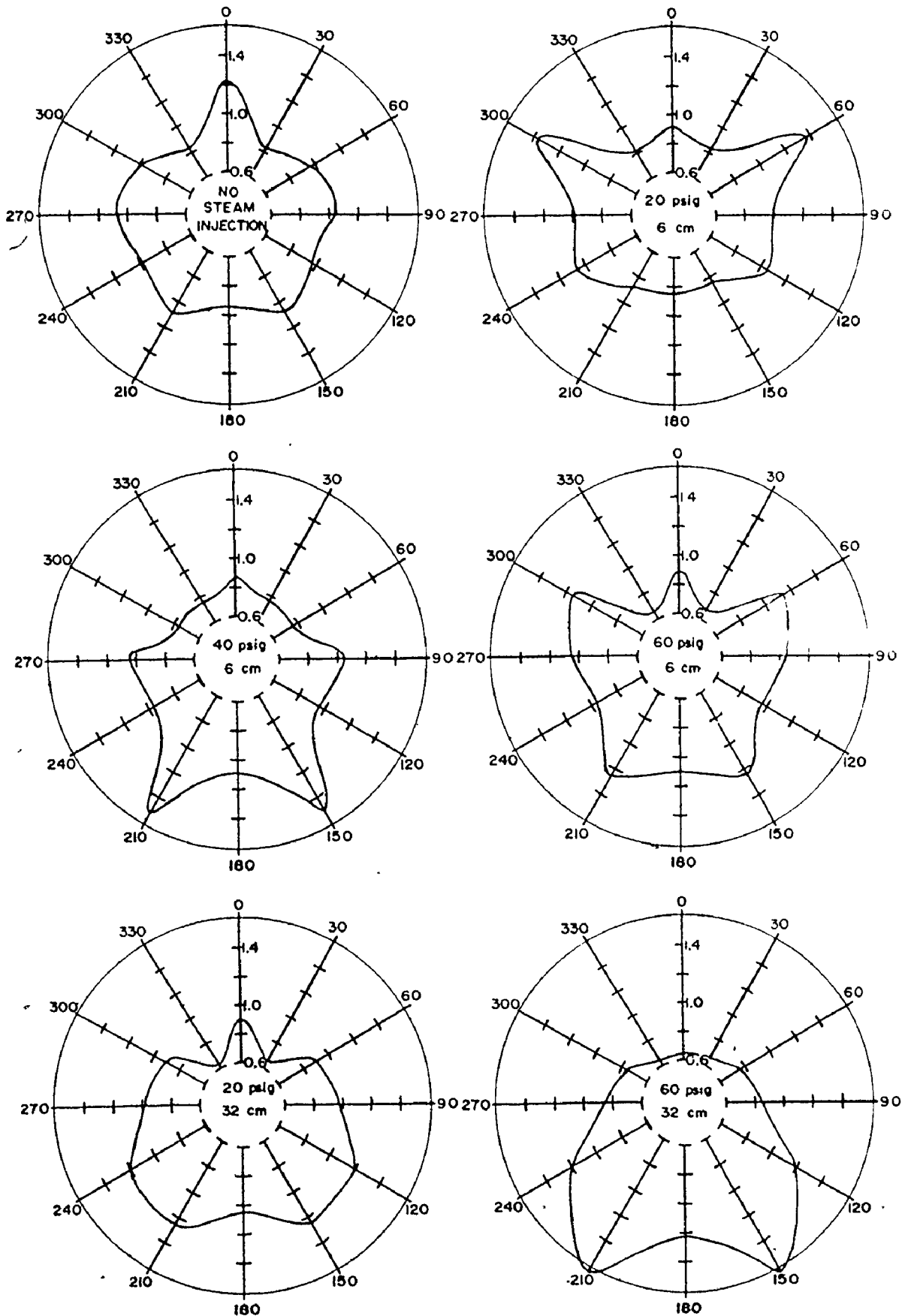


FIGURE 5.7 - VARIATION OF LOCAL CHF AROUND A CYLINDER OBTAINED WITH STEAM INJECTION

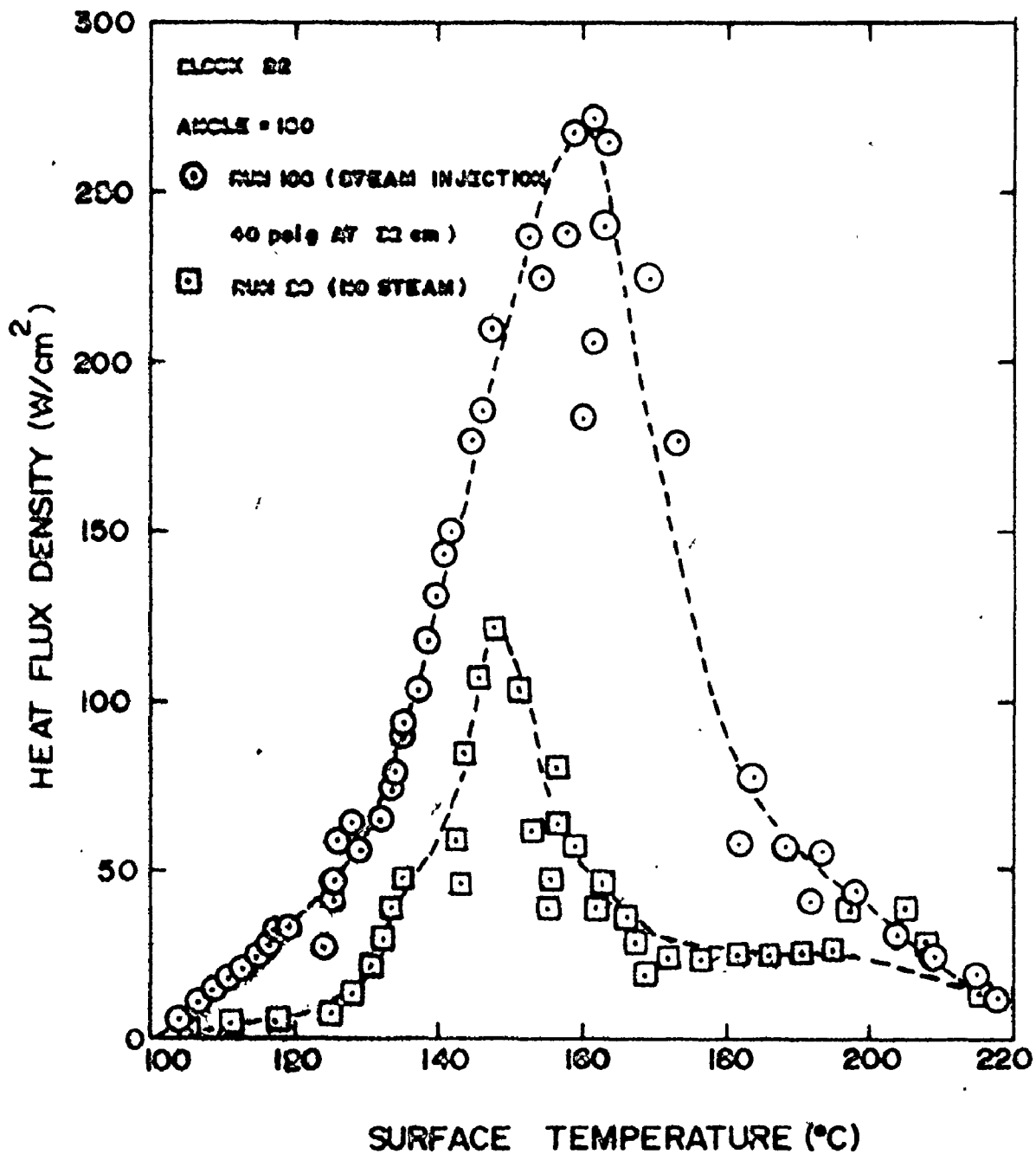


FIGURE 5-0- INFLUENCE OF STEAM INJECTION ON BOILING CURVES

To simulate this situation better in this current set of experiments, Cylinder 22 was insulated so that it had an active area subtended by an angle of 60° . The quenching experiments were performed with a steam flow corresponding to an orifice upstream pressure of 40 psig and the sparger-to-cylinder distance fixed at 32 cm. This steam flowrate corresponds to about six times the amount of vapour which would be produced by a partially insulated cylinder under critical heat flux conditions; the sparger-to-cylinder distance is about the distance between calandria tubes in a CANDU nuclear reactor. The local critical heat flux results for these experiments in which the active area and heat flux meter were centred at specific azimuthal angles are shown in Table 5.11; the observations with and without steam injection are listed along with the percentage change resulting from the steam injection. These results show once more that there was a considerable increase in CHF at the bottom of the cylinder. It is interesting to note that there was a relatively lower critical heat flux value at 30° . This observation supports the hypothesis that this lower critical heat flux under saturated boiling conditions is caused by the hydrodynamics of the upward vapour flow around the cylinder.

5.2.9 Boiling Curves with a Plated Cylinder

During the initial stages of this experimental program, an attempt was made to alleviate the copper oxidation problem by electroplating the cylinders with chromium, gold or nickel. This procedure, however, led to other unexpected problems as discussed below.

It was immediately apparent that there was substantially

different behaviour between bare and plated cylinders since the total cooling time for the plated cylinders was much longer than that for the bare one. For example, for one nickel-plated cylinder, the cooling time was 96 seconds whereas that for the unplated one was 46 seconds for the same temperature range (205°C to 116°C). Then the nickel was removed from about $1/3$ of the surface (in the region of the heat flux meter) and the corresponding cooling time was reduced to 78 seconds.

The reason for these observations becomes immediately apparent when the boiling curves are plotted for each of the quenching runs; these are shown in Figure 5.9 for the nickel-plated cylinder and for the nickel-plated one which had the nickel removed in the vicinity of the heat flux meter. It is noted that the boiling heat flux in the region of the critical heat flux is considerably reduced; in fact the maximum heat flux recorded for the plated cylinder is only 60% of that for the unplated one. At lower heat flux densities, the heat flux density does not seem to be influenced by the plating (comparing the results for the totally-plated and partially-plated cylinder). At heat fluxes above about 65 W/cm^2 , the plated cylinder indicates a progressively greater difference in heat flux density.

This observation may not be explained by the thermal resistance offered by the plated material. Indeed, the results are essentially the same for hard as well as decorative chrome whether it be a "flash electroplate" (0.0008 cm thick) or a more substantial thickness (0.0025 cm). On the other hand, this observation may be explained by postulating a substantial thermal contact resistance between the plated

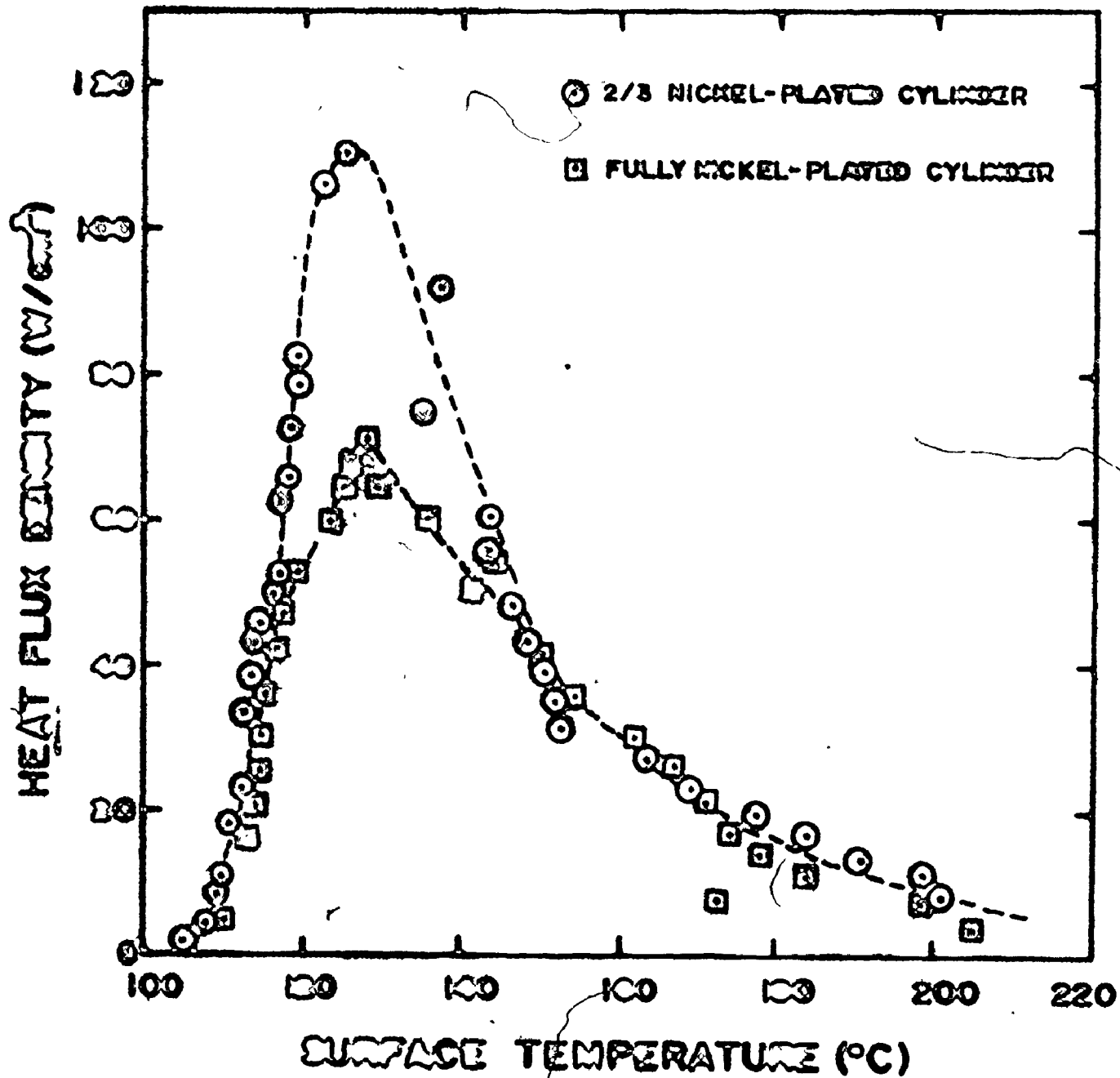


FIGURE 8.0- DOLING CURVES OF A PLATED CYLINDER

material and the underbearing copper surface. Hence, as the heat flux at the outer surface increases, a greater temperature difference exists between the copper surface and the outer nickel surface. As discussed by Hesse(H3), the outer surface temperature of the plating is determined by the instantaneous heat transfer rate to and from this thin metal layer and its thermal capacity. Since the resistance to transfer to the metal layer seems to be high and the thermal capacity of this layer is extremely small, the temperature history of the layer will be such that it only momentarily has a temperature corresponding to that at the critical heat flux. Therefore the critical heat flux is not achieved but rather some lower heat flux corresponding to a temperature where the instantaneous rate of heat transfer to the plated layer equals the instantaneous rate of heat transfer away from it. Thus the boiling curve is influenced considerably in the region of critical heat flux as was observed and as Hesse's analysis(H3) predicts.

Since the quenched specimen loses most of its heat content when it goes through the critical heat flux, it is not surprising that the total cooling time was drastically increased because of the lower maximum heat flux density.

A careful examination of Bradfield's results(B11) clearly demonstrates that he experienced the same problems in his study where a chrome-plated copper sphere (6cm in diameter) was quenched in a water bath. He obtained a critical heat flux value of 50.5 W/cm^2 for a 5° C . subcooling in distilled water. This value is approximately one third of the expected critical heat flux from a surface at these conditions. Therefore plating seems to bring about abnormal pool boiling data when

quenching techniques are used. This would not be the case in steady-state experiments because to obtain a given heat flux, a thermal driving force is applied to the boundary to keep the heat flow constant. Plated surfaces have been used to generate data for very high heat fluxes under steady-state conditions by many researchers without encountering any of the above problems. On the other hand, it should be emphasized that a heavily oxidized surface could manifest the same kind of behaviour as was observed with the plated specimen here. Again the thermal resistance of the oxide layer will not allow the outer surface temperature to be sustained for any appreciable time under high heat flux conditions; hence, lower maximum heat fluxes should be observed for quenching experiments only. These observations explain much of the controversy in the current literature(88) concerning the use of unsteady-state experiments to generate boiling curves.

5.3 Closing Remarks

Since the primary interest in this study was on the critical heat flux, the heat flux meter was designed to give greatest accuracy at high heat flux density. Hence the program concentrated on demonstrating effects and measuring the critical heat flux density as a function of angular location and subcooling of the boiling liquid. It was shown that the overall critical heat flux at saturation on a single copper cylinder is 110 W/cm^2 with a standard deviation of about 12 W/cm^2 . This value is exactly the critical heat flux density predicted by the Zuber's equation(24) for a flat plate. Lienhard's equation which is also based on the hydrodynamic stability model(55), predicts that the

critical heat flux for large cylinders should be 99 W/cm^2 , that is 0.9 times that predicted by Zuber's equation. Lienhard claims that his correlating equation has an accuracy of ± 20 percent. The experimental average critical heat flux densities are therefore within the range expected by either the Zuber or the Lienhard correlations. On the other hand, one cannot but feel that these predictions are somewhat fortuitous since neither analysis suggests any variation of CHF with position, nor do they consider the influence of vapour hydrodynamics other than that generated locally from the heat transfer surface. This experimental program has shown that the vapour flowing up around the cylinder does interact with the boiling phenomena to produce considerable variation in heat flux density around the cylinder.

Similarly it is shown that the percentage increase in average critical heat flux with level of subcooling is predicted very well by the equation proposed by Ponter and Haigh(P5) although again there is considerable variation of local CHF with position. Moreover, this variation can be attributed to the natural convective flow of liquid (hydrodynamic effect) and some to the local decrease in level of subcooling that occurs in the liquid as it is heated while flowing upward around the cylinder.

CHAPTER 6

RESULTS OBTAINED WITH THE ARRAY OF CYLINDERS

6.1 Introduction

In the postulated accident situation in a nuclear reactor, many fuel channels may undergo the same behaviour nearly simultaneously. Thus, the boiling phenomena that occurs on any one tube may be affected by the boiling phenomena which may be occurring on the others, particularly by those located below the tube in question. Intuitively, it is possible to state that there may be two effects which induce completely opposite results: One, an increase in heat flux brought about by the increased forced convection heat transfer arising from the upward vapour and induced liquid flow; the other, a decrease in heat flux resulting from partial blanketing of the tube by the upflowing vapour. An increase or decrease in heat flux will result depending upon which effect predominates. In the literature, these interactive effects are referred to as the "bundle effect"(R5). Note that as long as the liquid is sub-cooled, rising vapour will not exist and so the vapour blanketing effect does not exist. In such situations, however, the liquid may become locally saturated and then vapour will persist; hence the bundle effect becomes important for the problem at hand. Therefore, an experiment was designed to assess this bundle effect at the critical heat flux for saturated boiling conditions.

In this experimental system, a bundle comprising a maximum of 5 rows and 3 columns of 12.7 cm diameter by 7.62 cm long cylinders on a 2.18 pitch-to-diameter ratio was held in an open-structure frame containing rings which, in turn, held the insulating transite end pieces of the cylinders. The centre column was comprised of five instrumented precalibrated copper cylinders; the cylinders in the outer columns, which contained surface thermocouples only, maintained the vapour-liquid boundary conditions to simulate the conditions which could exist in the calandria of the CANDU nuclear reactor under the accident conditions.

The entire bundle (and frame) was heated to a temperature between 200° and 300°C in an electrically heated oven containing a nitrogen-hydrogen atmosphere, the flowrate of hydrogen gas to the oven was such that the hydrogen concentration never exceeded the combustion limits in air. The hydrogen was used to purge the oxygen by reaction with the red hot bare nichrome heating strips in the oven acting as catalyst. The gas in the oven was circulated continuously from top to bottom by an external blower in an attempt to improve the heat transfer rate to copper cylinders and to achieve a uniform temperature throughout. This latter objective was only partially achieved in practice; the upper cylinders were usually about $30\text{--}50^{\circ}\text{C}$ hotter than the lower ones.

After the array reached the desired temperature, the entire bundle was lifted from the oven and transferred to a track located in a 600 liters rectangular aluminum tank, in which the water had been previously heated (by an external steam-heated exchanger) to the desired

temperature. The bundle was then lowered quickly (in about 5 seconds) into the water and the signals from the thermocouples were fed continuously to and recorded in a minicomputer. For a more complete description of the experimental system the reader is referred to Chapter 3.

This chapter presents and discusses the main results obtained with this series of experiments.

6.2 Discussion of the Results

In the first phase of this experimental portion, only three rows were fitted with copper cylinders (Run 100-1 to 100-13). Since these experiments were used mainly to develop and perfect the experimental procedure, the study was restricted to saturated conditions and to the heat flux meters facing down (180°) only. Some information was obtained and is reported below. Later two more rows were added and the array was quenched in boiling water and in water at 20°C subcooling; again all the heat flux meters were facing down (180°). It was realized at that stage, that 5 rows were not enough to provide a decrease in heat flux at any point and it was decided to try to simulate additional tubes by injecting live steam underneath the centre column. The same steam injection system which was used with the single copper cylinder was employed. Some experiments were performed with the heat flux meter oriented at 180° and with pressures upstream of the orifice of 60 and 100 psig. A total of 31 quenching experiments were completed during the course of this experimental program. The complete set of data is contained in Appendix D. The results are summarized in Table 6.1. Each set of experiments will now be analysed and discussed in turn.

TABLE 6.1
AVERAGE % INCREASE OF CHF IN MULTIPLE CYLINDER ARRAY

POSITION IN BUNDLE	1	2	3	4	5
BLOCK NUMBER	12	13	9	17	20
OVERALL CHF WHEN CALIBRATED AS A SINGLE COPPER CYLINDER (W/cm^2)	105.2	113.3	117.2	117.7	96.5
	% INCREASE				
SATURATION ($\phi = 180^\circ$)	0.7	52	128	37	108
20°C SUBCOOLING ($\phi = 180^\circ$)	—	145	105	92	63
STEAM INJECTION (60 psig, $\phi = 180^\circ$)	—	47	109	36	67
STEAM INJECTION (100 psig, $\phi = 180^\circ$)	—	94	116	69	36
STEAM INJECTION (100 psig, $\phi = 90^\circ$)	11	32	5	-33	30
STEAM INJECTION (100 psig, $\phi = 0^\circ$)	-18	10	36	-13	-3

6.2.1 Saturation ($\phi = 180^\circ$)

A total of 18 experiments were done under saturated conditions and with the heat flux meter facing down. The results are summarized in Table 6.1. Unfortunately some difficulty was experienced with transferring all signals simultaneously to the computer; as a result, some of the experimental results recorded in Table 6.1 and in Appendix D are incomplete. The problem is believed to have been caused by water leaking into the shield and insulation of the thermocouple wires, thus grounding through the water tank; such grounding has caused similar "ground-loop" problem in the past. This problem was almost completely solved by coating the thermocouple leads with water impervious, high temperature Silicone Rubber (RTV 899). However, the temperature in the furnace was extremely high and at these temperatures the adhesive did crack somewhat and water could still penetrate; however fewer failures were encountered. The observations of these experiments may be summarized as follows:

- (i) No increase in heat flux was observed for the bottom cylinder. This implies that what happens above has very little, if any, effect on the boiling process below.
- (ii) The critical heat fluxes for the second row and above show an appreciable increase but not in a regular fashion (e.g. row 3 and 5 have a higher CHF than the other two rows). It should be noted, however, (Appendix D) that the time at which each cylinder passed through the critical heat flux was different. This occurred not only because each cylinder had a different starting temperature but also because each

exhibited different boiling curves during the quenching experiments. Different boiling curves were caused by the interaction between cylinders. The critical heat flux usually occurred at the bottom first and then was followed by rows 2 and 3 at about the same time. Finally, the critical heat flux then occurred on rows 4 and 5 at about the same time. This explains why rows 3 and 5 exhibited high increases in CHF as they were influenced by a lower cylinder going through the critical heat flux. In Run 100-7 the three cylinders passed through the critical heat flux condition at about the same time; at least the vapour generation was near the maximum on all three cylinders.

(iii) The complete boiling curves as a function of time for the three cylinders of Run 100-7 are presented on Figure 6.1. It is interesting to note that an increase in heat flux density occurred on the second cylinder as the lower one went through the critical heat flux. This indicates that there was an enhancement in heat flux arising from the natural convective flow of vapour and liquid from below. The results obtained here are in accordance with those reported in Chapter 5 for steam injection below the quenched cylinder.

6.2.2 20°C Subcooling ($\phi = 180^\circ$)

Quenching experiments with the 5 x 3 array were performed with the water initially subcooled 20°C; these experiments showed an expected behaviour as indicated in Table 6.1. The critical heat flux was increased but this increase was less for the upper cylinders. This observation can be explained by the effects of natural convection where

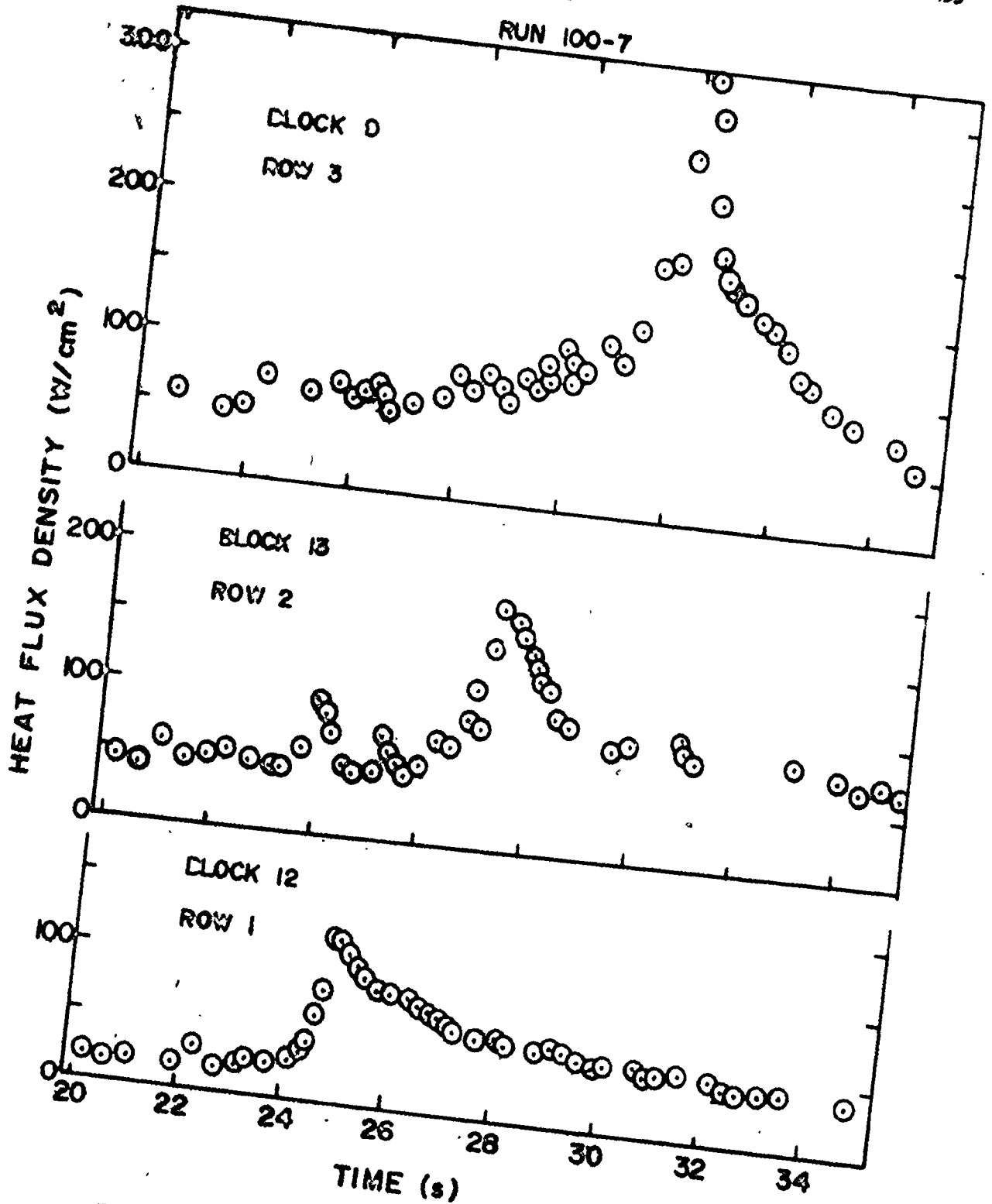


FIGURE 6-1 - BOILING CURVES FOR A 3-ROW BUNDLE

the rising water is heated progressively as it rises through the array. This means that the liquid environment around the upper cylinders is no longer subcooled at the initial level and hence the critical heat flux was less for the upper cylinders. On the other hand, there will be an enhancement in heat flux because of the larger natural convective flow from below. The data bear out this analysis: The average percentage increase in CHF for a single cylinder at 20°C subcooling was 80%. For the top cylinder in the array, the average increase was 63% so that the increase because of convective effect of the rising liquid was compensated by a decrease in subcooling. It is expected that at the point where the rising liquid becomes saturated (net production of vapour), the flow arising from natural convection will increase the CHF above that which would occur under the same conditions for a single cylinder. Therefore, the important experimental work is that associated with boiling in an array under saturated conditions.

6.2.3 Steam Injection System

With the saturation system with no steam injection it was seen that the critical heat fluxes rarely occurred at the same time so that little new information was obtained from these experiments which related to the effect of the steam generated from the tubes below on the heat flux on a particular tube higher in the bundle. Therefore it was decided to inject live steam underneath the centre column. In this way, additional rows of cylinders each undergoing boiling were simulated. The mass flowrate of steam, which was used, was equivalent to about

two and three times the amount of steam which would be evolved from a cylinder at critical heat flux conditions. The upstream pressure of the sonic orifice was set at 60 psig and 100 psig to achieve these two conditions. The 15-cylinder array was quenched in the same way as previously in water at near saturation conditions except that the steam flow was started prior to plunging the array. The results for this series of experiments are contained in Appendix D and are summarized in Table 6.1.

A substantial increase in heat flux is seen to occur at the bottom of the cylinder ($\phi = 180^\circ$); at the other two angles which were investigated no evident increase occurred. These results corroborate those found in Chapter 5 where the largest increase in heat flux density was observed to occur at the bottom portion of the cylinder. At $\phi = 180^\circ$, a higher increase was observed on the third row; lower increases occurred on the upper cylinders for the two steam flowrate investigated. At 100 psig, the increase on the second cylinder was much higher than that for the 60 psig case. These results suggest that after the third row, under these conditions, the blanketing effect of the rising vapour counteracted partially the induced forced convection effect of the rising steam-water mixture as far as the bottom of the cylinder was concerned. Therefore from the results obtained here it is not possible to predict under which situation a decrease in the overall critical heat flux would be observed. However, it is obvious that to produce a decrease in the obtainable CHF, many rows of cylinders would have to be at high heat fluxes simultaneously.

6.3 General Discussion and Conclusion

Since it is well known that under some conditions (particularly those occurring in reboilers), the upflowing vapour can cause the critical heat flux density to be substantially lower, it can be concluded from the results of this study that the effect of vapour generation on the critical heat flux must be strongly dependent on the clearance between the tubes in the calandria. Reducing the clearance to some critical value would inhibit the vapour-liquid flow and thus reduce the upward flow rate or cause vapour blanketing; the critical heat flux would be decreased accordingly. With the large pitch-to-diameter ratio used in CANDU reactors, the clearance seems to be so large that the vapour-liquid flow is not inhibited and thus an enhancement in the critical heat flux occurs because of the increased convection effect. A small spacing between two adjacent tubes in the same row can create an appreciable pressure loss in the vapour-liquid flow. The total pressure drop across the bundle must be equal to the available pressure head which is usually equal to the head of liquid outside the bundle. Therefore, if the spacing were very small, a smaller amount of liquid would be induced to flow through the bundle. With a large number of tubes (or a very large heat transfer area), all this liquid may be vaporized before it reaches the upper tubes. Under this condition, the upper tubes would not be surrounded by liquid but by vapour. This would have the effect of decreasing the average overall heat flux for the bundle although some tubes operate with a high heat flux density and others a very low one. Similarly, if the vertical spacing

between two adjacent tubes were small, the vapour bubbles generated at the top of one tube may touch the upper tube before they have a chance to detach from the surface and vapour blanketing may result. These effects do not seem to be important with the tube spacing associated with the current design of the CANDU reactors.

Some concern might be expressed as to whether the bundle simulates properly that which would occur in a calandria comprised of long tubes. Direct observation of the boiling phenomena through a window down the front of the tank indicated that the vapour flow was upward only; very little, if any, vapour passed horizontally outward through the open space in the support frame. Liquid may, however, have been drawn in through the frame by the upward flow of vapour and hence may have given a larger convective effect than would have occurred with a tube of larger length undergoing the same boiling phenomena. However in the postulated accident, not all the length of the pressure tube would touch the outside tube because there are spacers located at some axial locations.

Some concern might also be expressed concerning the relatively small number of tubes used in these experiments as it is an unfair representation of the boiling behaviour that would be observed for the many calandria tubes of a typical nuclear reactor. With the assumption that all the pressure tubes would sag at the same time and the fact that the duration of the transient may only last but a few seconds, any tube in the calandria would be affected by the boiling behaviour that prevails on only a few adjacent rows. Therefore, a tube should

be in a situation similar that which would be encountered in a relatively small bundle. The only situation where this would not prevail is when each tube would sag and experience boiling as the vapour of the lower tube just reached it so that the steam from any one tube would be added in phase to that which was generated below. However this fortuitous situation is most unlikely. Hence, this suggests that the results presented in this chapter are pertinent to the present problem.

CHAPTER 7

RESULTS OBTAINED WITH THE STEADY-STATE STEAM-HEATED TUBE BUNDLE

7.1 Introduction

As an extension to the unsteady-state bundle system, a steady-state steam-heated system was designed and fabricated to provide information concerning the steady-state boiling heat transfer performance to be expected on a 2.67 cm O.D. tube located in a bundle of similar tubes and undergoing the same boiling phenomena. The bundle system was comprised of four rows of three chrome-plated copper tubes having the same pitch-to-diameter ratio (2.18) as the calandria tubes of a typical nuclear reactor. A 100 psig steam supply was used as the energy source to allow operation in the transition boiling regime. Heptane was chosen as the boiling liquid because of its low critical heat flux value (because of steam supply restrictions) and the wall temperature range that could be achieved with the steam pressure available. Heptane was boiled off the surface of the tubes, condensed in a set of two heat exchangers and returned back to the boiling chamber. The heat flux density for each centre tube of each row was obtained from steam condensate flowrate measured independently from each tube. The complete boiling curve was obtained by varying the pressure of the steam inside the tube, which in turn dictated the outside wall temperature, and the heat flux density was measured for each pressure setting. The wall

temperature was measured with a thermocouple located near the surface of the tube. This system only provided the overall heat flux density on the tube and no information on possible angular or axial variations. For more information concerning the experimental system and the experimental procedure, the reader is referred to Chapter 3.

This chapter is concerned mainly with the presentation of the results obtained with the tube bundle system in which the heat transfer coefficient of one particular tube is affected by other rows also undergoing boiling. However, before the tube bundle results are discussed, some results relating to experiments performed with a single tube will be discussed in order to establish the critical heat flux for each tube when it is not influenced by others. The complete set of data obtained throughout this study is contained in Appendix 5.

7.2 Single Tube Experiments

7.2.1 Pool Boiling Curve on a Copper Tube

Unplated copper tubes were initially used in this project. Many sets of experiments were performed on several copper tubes. Complete boiling curves were generated for several tubes on different days. In some instance the tubes were cleaned between tests; on others the tubes were left in the apparatus and duplicate experiments were performed on them. Typical results of the latter set of experiments are presented on Figure 7.1. Six different runs were made on different days on this particular tube and the complete set of data is contained in Appendix B. The critical heat flux densities obtained for each of

these six runs are presented on Table 7.1. Only three runs are plotted here but these indicate the shift in the boiling curves that was observed during the course of these experiments. On the other hand, the reproducibility from run to run was good when the tube was cleaned between each test.

Careful examination of the tube after each experiment showed that the tube was oxidized somewhat and a green polymeric-like substance was deposited on the tube. This coating became progressively thicker as the experiments proceeded. Obviously the tube was being oxidized and contaminated by impurities in the liquid. Results on Figure 7.1 suggest that as fouling on the tube increases, the critical heat flux increases. It increased from about 185 kW/m^2 on a clean tube to about 215 kW/m^2 on a highly scaled tube as was obtained for Run 6. Furthermore, as fouling increases the critical heat flux occurs at much higher superheat. This shift in excess temperature is attributed mainly to build up of an oxide layer and in part to change in surface finish as noticed by Berenson (86). A large temperature gradient is required for heat to flow across this low thermal conductivity layer. The thermocouple on the tube reads a temperature somewhat below the surface because the bead of the thermocouple is inserted in the groove of the tube; it is, therefore, not recording the true temperature on the outside of the deposit and the shift in temperature is probably only an apparent shift.

The increase in the critical heat flux is attributed to the effect of scaling. Berenson (86) found the same result when he boiled

TABLE 7.1

CRITICAL HEAT FLUX DENSITY OBTAINED DURING
INDIVIDUAL CALIBRATION IN A SINGLE TUBE EXPERIMENT

Unplated Copper Tube

RUN	DATE	CHF (kW/m ²)	AVER. CHF. ^a (kW/m ²)
1	29 Jan. 75	186.1	183.5
2	30 Jan. 75	179.4	
3	31 Jan. 75	182.9	
4	1 Feb. 75	195.1	215.6
5	3 Feb. 75	215.6	
6	4 Feb. 75	217.7	

Plated Copper Tubes

TUBE NO.	DATE	CHF (kW/m ²)	AVER. CHF. (kW/m ²)
1	29 July 76	182.0	178.2
	30 July 76	176.4	
2	4 Aug. 76	199.8	207.4
	5 Aug. 76	201.3	
	12 Aug. 76	202.8	
	13 Aug. 76	196.4	
3	14 Aug. 76	185.7	195.7
	15 Aug. 76	191.8	
	17 Aug. 76	194.4	

^aRuns 4, 5 and 6 were not included in the average because fouling was influencing the results.

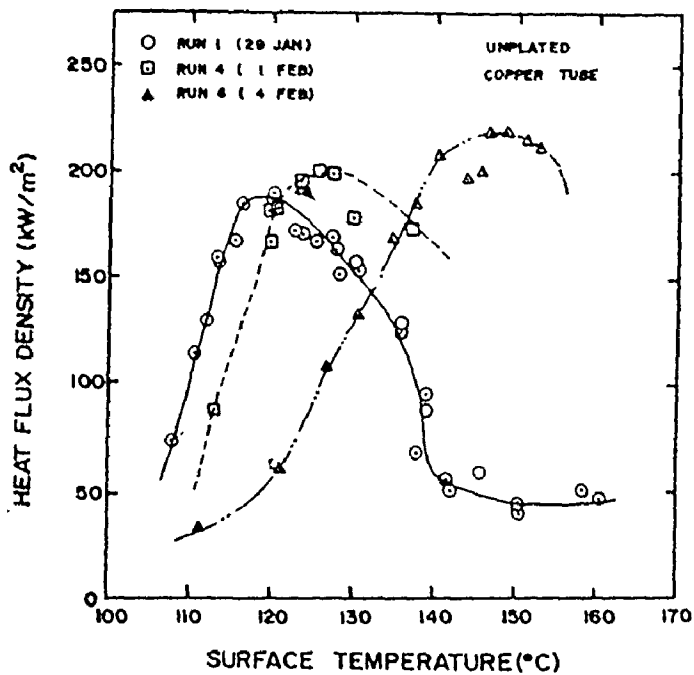


FIGURE 7.1 - TYPICAL BOILING CURVES FOR AN UNPLATED COPPER TUBE SHOWING THE EFFECT OF FOULING

A

pentane on a copper plate. He was able to show that the cause for the difference shown here was contamination in the form of dirt particles and dust on the heat transfer surface. He concluded that this dirt would tend to change the surface energy (contact angle) conditions of the surface and thus induced these effects. He observed, as was here, that it was necessary to clean the copper surface prior each experiment to obtain consistent results. In addition to the atmospheric dirt deposited between runs, it is believed that heptane upon vaporization, left impurities on the surface. The formation of polymeric material was traced to water entering the system through a small leak in the condenser. An experiment was done with a small boiler containing a short length of copper tubing; although some oxidation occurred, the green polymeric material did not appear. Hence it was still necessary to distill the heptane (yellow colour persisted), chrome-plate the tube to avoid oxidation and remove all water from the system.

Surface oxidation and contamination make this system very inefficient to transfer heat to a boiling liquid. It took approximately fifty hours for the evaporator to be inoperable; at this point the critical heat flux could not be achieved even with the full steam pressure of 100 psig (170°C). Another similar tube was used for a longer period of time and at the end the scaling started to peel off. Extremely low heat fluxes were obtained under these conditions as vapour was trapped under the scaling. Fouling effects have been recently reviewed by Taborek et al. (T1) and they concluded that fouling is the major unresolved problem in heat transfer. These results point to the

importance of scaling; any designer of industrial evaporators, must be very careful in his design to account for fouling. Fortunately, the fouling problem was resolved in the experimental system toward the end of the experimental program by preventing water leaks and by replacing neoprene gaskets and O-rings with teflon ones.

7.2.2 Pool Boiling Curve on a Chrome-Plated Tube

This experimental program strongly relies on the reproducibility of results obtained on a single tube since it must be possible to obtain a direct comparison of the observed heat flux on a single tube with the heat flux observed for the same tube when it is located in a bundle of tubes all undergoing the same boiling phenomena. Any transient effect, as observed on the copper tube, would confound the bundle effect and make any kind of analysis impossible. As mentioned above, the fouling problem was solved. On the other hand, to alleviate the previous oxidation problem a chrome-plated copper tube was used.

Two different chrome-plated copper tubes were used in single tube experiment to establish the pool boiling characteristics on each one in order to test the pool boiling curve reproducibility from run to run on the same tube and also from tube to tube. It was found that the critical heat flux density was reproducible from experiment to experiment on the same tube and on different tubes. The reproducibility of the nucleate boiling was also good. The critical heat flux value did not however occur at the same wall temperature from one tube to the other; this may be only an apparent shift and may relate to the

location and installation of the thermocouple. There was however no appreciable temperature shift from one experiment to another for any given tube.

Having established that reproducible results could be achieved for a chrome-plated tube, a characteristic boiling curve was obtained for each of the tubes which were used in the centre row of the bundle. These curves are shown in Figures 7.2, 7.3, 7.4 and 7.5 for Tubes 1, 2, 3 and 4 respectively. The full set of data is contained in Appendix B. It can be seen that the reproducibility from run to run for a particular chrome-plated copper tube is very good. There is only one boiling curve which differs appreciably from the other runs; this is the first run performed with Tube 3. The reason for this shift of the critical heat flux can be related to the insulation coating placed in the groove of the tube to prevent the boiling liquid to reach the thermocouple bead which was pinned into the copper on the top of the tube. In the first run an aluminum coating was used; however, this coating cracked by thermal expansion and the boiling liquid could reach the thermocouple bead. The resulting recorded temperature was lower than the actual one because of the cooling action of the liquid. In the other two runs performed on Tube 3 RTV Silicone adhesive was used to prevent heptane from contacting the tip of the thermocouple and good reproducibility was achieved.

Aluminum coating and many other coatings were used in an attempt to replace RTV because it was suspected that heptane was being contaminated with substances contained in RTV. However, in the end, RTV was

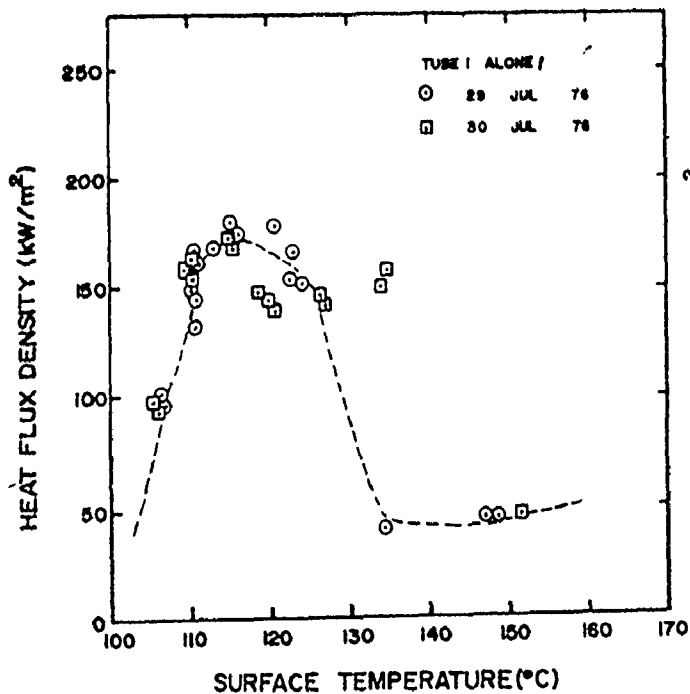


FIGURE 7.2 - BOILING CURVE FOR TUBE 1 OBTAINED WITH SINGLE TUBE EXPERIMENT.

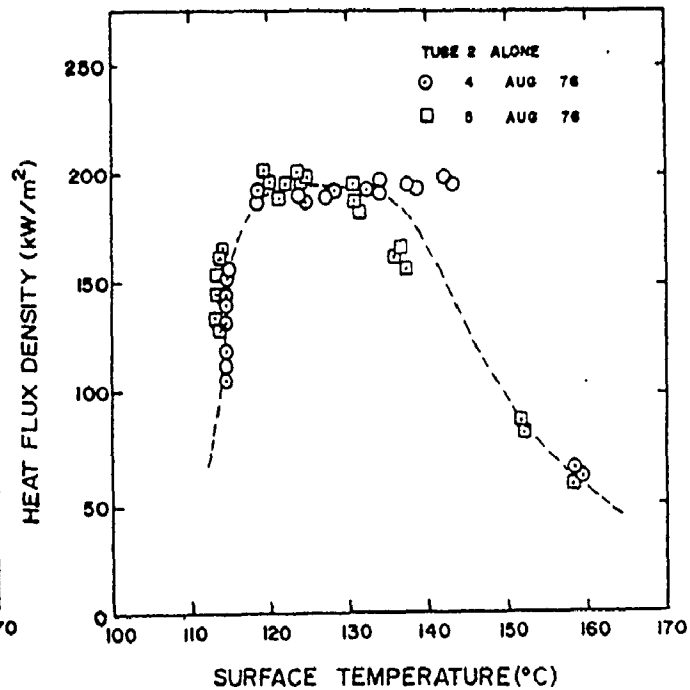


FIGURE 7.3 - BOILING CURVE FOR TUBE 2 OBTAINED WITH SINGLE TUBE EXPERIMENT.

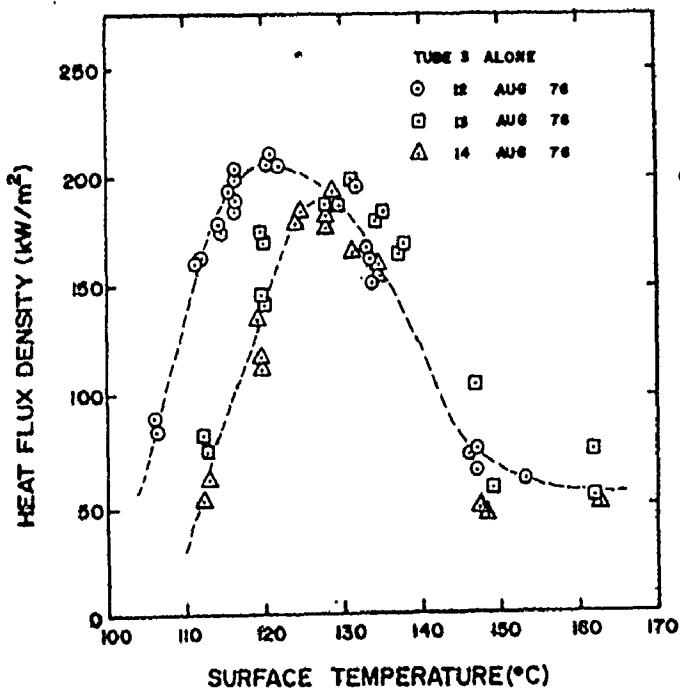


FIGURE 7.4 - BOILING CURVE FOR TUBE 3 OBTAINED WITH SINGLE TUBE EXPERIMENT.

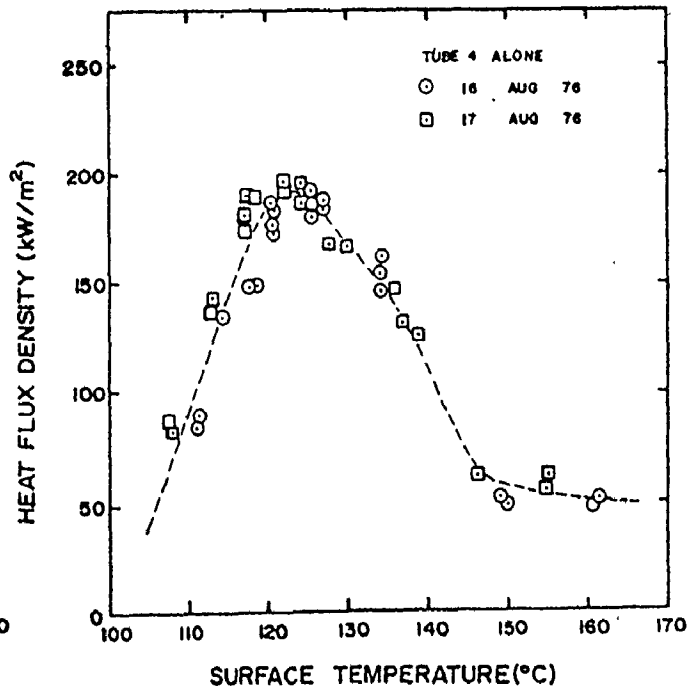


FIGURE 7.5 - BOILING CURVE FOR TUBE 4 OBTAINED WITH SINGLE TUBE EXPERIMENT.

used because of the need for an elastic coating which could sustain the thermal expansion and contraction; all the other coatings cracked and the temperature of the tube became unreliable after a few experiments.

The reproducibility of the boiling curves for different tubes is not as good as that obtained from experiments performed with the same tube. The shape of the different boiling curves and the excess temperature at which the critical heat flux occur vary slightly. The latter can in part be attributed to the different depth in which the thermocouple beads were inserted into the surface. On the other hand the critical heat fluxes obtained on each of these tubes are the same within experimental error. The results point out the importance of obtaining a characteristic boiling curve for each of the instrumented tubes in the bundle in order to analyse the tube bundle in the way suggested. This procedure should correct for differences in wall superheat.

Sometimes it was impossible to obtain any point in the major portion of the transition regime. For an increase of about 0.5 psi in the steam pressure, the wall superheat would jump from the critical heat flux to near the minimum heat flux value. Hesse(H3) described this instability and found that if the characteristic boiling curve in the transition region is steeper than the characteristic of the heating surface, there will be no stable operating points. Run 2 of Tube 1 and Run 1 of Tube 2 are typical examples of this phenomena. In the other run on the same tube, however, it was possible to obtain some operating points which suggest that the property of the surface had changed. In the cases where there was a sudden jump from the maximum heat flux to

near the minimum heat flux, the surface was such that the nucleate boiling could be maintained at a higher wall superheat and the corresponding transition regime was therefore steeper.

7.2.3 Critical Heat Flux Density

The critical heat flux densities on a fresh clean copper tube or a chrome-plated copper tube are presented on Table 7.1. An average value of 190 kW/m^2 with a standard deviation of 9.4 kW/m^2 was obtained. There does not seem to be any difference between an unplated copper tube and a plated one. McAdams(M2) reports a value of 167 kW/m^2 with a wall superheat of 30°C . An average wall superheat of about 23°C was observed here.

In the design of this experimental program, the critical heat flux was calculated with Equation 2.3 (Zuber, $K = 0.131$) and a value of 236 kW/m^2 was predicted. These experimental results are considerably lower than this predicted value. Equation 2.3 was derived for a flat plate and this lack of agreement may be attributable to the geometry used in these experiments. This geometry effect was investigated by Lienhard(81, 55); he derived that the critical heat flux density for a tube of the size used in this study should be about 90% of the critical heat flux value predicted by the Zuber's equation. The Lienhard's prediction for this tube size is about 212 kW/m^2 with a claimed accuracy of plus or minus 20%. The 190 kW/m^2 value obtained in this study is equivalent to 80% of the Zuber's prediction and within the range of accuracy of the Lienhard's prediction.

7.2.4 Influence of the Liquid Level

The steam pressure was set at approximately 60 psig which corresponded to near the critical heat flux point and the liquid level above the tube was varied from 2 to 16 cm above the tube. The results of this investigation are presented on Table 7.2. These results clearly show that the liquid level above the tube does not influence the critical heat flux value. These observations were very important in this study because the liquid level in the bundle system was different for each row and the recorded heat flux did not need to be corrected for differences in liquid level.

7.3 Multiple Tube Experiments

7.3.1 Pool Boiling Curves for Individual Rows

The experimental system was designed to allow separate control of the steam pressure on any row of tubes to establish a given wall superheat on the centre tube in the row. Furthermore, all rows or any combination of rows could be heated at any one time. In each case, the average heat flux for each centre tube could be measured from the steam condensate rate from it. This procedure allowed a direct comparison of the boiling curves for the tubes under all conditions and thus an evaluation of the interaction effect was possible. Some single tube experiments were performed during the experiments with the bundle to record any changes in the characteristic boiling curves for these tubes. This allowed a better comparison on a daily basis. This comparison also provided valuable information concerning the effect on the CHF of the

TABLE 7.2

INFLUENCE OF THE LIQUID LEVEL
ON THE CRITICAL HEAT FLUX

TUBE 4

August 17, 1976

Steam Pressure at 60 psig

LIQUID LEVEL ABOVE THE TUBE <hr style="width: 100%; border: 0.5px solid black; margin: 0;"/> (cm)	HEAT FLUX DENSITY <hr style="width: 100%; border: 0.5px solid black; margin: 0;"/> (kW/m ²)	AVERAGE HEAT FLUX DENSITY <hr style="width: 100%; border: 0.5px solid black; margin: 0;"/> (kW/m ²)
2	191.6 193.8	192.7
5	192.9 194.4	193.7.
9	192.3 193.5	192.9
16	191.9 192.9	192.4

centre tube by the two adjacent tubes located on the same row. This effect can be visualized on Figures 7.6, 7.7, 7.8 and 7.9 for Tubes 1, 2, 3 and 4 respectively.

Only Tube 2 shows a perfect agreement between the boiling curve obtained in a single tube experiment and the one obtained when a complete row was undergoing boiling. All the other tubes show an increase of their critical heat flux values when adjacent tubes of a given row are also boiling. Table 7.3 presents the CHF values obtained for this set of experiments. An average critical heat flux of roughly 206 kW/m^2 was obtained under these conditions which corresponds to an increase of about 8%. This substantial increase was not expected and is attributable to the additional fluid circulation produced by the two adjacent tubes. The bundle effect is therefore also influenced by what happens on a row of tubes.

This analysis also demonstrated that the characteristic pool boiling curve for any given tube did not change appreciably during the course of this investigation.

7.3.2 Downward Bundle Effect

If additional liquid circulation produced a beneficial effect within a single row, it is possible that a tube undergoing boiling could be influenced by boiling on tubes located above. To provide this information, the heat flux density for Tubes 1 and 2 was measured under conditions where boiling occurred on one or more tubes in the rows above. These results are plotted in Figure 7.10 and 7.11; the

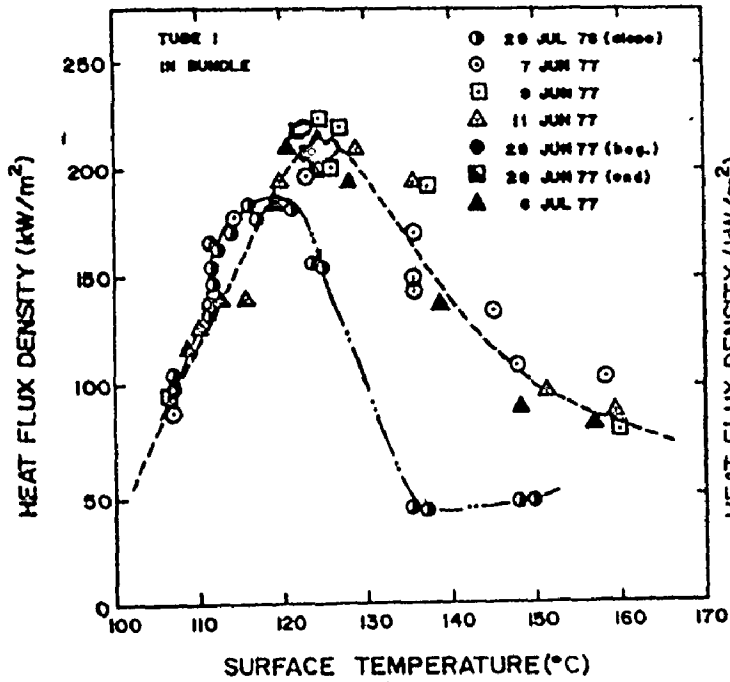


FIGURE 7.6 - BOILING CURVE FOR TUBE 1 OBTAINED WITH SINGLE ROW EXPERIMENT.

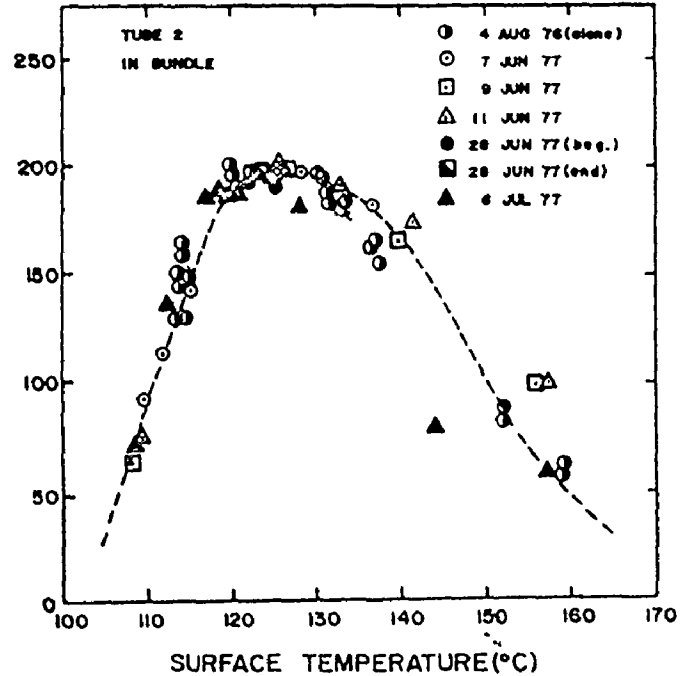


FIGURE 7.7 - BOILING CURVE FOR TUBE 2 OBTAINED WITH SINGLE ROW EXPERIMENT.

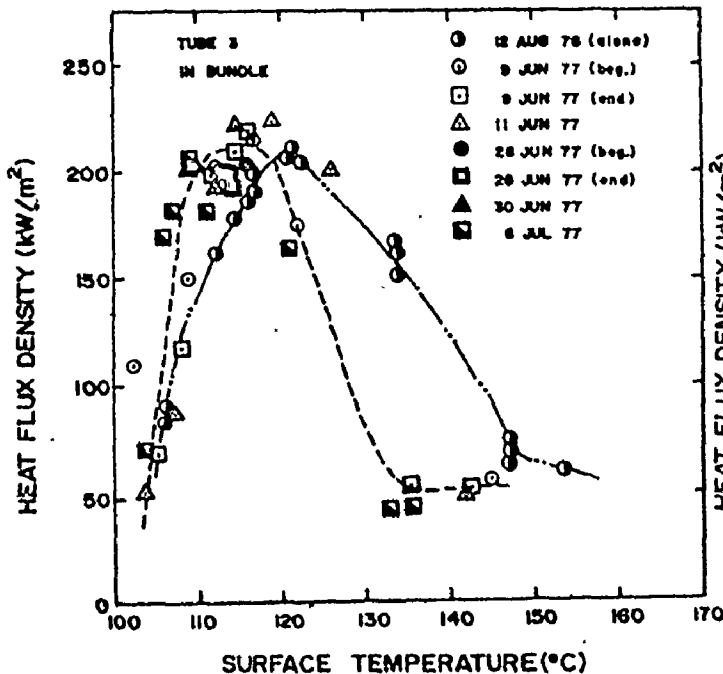


FIGURE 7.8 - BOILING CURVE FOR TUBE 3 OBTAINED WITH SINGLE ROW EXPERIMENT.

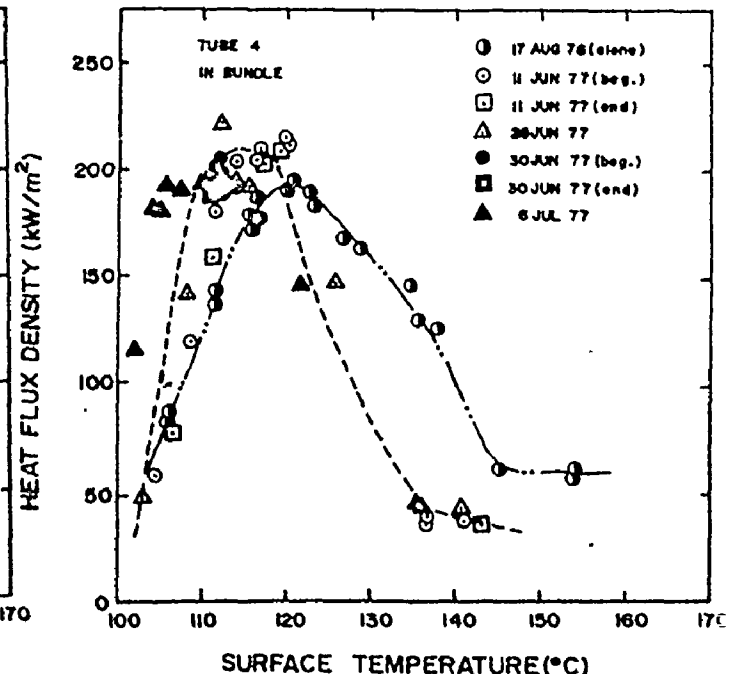


FIGURE 7.9 - BOILING CURVE FOR TUBE 4 OBTAINED WITH SINGLE ROW EXPERIMENT.

TABLE 7.3

CRITICAL HEAT FLUX VALUES DURING INDIVIDUAL
CALIBRATION IN THE BUNDLE (kW/m²)

<u>DATE</u>	<u>TUBE 1</u>	<u>TUBE 2</u>	<u>TUBE 3</u>	<u>TUBE 4</u>	<u>AVERAGE</u>
7 June 77	192.2	195.6			
9 June 77	223.0	201.4	214.2 218.3		
11 June 77	209.0	202.2	223.6	214.0 208.2	
28 June 77	218.4 207.6	193.3 197.7	203.7 199.7	220.7	
30 June 77				204.0 191.4	
6 July 77	<u>218.0</u>	<u>189.8</u>	<u>203.7</u>	<u>193.6</u>	
Average	211.4	196.7	209.2	205.3	205.7
Std. Dev.	11.1	4.8	9.4	11.4	6.5

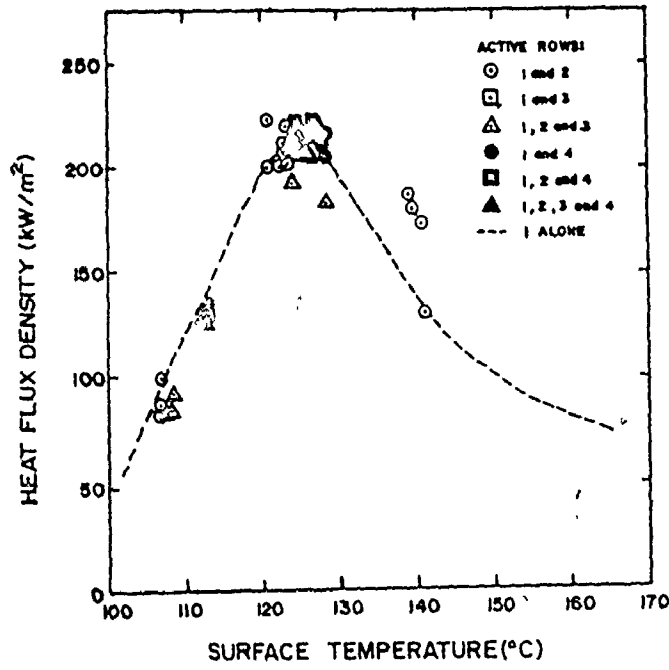


FIGURE 7.10 - BOILING CURVE FOR TUBE 1 OBTAINED WITH SINGLE ROW EXPERIMENT WHEN ABOVE TUBE(S) ARE UNDERGOING BOILING.

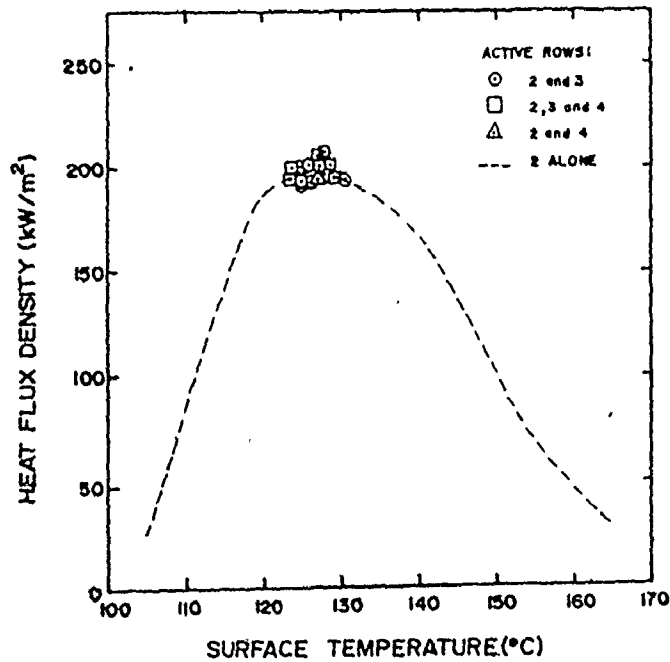


FIGURE 7.11 - BOILING CURVE FOR TUBE 2 OBTAINED WITH SINGLE ROW EXPERIMENT WHEN ABOVE TUBE(S) ARE UNDERGOING BOILING.

boiling curve for boiling on the particular row alone is shown for comparison. These results clearly show that the heat transfer coefficient of a given tube is not influenced by the boiling phenomena occurring above it. Wall and Park (W2) also found that there is little or no change in the boiling behaviour of a bottom tube in a vertical array due to tubes boiling above it.

7.3.3 Influence of Tube 1 on Tube 2

The first experiment performed to investigate the interaction of boiling on one tube by boiling on another one was to observe the effect that Tube 1 (the lower one) had on Tube 2. To obtain this information, the boiling curve for Tube 2 was established for three different heat fluxes on Tube 1. These results are plotted on Figure 7.12. The full set of data is contained in Appendix B. The following information can be deduced:

- (i) The nucleate boiling regime of the boiling curve is not affected by the vapour rising from Tube 1. All the measured heat fluxes corresponding to the three different heat fluxes of Tube 1 fall exactly on the boiling curve obtained when only row 2 was active. As the critical heat flux density is approached, the steep slope, characteristic to the nucleate boiling, fails to decrease and a higher critical heat flux density results. This phenomena is similar to the boiling curve that would be obtained under forced convection conditions as already discussed in Chapter 2.
- (ii) There is a substantial increase in the critical heat flux density. This beneficial effect is a function of the heat flux density

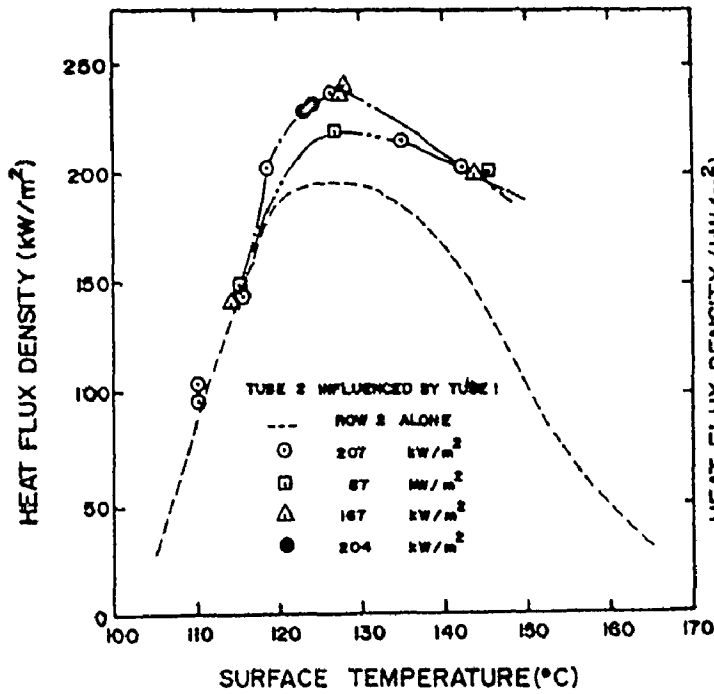


FIGURE 7.12 - BOILING CURVE OF TUBE 2 WHEN TUBE 1 IS ACTIVE.

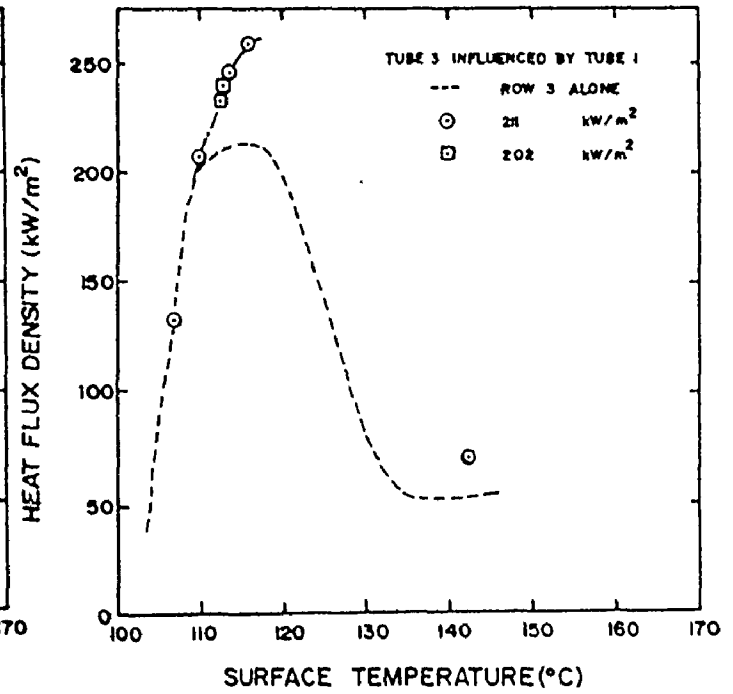


FIGURE 7.13 - BOILING CURVE OF TUBE 3 WHEN TUBE 1 IS ACTIVE.

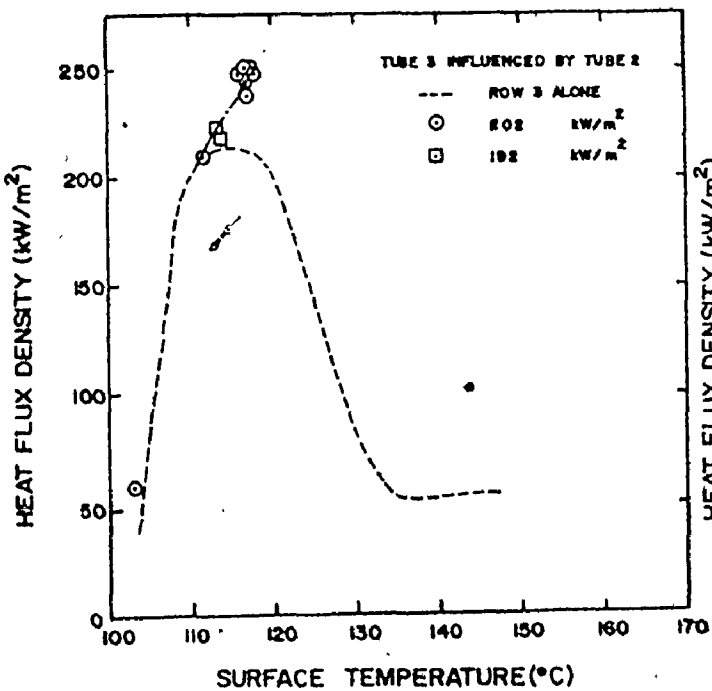


FIGURE 7.14 - BOILING CURVE OF TUBE 3 WHEN TUBE 2 IS ACTIVE.

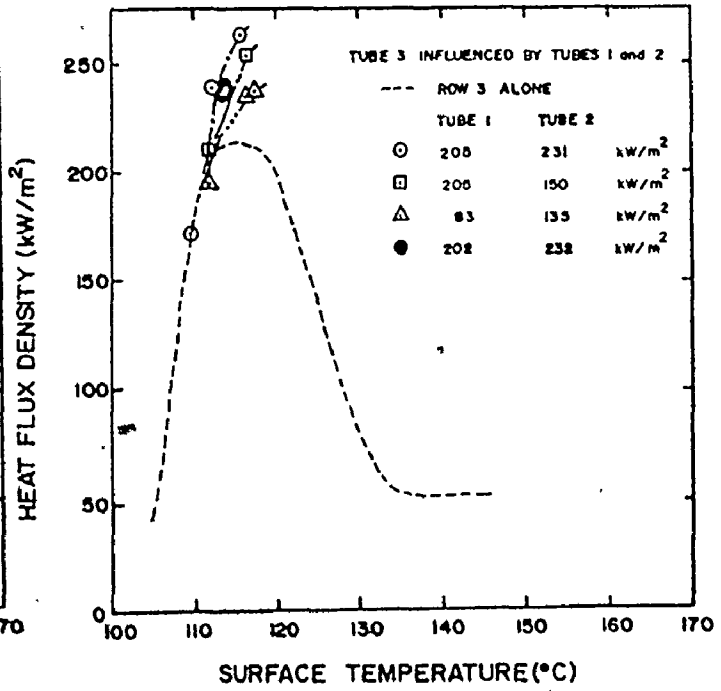


FIGURE 7.15 - BOILING CURVE OF TUBE 3 WHEN TUBES 1 AND 2 ARE ACTIVE.

prevailing on Tube 1 which, in turn, dictates the vapour mass flowrate and the attendant induced liquid flow which impinges on Tube 2. This effect, however, is not proportional to the quantity of vapour rising up to the next tube; rather, it seems to level off after a certain amount because the same increase was observed for a heat flux density of 167 and 207 kW/m^2 . A few days later, two other points, represented by black dots, were measured and good reproducibility was obtained. An average percentage increase of about 18% is observed for the CHF when compared with that obtained with Tube 2 in a single row experiments.

(iii) The transition regime also shows a marked increase in the heat flux density. The increase appears to be independent of the heat flux on the lower tube in the range investigated.

These results suggest that the increase observed for the critical heat flux density and for the transition regime occurs because the additional circulation produced by the rising vapour and liquid disrupts the formation of a film and enhances the contact between the boiling liquid and the heat transfer surface.

7.3.4 Influence of Tube(s) 1 and/or 2 on Tube 3

The results for these experiments are presented on Figures 7.13, 7.14 and 7.15 when Tubes 1 and 3, 2 and 3 and 1, 2 and 3 were active respectively. Similarly to what was observed with Tube 2, the heat flux density in the nucleate boiling regime was not influenced by boiling on the lower tubes. On the other hand, when Tube 1 was at its critical heat flux density, the average percentage increase in the

critical heat flux on Tube 3 was about 20%. When Tube 2 was also at its critical heat flux density, the average increase in CHF on Tube 3 was observed to be about 22%. Finally, the critical heat flux of Tube 3 increased by 17% when only Tube 2 was in active boiling at its CHF point. Tests were performed on different days and good reproducibility was obtained.

Only one observation was measured in the transition boiling regime because the maximum available pressure of the steam supply system corresponded to a point near the critical heat flux value. It was therefore impossible to create a stable film and operate Tube 3 at low heat fluxes in the transition regime. A stable film was created, however, when row 3 was operated alone. When steam was fed to the other rows, the pressure drop in the supply lines was increased so that the maximum pressure available at the boiler was decreased considerably. The resulting decrease in steam pressure combined with the circulation around Tube 3 (generated by the rising vapour) disrupted the boiling in the transition regime and nucleate boiling was restored. This problem was a limitation of the experimental system and may imply that possibly the critical heat flux was not achieved and that conservative increases are reported here. However, the results obtained with Tube 2 suggest that the CHF occurs at the same wall temperature independent of the vapour flowrate impinging on its surface. By analogy it can be visualized from the plotted boiling curves for Tube 3, that the high heat fluxes obtained correspond in most cases to the CHF value.

The only point obtained near the minimum heat flux suggests

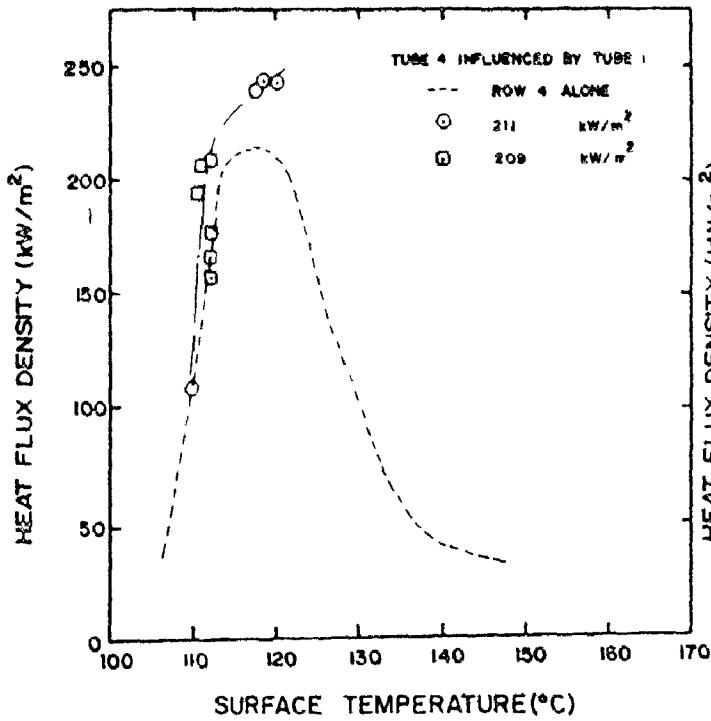


FIGURE 7.16 - BOILING CURVE OF TUBE 4 WHEN TUBE 1 IS ACTIVE.

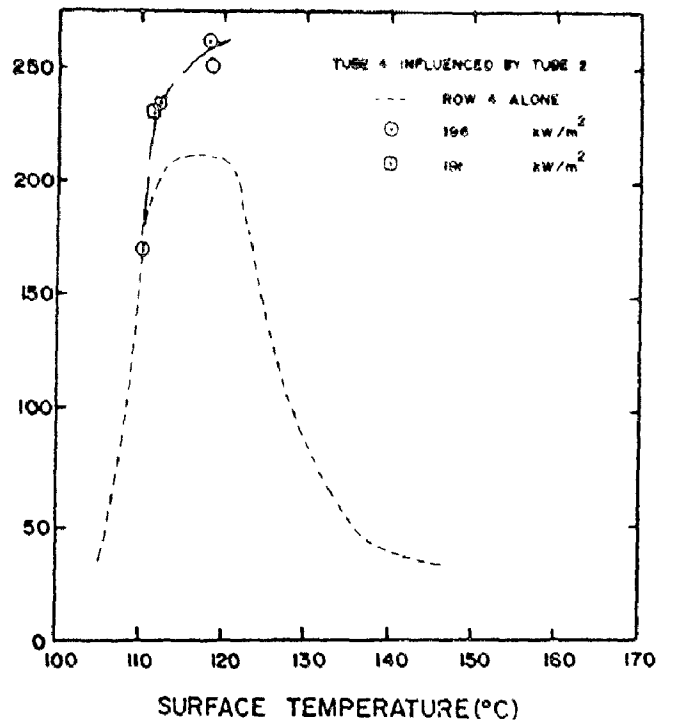


FIGURE 7.17 - BOILING CURVE OF TUBE 4 WHEN TUBE 2 IS ACTIVE.

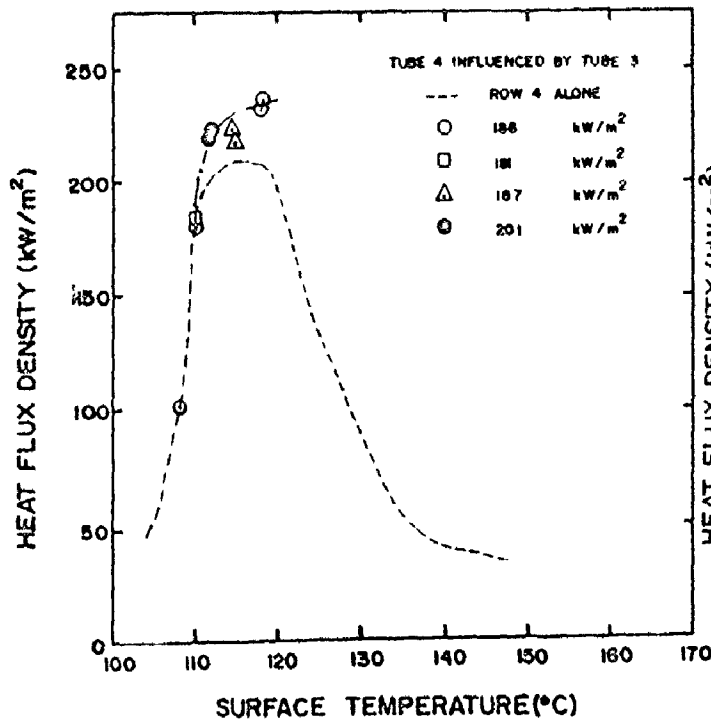


FIGURE 7.18 - BOILING CURVE OF TUBE 4 WHEN TUBE 3 IS ACTIVE.

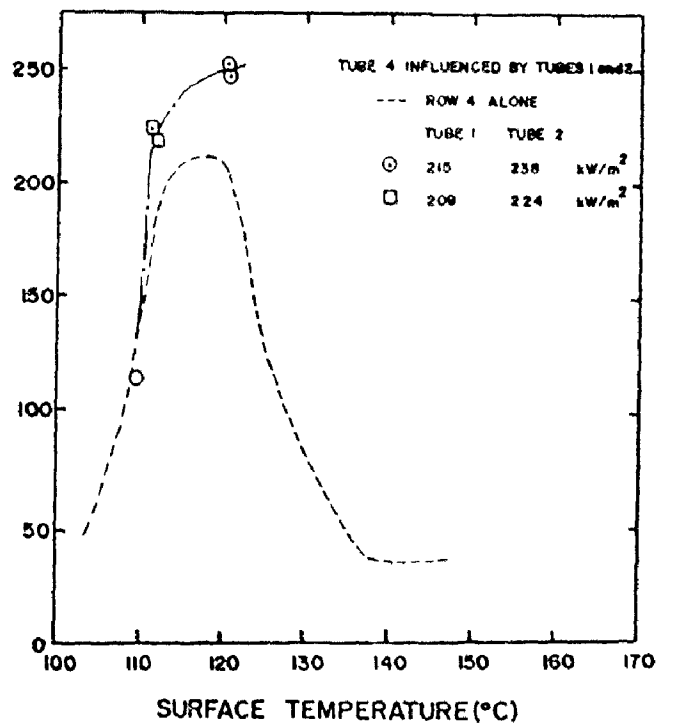


FIGURE 7.19 - BOILING CURVE OF TUBE 4 WHEN TUBES 1 AND 2 ARE ACTIVE.

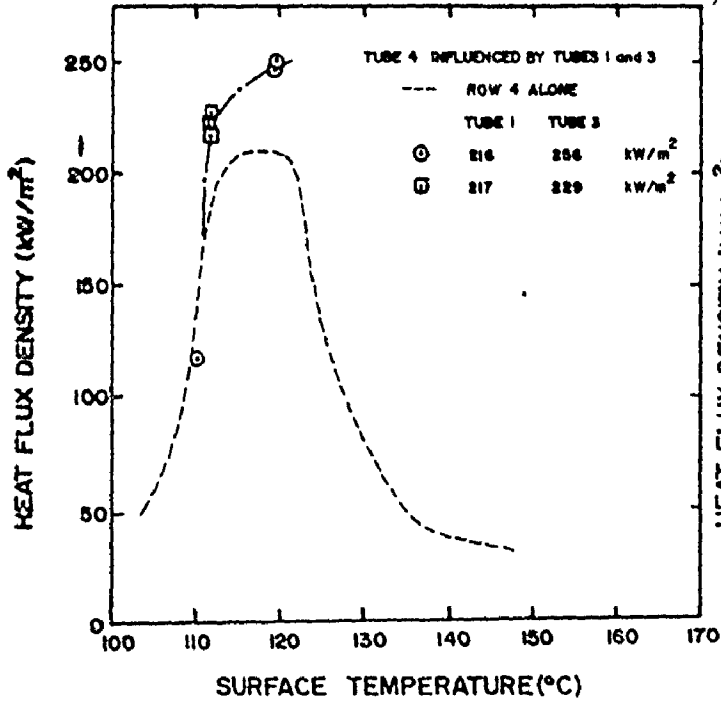


FIGURE 7.20 - BOILING CURVE OF TUBE 4 WHEN TUBES 1 AND 3 ARE ACTIVE.

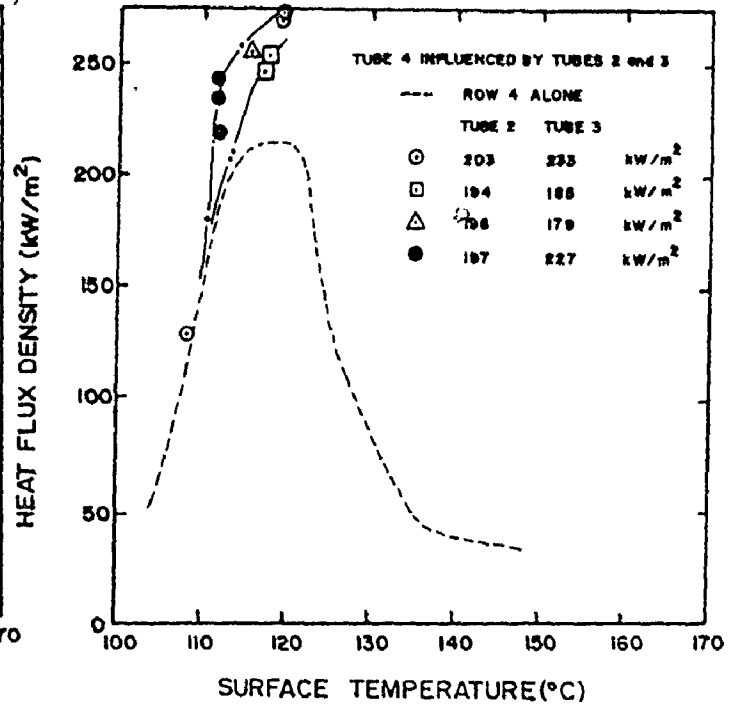


FIGURE 7.21 - BOILING CURVE OF TUBE 4 WHEN TUBES 2 AND 3 ARE ACTIVE.

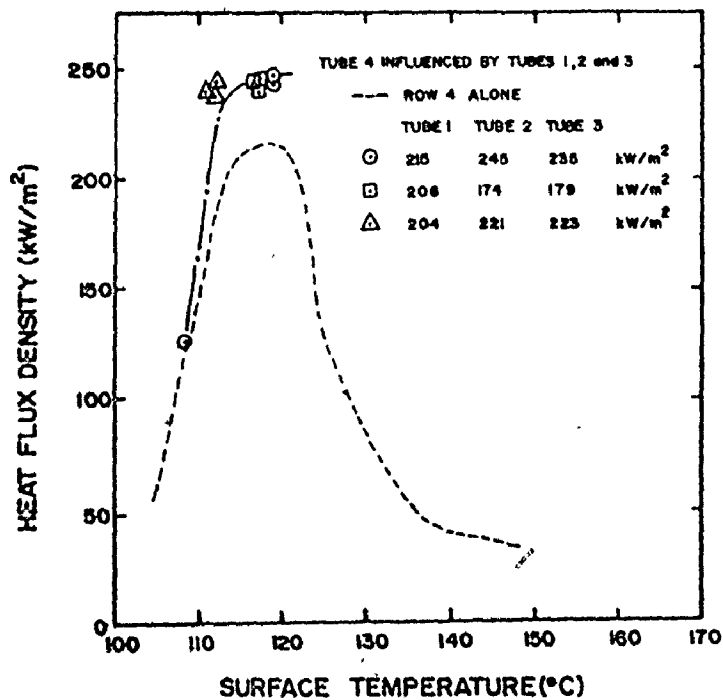


FIGURE 7.22 - BOILING CURVE OF TUBE

that when a stable film is formed, the heat flux is relatively unaffected by the occurred circulation.

7.3.5 Influence of Tube(s) 1, 2 and/or 3 on Tube 4

The results for the various combinations of operation of the three rows located below Tube 4 (alone, in pair or the three rows together) are graphically represented on Figures 7.16 to 7.22. The results for the influence on Tube 4 of boiling on the lower tubes are similar to that reported in the previous sections. It was impossible to operate row 4 beyond its critical heat flux value. The results obtained for the critical heat flux on Tube 4 (the maximum attainable) are summarized on Table 7.4 along with a summary of the results obtained on the other three tubes investigated. The average percentage increase recorded for Tube 4 varies from 12% when row 3 alone was active to a substantial 24% when rows 2 and 3 were at their critical heat flux values. It should be remembered that these percentages account only for the vertical bundle effect and the horizontal bundle effect (that is the influence of multiple tubes boiling activity on the heat flux density on adjacent tubes) was not determined. The average percentage increases tabulated in Table 7.4 were obtained by comparing the average critical heat flux density of a tube in the bundle with the average critical heat flux density obtained in a single row experiment.

7.4 Summary and General Discussion of the Results

The major portion of the information presented for the bundle

TABLE 7.4

AVERAGE PERCENTAGE INCREASE
OF THE CRITICAL HEAT FLUX
DENSITY WITHIN THE TUBE BUNDLE*

<u>ACTIVE ROW(S)</u>	<u>% INCREASE IN CHF ON</u>		
	<u>TUBE 2</u>	<u>TUBE 3</u>	<u>TUBE 4</u>
1	18	20	16
2	—	17	21
3	—	—	12
1 and 2	—	22	19
1 and 3	—	—	18
2 and 3	—	—	24
1, 2 and 3	—	—	20

*The % increase is obtained by comparing the average critical heat flux density of a tube in bundle with the average critical heat flux density obtained in a single row experiment.

effect has been analysed and reported in the previous sections. It has been shown that the nucleate boiling regime is not affected by the vapour impinging on the surface of the tube. On the other hand, the critical heat flux density showed a substantial increase; the observed increase was relatively independent of the amount of vapour rising from the tubes located below as long as a given minimum mass flowrate was exceeded. Now, the results will be analysed in an attempt to establish some pattern among the data tabulated in Table 7.4.

There seems to be a preferential spacing between two tubes which produces a higher CHF increase; the distance of two rows gives a greater increase of the CHF than only one row spacing or three rows spacing. An average increase of 20% was obtained for the two cases encountered in this study; 1 on 3 and 2 on 4. Moreover, the greatest increase observed during this investigation was obtained when two consecutive rows were acting on the next row (1 and 2 on 3; 2 and 3 on 4); an average percentage increase of 23% was recorded.

When the four rows of the bundle were at their critical heat flux values, an average increase of 20% was observed on Tube 4 and the overall bundle increase was roughly 15%. These results are in agreement with those reported by Palen et al.(P3) who concluded that with small tube bundles (4 to 6 rows), the additional circulation and turbulence caused by rising bubbles can increase the average heat transfer coefficient above that for a single tube. This increase would indicate that, instead of a vapour penalty, a multitube enhancement correction should be applied

to any single tube correlation for boiling. It is unknown how many rows would be required before a decrease would be observed, if, in fact, a decrease would be observed with the tube spacing employed. With the constraints of the available steam supply, it is not possible to increase the number of tubes in the bundle beyond the twelve used in this study.

The discrepancy between the present observations and those reported in the literature, that suggest a lower overall heat flux for a bundle because of vapour blanketing, may be due to several factors:

(i) Most of the data for large tube bundles reported in the literature are data which were obtained from tests on industrial boilers. The boiling surface condition was not reported. It is therefore possible that these bundles were heavily fouled with scaling and therefore extremely inefficient. The fouling aspect is extremely important in the present study because if the low heat fluxes reported on large bundles are caused strictly by fouling on tubes, the same penalty should not be applied to the calandria tubes which are essentially clean tubes.

Fouling has another important implication on the overall heat transfer coefficient. Extreme fouling may also reduce the available area (between adjacent tubes) through which the liquid-vapour mixture must flow; this decrease will increase the resistance to flow which in turn may decrease the overall bundle efficiency.

(ii) The large bundle may have a lower overall CHF than that for a single tube because insufficient liquid may be flowing into the bottom of the bundle to satisfy the liquid requirements in the bundle if all

tubes were boiling at the critical heat flux. This liquid can only flow into the bottom of the bundle because of the induced upward flow caused by the buoyancy of the vapour (the thermosyphon effect). This flow rate of liquid is determined by the available pressure head and integrated flow resistance offered by the tubes to the flowing two-phase mixture. Decreasing the tube spacing increases this resistance; increasing the fraction of the liquid vaporized also increases the resistance. Hence, it is quite reasonable to believe that in fact the so-called vapour blanketing effect (reduced overall heat flux) occurs not because the vapour somehow attaches to the tube and prevents the surrounding liquid from reaching the tube (implied by the term "blanketing") but because the upper tubes in the bundle are "starved" of liquid. This starving hypothesis suggests that better performance may be achieved in horizontal reboilers if the clearance between the tubes is increased so that the resistance to flow may be decreased. Alternatively, the pressure head (liquid head outside the bundle) could be increased to compensate for this increased resistance to flow.

This explanation is compatible with the literature data and the results obtained in the present study. It follows that to manufacture a more efficient boiler, it should be rectangular with a maximum of roughly eight rows deep with a reasonable pitch-to-diameter ratio (perhaps about 1.5).

7.5 Conclusion

From the results presented in this chapter, the following

conclusions can be made:

- (i) The reproducibility of the pool boiling data on a single tube has been established both on a copper tube and on a chrome-plated copper tube. The shape of the observed boiling curve varied from tube to tube but remained essentially unchanged for a given tube from experiment to experiment. Moreover, the critical heat flux density was nearly equal for all tubes investigated.
- (ii) The average critical heat flux density obtained in a single tube experiment on a 2.67 cm O.D. tube is 190 kW/m^2 with a standard deviation of about 5%. This value corresponds to about 80% of that predicted by Zuber's correlation and within the 20% range of accuracy claimed for Lienhard's extrapolation (90% of Zuber's prediction).
- (iii) The liquid level above a tube undergoing boiling has no effect on the critical heat flux density on that tube.
- (iv) The single row experiment showed that there is an interactive effect (enhancement) even when only one row is active. An average increase of about 8% was observed.
- (v) There is a significant "bundle effect" near the critical heat flux and in transition boiling regime with the present experimental system but no effect in the nucleate boiling regime. Table 7.4 summarizes the average percentage increase of the critical heat flux density when all active rows are at their CHF values. The increase reported is relatively independent of the amount of vapour rising from below if a given minimum quantity of vapour is exceeded. There is no evidence of a decrease, at least for the four row system investigated.

CHAPTER 8

SUMMARY AND CONCLUSIONS

8.1 Introduction

The objective of this experimental research program was to obtain boiling heat transfer data for the outside surface of any candria tube of a typical horizontal pressure tube nuclear reactor. This information was required for a single tube as well as a bundle of these tubes.

To achieve this objective a three-part experimental research program was initiated. The first part dealt with the acquisition of experimental boiling curves for various locations on the circumference of a 12.7 cm diameter copper cylinder. These boiling curves were established with a heat flux meter on cylinders of various lengths for different subcoolings of the quenching bath and for different areas of the boiling surface being active in the boiling process. The second portion of the experimental program provided unsteady-state boiling curves in a 5 by 3 bundle of copper cylinders for few angular locations and two levels of subcooling. A simulation of a larger array of tubes was achieved by injecting steam below the centre column of the array and measuring the effect on the boiling heat flux density on the cylinders in the array. Finally, the third part of this experimental program provided boiling heat transfer data for a 12-tube bundle under steady-

state conditions. The two bundles had the same pitch-to-diameter ratio (2.18) of the calandria tubes of a typical nuclear reactor.

The results obtained in each of these three parts have been presented and discussed in Chapter 5, 6 and 7 respectively. This chapter summarizes the major findings and presents the conclusions that can be drawn from the results.

8.2 Single Horizontal Cylinders

The results and the conclusions from this investigation are best summarized as they relate to local effects, on the one hand, and overall average effects on the other. These two aspects are discussed separately:

A. Local Heat Flux Density

1. A successful method for constructing a heat flux meter in a copper cylinder has been developed and has shown to provide instantaneous local boiling heat transfer densities during the quenching of the copper cylinder in saturated and subcooled water. Since difficulties arise in fabricating a meter to the ideal specifications, calibration of the meters was required. The calibration procedure which was developed was shown to be reasonable since:

- (i) Reproducibility of boiling curves by the quenching technique was achieved with different heat flux meters in different cylinders although the calibration factor for each was quite different.
- (ii) Solutions of the inverse conduction problem for the cylinders gave local cooling curves or heat flux densities which were comparable

to those indicated by a local temperature measurement or a calibrated heat flux meter, respectively.

(iii) A steady-state calibration procedure indicated that the calibration factors obtained by the quenching technique were reasonable.

On the other hand, it was found that the use of this type of heat flux meter is limited to unsteady-state experiments because of the inherent temperature depression on the heat flux meter and its vicinity.

2. The boiling curves generated for different angular locations around the cylinder show a severe variation which is attributable to the fluid hydrodynamics around the cylinder. This hydrodynamic effect shows a maximum influence in the CHF region. This large angular variation of CHF around a cylinder has heretofore not been reported. It was found, however, that the vapour-liquid flow around these large cylinders had a negligible effect on the boiling heat flux in the nucleate boiling regime. This effect was also demonstrated during the steady-state experiments.

Under subcooled conditions, the angular variation is less severe. The decrease in subcooling as the upward flowing liquid proceeds around the cylinder and other interactive effects of the natural convective flow and the forming and collapsing vapour bubbles should play a primary role in affecting local CHF under subcooled conditions.

In all cases, good reproducibility of the boiling curves was obtained.

3. The CHF at any point on a cylinder, whose surface is partially

insulated, is never less on the active boiling area than that which would be observed for a cylinder undergoing boiling over the entire area. At some angular locations, the heat flux density is considerably higher for the partially insulated cylinder. These results are a further indication that the variations in local heat flux density are a direct result of the interaction of the upflowing vapour with the boiling phenomena.

4. The results obtained with steam injection underneath a single copper cylinder indicate that the overall surface average CHF was essentially independent of the steam flowrate in the range investigated although the flowrate increased about threefold. On the other hand, it was observed that the local CHF over the lower portion of the cylinder (where the upflowing vapour first impinges) is much higher than over the rest of the cylinder. Similar results were also observed in the unsteady-state bundle experiments. In addition, the use of a partially insulated cylinder showed once more a considerable increase in CHF at the bottom location of the cylinder.

5. The wall temperature at which CHF occurs for a given cylinder was observed to vary considerably ($\pm 10^{\circ}\text{C}$ from the average) due in part to differences which were observed at different angular positions but mostly because of the difficulty in determining the exact temperature at which the CHF occurred. The variation from cylinder to cylinder was even greater, although an attempt was made to control the surface finish of the cylinders. Most of the variation from cylinder to

cylinder must be attributed to the difficulty in measuring the true surface temperature since it was known that the location of the actual thermocouple junction at the edge of the heat flux meter could not be controlled to the desired specifications.

As expected, when the level of subcooling was increased, it was observed that the CHF occurred at a higher wall superheat. This average increase is reported for the levels of subcooling investigated.

B. Overall Average Heat Flux Density

1. The overall average critical heat flux density at saturation on a single copper cylinder is about 110 W/cm^2 with a standard deviation of 12 W/cm^2 . This value is in excellent agreement with that predicted by Zuber's equation for boiling on a flat plate which is based on a hydrodynamic instability model. These results suggest that Lienhard's recommendation, which claims that the critical heat flux density for large cylinders should be 90 percent of that predicted for a flat plate, was not appropriate in this case, although CHF values found here are within the limits he suggests for his correlation. On the other hand, the seemingly good agreement between measured and predicted overall average critical heat flux density may be fortuitous given the rather large angular variation of CHF which was observed around the cylinder. Moreover, an increase in overall CHF was observed for a cylinder of twice the length.

2. The experimental overall average CHF obtained under subcooled conditions are very well correlated by the equations proposed by Ponter

and Haigh(P5) although, again, considerable variation of local CHF with position was observed.

3. The overall CHF for a 15.24 cm long cylinder is approximately 20% higher than that of both the 11.43 and 7.62 cm cylinders. Considerable effort was expended to determine the cause of this increase without success. It can be stated, however, that the cause of this increase can not be traced to the experimental system or procedure. It is suspected that this increase arises because the natural convective flow around the cylinder is larger for the longer cylinder.

4. It has been shown that adding a thermal resistance at the surface of the boiling surface (such as electroplated metal or oxidation product) changes the boiling curve that is obtained during a quenching experiment. The greatest effect occurs at the critical heat flux at which point the critical heat flux density may be reduced by as much as 40% when a copper cylinder is electroplated with a very thin layer of nickel. In this case, a thermal resistance is introduced at the nickel-copper interface.

8.3 Steady-State Calibration Experiments

Many experiments were performed under steady-state boiling conditions with an electrically-heated cylinder in an attempt to obtain a direct calibration of a heat flux meter which was installed in it. Although these experiments were not completely successful in achieving the stated objective, they did provide additional information which

was pertinent to the overall objectives of the program. These are summarized below:

(i) The rate of cooling did not affect the critical heat flux density as recorded by the heat flux meter. Furthermore these experiments demonstrated that the same critical heat flux was recorded whether the cylinder was heated from a low temperature (nucleate boiling) or whether it was cooled from some high temperature (transition boiling). This implied that there was no hysteresis effect. Hence the boiling curve obtained from the quenching experiments is representative of that which would have been measured under steady-state conditions.

(ii) An analysis to determine the temperature field in the vicinity of the heat flux meter was performed and it indicated that the heat flux meter, although very small relative to the overall heat transfer area, did affect the temperature distribution in the vicinity of the heat flux meter. The resulting temperature depression, along with the added effect of a thermal resistance between the copper plug which contained the meter, was determined as being the cause of the failure to achieve a direct calibration factor for the heat flux meter. This result was substantiated by direct visual observation of the boiling phenomena. Thus it is concluded that the particular design of the heat flux meter used in these quenching experiments cannot be used effectively under steady-state boiling conditions. It may be concluded, however, that this effect does not play an important role in the quenching experiments.

8.4 Unsteady-State Bundle Experiments

A substantial increase in heat flux was observed with the unsteady-state bundle system. The largest increase occurred at the bottom of the cylinder. The results obtained with this system corroborate those found with steam injection underneath a single copper cylinder. There was no evidence of a decrease in CHF with the 5 row system even when live steam was injected underneath to simulate additional rows.

8.5 Steady-State Bundle Experiments

1. The reproducibility of the local data on a single tube has been established both on a copper tube and a chrome-plated copper tube. Although the shape and the position of the boiling curves measured varied from tube to tube, it remained roughly unchanged for a given tube from experiment to experiment. Moreover, the CHF density was roughly equal for all tubes investigated.
2. The average critical heat flux density obtained in a single tube experiment on a 2.67 cm O.D. tube was about 190 kW/m^2 with a standard deviation of roughly 5%. This value corresponds to about 80% of the Zuber's prediction.
3. The average CHF for the 12-tube bundle was approximately 20% higher than the one observed for a single tube. Since it is well known that under some conditions (particularly those occurring in re-boilers), the upflowing vapour can cause the critical heat flux density

to be substantially lower, it can be concluded from the results obtained with the two bundles that the effect of vapour generation on the critical heat flux must be strongly dependent on the clearance between tubes in the bundle. Reducing the clearance to some value would inhibit the vapour-liquid flow and thus reduce the upward flow-rate or cause vapour blanketing; the CHF of the bundle would decrease accordingly. There is no evidence of a decrease in CHF at least for the two systems investigated.

CHAPTER 9

RECOMMENDATIONS FOR FUTURE WORK

As with any major research study, many aspects arise during the course of it, either by direct observation or through analysis, which require further study or investigation. Some of these are suggested below:

1. Length of Cylinder

One major problem which was left unresolved was the influence of length of cylinder on the critical heat flux density. The approximately 20 percent increase in CHF which was observed for a cylinder having twice the length of the cylinder, which was used in this study, was observed with three different cylinders and therefore length must play a real role in determining the critical heat flux on a large diameter cylinder. It was suggested that the increased natural convection caused by the longer length could be responsible for this increase.

There is also a possibility that the larger CHF could be caused by a hydrodynamic effect whereby the heat transfer on the surface is limited by the number of possible escaping jets that the length of the cylinder can accommodate. This effect may be resolved by performing quenching experiments on a very long cylinder (say 30 cm), equipped with a heat flux meter, and then reducing the length progressively (say in 5 cm steps).

2. Diameter of the Cylinder

The overall average critical heat flux was well predicted by Zuber's equation. It was suggested, however, that in the light of the severe variations of CHF around the cylinder that this excellent agreement may be somewhat fortuitous. This effect may be resolved by performing quenching experiments on cylinders of larger and smaller diameter.

3. Tube Bundle Effect

A. Experimental Program

There is a considerable amount of data accumulated on boiling in tube bundles which contain a large number of tubes. In most cases, there is a substantial reduction of the overall CHF for the bundle compared to that for a single tube. The results presented in this thesis and elsewhere (P3, W2) show that for a small bundle there is an appreciable increase and a vapour enhancement rather than a penalty should be applied. Therefore there is a need for a systematic investigation of boiling in tube bundles to understand the intrinsic boiling phenomena within the bundle.

As a first step, there is a need to investigate the effect of the pitch-to-diameter ratio with the steady-state tube bundle system used in this investigation. Experiments should be performed with the pitch-to-diameter ratios usually used in industry (1.25 and 1.50). If it is demonstrated that the tube spacing or arrangement is not a

significant parameter for small bundles, than larger bundles (greater number of rows) should be used. If the bundle size is limited by the steam supply, as it was in this investigation, then perhaps a new experimental system should be designed in which:

- (a) A liquid with lower latent heat of vaporization (e.g. Freon 13) is used.
- (b) Smaller diameter tubes are used (say 1.25 cm or 1.75 cm tubes)

B. Development of a Boiling Two-Phase Flow Hydrodynamic Model

It has been suggested in this thesis that the low overall average CHF values for the bundle may be caused not by a "vapour blanketing" effect but by a "liquid starvation" effect. This means that the liquid flow into the bottom of the tube bundle may not be sufficient to satisfy the demand if all tubes are operating at this critical heat flux. This hypothesis can be tested in two ways:

(i) Direct measurement of velocity profiles in the cross-section between the lower row of tubes and hence the liquid mass flowrate under given operating conditions.

(ii) Development of a mathematical model for the system based on the boiling and two-phase flow phenomena which occurs in bundles. This model requires:

- (a) Boiling curves for the tubes of the type generated by this study which include the effect of rising vapour and liquid.
- (b) Pressure drop of two-phase mixtures through tube banks under various gas and liquid flowrates.

- (c) Vapour hold-up correlations in two-phase flow for tube banks as a function of gas and liquid flowrate.

Each of these two-phase flow studies would be a major undertaking. Obviously the velocity profile measurements would be a way to test the model as would the direct measurement of heat flux density on each tube in the array.

These studies would provide very valuable information which could be used to improve the design criteria for horizontal reboiler systems.

REFERENCES

- A1 - Archambault, P. and Chevrier, J.C.,
"Distribution de la température au sein d'un cylindre trempé dans un liquide vaporisable",
Int. Journal of Heat and Mass Transfer, 20, 1, 1977.
- 81 - Bakru, N. and Lienhard, J.H.,
"Boiling from Small Cylinders",
Int. Journal of Heat and Mass Transfer, 15, 11, 2011, 1972.
- 82 - Bankoff, S.G.,
"A Note on Latent Heat Transport in Nucleate Boiling",
A.I.Ch.E. Journal, 8, 63, 1962.
- 83 - Bankoff, S.G. and Mehra, V.S.,
"A Quenching Theory for Transition Boiling",
IEC Fundamentals, 1, 1, 38, 1962.
- 84 - Beck, J.V.,
"Surface Heat Flux Determination Using an Integral Method",
Nuc. Eng. and Design, 7, 170, 1968.
- 85 - Berenson, P.J.,
"Film-Boiling Heat Transfer from a Horizontal Surface",
J. of Heat Transfer, 83, 351, 1961.
- 86 - Berenson, P.J.,
"Experiments on Pool-Boiling Heat Transfer",
Int. Journal of Heat and Mass Transfer, 5, 985, 1962.
- 87 - Bergles, A.E. and Rohsenow, W.M.,
"The Determination of Forced-Convection Surface-Boiling Heat Transfer",
J. of Heat Transfer, 86, 365, 1964.
- 88 - Bergles, A.E. and Thompson, Jr., W.G.,
"The Relationship of Quench Data to Steady-State Pool Boiling Data",
Int. Journal of Heat and Mass Transfer, 13, 55, 1968.
- 89 - Bernath, L.,
"Prediction of Heat Transfer Burnout",
Chem. Eng. Progress Symp. Series, 52, 18, 1, 1956.

- 810 - Bernath, L.,
"A Theory of Local-Boiling Burnout and Its Application to Existing Data",
Chem. Eng. Progress Symp. Series, 56, 95, 1960.
- 811 - Bradfield, W.S.,
"On the Effect of Subcooling on Wall Superheat in Pool Boiling",
J. of Heat Transfer, 89, 269, 1967.
- 812 - Breen, B.P. and Westwater, J.W.,
"Effect of Diameter of Horizontal Tubes of Film Boiling Heat Transfer",
Chem. Eng. Progress, 58, 7, 67, 1962.
- 813 - Brodkey, R.S.,
"The Phenomena of Fluid Motions",
Addison-Wesley Publishing Co., 1967.
- 814 - Brodsky, A.Z.,
Personal Communication,
January, 1978.
- 815 - Burggrof, O.R.,
"An Exact Solution of the Inverse Problem in Heat Conduction Theory and Applications",
J. of Heat Transfer, 86, 3, 373, 1964.
- C1 - Carnahan, B., Luther, H.A. and Wilkes, J.D.,
"Applied Numerical Method",
John Wiley and Sons, Inc., 1969.
- C2 - Chang, Y.P.,
"Some Possible Critical Conditions in Nucleate Boiling",
J. of Heat Transfer, 85, 89, 1963.
- C3 - Chaudhri, I.H. and McDougall, I.R.,
"Ageing Studies in Nucleate Pool Boiling of Isopropyl Acetate and Perchloroethylene",
Int. Journal of Heat and Mass Transfer, 12, 681, 1969.
- C4 - Chen, C.J. and Chiou, J.S.,
"Prediction of Surface Temperature and Heat Flux from an Interior Temperature Response",
Letters in Heat and Mass Transfer, 3, 539, 1976.
- C5 - Chen, C.J. and Thomsen, D.M.,
"On Transient Cylindrical Surface Heat Flux Predicted from Interior Temperature Response",
AIAA Journal, 13, 5, 697, 1975.

- C6 - Chen, J.C.,
"Correlation for Boiling Heat Transfer fo Saturated Fluids in Convective Flow",
I.E.C. Proc. Des. Dev., 5, 322, 1966.
- C7 - Cobb, C.B. and Park, Jr., E.L.,
"Correlation of the Maximum Heat Flux and Temperature Difference in the Nucleate Boiling of Corresponding States Liquids",
Advanced Cryogenic, 12, 381, 1967.
- C8 - Collier, J.G.,
"Convective Boiling and Condensation",
McGraw-Hill Book Co., London, 1972.
- C9 - Cooper, M.G. and Lloyd, A.J.P.,
"Transient Local Heat Flux in Nucleate Boiling",
Proc. Third International Heat Transfer Conference, Chicago, Vol III, 193, 1966.
- C10 - Corty, C. and Foust, A.S.,
"Surface Variables in Nucleate Boiling",
Chem. Eng. Progress Symp. Series, 51, 1, 1955.
- C11 - Costello, C.P. and Frea, W.J.,
"The Roles of Capillary Wicking and Surface Deposits in the Attainment of High Pool Boiling Burnout Heat Fluxes",
A.I.Ch.E. Journal, 10, 393, 1964.
- C12 - Cowley, C.W., Timson, W.J. and Sawdye, J.A.,
"A Method for Improving Heat Transfer to a Boiling Fluid",
IEC Process, Design and Development, 1, 2, 81, 1962.
- D1 - Dervedde, E.,
"Boiling Heat Transfer to Turbulent Liquid Film",
M. Eng. Thesis, McMaster University, 1966.
- F1 - Fand, R.M. and Ho, R.C.C.,
"An Evaluation of Rohsenow's Pool Boiling Correlation Equation",
Letters in Heat and Mass Transfer, 4, 239, 1977.
- F2 - Farber, E.A. and Scoriah, R.L.,
"Heat Transfer to Water Boiling Under Pressure",
Trans. ASME, 70, 369, 1948.
- F3 - "Fluid Meters, Their Theory and Application",
Fifth Edition ASME Publication, 1959.
- F4 - Forster, K.E. and Greif, R.,
"Heat Transfer to a Boiling Liquid-Mechanism and Correlations",
J. of Heat Transfer, 81, 43, 1959.

- G1 - Gaertner, R.F.,
"Effect of Surface Chemistry on the Level of Burnout Heat Flux
in Pool Boiling",
G.E. Report No. 63-RL-3449C, 1963.
- G2 - Gaertner, R.F.,
"Photographic Study of Nucleate Pool Boiling on a Horizontal
Surface",
J. of Heat Transfer, 87, 17, 1965.
- G3 - Gambill, W.R.,
"A Survey of Boiling Burn-Out",
British Chemical Engineering, 8, 2, 93, 1963.
- G4 - Gardon, R.,
"An Instrument for Direct Measurement of Intense Thermal Radia-
tion",
The Review of Scientific Instrument, 24, 366, 1953.
- G5 - Gardon, R.,
"A Transducer for the Measurement of Heat-Flow Rate",
J. of Heat Transfer, 82, 396, 1960.
- G6 - Githinji, P.M. and Sabersky, R.H.,
"Some Effects of the Orientation of the Heating Surface in
Nucleate Boiling",
J. of Heat Transfer, 85, 379, 1963.
- H1 - Han, C.Y. and Griffith, P.,
"The mechanism of Heat Transfer in Nucleate Pool Boiling-Part I",
Int. Journal of Heat and Mass Transfer, 8, 887, 1965.
- H2 - Han, C.Y. and Griffith, P.,
"The Mechanism of Heat Transfer in Nucleate Pool Boiling-Part II",
Int. Journal of Heat and Mass Transfer, 8, 905, 1965.
- H3 - Hesse, G.,
"Heat Transfer in Nucleate Boiling, Maximum Heat Flux and
Transition Boiling".
Int. Journal of Heat and Mass Transfer, 16, 1611, 1973.
- H4 - Hosler, E.R. and Westwater, J.W.,
"Film Boiling on a Horizontal Plate",
ARS Journal, 553, 1962.
- H5 - Hsu, Y.Y.,
"Gradual Transition of Nucleate Boiling from Discrete Bubble
Regime to Multibubble Regime".
Chem. Eng. Progress Symp. Series, 61, 59, 290, 1965.

- I1 - Imber, M. and Khan, J.,
"Prediction of Transient Temperature Distributions with Embedded Thermocouples",
AIAA Journal, 10, 6, 784, 1972.
- I2 - Ivey, H.J. and Morris, D.J.,
"Critical Heat Flux of Saturation and Subcooled Pool Boiling in Water at Atmospheric Pressure",
Proc. Third International Heat Transfer Conference, Chicago, Vol III, 129, 1966.
- J1 - Johnson, H.A.,
"Transient Boiling Heat Transfer to Water",
Int. Journal of Heat and Mass Transfer, 14, 67, 1971.
- J2 - Judd, R.L. and Merte, Jr., H.,
"Evaluation of Nucleate Boiling Heat Flux Predictions at Varying Levels of Subcooling and Acceleration",
Int. Journal of Heat and Mass Transfer, 15, 1075, 1972.
- K1 - Katto, Y. and Kikuchi, K.,
"Study of Forces Acting on a Heated Surface in Nucleate Boiling at High Heat Fluxes",
Heat Transfer - Japanese Research, 1, 4, 36, 1972.
- K2 - Kern, D.Q.,
"Process Heat Transfer",
McGraw-Hill Book Co., New York, 1950.
- K3 - Khosla, J.K.,
"Opposing Free and Forced Convective Heat Transfer to Turbulent Air Flow in a Vertical Pipe",
Ph.D. Thesis, McMaster University, 1973.
- K4 - Kreith, F.,
"Principles of Heat Transfer",
2nd ed., International Textbook Co., Pennsylvania, 1965.
- K5 - Kutateladze, S.S.,
"Fundamentals of Heat Transfer",
2nd ed., Edwards Arnold Ltd., 1963.
- L1 - Lance, R.P. and Myers, J.E.,
"Local Boiling Coefficients on Horizontal Tube",
A.I.Ch.E. Journal, 4, 1, 75, 1958.
- L2 - Leppert, G. and Pitts, C.C.,
"Boiling", drawn from "Advances in Heat Transfer",
ed. by T.F. Irving Jr. and J.P. Harnett, V.1, Academic Press, 1964.

- L3 - Lienhard, J.H. and Dhir, V.K.,
"Hydrodynamic Prediction of Peak Pool-Boiling Heat Fluxes from Finite Bodies",
J. of Heat Transfer, 95, 152, 1973.
- L4 - Lienhard, J.H., Dhir, V.K. and Rihard, D.M.,
"Peak Pool Boiling Heat Flux Measurements on Finite Horizontal Flat Plates",
J. of Heat Transfer, 95, 477, 1973.
- L5 - Lienhard, J.H. and Schrock, V.E.,
"The Effect of Pressure, Geometry, and the Equation of State Upon the Peak and Minimum Boiling Heat Flux",
J. of Heat Transfer, 85, 261, 1963.
- L6 - Lienhard, J.H. and Watanabe, K.,
"On Correlating the Peak and Minimum Boiling Heat Fluxes With Pressure and Heater Configuration",
J. of Heat Transfer, 88, 94, 1966.
- L7 - Lienhard, J.H. and Wong, P.T.Y.,
"The Dominant Unstable Wavelength and Minimum Heat Flux During Film Boiling on a Horizontal Cylinder",
J. of Heat Transfer, 86, 220, 1964.
- M1 - Malek, R.G.,
"Predict Nucleate Boiling Transfer Rates",
Hydrocarbon Processing, 52, 2, 89, 1973.
- M2 - McAdams, W.H.,
"Heat Transmission",
3rd ed., McGraw-Hill Book Co., New York, 1954.
- M3 - McAdams, W.H. et al.,
"Heat Transfer from Single Horizontal Wires to Boiling Water",
Chem. Eng. Progress, 44, 639, 1948.
- M4 - Merte, Jr., H. and Clark, J.A.,
"Boiling Heat Transfer with Cryogenic Fluids at Standard, Fractional, and Near-Zero Gravity",
J. of Heat Transfer, 86, 3, 351, 1964.
- M5 - Moissis, R. and Berenson, P.J.,
"On the Hydrodynamic Transitions in Nucleate Boiling",
J. of Heat Transfer, 85, 221, 1963.
- M6 - Moore, F.D. and Mesler, R.B.,
"The Measurement of Rapid Surface Temperature Fluctuations During Nucleate Boiling of Water",
A.I.Ch.E. Journal, 7, 620, 1961.

- N1 - Nishikawa, K. et al.,
"Pool Film Boiling Heat Transfer from a Horizontal Cylinder to Saturated Liquids",
Int. Journal of Heat and Mass Transfer, 15, 853, 1972.
- N2 - Nishikawa, K. and Yamagata, K.,
"On the Correlation of Nucleate Boiling Heat Transfer",
Int. Journal of Heat and Mass Transfer, 1, 219, 1960.
- N3 - Northover, E.W. and Hitchcock, J.A.,
"A Heat Flux Meter for Use in Boiler Furnaces",
J. Sci. Instr., 44, 371, 1967.
- N4 - Nukiyama, S.,
"The Maximum and Minimum Values of the Heat Q Transmitted from Metal to Boiling Water Under Atmospheric Pressure",
Int. Journal of Heat and Mass Transfer, 9, 1419, 1966.
- P1 - Palen, J.W. and Small, W.M.,
"A New Way to Design Kettle and Internal Reboilers",
Hydrocarbon Processing and Petroleum Refiner, 43, 11, 199, 1964.
- P2 - Palen, J.W. and Taborek, J.J.,
"Refinery Kettle Reboilers Proposed Method for Design and Optimization",
Chem. Eng. Progress Symp. Series, 7, 58, 37, 1962.
- P3 - Palen, J.W., Yarden, A. and Taborek, J.,
"Characteristics of Boiling Outside Large-Scale Horizontal Multitube Bundles",
A.I.Ch.E. Symp. Series, 68, 118, 50, 1972.
- P4 - Paschkis, V. and Stolz, Jr., G.,
"Research and Development With Respect to Heat Transfer in Quenching",
Final Report, Columbia University.
Heat and Mass Flow Analyser Lab., New York, 1962.
52pp. ARDD-1540:6.
- P5 - Ponter, A.B. and Haigh, C.P.,
"The Boiling Crisis in Saturated and Subcooled Pool Boiling at Reduced Pressures",
Int. Journal of Heat and Mass Transfer, 12, 429, 1969.
- P6 - Pramuk, F.S. and Westwater, J.W.,
"Effect of Agitation on the Critical Temperature Difference for a Boiling Liquid",
Chem. Eng. Progress Symp. Series, 52, 18, 79, 1956.

- R1 - Rallis, C.J. and Jawurek, H.H.,
"Latent Heat Transport in Saturated Nucleate Boiling",
Int. Journal of Heat and Mass Transfer, 7, 1051, 1964.
- R2 - Rao, S.N.,
"Effect of Surface Active Agents in Boiling Heat Transfer",
M. Eng. Thesis, McMaster University, 1967.
- R3 - Reinsch, C.H.,
"Smoothing by Spline Functions",
Numerische Mathematik, 10, 3, 177, 1967.
- R4 - Robinson, D.B. and Katz, D.L.,
"Effect of Vapor Agitation on Boiling Coefficients",
C. E. P., 47, 6, 317, 1951.
- R5 - Rogers, J.T.,
Unpublished Report,
August, 1972.
- R6 - Rohsenow, W.M.,
"Heat Transfer With Boiling",
Drawn from "Developments in Heat Transfer", Chap. 8,
The M. I. T. Press, Cambridge, 1964.
- R7 - Rohsenow, W.M. and Clark, J.A.,
"A Study of the Mechanism of Boiling Heat Transfer",
Trans. ASME, 73, 609, 1951.
- R8 - Rohsenow, W.M. and Griffith, P.,
"Correlation of Maximum-Heat-Flux Data for Boiling of Saturated
Liquids",
Chem. Eng. Progress Symp. Series, 52, 18, 47, 1956.
- R9 - Rohsenow, W.M. and Hartnett, J.P.,
"Handbook of Heat Transfer",
McGraw-Hill, 1973.
- R10 - Roll, J.B. and Myers, J.E.,
"The Effect of Surface Tension on Factors in Boiling Heat
Transfer",
A.I.Ch.E. Journal, 10, 530, 1964.
- R11 - Rosta, P.Z.,
Unpublished Report,
April 1972.
- S1 - Sainsbury, J.D.,
Unpublished Symposium.

- S2 - Sparrow, E.M., Haji-Sheikh, A. and Lundgren, T.S.,
"The Inverse Problem in Transient Heat Conduction",
J. of Applied Mechanics, 31, 369, 1964.
- S3 - Stolz, Jr., G.,
"Numerical Solutions to an Inverse Problem of Heat Conduction
for Simple Shapes",
J. of Heat Transfer, 82, 20, 1960.
- S4 - Stolz, Jr., G. et al.,
"Thermal Considerations in Oil Quenching",
J. of The Iron and Steel Institute, 193, 116, 1959.
- S5 - Sun, K.H. and Lienhard, J.H.,
"The Peak Pool Boiling Heat Flux on Horizontal Cylinders",
Int. Journal of Heat and Mass Transfer, 13, 9, 1425, 1970.
- T1 - Taborek, J. et al.,
"Fouling-The Major Unresolved Problem in Heat Transfer",
A.I.Ch.E. Symp. Series, 68, 118, 45, 1972.
- T2 - Tachibana, F., Akiyama, M. and Kawamura, H.,
"Heat Transfer and Critical Heat Flux in Transient Boiling,
(I) An Experimental Study in Saturated Pool Boiling",
Journal of Nuclear Science and Technology, 5, 3, 117, 1968.
- T3 - Tachibana, F and Enya, S.,
"Heat Transfer Problems in Quenching",
Bulletin of the JSME, 16, 91, 101, 1973.
- T4 - Thibault, J. and Hoffman, T.W.,
Letter to the Editor
To be Published in the Int. Journal of Heat and Mass Transfer.
- V1 - Vereas, D.R. and Florschuetz, L.W.,
"A Comparison of Transient and Steady-State Pool-Boiling Data
Obtained Using the Same Heating Surface",
J. of Heat Transfer, 93, 229, 1971.
- V2 - Voutsinos, C.M. and Judd, R.L.,
"Laser Interferometric Investigation of the Microlayer Evapo-
ration Phenomena",
J. of Heat Transfer, 97, 1, 88, 1975.
- W1 - Wall, K.W.,
"Nucleate Boiling of n-Pentane, n-Hexane and Several Mixtures
of the Two in Various Tube Arrays",
Ph.D. Thesis, University of Missouri-Rolla, 1974.

- W2 - Wall, K.W. and Park, Jr., E.L.,
"Nucleate Boiling on n-Pentane, n-Hexane and Several Mixtures
of the Two from Various Tube Arrays",
Int. Journal of Heat and Mass Transfer, 21, 73, 1978.
- W3 - Welly, J.R., Wicks, C.E. and Wilson, R.E.,
"Fundamentals of Momentum, Heat and Mass Transfer",
John Wiley & Sons Inc., New York, 1969.
- W4 - Westwater, J.W. and Santagelo, J.C.,
"Photographic Study of Boiling",
I.E.C., 47, 1605, 1955.
- Y1 - Yamagata, K. et al.,
"Nucleate Boiling of Water on the Horizontal Heating Surface",
Mem. Fac. Eng., Kyushu Univ., Japan, 15, 1, 97, 1955.
- Y2 - Yamanis, J.,
"The Instantaneous Local Heat Flux in a Scraped-Surface Heat
Exchanger",
M. Eng. Thesis, McMaster University, 1970.
- Z1 - Zuber, N.,
"On the Stability of Boiling Heat Transfer",
Trans. ASME, Paper No. 57-HT-4, 1957.
- Z2 - Zuber, N.,
"Nucleate Boiling. The Region of Isolated Bubbles and the
Similarity with Natural Convection",
Int. Journal of Heat and Mass Transfer, 6, 53, 1963.
- Z3 - Zuber, N.,
"Recent Trends in Boiling Heat Transfer Research-Part I:
Nucleate Pool Boiling",
Applied Mechanics Review, 17, 9, 663, 1964.
- Z4 - Zuber, N., Tribus, M. and Westwater, J.W.,
"The Hydrodynamic Crisis in Pool Boiling of Saturated and
Subcooled Liquids",
Paper 27, Second International Heat Transfer Conference,
Boulder, Colorado, 1961.

APPENDIX A

TABLE OF PROPERTIES USED IN THIS STUDY

Properties	Unit	Water	Heptane	Copper
Molecular Weight	g/mole	18	100.2	63.5
Boiling Point	deg. C	100	98.4	—
Lat. Heat of Vap.	J/g	2256	320	—
Thermal Capacity	J/gC	4.216	2.242	.381
Vapour Density	g/cc	.000598	.00348	—
Liquid Density	g/cc	.958	.679	—
Viscosity	g/cms	.00282	.00209	—
Surface Tension	Dyne/cm	58.8	12.6	—
Thermal Cond.	w/cm C	.00681	.00133	3.738
Solid Density	g/cc	—	—	8.894
Zuber's CHF	w/cm ²	110.7	23.6	—

1 Dyne = 1 g.cm/s² = 10⁻⁵N

INDIVIDUAL CALIBRATION

Tube No.	Raw Data				Boiling Curve	
	Pressure (psig)	Temp. (mV)	Volume (cc)	Time (s)	Temp. (°C)	Heat Flux (MW/m ²)
July 29, 1976						
1	30	4.82	762.	480.0	110.5	134.1
1	40	4.81	794.	505.2	110.3	132.8
1	41.	5.03	922.	420.0	114.9	182.0
1	51.	5.07	846.	397.8	115.8	176.3
1	51.	5.28	933.	430.2	120.2	179.8
1	51	5.38	870.	438.0	122.3	155.2
1	51	5.45	795.	430.2	123.7	153.4
1	51	4.81	866.	499.8	110.3	144.1
1	32	4.80	848.	478.8	110.1	141.4
1	32	4.79	774.	435.0	109.9	150.0
1	31	4.84	817.	424.2	110.9	161.6
1	37.	4.84	931.	475.8	110.9	164.2
1	62	5.95	383.	781.8	134.1	40.3
1	62.	5.95	345.	691.8	134.1	41.0
1	43.	4.92	794.	388.8	112.6	170.4
1	43.	4.93	847.	423.4	112.8	170.1
1	35	4.80	727.	370.8	110.1	164.8
1	35.	4.80	829.	435.0	110.1	160.2
1	31	4.80	710.	364.8	110.1	163.3
1	99	6.65	352.	621.0	148.4	45.4
1	99.	6.58	366.	646.8	147.0	45.4
1	18.	4.60	690.	577.2	105.8	102.4
1	18	4.50	670.	594.0	105.8	96.6
1	37.	4.80	642.	322.8	110.1	166.9

Tube No.	Raw Data				Boiling Curve	
	Pressure (psig)	Temp. (mV)	Volume (cc)	Time (s)	Temp. (°C)	Heat Flux (MW/m ²)
August 5, 1976						
2	25.	4.96	706.	460.8	113.5	110.2
2	24.	4.95	531	346.8	113.2	130.1
2	86	6.80	461.	433.2	151.5	84.0
2	86	6.80	525	508.8	151.5	83.4
2	55	5.44	740	377.8	123.4	201.1
2	56	5.46	717	303.0	123.9	191.9
2	56	5.48	652.	277.0	124.4	199.3
2	31	4.96	936	490.8	113.5	161.0
2	31	4.96	775	396.0	113.5	164.1
2	49.	5.23	680	285.0	119.5	198.1
2	49	5.24	781	322.8	119.3	200.9
2	96	6.09	663	348.0	137.0	107.1
2	66.	6.05	860	426.0	136.4	105.4
2	66.	6.04	826.	418.8	136.0	101.6
2	29	4.96	869.	493.2	113.5	169.0
2	29	4.95	920.	514.2	113.2	151.4
2	52.	5.36	709	298.8	121.9	196.5
2	52	5.33	775.	337.8	121.2	190.0
2	102.	7.15	397	549.0	158.5	57.9
2	104.	7.15	385.	525.0	158.5	58.6
2	28.	4.96	618	358.2	113.5	146.1
2	28.	4.96	542.	318.0	113.5	144.3
2	65.	5.79	744.	325.8	130.8	187.2
2	65	5.77	658	276.0	130.4	185.5
2	65.	5.79	661	294.0	130.8	184.3

July 30, 1976						
1	36.	4.80	990.	502.8	110.1	165.4
1	43.	4.81	836.	426.0	110.3	164.8
1	43.	5.27	783.	460.8	120.0	141.8
1	43.	5.26	876.	499.8	119.8	146.1
1	43	5.20	845.	471.0	118.5	149.7
1	53.	5.58	1004.	571.0	124.4	145.0
1	53	5.57	800.	448.8	116.2	147.5
1	31	4.80	679.	360.0	110.1	159.2
1	32.	4.80	709.	366.0	110.1	163.4
1	32	4.80	957.	490.8	110.1	166.2
1	13.	4.56	670.	389.8	105.0	98.0
1	13	4.56	728.	418.8	105.0	75.6
1	45	5.02	873.	418.8	114.7	174.4
1	40	5.02	765.	375.2	114.7	171.4
1	31.	4.80	635.	340.2	110.1	157.8
1	100	6.80	318.	543.0	151.5	46.9
1	71	5.98	750.	390.0	134.7	158.9
1	73	5.97	697.	370.2	134.5	151.5
1	31	4.80	754	400.2	110.1	159.0

August 12, 1976						
3	48.	5.09	790.	373.0	116.2	180.8
3	48	5.07	756.	342.0	115.8	183.7
3	33.	4.88	742.	405.8	111.3	150.9
3	31.	4.86	937.	521.2	111.3	150.9
3	66	5.92	780	418.8	144.1	142.5
3	66	5.90	886.	466.8	133.1	142.5
3	66	5.92	832	480.0	133.5	142.5
3	14	4.81	537	633.0	105.1	113.1
3	14	4.60	648.	694.2	105.8	80.4
3	82.	6.57	452	654.0	144.8	46.0
3	82	6.46	514	639.0	144.8	44.2
3	82.	6.36	403.	534.8	144.8	44.2
3	43.	5.09	895.	421.2	116.2	177.3
3	43	5.06	788.	355.8	115.6	184.8
3	63	5.00	838.	418.8	114.3	157.8
3	18.	4.99	747	369.0	114.7	114.7
3	57	5.36	1271.	534.0	121.9	196.3
3	57	5.31	773.	316.4	120.8	202.8
3	57	5.29	671	280.2	120.4	197.4
3	102	6.88	371.	586.2	153.1	50.7
3	102	6.88	387	610.2	153.1	50.8
3	48	5.09	649.	274.8	116.2	196.2
3	48.	5.09	702	304.2	116.2	191.8

August 4, 1976						
2	33.	5.01	958.	520.8	114.5	155.0
2	33.	5.01	878.	474.0	114.5	156.0
2	45.	5.19	776.	434.4	118.3	187.2
2	45.	5.19	849.	367.2	118.3	192.6
2	102.	7.18	496.	640.8	159.1	61.9
2	102.	7.16	533.	661.2	158.7	64.4
2	22	5.00	806.	649.2	114.3	105.9
2	23.	5.00	746.	370.0	114.3	111.5
2	24.	5.00	846.	634.8	114.3	112.7
2	52	5.46	787.	343.8	123.9	189.6
2	52	5.40	865.	390.0	124.4	188.1
2	58	5.62	858.	372.0	127.3	190.1
2	57.	5.65	813.	348.0	127.9	192.6
2	28.	5.00	814.	487.8	114.3	141.3
2	28	5.00	908.	538.2	114.3	142.9
2	68.	5.74	91	405.0	133.9	192.1
2	68.	5.94	872	361.2	133.9	197.3
2	67.	5.86	847.	358.8	132.2	193.3
2	71.	6.13	711.	292.8	137.8	197.3
2	71.	6.15	756.	310.2	138.2	198.0
2	71.	6.37	808.	325.2	142.7	199.8
2	70.	6.38	773.	316.8	142.9	198.7
2	24	5.07	604.	490.2	114.3	118.7
2	25.	5.00	509.	330.0	116.3	131.1

August 18, 1976						
3	44	5.26	768.	373.2	119.8	171.0
3	44	5.26	842.	406.2	119.8	172.8
3	64	6.12	575.	285.0	137.6	165.5
3	64	6.14	632.	307.2	138.0	168.8
3	17	4.93	370.	409.2	112.8	77.6
3	17	4.93	342.	388.2	112.8	75.6
3	103.	7.34	359.	546.0	162.3	52.6
3	94.	7.33	372.	397.8	162.1	75.2
3	58.	5.99	514.	232.8	134.9	182.0
3	58	6.01	607	273.0	135.3	183.3
3	53.	5.67	575	253.8	128.3	187.4
3	53.	5.66	591.	262.2	128.1	186.5
3	79	6.59	440	343.2	147.2	104.1
3	79	6.70	267.	385.8	149.4	56.2
3	57	5.81	575.	238.0	131.2	190.6
3	57	5.83	474.	241.2	131.6	196.1
3	37.	5.26	517	310.2	119.8	145.3
3	37.	5.26	645.	385.2	119.8	140.5

INDIVIDUAL CALIBRATION

Tube No.	Raw Data				Rolling Curve	
	Pressure (psig)	Temp. (mV)	Volume (cc)	Time (s)	Temp. (°C)	Heat Flux (kW/m ²)
August 14, 1976						
3	37.	5.25	728.	435.6	119.5	140.2
3	37.	5.26	622.	372.0	119.8	140.3
3	58.	5.96	591.	309.0	134.3	157.6
3	58.	5.97	613.	324.0	134.5	158.9
3	104.	7.37	597.	993.0	162.9	168.1
3	104.	7.37	277.	448.2	162.9	168.1
3	14.	4.91	332.	583.2	112.4	139.0
3	14.	4.92	366.	403.8	112.6	139.0
3	14.	4.91	334.	487.2	112.8	139.1
3	14.	5.83	949.	472.2	131.6	165.9
3	14.	5.83	656.	325.8	131.6	166.2
3	53.	5.47	568.	259.8	124.1	180.9
3	53.	5.47	820.	377.4	124.1	179.8
3	69.	6.61	241.	415.2	147.6	175.5
3	69.	6.63	327.	585.0	148.0	175.5
3	57.	5.65	860.	388.2	127.9	182.7
3	57.	5.65	695.	321.6	127.9	178.3
3	57.	5.67	651.	289.2	128.3	185.7
3	31.	5.26	451.	336.6	119.8	113.1
3	31.	5.26	415.	304.2	119.8	115.2

August 16, 1976

4	49.	5.29	737.	330.0	120.4	185.4
4	49.	5.30	973.	439.8	120.6	183.7
4	75.	6.73	334.	580.2	150.1	146.9
4	75.	6.71	418.	674.4	149.6	150.5
4	35.	5.18	894.	508.2	110.1	147.9
4	35.	5.15	911.	520.2	117.5	147.2
4	60.	5.53	864.	370.8	123.4	191.8
4	60.	5.54	868.	385.8	125.6	185.2
4	70.	5.54	922.	423.0	125.6	179.4
4	67.	5.76	846.	432.6	134.3	160.5
4	67.	5.96	753.	399.0	134.3	153.9
4	7	5.96	744.	415.8	134.3	146.5
4	4	5.30	907.	427.2	120.6	176.3
4	49.	5.30	911.	428.4	120.6	176.5
4	19.	4.05	608.	586.8	111.1	180.7
4	19.	4.84	619.	649.8	110.9	181.5
4	103.	7.31	387.	630.0	161.7	149.1
4	103.	7.31	426.	676.8	161.7	150.6
4	29.	5.00	837.	528.0	114.3	134.1
4	62.	5.60	900.	398.4	126.9	185.6
4	62.	5.60	821.	360.0	126.9	187.4
4	44.	5.33	747.	360.0	120.6	172.4
4	44.	5.30	763.	360.0	120.6	176.1

August 17, 1976

4	48.	5.10	849.	396.0	116.4	178.1
4	48.	5.11	892.	427.2	116.6	173.5
4	48.	5.11	830.	393.0	116.6	175.5
4	68.	5.62	763.	373.8	127.3	167.0
4	68.	5.72	952.	471.0	129.3	165.4
4	17	4.64	555.	585.0	106.7	181.4
4	17	4.64	568.	580.2	106.7	184.0
4	103	6.96	432.	619.8	154.7	155.8
4	101.	6.97	447.	598.2	154.9	159.8
4	77.	6.02	879.	487.8	135.5	146.5
4	77.	6.07	780.	486.0	136.6	130.5
4	77.	6.17	680.	442.2	138.6	125.0
4	49.	5.11	828.	364.8	116.6	188.4
4	49.	5.13	994.	439.8	117.0	187.6
4	31.	4.91	940.	577.8	112.4	137.3
4	31.	4.91	792.	475.2	112.4	140.7
4	60.	5.33	900.	384.0	121.2	192.9
4	60.	5.34	917.	388.2	121.4	194.4
4	61.	5.45	738.	325.8	123.7	185.0
4	61.	5.43	868.	375.0	123.3	190.1
4	44.	6.53	445.	600.0	146.0	160.1
4	44.	5.09	747.	354.0	116.2	175.9
4	44.	5.09	736.	343.2	116.2	178.8

TUBE BUNDLE

Tube No.	Raw Data				Rolling Curve	
	Pressure (psig)	Temp. (mV)	Volume (cc)	Time (s)	Temp. (°C)	Heat Flux (kW/m ²)
June 7, 1977						
1	61.	6.02	689.	396.9	115.5	142.8
1	60.	6.02	577.	318.8	115.5	149.0
1	99.	7.13	520.	407.9	148.1	102.3
1	7.	4.30	575.	426.7	99.4	117.4
1	38.	5.00	835.	393.9	114.3	177.8
1	51.	5.40	845.	357.2	122.7	192.2
1	63.	6.02	690.	334.2	135.5	169.5
1	77.	6.61	503.	379.9	147.6	107.7
1	16.	4.64	405.	402.4	106.7	86.5
2	24.	4.87	521.	394.6	111.6	111.4
2	68.	6.06	770.	348.7	136.4	180.8
2	7.	4.40	740.	358.3	101.6	179.9
2	2.	4.23	218.	427.1	98.0	141.9
2	19.	4.77	375.	351.4	109.4	97.4
2	57.	5.65	942.	397.4	127.9	195.5
2	92.	6.78	825.	375.1	151.1	177.2
2	50.	5.28	838.	366.2	120.2	189.9
2	30.	5.04	512.	304.9	115.1	142.0

1	53.	5.42	886.	337.1	123.1	217.6
2	70.	5.60	975.	348.7	126.9	236.4
1	53.	5.40	850.	352.4	122.7	199.7
2	19.	4.80	398.	410.1	110.1	96.7
1	53.	5.42	929.	385.4	123.1	199.5
2	19.	4.80	470.	410.1	110.1	104.4
1	52.	5.40	824.	328.2	122.7	206.0
2	75.	6.00	870.	348.7	135.1	215.9
1	49.	5.30	781.	326.7	120.6	194.6
2	49.	5.20	801.	318.5	118.5	203.7
1	50.	5.30	887.	330.9	120.6	222.5
2	83.	6.35	831.	342.3	142.3	203.5
1	15.	4.64	310.	334.7	106.7	107.7
2	87.	6.51	837.	342.3	145.6	202.1
1	15.	4.64	474.	413.1	106.7	98.8
2	67.	5.60	1154.	342.3	126.9	220.3
1	14.	4.64	356.	375.4	106.7	81.6
2	37.	5.05	658.	342.3	115.4	148.0
1	72.	6.30	655.	412.0	141.1	170.0
2	30.	5.00	682.	342.3	114.3	174.4
1	72.	6.23	722.	326.6	119.9	179.9
2	72.	5.65	953.	342.3	127.9	239.7
1	71.	6.28	785.	372.3	140.9	172.2
2	86.	6.42	916.	342.3	143.7	199.0
1	71.	6.20	779.	341.1	139.2	185.6
2	74.	5.63	966.	342.3	127.5	215.0
1	43.	5.40	839.	336.7	122.7	205.1
2	30.	5.05	584.	342.3	115.4	146.6

June 9, 1977

1	61.	5.60	840.	315.2	126.9	219.3
1	60.	5.55	818.	336.4	125.8	200.2
1	100.	7.21	390.	405.7	159.7	77.1
1	12.	4.02	496.	455.9	106.3	94.0
1	55.	5.48	845.	313.3	124.4	223.0
1	69.	6.10	825.	352.5	137.2	191.4
2	60.	5.58	910.	372.0	126.4	201.4
2	12.	4.70	295.	402.0	108.0	63.4
2	71.	6.23	712.	350.6	139.9	165.9
2	96.	7.02	465.	378.5	155.9	96.7
3	64.	4.89	1055.	428.2	112.0	202.1
3	97.	6.46	290.	437.4	144.6	53.3
3	83.	5.35	878.	409.4	121.5	173.8
3	11.	4.42	483.	385.5	102.0	108.4
3	40.	4.72	700.	392.4	108.4	149.4
3	78.	5.30	960.	364.4	116.4	214.2
1	57.	5.48	894.	333.7	124.4	221.1
3	78.	4.97	1210.	413.7	113.7	246.7
1	56.	5.48	845.	329.5	124.4	211.8
3	34.	4.64	520.	328.5	106.7	132.9
3	58.	5.50	824.	328.5	124.8	206.9
3	57.	4.78	827.	328.5	109.7	207.8
3	58.	5.42	792.	304.5	123.1	206.4
3	95.	6.35	251.	142.3	142.3	49.5
1	57.	5.42	780.	306.4	123.1	210.1
3	94.	5.07	988.	342.3	115.8	259.5

APPENDIX C

EXPERIMENTAL RESULTS OBTAINED WITH SINGLE COPPER CYLINDERS

The data presented in this appendix were obtained on single 12.7 cm diameter horizontal copper cylinders which were instrumented with a heat flux meter. A complete boiling curve was obtained for each experiment. However, only the critical heat flux density (CHF), the temperature at which the critical heat flux occurred (TCHF) and the inverse calibration ratio (I.C.R.) are presented in this appendix. The block number and the quenching bath subcooling are given for each set of data. The data presented are for a 7.62 cm long cylinder, for side number 1 of the heat flux meter, in distilled water and with no external agitation unless specified otherwise.

DEFINITION OF VARIABLES

BN - Block number

SN - Side number

CN - Code number

0 - 7.62 cm long, uninsulated

1 - 7.62 cm long, insulated to 60° angle

2 - 7.62 cm long, insulated to 30° angle

3 - 15.24 cm long, uninsulated

4 - 15.24 cm long, insulated axially to leave 10.16 cm length

5 - 15.24 cm long, insulated axially to leave 6.35 cm length

6 - 11.43 cm long, uninsulated

10 - +0.020 mV to normal difference temperature offset

11 - -0.020 mV to normal difference temperature offset

12 - codes 1 and 83 together

IJ - vapour injection system

I = 7 - orifice upstream pressure = 20 psig

I = 8 - orifice upstream pressure = 40 psig

I = 9 - orifice upstream pressure = 60 psig

J = 1 - distance between the sparger and the cylinder = 6 cm

J = 2 - distance between the sparger and the cylinder = 19 cm

J = 3 - distance between the sparger and the cylinder = 32 cm

RUN - Run number

ANGLE - Angular location of the heat flux meter

TCHF - Temperature at which CHF occurred

CHF - Critical heat flux density

The following calibration factors were used in this study:

<u>BLOCK NUMBER</u>	<u>CALIBRATION FACTOR</u>
2	.528
5	.705
5*	.942
7	.906
8	.786
9	1.008
11	.279
12	.483
13	.946
14	.508
15	.704
17	.644
20	1.353
22	.873
23	.706
23*	.532

* Side number 2

BY	NSUB	ICF	DF	I.C.P.
	(°C)	(°C)	(W/cm ²)	(ft ²)
11	11	11	11	11
12	12	12	12	12
13	13	13	13	13
14	14	14	14	14
15	15	15	15	15
16	16	16	16	16
17	17	17	17	17
18	18	18	18	18
19	19	19	19	19
20	20	20	20	20
21	21	21	21	21
22	22	22	22	22
23	23	23	23	23
24	24	24	24	24
25	25	25	25	25
26	26	26	26	26
27	27	27	27	27
28	28	28	28	28
29	29	29	29	29
30	30	30	30	30
31	31	31	31	31
32	32	32	32	32
33	33	33	33	33
34	34	34	34	34
35	35	35	35	35
36	36	36	36	36
37	37	37	37	37
38	38	38	38	38
39	39	39	39	39
40	40	40	40	40
41	41	41	41	41
42	42	42	42	42
43	43	43	43	43
44	44	44	44	44
45	45	45	45	45
46	46	46	46	46
47	47	47	47	47
48	48	48	48	48
49	49	49	49	49
50	50	50	50	50
51	51	51	51	51
52	52	52	52	52
53	53	53	53	53
54	54	54	54	54
55	55	55	55	55
56	56	56	56	56
57	57	57	57	57
58	58	58	58	58
59	59	59	59	59
60	60	60	60	60
61	61	61	61	61
62	62	62	62	62
63	63	63	63	63
64	64	64	64	64
65	65	65	65	65
66	66	66	66	66
67	67	67	67	67
68	68	68	68	68
69	69	69	69	69
70	70	70	70	70
71	71	71	71	71
72	72	72	72	72
73	73	73	73	73
74	74	74	74	74
75	75	75	75	75
76	76	76	76	76
77	77	77	77	77
78	78	78	78	78
79	79	79	79	79
80	80	80	80	80
81	81	81	81	81
82	82	82	82	82
83	83	83	83	83
84	84	84	84	84
85	85	85	85	85
86	86	86	86	86
87	87	87	87	87
88	88	88	88	88
89	89	89	89	89
90	90	90	90	90
91	91	91	91	91
92	92	92	92	92
93	93	93	93	93
94	94	94	94	94
95	95	95	95	95
96	96	96	96	96
97	97	97	97	97
98	98	98	98	98
99	99	99	99	99
100	100	100	100	100

Angle	Run	W/F	Avg. CHF (W/cm ²)	IQF (°C)	L.G.B.	L.Aver. G.D. (mm)	Angle	Run	W/F	Avg. CHF (W/cm ²)	IQF (°C)	L.G.B.	L.Aver. G.D. (mm)	
Block Number 2 Saturation							Block Number 2 10°C Subcooling							
0	15	217.3	226.5	122.6	.1451	.1323	0	86	307.5	316.2	138.3	.1666	.1754	
	16	238.4		122.4	.1451			87	324.8		145.0	.1852		
	26	246.6		132.8	.1225									
	27	255.8		131.1	.1161		30	76	246.3	263.2	126.1	.1400	.1522	
	58	175.0		127.2	.1282			77	280.0		151.7	.1668		
	59	236.1		125.0	.1429									
30	13	132.2	157.7	118.3	.1975	.1831	60	88	225.8	222.7	118.8	.1230	.1317	
	14	209.1		117.6	.1600			89	220.4		122.8	.1519		
	24	173.5		131.0	.1613			90	241.6		123.3	.1149		
	25	184.2		134.1	.1561			92	200.6		137.2	.1436		
	54	141.9		128.9	.1964									
	55	121.7		128.3	.2601		90	78	272.8	264.5	135.4	.1127	.1125	
	73	153.1		120.0	.1650			79	256.1		143.3	.1124		
	74	155.5		126.1	.1857		120	84	281.9	276.3	133.9	.0999	.1126	
	75	142.2		124.4	.2064			85	270.6		140.0	.1290		
0	11	128.0	204.1	122.9	.1236	.1407	150	81	304.6	289.8	141.7	.0953	.1028	
	12	219.4		120.1	.1195			83	275.0		146.1	.1004		
	31	197.1		121.7	.1949									
	34	189.4		131.1	.1519		180	93	239.7	235.9	125.0	.1112	.1157	
	7	199.9		130.0	.1395			94	246.9		120.0	.1123		
	73	175.3		118.9	.1372			95	246.9		125.0	.1048		
								96	210.0		130.0	.1005		
	18	161.9	183.8	131.2	.1554	.1540	Overall						265.3	.1210
	20	200.9		126.3	.1393		Block Number 2 20°C Subcooling							
	21	182.3		134.1	.1629		0	44	311.1	334.3	135.6	.2046	.1892	
	30	172.4		138.3	.2037			45	337.4		149.4	.1760		
	39	109.7		128.9	.1408		30	52	346.9	317.4	146.1	.1483	.1370	
	46	162.4		143.9	.1518			53	387.9		145.6	.1277		
	57	205.3		133.9	.1408		60	46	340.	345.4	142.2	.1212	.1158	
120	9	181.0	206.1	127.7	.1083	.1198		47	350.1		146.7	.1108		
	10	194.6		127.0	.1181		90	40	343.9	353.1	152.7	.112	.119	
	30	194.0		133.3	.1221			41	362.1		137.8	.1099		
	31	218.2		132.2	.1238		120	50	309.4	326.6	141.2	.119	.112	
	66	216.3		122.8	.1287			51	343.8		141.2	.1075		
	67	196.5		131.1	—		150	48	387.9	372.2	133.3	.1076	.1117	
150	6	174.7	170.6	119.6	.1692	.1528		49	356.4		130.7	.1161		
	7	103.9		118.6	.1205		180	42	387.9	387.9	141.1	.1024	.1042	
	8	173.9		117.7	.1304			43	387.9		137.8	.1061		
	12	171.		126.5	.1369		Overall						354.3	.1224
	23	172.		124.8	.1553		Block Number 2 30°C Subcooling							
	60	171.		129.4	.1746		120	48	432.1	422.6	144.1	—	—	
	61	171.6		132.2	.1896			49	432.1		150.0	—	—	
	112	172.3		139.1	.1488			0	423.7		121.6	—	—	
	123	170.1		131.4	.1802		180	2	389.5	319.5	131.7	—	—	
180	1	—	187.3	115.6	.1874	.1283	Overall						411.6	—
	3	170.9		115.1	.1168		Block Number 2 Saturation Insulated along the circumference to leave 60° angle active boiling area.							
	4	199.1		113.4	.0828		0	158	221.7	235.3	127.9	.0850	.0792	
	5	180.3		122.9	.1344			164	248.8		125.0	.0741		
	18	171.1		—	—		30	176	218.1	218.1	129.6	.1173	.1173	
	29	171.		134.4	.1172		90	166	196.6	196.2	130.4	.0939	.1042	
	34	171.7		120.0	.1403			170	193.7		123.4	.1171		
	65	172.1		132.2	.1817		180	126	209.0	209.7	—	—	.0826	
Overall			108.4			.1441		127	222.0		—	—		
								128	222.0		—	—		
								130	222.0		—	—		
								130	216.3		134.0	.1280		
								131	215.1		129.3	.0757		
								132	194.9		144.9	.1069		
								133	182.2		127.7	.1070		
								134	180.5		133.6	.0931		
								139	183.0		139.6	.1096		
								141	233.5		125.0	.1099		
								140	265.2		122.6	.1076		
								141	242.6		121.2	.1045		
Overall			223.4			.1257	Overall						212.2	.1084

Angle Run CHF Aver. CHF IDF I.C.R. I. Aver. C.R.
(W/cm²) (BC) (Ft²)

Block Number 2
5°C Subcooling
Insulated along the circumference to leave
60° angle active boiling area.

0	165	242.5	242.5	131.2	.0895	.0895
90	171	209.0	209.0	122.8	.1060	.1060
180	140	256.2	246.9	124.2	.0667	.0727
	142	234.1		133.9	.0600	
	145	243.5		120.3	.1193	
	146	253.6		124.3	.0666	
Overall			226.8			.0913

Block Number 2
10°C Subcooling
Insulated along the circumference to leave
60° angle active boiling area.

0	160	283.5	283.5	132.1	.0894	.0894
90	172	365.0	355.0	140.4	.0502	.0502
180	135	292.7	298.4	126.5	.0619	.0573
	136	324.9		127.5	.0562	
	147	277.8		126.4	.0544	
Overall			328.0			.0584

Block Number 2
20°C Subcooling
Insulated along the circumference to leave
60° angle active boiling area.

0	159	326.5	326.5	130.5	.0906	.0906
90	167	434.7	454.9	145.9	.0548	.0584
	169	475.1		140.9	.0626	
180	137	326.3	337.0	113.9	.0401	.0398
	138	367.7		126.0	.0395	
Overall			393.3			.0518

Block Number 5
Saturation

5	149.0		173.4	129.8	.1825	.1883
6	137.0		136.0	.1547		
7	127		141.3	.1613		
22	111.1		134.6	.1756		
23	101.1		148.6	.1655		
30		117.1	139.0	118.1	.2925	.2992
		114.0		125.1	.3009	
		110.0		125.4	.3043	
60	8	141.0	161.0	140.4	.1766	.1796
	9	181.0		134.7	.1827	
90	13	157.5	151.7	127.2	.1987	.1973
	14	150.0				
	15	140.0		142.1	.1953	
120	10	123.0	136.2	127.8	.2075	.2049
	11	142.6		135.5		
	12	143.0		135.5	.2024	
180	19	144.0	123.3	125.4	.1200	.1600
	20	116.0		144.2	.1874	
	21	128.0		137.9	.1968	
180	1	155.0	152.0	120.6	.1345	.1595
	2	165.0		121.8	.1605	
	3			130.8		
	4	136.0		138.2	.1925	
	41	131.0		145.5	.1607	
Overall			141.7			.1922

Angle Run CHF Aver. CHF IDF I.C.R. I. Aver. C.R.
(W/cm²) (BC) (Ft²)

Block Number 5
Saturation
Side number 2 of the heat flux meter.

0	24	165.0	156.0	145.7	.2100	.2099
	25	147.0		134.1	.2099	
30	35	92.6	92.0	128.3	.3142	.3078
	36	91.3		130.9	.3016	
60	26	147.0	152.0	140.8	.2537	.2784
	27	157.0		138.0	.3085	
90	31	111.0	116.5	145.7	.2537	.2493
	32	122.0		139.3	.2450	
120	37	99.0	103.5	131.8	.2140	.2088
	38	108.0		134.9	.2221	
150	29	117.0	109.5	134.2	.2589	.2977
	30	105.0		135.7	.2945	
	33	114.0		135.9	.3281	
	34	101.0		129.3	.3106	
180	39	100.5	99.6	154.9	.2619	.2529
	40	98.6		139.0	.2445	
Overall			116.9			.2568

Block Number 5
5°C Subcooling

0	72	236.0	236.0	136.9	.1846	.1846
30	53	154.9	133.8			.2889
	54	132.7		137.8	.2889	
60	64	180.0	180.0	136.6	.2015	.2015
90	48	171.0	171.0	137.5	.1597	.1597
120	67	167.0	167.0	139.5	.1973	.1973
150	61	156.0	146.0	138.3	.1555	.1555
180	46	172.0	163.0	131.3	.1297	.1297
	47	154.0		159.8	.1808	
Overall			169.6			.1885

Block Number 5
10°C Subcooling

0	71	238.0	241.0	145.1	.2494	.232
	73	244.0		143.7	.2319	
30	52	200.0	219.0	131.9	.1672	.2112
	74	193.0		135.4	.2411	
	75	194.0		131.9	.2432	
60	65	219.0	219.0	135.1	.1925	.1925
90	50	208.0	208.0	140.2	.1776	.1776
120	69	187.0	187.0	145.8	.2399	.2399
150	60	150.0	158.0	137.4	.1855	.1855
180	45	181.0	181.0	134.1	.1872	.1872
Overall			200.3			.2008

Block Number 5
20°C Subcooling

0	70	239.0	239.0	148.4	.3107	.3107
30	57	191.0	220.5	161.9	.3472	.2967
	58	250.0		151.6	.2591	
60	66	252.0	252.0	150.9	.2232	.2272
90	51	273.0	273.0	151.9	.1784	.1784
120	68	228.0	228.0	151.3	.2414	.2414
150	62	272.0	272.0	151.4	.1986	.1986
180	42	275.0	266.0	149.5	.1697	.1566
	43	257.0		140.3	.1642	
Overall			249.7			.2142

Angle Run DIF Aver. DIF (W/cm²) ICH (°C) I.C.B. I.Aver.I.B. (11%)

Block Number 5

Saturation
Insulated along the circumference to leave
60° angle active boiling area.

0	89	189.0	189.0	129.1	.0674	.0674
30	77	169.0	165.5	134.5	.0948	.0818
	82	182.0		133.6	.0719	
60	95	156.0	156.0	130.3	.0596	.0596
90	85	211.0	211.0	134.9	.1134	.1134
150	97	139.0	139.0	126.0	.0738	.0738
180	85	167.0	167.0	120.8	.0735	.0735
Overall			189.9			.075

Block Number 6

Saturation
Insulated along the circumference to leave
60° angle active boiling area.

30	81	194.1	182.3	134.2	.1245	.0913
	81	170.5		134.5	.0720	
Overall			182.3			.0913

Block Number 5

Saturation
Insulated along the circumference to leave
60° angle active boiling area.

0	31	171.4	181.4	132.8	.1624	.1624
30	60	225.0	220.0	136.7	—	.0569
	60	214.0		134.0	.0569	
60	73	166.9	168.9	132.5	.0636	.0636
90	87	227.1	227.1	129.9	.0635	.0635
120	120	225.0	225.0	133.0	.0509	.0509
150	83	229.7	229.7	133.5	.0567	.0567
Overall			213.3			.0620

Block Number 6

Saturation
Insulated along the circumference to leave
60° angle active boiling area.

0	16	201.0	201.0	133.7	.0850	.0850
30	9	261.4	261.4	142.4	.0760	.0760
60	34	243.6	243.6	115.4	.0617	.0617
90	24	251.8	251.8	115.7	.0594	.0594
120	30	116.8	116.8	141.3	.0483	.0483
180	24	269.0	269.0	144.5	.0432	.0432
Overall			212.4			.0572

Angle Run DIF Aver. DIF (W/cm²) ICH (°C) I.C.B. I.Aver.I.B. (11%)

Block Number 7

Saturation
15.24 cm long copper cylinder
The 3 constantan wires are oriented
along the circumference of the cylinder.

0	16	174.0	178.4	142.1	.1743	.1795
	17	170.4		148.2	.1971	
	18	190.0		148.1	.1993	
30	9	96.4	85.8	134.8	.1491	.1433
	10	53.1		133.2	.1421	
	11	91.4		133.7	.1383	
	12	86.2		121.7	.1359	
60	19	132.1	120.8	134.1	.1311	.1455
	20	124.4		143.3	.1710	
	21	112.1		137.8	.1416	
	22	113.6		138.4	.1315	
90	2	144.5	134.9	140.5	.1415	.1848
	28	111.0		146.1	.1302	
	29	121.0		138.1	.1478	
	30	131.4		149.7	.1487	
120	13	144.0	152.8	138.0	.1676	.1862
	14	172.3		138.8	.1451	
	31	161.8		143.1	.1700	
	32	148.0		144.4	.1646	
150	23	165.9	152.3	144.8	.1745	.1453
	24	141.6		136.2	.1793	
	25	149.2		140.8	.1615	
	26	152.4		140.6	.1747	
180	3	132.1	138.1	129.9	.1544	.1416
	8	144.3		135.8	.1774	
	33	149.0		136.5	.1647	
	34	137.6		138.9	.1671	
Overall			135.0			.1717

Block Number 8

Saturation
15.24 cm long copper cylinder

0	12	111.9	228.8	139.1	.1071	.1914
	13	251.4		133.8	.1161	
	14	272.4		126.7	.1716	
	15	215.9		135.2	.1677	
	11	252.5		134.6	.1671	
	32	236.9		138.2	.1956	
30	8	122.8	129.0	137.0	.1445	.1450
	9	124.3		137.8	.1481	
	10	106.4		138.9	.1474	
	11	147.4		126.6	.1418	
60	9	134.3	166.2	122.1	.1511	.1515
	20	118.3		136.4	.1921	
	21	94.9		121.3	.1445	
	24	113.0		124.4	.1411	
	25	114.9		124.4	.1074	
	26	114.4		—	—	
	29	119.0		130.2	.1246	
90	15	111.1	175.1	144.2	.1717	.1477
	16	136.1		130.9	.1961	
120	5	104.2	190.9	132.7	.1418	.1920
	6	127.5		134.1	.1963	
	7	207.4		133.7	.1810	
150	17	110.0	197.2	134.2	.1854	.1808
	18	184.4		138.8	.1919	
180	1	224.5	207.2	135.5	.1945	.1854
	3	187.6		127.9	.1251	
	4	209.4		129.6	.1622	
Overall			180.4			.1718

Experiments were performed in a 60 liter tank (the one used to quench the bundle)



Angle Run DIF Aver DIF I DIF I.C.R. I Aver C.R

Angle Run DIF Aver DIF I DIF I.C.R. I Aver C.R

Block Number 8
Saturation
11.34 cm long copper cylinder

Angle	Run	DIF	Aver DIF (u/cm ²)	I DIF (°C)	I.C.R.	I Aver C.R (Ft ²)
0	35	149.9	169.1	141.7	.3963	.3171
	36	219.1		132.1	.2017	
	37	135.1		129.9	.6422	
	44	172.4		142.7	.2795	
30	43	107.9	107.9	133.3	.7307	.7307
60	40	147.1	147.6	137.2	.3445	.3445
90	39	152.0	152.0	138.8	.3226	.3226
120	38	133.5	133.5	135.9	.2700	.2700
150	41	166.4	166.4	138.9	.3128	.3128
	42	121.1	115.9	121.9	.2796	.2795
	42	144.1		137.9	.2795	
Overall			143.4			.3402

Block Number 8
Saturation
Insulated along the circumference to leave 60° angle active boiling area

Angle	Run	DIF	Aver DIF (u/cm ²)	I DIF (°C)	I.C.R.	I Aver C.R (Ft ²)
0	100	173.5	189.5	136.2	.7807	.1678
	119	185.8		126.1	.1250	
	120	209.1		134.3	.1163	
30	111	187.5	189.3	129.1	.0942	.0991
	112	191.0		127.8	.1039	
60	97	139.3	153.4	136.9	.1171	.1009
	115	157.9		133.7	.0796	
	116	163.1		135.4	.0923	
90	102	137.7	150.3	133.1	.1109	.1170
	103	163.3		134.7	.1034	
120	94	141.4	149.2	139.8	.1415	.1273
	95	115.8		137.4	.1045	
150	101	158.1	157.8	121.2	.1105	.1091
	108	117.3		137.3	.1777	
180	88	168.2	164.2	138.2	.1244	.1272
	90	158.1		133.1	.1218	
	91	164.2		135.2	.1114	
Overall			162.8			.1117

Block Number 8
Saturation
62 cm long copper cylinder

Angle	Run	DIF	Aver DIF (u/cm ²)	I DIF (°C)	I.C.R.	I Aver C.R (Ft ²)
0	51	156.0	182.7	135.6	.2261	.2151
	50	178.7		128.9	.1997	
	71	213.1		145.4	.2214	
30	49	182.9	113.9	135.2	.3354	.3334
	50	124.8		133.2	.3315	
60	47	182.0	125.4	134.4	.2975	.2882
	58	114.5		128.2	.2794	
	78	139.9		117.5	—	
90	47	125.5	130.3	134.3	.2718	.1933
	48	135.0		141.7	.1838	
120	44	139.0	165.9	121.4	.1896	.1151
	54	112.7		111.2	.1627	
150	45	117.0	140.1	131.0	.2553	.2548
	53	149.0		141.0	.2526	
180	45	121.7	137.4	124.8	.1949	.2025
	46	143		131.2	.2095	
	47	134.5		130.0	—	
	48	143.8		135.0	—	
Overall			139.2			.2307

Block Number 8
20° Subcooling
Insulated along the circumference to leave 60° angle active boiling area

Angle	Run	DIF	Aver DIF (u/cm ²)	I DIF (°C)	I.C.R.	I Aver C.R (Ft ²)
0	121	260.8	246.4	143.7	.1284	.1398
	122	231.9		132.8	.1534	
30	113	242.0	266.5	144.7	.1188	.1313
	114	271.0		151.4	.1245	
60	117	278.9	292.3	149.9	.1224	.1377
	118	175.7		147.7	.1124	
90	104	267.9	265.4	144	.1444	—
	105	262.9		147.6	.1445	
120	107	332.7	332.7	147.9	.1516	.1516
150	109	270.4	287.4	152.6	.1331	.1349
	110	174.3		153.2	.1198	
180	92	212.9	272.0	141.7	.1177	.1707
	93	242.1		139.6	.1333	
Overall			284.0			.1316

Block Number 8
20° Subcooling
74.7 cm long copper cylinder

Angle	Run	DIF	Aver DIF (u/cm ²)	I DIF (°C)	I.C.R.	I Aver C.R (Ft ²)
0	114	137.0	133.0	137	.5248	
	115	134.4		131.4	.4248	
	124	154.3		135.7	.5513	
30	111	158.2	221.4	133.5	.3371	.3419
	112	114.1		141.7	.1594	
60	107	212.2	243	134.5	.3788	.3109
	108	140.1		117.5	.3790	
90	106	239	271.7	131.3	.3379	.3253
	107	113.1		111.3	.3162	
120	111	249.7	240.4	138.1	.2876	.3079
	112	231.0		144.7	.3312	
150	108	237.1	250.3	150.3	.2943	.2773
	109	263.5		151.1	.2621	
180	109	229.9	219.6	142.2	.2031	.2438
	110	207.3		141.3	.3049	
Overall			243.7			.3254

Block Number 8
Saturation
Insulated along the circumference to leave 30° angle active boiling area

Angle	Run	DIF	Aver DIF (u/cm ²)	I DIF (°C)	I.C.R.	I Aver C.R (Ft ²)
0	118	157.5	152.5	131.7	.1411	.1431
30	130	161.4	161.4	127.7	.1024	.1024
60	137	166.0	166.0	131.6	.1094	.1094
90	121	168.3	161.2	131.4	.0918	.0893
	124	174.0		133.7	.0870	
120	126	168.4	168.4	137.0	.0822	.0822
150	135	166.5	166.5	125.6	.1098	.1098
180	113	129.7	129.7	128.2	.2054	.2054
Overall			164.1			.1055

Angle	Run	Diff	Aver. μF (μ/cm^2)	TCF ($^{\circ}C$)	I.C.R.	I. Aver. C.R. (ft 2)
Block Number 8						
No. of coils Insulated along the circumference to leave 30° angle active boiling area.						
0	129	324.9	324.9	149.4	.0997	.0997
30	131 132	331.2 314.7	323.0	139.2 137.4	.0791 .0857	.0821
60	138	371.9	371.9	139.5	.1051	.1051
90	125	367.4	367.4	147.8	.0483	.0483
120	127	335.1	335.1	145.6	.0900	.0900
150	36	317.7	317.7	136.4	.0849	.0849
180	134	312.9	312.9	129.5	.0949	.0949
Overall			336.6			.0754
Block Number 9						
Saturation						
0	0 7	129.4 147.1	138.3	161.5 167.2	.2350 .2350	.2350
30	15 16 17	146.0 145.0 113.6	125.8	148.0 154.3 —	.4066 .3606 —	.3771
60	17 18 19 20 21	124.1 111.3 111.1 111.1 111.1	115.4	141.5 156.9 159.6 159.8 —	.2822 .2650 .3247 —	.2889
90	2 3 4 5 6 7	— — — — — —	121.1	157.4 151.9 148.5 151.4 — —	.2375 .2370 .229 .2487 — —	.2435
120	8 9 10 11	— — — —	107.3	152.6 158.0 145.8 —	.2727 .3116 .2455 —	.2725
150	12 13 14 15	— — — —	114.5	151.9 158.1 — —	.2778 .2493 — —	.2731
180	16 17 18 19 20 21	— — — — — —	114.5	151.9 158.1 — — — —	.2778 .2493 — — — —	.2731
Overall			111.3			.2749
Block Number 11						
Saturation						
0	11 12	164.5 143.0	147.1	151.5 154.5	.2691 .2639	.2664
30	13 14	199.9 153.0	176.9	143.4 144.2	.1076 .0969	.1019
60	15 16	— 410.2	331.4	147.7 146.9	.0771 .0700	.0730
90	17 18	159.5 305.5	172.5	145.3 148.3	.0781 .0831	.0805
120	19	425.7	425.7	150.8	.0592	.0592
150	20 21	327.9 337.3	332.6	146.3 145.4	.0821 .0801	.0811
180	22 23 24 25	270.0 291.1 286.7 382.4	307.6	135.7 140.7 140.9 148.5	.0832 .1275 .1079 .0842	.0843
Overall			169.4			.0740

Angle	Run	Diff	Aver. μF (μ/cm^2)	TCF ($^{\circ}C$)	I.C.R.	I. Aver. C.R. (ft 2)
Block Number 12						
Saturation						
0	7 8	111.4 213.4	202.4	121.0 121.1	.1109 .1106	.1107
30	9 10	195.5 159.0	172.3	231.1 133.7	.1564 .1697	.1640
60	19 20	231.0 183.0	207.5	132.8 121.5	.1367 .1539	.1434
90	11 12	226.4 229.4	227.9	124.0 111.9	.1147 .1279	.1188
120	13 14 15 16	243.7 234.4 235.3 251.8	241.2	124.6 120.1 111.4 111.8	.1147 .1177 .1177 .1172	.1162
150	5 6	12 213.4	218.1	117.9 123.9	.1177 .1371	.1178
180	7 8 9 10 11 12	127.3 102.1 192.0 148.2 163.3	168.1	119.1 117.7 120.1 121.1 119.0	.1413 .1285 .1336 .1442 .132	.1348
Overall			217.4			.1317
Block Number 13						
Saturation						
0	9 10	112.4 112.1	167.1	118.5 120.5	.2624 .2313	.2418
30	11 12	11.4 11.2	87.3	119.2 117.3	.3378 .3168	.3243
60	13 14	118.9 118.1	128.4	120.1 127.2	.2154 .2171	.2164
90	15 16	130 124.0	127.0	121.0 121.8	.238 .2771	—
120	17 18	112.1 118.2	124.2	122.1 122.1	.2478 .2395	.2435
150	19 20	115.6 111.1	118.9	129.6 131.4	.2748 .2773	.2901
180	21 22 23 24 25	115.6 115.6 111.1 111.1 111.1	118.9	129.6 131.4 131.4 131.4 131.4	.2748 .2773 .2773 .2773 .2773	.2901
Overall			118.3			.2607
Block Number 14						
Saturation						
0	5 6	121.5 133.8	224.1	113.1 118.6	.1271 .1378	.1301
30	7 8	119.1 164.2	171	116.7 112.9	.1644 .1854	.1651
60	9 10	140.8 162.8	161.7	114.2 117.3	.1644 .1671	.1626
90	11 12	140.1 206.7	173.4	111.4 121.0	.1371 .1212	.1287
120	13 14	204.9 178.1	191.8	114.5 114.8	.1196 .1199	.1197
150	15 16	167.7 136.8	152.3	— 113.9	.1100 .1639	.1366
180	17 18 19	141.4 141.2 191.9	144.8	124.6 118.7 111.9	.1524 .1615 .1232	.1480
Overall			174.4			.1385

Angle Run (of Aver of CHF I.C.R. I.Aver.C.R

Angle Run CHF Aver of CHF I.C.R. I.Aver.C.R

Block Number 14
Saturation
Insulated along the circumference to leave
90 degree active boiling area.
Obtained through a steady-state experiment.

Angle	Run	(of	Aver of	CHF	I.C.R.	I.Aver.C.R
			(d/cm)	(°C)		(%)
0	37	228.5	230.5	110.5	—	—
	38	254.5	—	106.1	—	—
	39	247.7	—	100.8	—	—
	40	232.5	—	109.7	—	—
	41	197.0	—	118.4	—	—
	42	230.9	—	118.5	—	—
Overall			230.5			

Block Number 15
Saturation
11.24 cm long copper cylinder

Angle	Run	(of	Aver of	CHF	I.C.R.	I.Aver.C.R
			(d/cm)	(°C)		(%)
0	8	112.1	209.4	127.0	1649	1470
	9	133	—	129.1	1304	—
	10	104.3	—	148.9	1798	—
	19	127.1	—	147.2	1281	—
30	11	148.8	160.3	125.0	2766	2573
	11	175.0	—	130.9	2405	—
60	14	187.0	190.1	133.2	2141	2028
	15	192.6	—	139.7	1926	—
90	1	191.1	177.5	127.2	1981	1821
	5	221.4	—	122.3	1703	—
120	15	177.1	180.0	131.5	1538	1749
	17	195.9	—	135.4	1908	—
150	12	194.4	193.4	137.5	2232	1873
	13	192.3	—	131.8	1614	—
180	5	214.1	211.5	137.1	1680	1657
	7	214.1	—	143.3	1635	—
Overall			190.5			1692

Block Number 15
Saturation
Insulated axially to leave an active boiling
length of 10.16 cm

Angle	Run	(of	Aver of	CHF	I.C.R.	I.Aver.C.R
			(d/cm)	(°C)		(%)
0	23	117.0	207.5	141.4	1347	1447
	24	115.0	—	144.9	1301	—
	34	121.7	—	144.1	1633	—
	41	136	—	130.5	1880	—
	42	—	—	133.7	1455	—
30	11	137.0	141.1	127.0	2067	1715
	17	134.4	—	138.9	2000	—
60	11	157	152.9	140.1	1547	1770
	12	137	—	142.5	1904	—
90	11	—	143.3	137.4	1848	1717
	11	—	143.7	143.7	1630	—
	11	—	143.5	136.5	1104	—
120	11	161.1	141.1	141.1	1799	—
	14	161.1	174.4	147.1	1727	1611
150	16	161.1	174.4	147.1	1727	1611
	16	138.7	—	133.5	1797	—
180	6	138.7	177.5	147.5	1491	1626
	17	—	—	129.1	1633	—
	20	137	—	137.7	1776	—
1	20	167.3	145.3	145.3	1590	1517
	21	164.5	—	140.6	1541	—
	42	170.6	—	141.0	1439	—
	43	158.9	—	149.3	1678	—
	Overall			164.4		

* Experiments were done with transite rings placed at the edge of the insulation on the outside of the copper plate to simulate the shape boundary of a shorter cylinder.

Block Number 15
Saturation
Insulated axially to leave an active
boiling length of 6.35 cm

Angle	Run	CHF	Aver of CHF	I.C.R.	I.Aver.C.R
			(d/cm)		(%)
0	4	227.6	226.7	142.7	1031
	48	234.1	—	148.0	1008
	64	219.1	—	131.4	1354
30	55	226.1	—	136.1	1156
	50	134.8	176.2	132.9	1105
60	51	117.6	—	130.7	1688
	49	148.4	152.1	141.0	1115
	62	139.1	—	137.5	1385
90	53	168.8	—	136.4	1109
	51	149.3	179.3	141	1423
	51	193.0	—	134.7	1141
120	54	174.2	—	134.3	1459
	58	189.6	174.0	136.7	1349
	59	158.3	—	132.5	1221
150	54	194.3	185.7	138.3	1227
	55	171.1	—	142.5	1251
180	60	137.1	152.6	132.6	1324
	61	132.8	—	135.1	1198
	67	107.2	—	145.8	1074
Overall			167.8		1132

Block Number 15
Saturation
11.42 cm long copper cylinder

Angle	Run	CHF	Aver of CHF	I.C.R.	I.Aver.C.R
			(d/cm)		(%)
0	11	191.3	221.2	142.4	1441
	16	164.1	—	144.4	1095
	17	127.7	—	142.5	1940
30	87	94.1	106.5	141.7	1164
	84	122.3	—	135.7	1434
	85	94.1	—	133.7	1338
60	71	134.6	141.2	138.3	1248
	74	147.7	—	143.0	1253
90	71	158.8	175.4	145.3	1435
	72	192.0	—	140.8	1160
120	80	149.0	182.3	141.5	1171
	81	154.5	—	147.4	1421
150	88	171.4	163.5	137.6	1132
	89	171.3	—	147.3	1419
	89	194.4	—	138.7	1419
180	86	147.4	151.7	140.8	1432
	86	147.4	—	144.3	1427
Overall			159.7		1239

Block Number 15
Saturation
12 cm long copper cylinder

Angle	Run	CHF	Aver of CHF	I.C.R.	I.Aver.C.R
			(d/cm)		(%)
0	89	—	215.3	139.2	—
	90	—	—	136.1	—
	91	—	—	143.4	—
	111	211.8	—	144.8	—
	112	221.8	—	146.3	1187
30	130	210.4	—	149.5	1870
	92	131.2	118.2	128.8	2648
	93	126.6	—	134.3	1780
60	94	95.7	—	130.1	2297
	99	179.8	178.5	129.6	574
	110	172.1	—	138.5	1122
90	117	152.9	158.4	144.1	2274
	98	—	—	151.1	—
	109	134.9	—	147.4	2258
120	95	152.1	149.4	141.2	1151
	96	—	—	142.9	—
	108	141	—	140.6	2038
150	102	189.1	180.8	130.7	1459
	106	172.5	—	134.2	1127
180	86	170.4	171.2	144	1507
	88	168.6	—	142.7	1443
Overall			160.4		2279

Angle	Run	CHF	Aver. CHF (W/cm ²)	TCF (°C)	I.C.R.	I.Aver.C.R. (F/F)
Block Number 15 20°C Subcooling 7.62 cm long copper cylinder						
0	113	272.8	275.6	139.6	.3877	.3790
	114	283.1		144.6	.3597	
	129	270.9		148.4	.3912	
30	121	253.2	298.7	140.3	.2542	.2548
	122	344.1		152.7	.2555	
60	115	290.9	296.6	145.9	.2369	.2394
	116	302.3		159.0	.2419	
90	123	277.5	281.1	154.6	.2365	.2378
	124	284.5		155.5	.2392	
120	117	304.5	311.9	152.6	.2140	.2172
	118	319.2		154.2	.2206	
150	119	313.5	340.8	152.2	.2248	.2123
	120	368.0		149.0	.2012	
180	125	305.8	287.4	151.3	.2137	.2213
	126	287.1		145.1	.2252	
	127	289.3		146.6	.2243	
	128	256.3		149.2	.2225	
Overall		301.7				.2381

Angle	Run	CHF	Aver. CHF (W/cm ²)	TCF (°C)	I.C.R.	I.Aver.C.R. (F/F)
Block Number 15 Saturation Insulated along the circumference to leave 30° angle active boiling area.						
0	146	174.2	177.0	128.4	.1191	.1060
	147	179.7		134.1	.0958	
30	148	130.5	154.5	125.5	.0679	.0792
	150	192.5		131.8	.0950	
60	142	163.5	166.0	134.1	.0855	.0813
	143	168.4		132.7	.0774	
90	152	162.5	187.1	130.6	.0876	.0927
	153	191.6		134.3	.0984	
120	139	193.3	182.6	144.1	.0889	.0865
	140	181.4		142.4	.0842	
150	156	175.6	180.5	133.1	.0672	.0664
	158	185.3		135.1	.0656	
180	132	190.8	175.5	134.5	—	.0518
	131	178.2		143.1	.0775	
	135	150.8		132.3	.0355	
	136	182.2		144.2	.0634	
Overall		176.1				.0702

Angle	Run	CHF	Aver. CHF (W/cm ²)	TCF (°C)	I.C.R.	I.Aver.C.R. (F/F)
Block Number 15 20°C Subcooling Insulated along the circumference to leave 30° angle active boiling area.						
0	140	257.5	270.7	137.0	.0773	.0712
	151	290.3		143.7	.0562	
30	149	277.1	317.6	144.8	.1084	.0942
	151	350.0		151.1	.0845	
	144	203.4	203.1	157.2	.0998	.0877
90	145	282.7		150.4	.0782	
	154	334.9	341.4	156.0	.1104	.0970
120	155	347.9		149.1	.0865	
	141	349.3	345.4	153.6	.0650	.0773
150	157	341.4		148.2	.0943	
	159	315.5	318.0	141.0	.0643	.0682
180	162	320.5		152.0	.0725	
	137	326.9	338.1	150.5	.0754	.0723
Overall	138	349.3		153.6	.0695	
			318.3			.0812

Angle	Run	CHF	Aver. CHF (W/cm ²)	TCF (°C)	I.C.R.	I.Aver.C.R. (F/F)
Block Number 15 Saturation Insulated along the circumference to leave 30° angle active boiling area.						
0	160	212.4	212.4	133.5	.0735	.0735
	170	174.1	174.1	138.6	.0672	.0672
60	177	196.7	196.7	128.2	.0736	.0736
	163	200.1	196.0	131.5	.0612	.0685
90	164	191.9		137.3	.0778	
	120	166	189.0	140.9	.0686	.0586
150	175	177.3	177.3	133.0	.0664	.0664
	180	173	173.8	133.3	.1110	.1110
Overall			187.7			.0714

Angle	Run	CHF	Aver. CHF (W/cm ²)	TCF (°C)	I.C.R.	I.Aver.C.R. (F/F)
Block Number 15 20°C Subcooling Insulated along the circumference to leave 30° angle active boiling area.						
0	172	261.3	261.3	136.0	.0776	.0776
	171	351.9	351.9	143.0	.0531	.0531
60	178	420.1	420.1	148.2	.0499	.0499
	165	397.1	397.1	150.0	.0521	.0521
120	157	386.7	386.7	148.9	.0492	.0492
	176	344.3	344.3	145.7	.0451	.0451
180	174	308.1	308.1	145.9	.0397	.0397
	Overall		363.0			.0502

Angle	Run	CHF	Aver. CHF (W/cm ²)	TCF (°C)	I.C.R.	I.Aver.C.R. (F/F)
Block Number 17 Saturation						
0	30	221.6	222.1	140.3	.1283	.1342
	31	222.6		137.4	.1407	
30	24	126.2	135.0	148.1	.2751	.3337
	25	143.7		147.4	.4239	
60	32	173.8	190.1	149.5	.1708	.1654
	33	206.3		141.4	.1604	
90	28	171.5	183.8	141.5	.1403	.1409
	29	194.1		137.8	.1416	
120	26	184.7	180.6	137.7	.1774	.1549
	27	176.4		139.7	.1545	
150	20	193.1	194.8	139.4	.1946	.1957
	21	196.5		132.9	.1920	
180	22	209.5	204.8	144.3	.1784	.1762
	23	200.1		146.5	.1740	
Overall			182.9			.1755

Angle	Run	U/F	Aver. Cf (W/cm ²)	CHF (W)	I.C.H.L.	I.Aver.C.H.L. (F ²)
Block Number 20 Saturation						
0	6 7	83.3 77.3	80.3	129.9 130.8	.3226 .3371	.3297
30	11 12	68.6 61.5	65.1	128.0 127.7	.5559 .6922	.6166
60	9 10	61.1 77.7	69.4	128.3 128.3	.3941 .4722	.4296
90	15 16	75.3 55.1	70.2	133.3 131.9	.3201 .3198	.3199
120	5 13	73.9 72.8	73.4	133.4 133.4	.2906 .3261	.3073
150	8 14	75.8 75.3	75.6	130.2 135.6	.3160 .4025	.3553
180	3 4 17 18	57.3 73.0 71.7 71.7	68.4	122.4 130.3 127.9 139.4	.3708 .3501 .2504 .3064	.3122
Overall			71.3			.3690

Angle	Run	U/F	Aver. Cf (W/cm ²)	CHF (W)	I.C.H.L.	I.Aver.C.H.L. (F ²)
Block Number 22 Saturation						
0	11 12 17 18	181.3 103.7 176.7 191.5	184.7	148.4 144.8 156.4 147.2	.1998 .2125 .1800 .2008	.1976
30	14 15 16	113.1 113.8 148.1	125.0	136.5 140.3 141.2	.4092 .3532 .3903	.3828
60	21 22	169.3 159.5	169.4	141.8 141.3	.2741 .2463	.2704
90	7 9 10 23 24	155.8 127.4 142.7 191.2 133.7	162.4	141.1 145.6 146.3 149.6 148.3	.2139 .1934 .2717 .2380 .2156	.2220
120	19 20	157.9 148.1	150.5	147.1 146.0	.2098 .1519	.1828
150	25 26	124 171.1	145.8	141.3 151.0	.2285 .3378	.2301
180	27 29 30	113.4 153.7 115.3	143.8	145.8 148.2 155.5	.2423 — .2575 .2840	.2502
Overall			153.0			.2380

Angle	Run	U/F	Aver. Cf (W/cm ²)	CHF (W)	I.C.H.L.	I.Aver.C.H.L. (F ²)
Block Number 22 100% Subcooling						
0	42 46 53	306.8 363.3 255.1	338.4	156.0 175.5 179.0	.1202 .1729 .3837	.1795
30	39 40	345.0 356.6	356.8	179.5 182.6	.3209 .3045	.3325
60	47 58	338.0 412.4	371.2	181.7 188.1	.3951 .2498	.3061
90	41 42 59	272.7 247.6 313.2	277.8	181.1 179.3 176.8	.3477 .2735 .3146	.3073
120	51 52	315.0 355.4	335.2	180.0 178.5	.3103 .3296	.3197
150	43 44	343.6 294.9	319.3	167.2 174.0	.2540 .2306	.2417
180	49 50	278.3 302.8	290.6	169.6 173.2	.2592 .2792	.2688
Overall			329.1			.2774

Angle	Run	U/F	Aver. Cf (W/cm ²)	CHF (W)	I.C.H.L.	I.Aver.C.H.L. (F ²)
Block Number 22 Saturation With steam injection underneath the copper cylinder. Pressure upstream of orifice = 20 psig. Steam sparger located at 6 cm from the bottom of the cylinder.						
0	65	152.7	152.7	147.7	.3048	.3048
30	68 94	100.6 179.6	140.1	142.6 145.5	.2296 .2968	.3565
60	92	232.5	232.5	159.2	.4308	.4308
90	85	166.8	166.8	157.2	.3465	.3465
120	79	179.4	179.4	153.1	.3744	.3744
150	86 99	131.3 158.5	144.9	155.5 155.1	.2797 .2943	.2858
180	34 76	150.3 132.4	141.4	145.9 156.7	.2573 .2766	.2666
Overall			168.5			.3393

Angle	Run	U/F	Aver. Cf (W/cm ²)	CHF (W)	I.C.H.L.	I.Aver.C.H.L. (F ²)
Block Number 22 Saturation With steam injection underneath the copper cylinder. Pressure upstream of orifice = 40 psig. Steam sparger located at 6 cm from the bottom of the cylinder.						
0	62	148.3	148.3	144.2	.3264	.3264
30	37 69 71 93	152.0 111.9 102.2 159.5	133.4	146.7 147.7 140.1 147.4	.4477 — .6327 .6211	.5536
60	90	132.9	132.9	149.0	.2632	.2632
90	83	180.3	180.3	160.0	.5427	.5427
120	80	164.7	164.7	154.2	.4480	.4480
150	89 100	382.8 135.8	259.8	175.9 158.9	.4397 .3138	.1933
180	31 32 33 36 74 101 102	185.5 205.0 137.1 130.1 199.7 214.7 232.3	190.5	173.2 171.3 147.7 148.5 164.5 149.4 171.4	.1914 .1122 .2851 .2055 .2124 .2299 .2126	.2145
Overall			173.4			.3590

Angle	Run	U/F	Aver. Cf (W/cm ²)	CHF (W)	I.C.H.L.	I.Aver.C.H.L. (F ²)
Block Number 22 Saturation With steam injection underneath the copper cylinder. Pressure upstream of orifice = 60 psig. Steam sparger located at 6 cm from the bottom of the cylinder.						
0	63	148.6	148.6	157.8	.3077	.3077
30	38 70 96	137.7 59.5 133.3	110.2	145.8 142.3 150.8	.4143 .4841 .6063	.5071
60	91	192.6	192.6	156.8	.4461	.4461
90	84	174.1	174.1	158.1	.4285	.4285
120	81 82	159.8 149.7	154.8	150.6 149.0	— .2461	.2461
150	87 88 97 98	297.8 195.4 192.3 136.8	205.6	179.7 181.3 168.2 158.9	.1425 .2278 .2900 .3381	.2246
180	35 77 78	166.9 130.4 241.6	182.3	164.3 173.2 203.5	.2484 .2793 .1871	.2211
Overall			167.1			.3223

Block Number 22
 Saturation
 With steam injection underneath the copper cylinder.
 Pressure upstream of orifice = 20 psig.
 Steam sparger located at 19 cm from the bottom of the cylinder.

Angle	Run	IF	Aver. IF (W/cm ²)	IDF (°C)	I.C.R.	I.Aver. I.R. (%)
	100	105	217.4	217.4	145.3	.3216
Overall			217.4			.3216

Block Number 22
 Saturation
 With steam injection underneath the copper cylinder.
 Pressure upstream of orifice = 40 psig.
 Steam sparger located at 19 cm from the bottom of the cylinder.

Angle	Run	IF	Aver. IF (W/cm ²)	IDF (°C)	I.C.R.	I.Aver. I.R. (%)
	100	103	230.1	241.1	165.4	.2571
	104	104	240.9			
Overall			241.1			.2571

Block Number 22
 Saturation
 With steam injection underneath the copper cylinder.
 Pressure upstream of orifice = 60 psig.
 Steam sparger located at 19 cm from the bottom of the cylinder.

Angle	Run	IF	Aver. IF (W/cm ²)	IDF (°C)	I.C.R.	I.Aver. I.R. (%)
	110	106	312.4	312.8	161.5	.2056
Overall			312.8			.2056

Block Number 22
 Saturation
 With steam injection underneath the copper cylinder.
 Pressure upstream of orifice = 20 psig.
 Steam sparger located at 32 cm from the bottom of the cylinder.

Angle	Run	IF	Aver. IF (W/cm ²)	IDF (°C)	I.C.R.	I.Aver. I.R. (%)
	0	116	178.2	178.2	142.5	.3131
	30	117	121.2	121.2	143.4	.2546
	60	121	177.7	177.7	147.1	.5088
	90	123	193.5	193.5	155.0	—
	120	113	233.5	233.5	147.7	.1775
	150	111	244.7	244.7	145.0	.2587
	180	109	175.2	220.4	157.4	.2552
		111	175.5		159.3	.2278
Overall			194.0			.2644

Block Number 22
 Saturation
 With steam injection underneath the copper cylinder.
 Pressure upstream of orifice = 40 psig.
 Steam sparger located at 32 cm from the bottom of the cylinder.

Angle	Run	IF	Aver. IF (W/cm ²)	IDF (°C)	I.C.R.	I.Aver. I.R. (%)
	160	177	214.2	223.3	150.5	.2880
	180	180	232.4		155.5	.3154
Overall			223.3			.3011

Block Number 22
 Saturation
 With steam injection underneath the copper cylinder.
 Pressure upstream of orifice = 60 psig.
 Steam sparger located at 32 cm from the bottom of the cylinder.

Angle	Run	IF	Aver. IF (W/cm ²)	IDF (°C)	I.C.R.	I.Aver. I.R. (%)
	0	115	121.6	121.6	141.6	.6544
	30	118	120.1	120.1	142.0	.4457
	60	122	148.6	148.6	—	—
	90	124	161.9	161.9	156.1	.2516
	120	114	229.6	229.6	159.9	.1776
	150	120	317.7	317.1	150.1	.280
	180	108	220.4	235.0	144.6	.2745
		112	251.6		170.5	.2432
Overall			192.7			.2735

Block Number 22
 30°C Subcooling
 Insulated along the circumference to leave 50% angle active boiling area.

Angle	Run	IF	Aver. IF (W/cm ²)	IDF (°C)	I.C.R.	I.Aver. I.R. (%)
	0	131	290.1	269.6	151.2	.1278
		132	241.0		150.1	.0990
	30	133	377.2	379.2	177.6	.0864
	60	134	368.2	368.2	181.3	.0929
	90	129	397.4	377.9	169.5	.0944
		130	358.4		181.2	.0960
	120	135	352.8	354.2	144.3	.0954
		137	355.		174.1	.1037
	150	128	399.1	399.1	175.9	.0946
	180	126	424.1	399.2	157.3	.0944
		127	374.3		170.5	.09820
Overall			368.8			.0899

Block Number 22
 Saturation
 Insulated along the circumference to leave 50% angle active boiling area.
 With steam injection underneath the copper cylinder.
 Pressure upstream of orifice = 40 psig.
 Steam sparger located at 32 cm from the bottom of the cylinder.

Angle	Run	IF	Aver. IF (W/cm ²)	IDF (°C)	I.C.R.	I.Aver. I.R. (%)
	0	142	233.1	233.1	149.3	.0974
	30	140	177.1	122.3	—	—
		141	167.5		134.6	.1335
	60	145	149.4	148.4	130.6	.1827
	90	146	174.1	174.1	134.3	.1764
	120	144	183.0	183.0	151.2	.0862
	150	143	229.8	229.8	150.6	.1012
	180	138	212.9	243.2	147.2	.1090
		139	273.4		166.3	.1049
Overall			182.6			.1204

Angle	Run	DF	Avg. DF (W/cm ²)	TDH (°C)	I.C.P. (%)	I.Avg.C.P. (%)
Block Number 23						
Saturation						
0	17	222.3	246.7	144.5	.1467	.1483
	18	271.1		150.8	.1500	
30	15	135.2	114.4	131.5	.1345	.1323
	16	93.5		128.3	.4293	
60	10	184.6	187.2	141.0	.1700	.1781
	11	189.7		150.9	.1871	
90	8	214.7	229.3	146.0	.1601	.1672
	9	243.8		144.9	.1749	
120	19	210.0	204.6	144.3	.1976	.1916
	20	199.1		150.0	.1863	
150	4	227.2	220.2	134.8	.1811	.1871
	5	213.2		141.8	.1936	
180	12	150.1	179.2	135.2	.2142	.1955
	13	161.6		133.4	.1969	
	14	227.4		143.9	.1822	
	21*	224.6		143.4	.2558	
	22*	158.0		141.6	.1780	
	23*	214.4		144.2	.1828	
	24	168.4		139.4	.2221	
	25	181.9		142.6	.1788	
	26*	152.3		134.1	.1471	
	27*	161.5		133.6	.1968	
	28*	170.5		145.4	.2440	
Overall			194.7			.1955

*Experiments using tap water liquid level = 15 cm

*Experiments using tap water liquid level = 28 cm

*Experiments using tap water liquid level = 41 cm

The liquid level is measured from the top of the cylinder.

Angle	Run	DF	Avg. DF (W/cm ²)	TDH (°C)	I.C.P. (%)	I.Avg.C.P. (%)
Block Number 23						
Saturation						
0.02 mV was added from the normal offset of the disc temperature difference to correct for zero heat flux density						
0	17	216.8	241.3	144.7	.1676	.1735
	18	265.7		151.0	.1799	
30	15	129.7	106.8	131.7	.1504	.1579
	16	87.9		126.5	.6866	
60	10	179.1	181.7	141.3	.1915	.2081
	11	184.3		151.1	.2278	
90	8	209.3	223.9	146.2	.1922	.1950
	9	238.4		145.1	.1978	
120	19	204.6	199.2	144.5	.2271	.2268
	20	193.7		150.2	.2265	
150	4	221.7	214.7	135.0	.2200	.2330
	5	207.7		142.0	.2383	
180	12	144.6	174.2	135.4	.2117	.2295
	13	156.0		133.6	.2640	
	14	221.9		144.1	.2207	
Overall			189.3			.2360

Block Number 23
Saturation
Side 2 of the Heat Flux Meter

Angle	Run	DF	Avg. DF (W/cm ²)	TDH (°C)	I.C.P. (%)	I.Avg.C.P. (%)
0	53	254.1	254.1	128.3	.1171	.1171
30	52	138.4	138.4	127.9	.2111	.2111
60	51	192.9	192.9	145.0	.1177	.1177
90	56	209.6	209.6	127.7	.1256	.1256
120	57	225.3	225.3	127.1	.1341	.1341
150	54	203.4	203.4	139.1	.1853	.1853
180	55	207.5	207.5	134.1	.1664	.1664
Overall			200.1			.1452

Angle	Run	DF	Avg. DF (W/cm ²)	TDH (°C)	I.C.P. (%)	I.Avg.C.P. (%)
Block Number 23						
Saturation						
0.02 mV was subtracted from the normal offset of the disc temperature difference to correct for zero heat flux density						
0	17	227.7	252.1	144.3	.1240	.1247
	18	274.5		150.6	.1254	
30	15	140.8	119.9	131.3	.2351	.2484
	16	99.0		128.1	.2634	
60	10	190.1	192.6	140.8	.1375	.1425
	11	195.1		150.7	.1479	
90	8	220.1	234.7	145.8	.1332	.1383
	9	249.3		144.7	.1439	
120	19	215.5	210.0	144.1	.1599	.1546
	20	204.4		149.7	.1497	
150	4	232.8	225.7	134.6	.1468	.1505
	5	218.6		141.6	.1543	
180	12	155.6	185.2	135.0	.1681	.1557
	13	167.1		133.2	.1521	
	14	232.8		143.7	.1482	
Overall			200.2			.1554

Block Number 23
Saturation
with steam injection underneath the copper cylinder.
Pressure upstream of orifice = 40 psig.
Steam sparger located at 32 cm from the bottom of the cylinder.

Angle	Run	DF	Avg. DF (W/cm ²)	TDH (°C)	I.C.P. (%)	I.Avg.C.P. (%)
0	34	154.3	154.3	142.2	.3576	.3576
30	35	198.3	182.7	151.2	.2427	.3400
	36	167.1		135.0	.5876	
60	39	162.1	162.1	138.6	.2605	.2605
90	41	234.0	234.0	144.0	.3212	.3212
120	31	195.3	242.5	144.9	.3016	.2712
	42	289.8		151.3	.2464	
150	37	334.0	329.5	151.8	.1707	.1837
	38	325.0		158.1	.1988	
180	29	298.9	325.0	151.8	.1939	.2073
	30	351.1		139.1	.2227	
Overall			231.7			.2628

Block Number 23
Saturation
Re-calibration after the distilled water system was cleaned.

Angle	Run	DF	Avg. DF (W/cm ²)	TDH (°C)	I.C.P. (%)	I.Avg.C.P. (%)
0	48	253.2	253.2	142.1	.1392	.1392
30	49	126.5	126.5	146.9	.2572	.2572
60	50	177.6	177.6	—	.1622	.1622
90	44	167.7	167.7	149.9	.2393	.2393
120	45	200.7	200.7	148.8	.1770	.1770
150	47	211.0	211.0	158.8	.1638	.1638
180	46	221.4	221.4	148.5	.1899	.1899
Overall			186.9			.1463

APPENDIX D

EXPERIMENTAL RESULTS OBTAINED WITH THE MULTIPLE CYLINDER ARRAY

RUN NUMBER	RAY NUMBER	POSITION IN BUNDLE	ANGLE	DEVIATION OF DIAPHRAGM (°)	CRITICAL HEAT FLUX (W/cm ²)	% INCREASE*	INITIAL TEMPERATURE (°C)	TIME AT CHF (s)
100-1	12	1	180	0	202.9	-7	182	5.5
	13	2	180	0	451.6	27	231	87.1
	9	3	180	0	229.9	98	293	79.1
100-1	12	1	180	0	—	—	—	—
	13	2	180	0	166.0	39	205	23.8
	9	3	180	0	218.7	88	232	17.8
100-4	12	1	180	0	—	—	—	—
	13	2	180	0	—	—	—	—
	9	3	180	0	319.4	174	230	22.4
100-5	12	1	180	0	—	—	—	—
	13	2	180	0	—	—	—	—
	9	3	180	0	249.3	114	228	18.7
100-7	12	1	180	0	243.0	12	209	24.8
	13	2	180	0	183.3	53	232	27.4
	9	3	180	0	316.6	172	244	30.3
100-8	12	1	180	0	—	—	—	—
	13	2	180	0	192.2	60	232	18.7
	9	3	180	0	274.3	136	240	22.0
100-9	12	1	180	0	—	—	—	—
	13	2	180	0	—	—	—	—
	9	3	180	0	262.8	126	227	24.5
100-10	12	1	180	0	—	—	203	—
	13	2	180	0	—	—	231	—
	9	3	180	0	267.4	130	252	28.5
100-11	12	1	180	0	—	—	206	—
	13	2	180	0	208.0	74	225	34.4
	9	3	180	0	282.2	143	243	28.9
100-12	12	1	180	0	—	—	205	—
	13	2	180	0	218.5	82	231	31.5
	9	3	180	0	292.6	152	257	33.4
100-13	12	1	180	0	212.7	-2	187	8.1
	13	2	180	0	—	—	234	—
	9	3	180	0	311.6	168	230	22.0
100-14	12	1	180	0	—	—	226	—
	13	2	180	0	114.0	-5	258	94.5
	9	3	180	0	—	—	299	>103.0
	17	4	180	0	—	—	>302	>103.0
	20	5	180	0	—	—	>302	>103.0
100-15	12	1	180	0	—	—	204	—
	13	2	180	0	210.5	76	241	36.2
	9	3	180	0	220.4	90	246	48.5
	17	4	180	0	229.6	26	281	88.0
	20	5	180	0	337.6	93	292	95.3
100-16	12	1	180	0	—	—	207	—
	13	2	180	0	—	—	230	—
	9	3	180	0	246.0	112	255	54.0
	17	4	180	0	232.1	27	265	89.8
	20	5	180	0	341.2	98	270	97.2
100-17	12	1	180	0	218.4	0	202	27.1
	13	2	180	0	194.1	62	—	20.5
	9	3	180	0	210.4	81	238	23.9
	17	4	180	0	287.1	57	247	38.8
	20	5	180	0	349.6	110	261	50.6
100-18	12	1	180	0	—	—	203	—
	13	2	180	0	—	—	—	—
	9	3	180	0	—	—	250	—
	17	4	180	0	—	—	260	—
	20	5	180	0	164.9	131	274	117.5
100-19	12	1	180	20	—	—	209	—
	13	2	180	20	287.3	140	259	4.9
	9	3	180	20	248.1	113	264	10.0
	17	4	180	20	—	—	>303	—
	20	5	180	20	—	—	>303	—
100-20	12	1	180	20	—	—	223	—
	13	2	180	20	279.0	133	257	14.2
	9	3	180	20	206.3	77	298	23.8
	17	4	180	20	—	—	—	—
	20	5	180	20	138.9	95	296	35.4

* As compared to the overall CHF at saturation when individually calibrated.

R/N NUMBER	BLOCK NUMBER	POSITION IN BLOCK	ANGLE	DEGREE OF COOLING (°C)	CRITICAL HEAT FLUX (W/cm ²)	% INCREASE	INITIAL TEMPERATURE (°C)	TIME AT CHF (s)
100-21	12	1	180	20	—	—	223	—
	13	2	180	20	312.9	161	—	9.1
	9	3	180	20	260.0	124	—	15.4
	17	4	180	20	430.4	135	—	17.3
	20	5	180	20	96.0	35	—	23.8
100-22	12	1	180	20	—	—	225	—
	13	2	180	20	—	—	262	—
	9	3	180	20	—	—	3302	—
	17	4	180	20	271.5	48	3302	34.8
	20	5	180	20	113.4	59	3302	40.8
100-23	12	1	180	Vap. (60)	—	—	204	—
	13	2	180	0	158.5	32	251	27.8
	9	3	180	0	267.4	130	285	47.9
	17	4	180	0	248.5	36	3302	95.6
	20	5	180	0	115.2	62	290	87.4
100-24	12	1	180	Vap. (60)	—	—	198	—
	13	2	180	0	193.1	61	236	28.4
	9	3	180	0	197.3	70	272	56.3
	17	4	180	0	—	—	277	—
	20	5	180	0	143.3	101	286	138.2
100-25	12	1	180	Vap. (60)	—	—	174	—
	13	2	180	0	—	—	229	—
	9	3	180	0	260.7	124	245	45.1
	17	4	180	0	200.1	9	293	74.5
	20	5	180	0	110.0	34	266	81.2
100-26	12	1	180	Vap. (60)	—	—	173	—
	13	2	180	0	176.9	48	218	17.3
	9	3	180	0	247.3	113	248	29.0
	17	4	180	0	297.4	63	262	51.7
	20	5	180	0	107.7	51	255	55.1
100-27	12	1	180	Vap. (100)	—	—	184	—
	13	2	180	0	232.8	94	242	50.0
	9	3	180	0	251.7	116	266	76.2
	17	4	180	0	309.8	69	242	70.6
	20	5	180	0	96.8	36	224	63.2
100-28	12	1	90	Vap. (100)	242.8	11	192	25.7
	13	2	90	0	216.1	80	241	24.1
	9	3	90	0	121.1	4	276	56.7
	17	4	90	0	147.5	19	250	51.0
	20	5	90	0	106.4	49	234	44.9
100-29	12	1	90	Vap. (100)	240.7	10	202	14.3
	13	2	90	0	100.2	-16	270	75.0
	9	3	90	0	123.1	6	269	132.5
	17	4	90	0	95.5	-48	283	149.7
	20	5	90	0	80.2	12	290	165.5
100-30	12	1	0	Vap. (100)	209.1	-4	188	17.6
	13	2	0	0	131.5	10	251	44.8
	9	3	0	0	152.6	31	285	78.9
	17	4	0	0	86.5	-53	263	106.9
	20	5	0	0	75.3	6	251	77.0
100-31	12	1	0	Vap. (100)	164.8	-33	181	23.1
	13	2	0	0	—	—	242	—
	9	3	0	0	164.3	41	275	99.6
	17	4	0	0	231.4	27	297	125.7
	20	5	0	0	62.9	-12	243	139.9

APPENDIX E

DEVELOPMENT OF THE HEAT FLUX METER - PROBLEMS ENCOUNTERED

Too often, in the literature, problems encountered with the construction of a piece of equipment or with the acquisition of data are not discussed. As a result, other researchers, doing similar experiments, may experience the same problems and consequently lose considerable time and money going through many of the same development steps. Therefore, it is the purpose of this appendix to describe all the different problems encountered in the construction of the heat flux meter which finally gave reliable and consistent results for a significant number of runs.

As indicated in the equipment description section, this experimental program used a disk-type heat flux meter which was an integral part of a copper cylinder. Many problems were encountered during the silver soldering of the constantan wires into the edge and centre of this disk. For consistent and reliable results, it was necessary that the constantan wires and the copper cylinder form a good joint to produce a high thermal conductance between the two metals. If there were flaws in the solder then poor contact resulted and erroneous results were obtained. In the paragraphs to follow, the different techniques used to produce this solder joint are discussed.

Acetylene Torch

The first obvious method was to use an acetylene torch to heat the block to a temperature higher than the melting point of silver solder. However this technique was not too successful. Due to the mass of copper involved and its high thermal conductivity, it took a relatively long time to heat the entire block; excessive oxidation of the copper surface resulted and hence this method was abandoned.

Electric Furnace

The next method was to place the copper block in a steel container, 18 cm diameter by 30 cm long, which in turn was placed in an electrically heated furnace. The wires (.254 mm) were placed in the holes (.279 mm) of the disk. The silver solder and flux were placed around the wire, which protruded through the holes prior to placing it into the heater. The steel container was purged with nitrogen gas to minimize oxidation of the copper cylinder and then brought to a temperature of about 700°C. Hopefully when the solder melted, it would flow down the wires and join the constantan wire to the copper. The block was machined in a lathe to remove excess silver solder after the soldering was completed.

This method required that the silver solder should flow down the wire to fill the gap and form a joint between constantan wires and the copper. However this method produced poorly solder joints, in fact sometimes the wires could be detached from the surface by simply pulling gently on the wire. This suggested that the joint between the two

metals was very weak and irregular. Moreover, microscopic examination of the joint showed cracks in it. Twelve heat flux meters were constructed by this method and tested; all of them gave spurious results or failed completely which indicated that the solder joint was poor. Other types of silver solder did not alleviate the problem.

This experience led to a new method of making the couple. In this case, a copper wire, 0.0787 cm in diameter was fused together with a .0254 cm constantan wire to form a copper-constantan junction using an arc. The larger copper wire was then silver soldered into a hole only slightly larger than the wire. The thermocouple junction was pulled up tight against the under surface of the disk before soldering. This scheme should provide a good junction and the conduction from the copper insert to the junction should be sufficient to ensure that the junction will be very near the temperature of the copper insert. However, this method did not yield the expected results because here again it was impossible to get a good contact between the copper wire and the copper block using this soldering method.

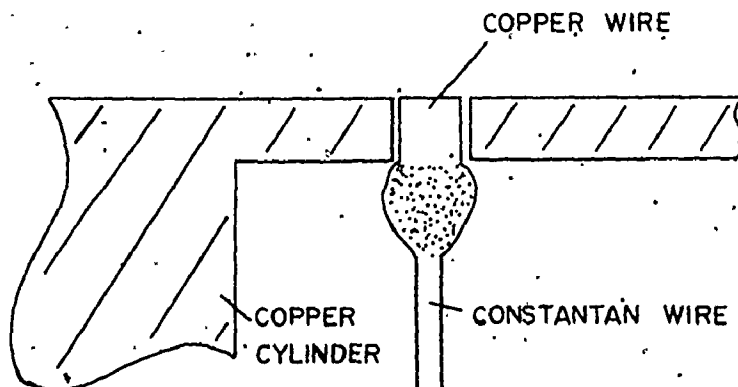


FIGURE E.1 - HEAT FLUX METER WITH A COPPER WIRE

Induction Furnace

After considerable experimentation with this soldering technique, it was decided to abandon it and attempt a different method of heating the block. Moreover, the soldering literature suggested that small amounts of oxidation products at the joint could have detrimental effects on its strength. This led to attempting the soldering in an induction furnace purged with first nitrogen, then hydrogen. In this case, the block was placed on transite supports in an 20 cm diameter by 25 cm long glass tube and with the ends sealed with aluminum flanges. Nitrogen was admitted continuously to this container. Solder flux along with a ring of silver solder wire were put around the wires. A water-cooled copper tube induction coil was placed around the glass tube to include the copper block. The block was heated until the solder was well melted and then allowed to cool in the nitrogen atmosphere. The block was subsequently machined to remove the excess solder.

There are many things which were made in an attempt to obtain a good joint:

- (i) Silver soldering in a hydrogen atmosphere.
- (ii) To feed silver solder through a hole in the pyrex glass when the block was at required temperature. However big sparks were produced by this procedure. These sparks could have been eliminated by turning the induction furnace off. However the block would have cooled very fast and it is unknown whether the surface temperature would have been high enough.
- (iii) Soldering in a hydrogen atmosphere but using gold solder

(82.5% Au, 17.5% Ni) which is recommended for corrosive, high-temperature service. The melting temperature of this solder is 950°C .

Four good experimental runs were obtained with one block using technique (i); however, at the fifth run the heat flux meter gave spurious results which suggested that the joint was poor.

Copper Plug Insert

The problem with all previous attempts was that a very poor solder joint was made between the wires and the copper. In conventional soldering where a torch is used, the silver solder can be fed easily and a certain pressure on the solder makes the solder flow down the hole and fill it completely. Moreover, the jet of the torch helps the solder to flow down the thermocouple wires. Therefore, a cylindrical copper plug was made in which a heat flux meter was constructed. The small dimensions of the plug allowed the constantan wires to be silver soldered easily with an acetylene torch. A hole, which was .002 cm to .005 cm smaller than the plug, was drilled in the cylinder. This plug was then press-fitted into the copper cylinder via an Instron testing machine; pressures in excess of 40 MPa were necessary. This method, in contrast with others, gave consistent and reliable results in boiling heat transfer.

Two different plugs were used; one was 2 in. in diameter by 1 in. deep and the second one was 0.5 in. in diameter by 1 in. deep. The cylinder with the smaller plug cooled in approximately the same time as the cylinders where the heat flux meter was an integral part of the block; the larger plug indicated a faster cooling. This was

probably because the surface area over which the plug was cooled by boiling was about the same as the copper-copper area through which heat was transferred by conduction. Some thermal contact resistance obviously still existed at this interface. By making this area large relative to the cooled area, the relative importance of this interfacial resistance can be minimized. Hence all heat flux meters were constructed using the smaller plug.

This technique, however, led to other difficulties such as different calibration factors from copper cylinder to copper cylinder; in addition, there was a different response depending upon which centre-to-edge thermocouple was used. In an attempt to explain the difference in calibration factors for different meters installed in different cylinders, an analysis of the heat transfer behaviour of the meter under a variety of conditions was performed. These will be briefly discussed in turn.

The calibration factor will obviously be different from unity if the dimensions of the meter are different from those specified. The radius of the disk can be made very accurate according to the drill used in making the hole so that little error is expected here. The thickness of the disk, on the other hand, is less accurate. It is made by drilling the hole for the plug to a prespecified depth. The plug and the disk are fabricated separately with the disk thickness determined by the expected depth that the plug will be inserted into the hole in the cylinder. After insertion the extra material is machined from the outer surface of the plug and the disk thickness is determined by this operation. If the plug is not pressfitted into the hole to the

expected depth, the thickness of the disk will be more or less than expected. This procedure can not only give rise to a different disk thickness, but also can result in another problem. Since a considerable force is required to force fit the plug into the cylinder, it is possible that one side of the plug may exert a greater frictional force than another thus leading to distortion of the plug (that is the plug axis would not be exactly coincident with the radius of the cylinder). The machining operation would then give a disk which did not have parallel faces. Calculations indicate that with a 3° misalignment, the copper disk could vary from 0.51 mm on one side to 0.25 mm on the other.

The effect of this variation in thickness on the temperature field in the disk was evaluated by analysing that in an infinitely long strip of uniform and non-uniform thickness cut into a copper block of infinite dimensions. This simpler system was chosen since the circular geometry with an asymmetric temperature field would be much more difficult to analyse.

This analysis is reported in Appendix G. In summary, this analysis does explain the lower calibration factors, since the centre-to-edge temperature difference was considerably greater than that for a uniform disk of the same average thickness, regardless of which side temperature was measured. It follows that the calibration factor would depend on which side was used. This observation is consistent with the experience with the heat flux meters used in this study, that is, differences in calibration factors were observed depending upon which of the two edge thermocouples were used to indicate the heat flux. Both,

however as shown by experiments performed on Block 5 and Block 23 gave roughly the same overall calibrated results.

Fabrication problems can give rise to other effects which have been observed for Block 14. The actual cross-section of the disk was observed by cutting the cylinder and then slowly machining the cylinder to expose the disk along its diameter. Photographs of this are shown in Figure E.3. The thickness of the disk was measured and found to be of a uniform thickness of 0.76 mm, which is 50% thicker than expected. This greater thickness resulted because the plug was inserted to a greater depth than desired as indicated by the depression in the bottom face of the hole into which the plug was inserted (Figure E.2). This effect would have made the disk thickness about 50% greater than expected and would have resulted in a calibration factor of 1.5. The calibration factor, however, was found to be one-third of this value. Figure E.3 suggests the reason for this. It shows that the edge thermocouple was not silver soldered at the edge of the disk, but at some point on the wall of the hole about 2 mm below the surface. This was caused by the silver solder running down the wire during the soldering operation. Since a conduction analysis indicates a considerably higher temperature at this point, the centre-to-edge temperature difference which would be measured would be considerably higher than expected. This would give rise to a low calibration factor. Block 14 was in fact the worst case encountered as it gave extremely low overall CHF and did not show the typical CHF pattern around the cylinder. Although, the seriously abnormal design, the overall CHF was within 30% of the overall



FIGURE E.2 - PHOTOGRAPH SHOWING THE BOTTOM SECTION OF THE PLUG INSERT



FIGURE E.3 - PHOTOGRAPH SHOWING THE LOCATION OF THE EDGE THERMOCOUPLE

CHF normally obtained. This shows that the unsteady-state calibration procedure has a damping effect of the error introduced in the design.

APPENDIX F

DATA ACQUISITION AND ANALYSIS OF RAW DATA

This appendix describes the method used to acquire the data and the technique used to analyse them.

1- Data Acquisition

As described earlier, the instrumented copper cylinder was heated to a temperature varying between 200°C and 300°C and then plunged into a pool of stagnant water at the desired level of subcooling. During the cooling period, both the surface temperature and the temperature difference signals were continuously fed to thermocouple transmitters where millivolts were converted to milliamperes. These thermocouple transmitters were equipped with two 20-twin metal film infinite resolution potentiometers to provide wide-range span and zero adjustment. The transmitters were calibrated in the range of 0 to 2 mV for the temperature difference and from 3 to 15 mV for temperature measurements. There were 6 transmitters (Acromag, 315-WM-50); One of which was used for surface temperature measurement; the other five were used for temperature difference measurements. The output of these transmitters was in milliamperes and range from 10 mA to 50 mA. In addition to the six Acromag transmitters, there were sixteen home-made transmitters which were calibrated in the same way as the others and simply amplified the millivolt signals to a range varying between 2 and 10 Volts. The

transmitters were calibrated daily. Since the Acromag transmitters were more stable and accurate, they were used to transmit any small temperature difference signals where their accuracy was most important.

The output signal of the transmitters was sent to the Nova minicomputer interface panel via a shielded cable (Belden Corporation, NO. 8775). The milliampere signal flowed through a 200 ohm resistor; the potential difference (2-10V) was fed to the appropriate A/D channel. The voltage signal from the other type of transmitters was fed directly to its appropriate A/D channel. There were 16 A/D 10-bit converters in the Nova computer used and accepted voltages varying between 2 and 10 Volts. The minicomputer was programmed to read at discrete time intervals at a rate of 100 readings/second. These values were averaged over a short time span, the interval (0.05 sec. to 2 sec.) depending upon the level of subcooling and the amount of the surface participating in the boiling process. The main minicomputer programs written in Assembly language are listed in Appendix Y. This Appendix also describes how to use the program. The main feature of this program was its ability to be started at the remote location of the experiment and to have the averaging rate changed during the experiment to accommodate rapid and slow cooling via a set of 3 contact senses. For instance, during saturation boiling, the temperatures were averaged over a period of 1 s (100 values) in the region of low heat fluxes and over 0.1 s (10 values) when the heat flux was within about 30% of the critical heat flux. For experiments performed under subcooled conditions, averages were taken even more frequently (0.05 s).

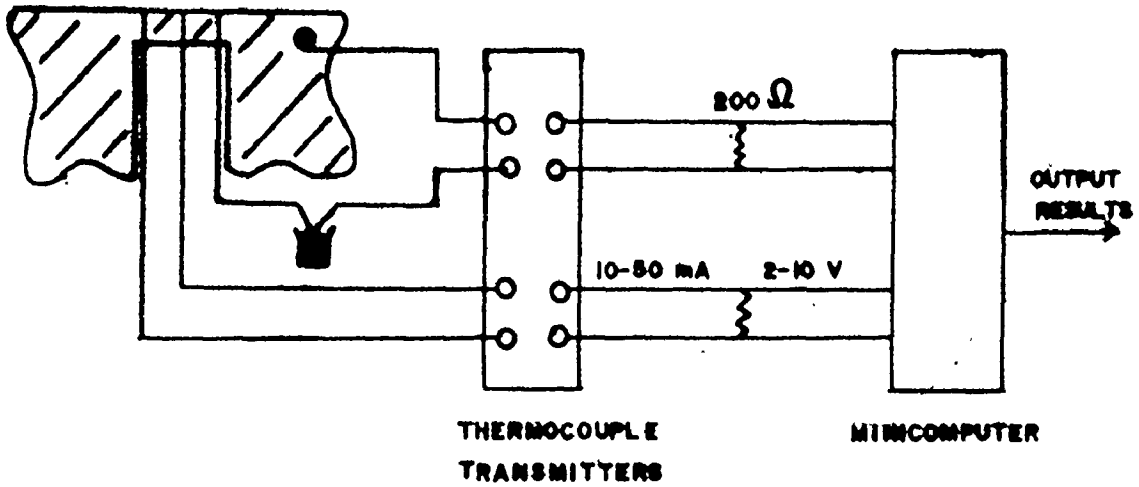


FIGURE F-1 - DATA ACQUISITION SYSTEM

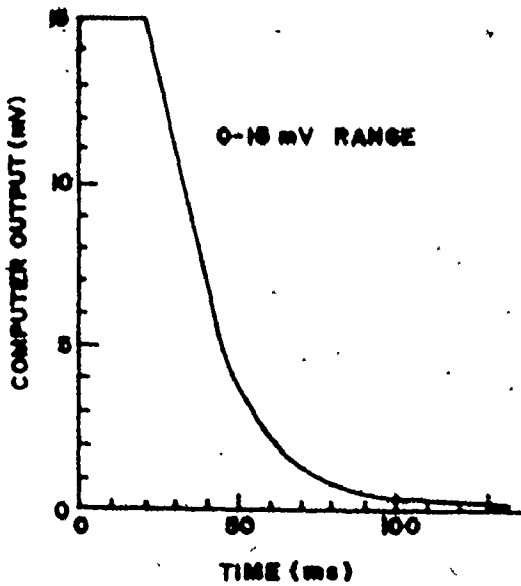


FIGURE F-2 - TRANSMITTER RESPONSE TO A STEP CHANGE

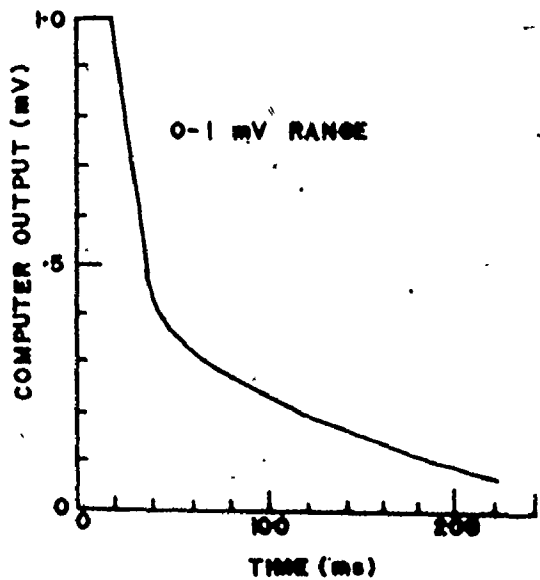


FIGURE F-3 - TRANSMITTER RESPONSE TO A STEP CHANGE

A minicomputer offers many advantages over a strip chart recorder, which was used initially in this project. With a chart recorder, the data reduction was time consuming and extremely limited. Moreover, its use introduced an element of subjectivity which should be eliminated. A minicomputer provided direct reading of the variables and then allowed direct analysis of the raw data; a chart recorder required considerable labour to transfer chart units into millivolts and then additional calculations to obtain temperatures and heat fluxes from these data. Moreover, there was always the problem of determining zero-time for the recorders when two single pen recorders were used to record the two signals from each heat flux meter. This problem would have become more severe when dealing with a bundle of cylinders.

Both kinds of transmitters had linear amplification. The time response of the Acromag transmitters depended on the range of calibration. For a calibration range of 3-15 mV and 0-1 mV, the output of the transmitters to a step change is presented on Figure F.2 and F.3. The transmitters indicated 90% of the step change in 56 msec and 180 msec for the ranges mentioned above. The home-made transmitters cover 99% of a step change in less than 100 msec.

2- Analysis

The experimental data of each experiment were stored on a disk file. When sufficient data have been collected, the disk file was transferred onto a paper tape. The data stored on paper tape were transferred to computer cards using the McMaster University CDC 6400 library subroutine "COPYPT". A Fortran program was written to accept

the original temperature-time and temperature difference-time data as input and computed the local temperatures and heat fluxes at the surface. This Fortran program is listed in Appendix Z. In this program, the data were read and discriminated in such a way as indicated below, to eliminate an excessive number of points on the boiling curve and still provide sufficient data to define the boiling curve. If a temperature difference deviated from the previous one by more than 0.010 mV, or if the surface temperature reading deviated from the previous one by more than 0.015 mV then this data point was recorded as another point on the boiling curve. The heat flux was calculated and the boiling curve was plotted using the Benson-Lehner plotting system.

With a simultaneous reading of the surface temperature and the temperature between the edge and the centre of the disk, it was possible to calculate the heat flux at the surface for a given wall superheat. It is relatively easy to derive an equation relating the heat flux at the surface as a function of the temperature difference on the disk surface (Equation 2.15). Darnedde(D1) expressed the edge-to-centre temperature difference as a millivoltage output (ΔE) for copper-constantan thermocouples:

$$(q/A) = \frac{4 k_o t_d}{R_o^2} \frac{\Delta E}{C} \quad (F-1)$$

The variable C is function only of the thermal characteristics and the temperature of the surface and is given by the following equation:


$$C = \frac{(\beta + 2\gamma \Delta T_w)}{(\beta + \alpha \Delta T_w)} \quad (F-2)$$

In this equation, $\Delta T_w (= T_D - T_{REF})$ and T_D was taken as the average of the edge and centre temperatures; $T_{REF} = 0^\circ\text{C}$.

APPENDIX G

STEADY-STATE TEMPERATURE DISTRIBUTION IN A TILTED HEAT FLUX METER

The response of the heat flux meter used in this study presented an unexpected behaviour in that two different boiling curves could be generated depending upon which of the two thermocouples located at the edge of the heat flux meter was used to record the temperature difference across the disk. If the meter had been constructed properly, the boiling curves should have been the same. Many possible causes for this behaviour have been investigated such as contact resistance between the thermocouple and the copper surface, formation with silver solder of a new couple, different calibration of the thermocouples, etc. However none of these could really explain the abnormal behaviour. There are now two known main effects of this discrepancy: First, an inclination of only few degrees of the press-fitted copper plug could produce an appreciable thickness variation across the disk and, secondly, the thermocouple may not be silver soldered at the edge of the disk, but at some point on the wall of the hole as shown in Appendix E. This appendix presents the analysis of the first of these effects. Only a 3° angle-inclination induces a variation of .25 mm in thickness across a nominally .5 mm thick heat flux meter. It was expected that the adiabatic and isotherm lines in the tilted heat flux meter and its vicinity could provide some information concerning the unexpectedly low calibration factors observed.

To verify the contribution of a tilt to the calibration factor of the heat flux meter, a computer program was written to compute the temperature distribution in the heat flux meter and its vicinity. In the program, the Laplace equation of a rectangular system was solved numerically instead of circular system to keep the system two-dimensional and reasonably tractable. A circular system with the asymmetry involved would require the solution of a three-dimensional system of equations which would have been beyond the capacity of the computer. A two-dimensional rectangular system should provide the desired information. This appendix describes the method used to solve the problem and presents the results obtained for a uniform and tilted heat flux meter.

G.1 Method of Solution

The temperature distribution in the rectangular heat flux meter can be described by the Laplace equation as there is no internal source of energy.

$$\frac{\partial^2 T}{\partial x^2} + \frac{\partial^2 T}{\partial y^2} = 0 \quad (G.1)$$

This is an elliptic equation so that the boundaries of the region of solution must be defined everywhere and the system of equations must be solved simultaneously. To satisfy the required boundary conditions the following assumptions are made:

- (1) At the boiling surface, it is assumed that a uniform heat flux

of 110 W/cm^2 ($350,000 \text{ Btu/hr ft}^2$) prevails.

(ii) At a certain distance away from the heat flux meter, it is assumed that conduction in the x-direction is negligible, and only an outward (y-direction) temperature gradient prevails. This boundary condition is set by specifying a temperature at the surface and then calculating the temperature of the inside mesh points using Fourier's law of conduction along that line with the specified heat flux density.

(iii) Similarly, it is assumed that at a certain depth below the surface the recess in the metal does not influence the temperature distribution so that a constant temperature line prevails.

(iv) Finally, it is assumed that there is a zero heat flow at the internal boundary of the heat flux meter, that is, the gradient normal to the surface is zero.

Figure G.1 describes the equations used for the different mesh points in the given system. These equations form a matrix of coefficients which must be inverted, using Gauss elimination, in order to obtain the temperature at each mesh point.

G.2 Results

G.2.1 The Temperature Distribution

The temperature distribution in the heat flux meter and its vicinity has been established for four different cases. A total of more than 400 mesh points have been used which therefore involves solving a system of more than 400 equations. However this huge matrix has fortunately no more than five entries per row and a sparse matrix solver

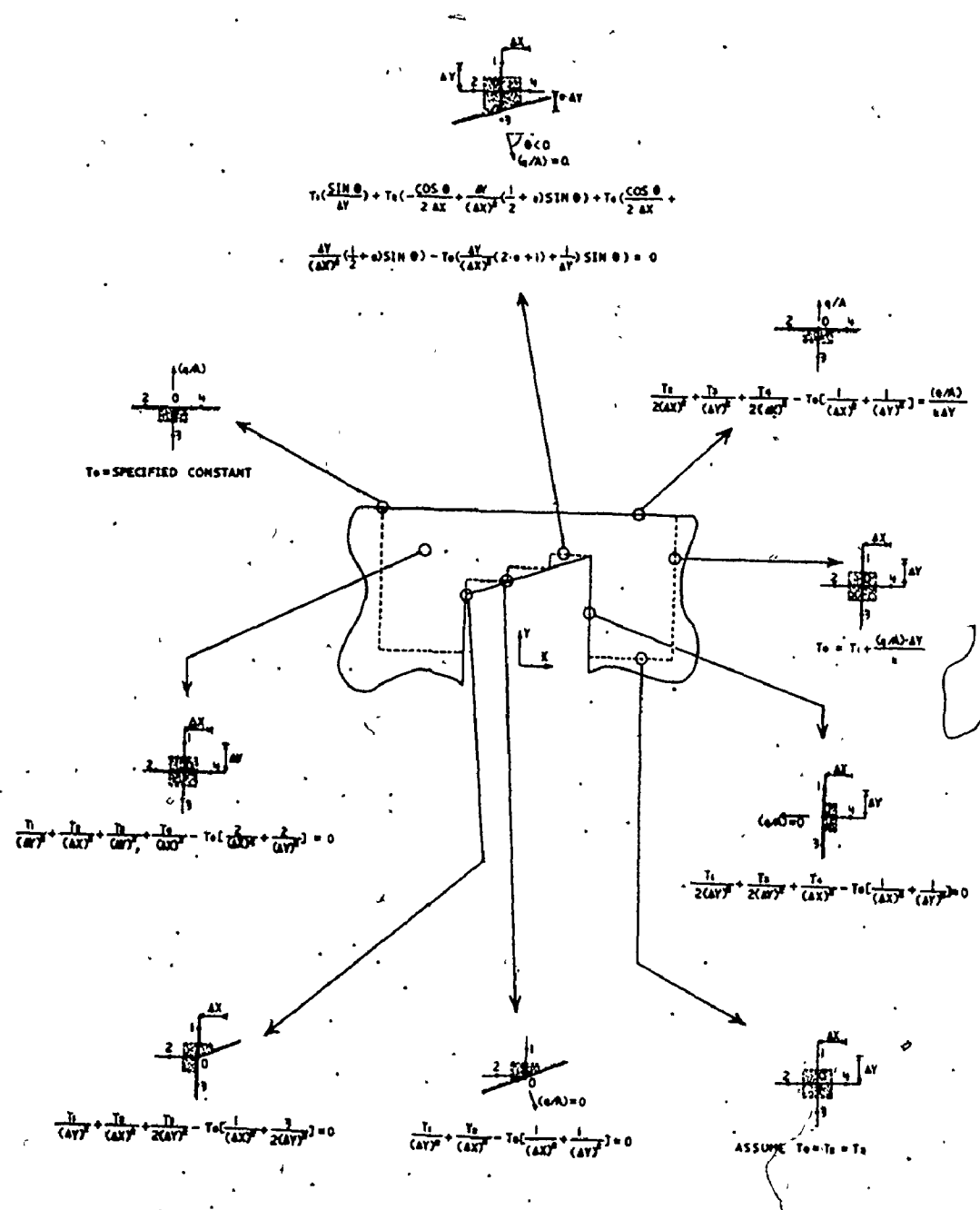


FIGURE G.1 - SYSTEM OF EQUATIONS FOR A TILTED HEAT FLUX METER

TABLE G.1

SUMMARY OF THE RESULTS OBTAINED
WITH A NUMERICAL METHOD FOR A UNIFORM
AND A TILTED HEAT FLUX METER

	<u>CASE NUMBER</u>			
	1	2	3	4
Temperature Difference (Predicted)				
At right ($^{\circ}\text{F}$)	62	30	50	40
At left ($^{\circ}\text{F}$)	62	30	60	50
Temperature Difference (Analytical)				
At right ($^{\circ}\text{F}$)	60	30	40	40
At left ($^{\circ}\text{F}$)	60	30	50	50
Calculated Heat Flux				
At right (W/cm^2)	113	113	183	146
At left (W/cm^2)	113	110	219	182
Applied Heat Flux	110	110	110	110
Calibration Factor				
At right	.97	1.0	.60	.75
At left	.97	1.0	.50	.60
Tilt (Degree)	0	0	3	3

was used. It took about 400 seconds (CPU time on a CDC 6400 computer) to solve the complete system.

Two cases were run with a uniform thickness in order to have a comparison with the one-dimensional method of solution. One case was run with a .254 mm thick disk and the other with a .51 mm thick disk. The temperature distribution for each case are presented on Figures G.2 and G.3 respectively. Two other cases were run with a tilted disk for two different sizes of the mesh. These are presented on Figures G.4 and G.5. Table G.1 summarizes the main values obtained with this study and compares it with an analytical solution.

G.2.2 Analytical Solution

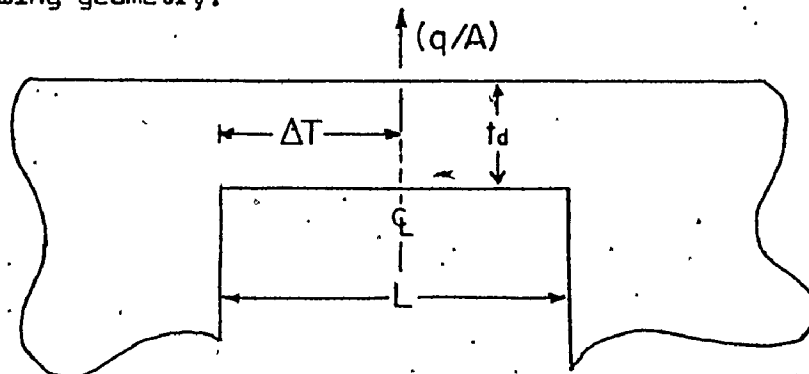
The equation for a uniform and non-uniform heat flux meter in Cartesian geometry will be derived in turn.

(1) Uniform Heat Flux Meter

It is relatively easy by performing a heat balance on the heat flux meter to derive the following equation:

$$(q/A) = \frac{8 k t_d \Delta T}{L^2} \quad (G.2)$$

for the following geometry:



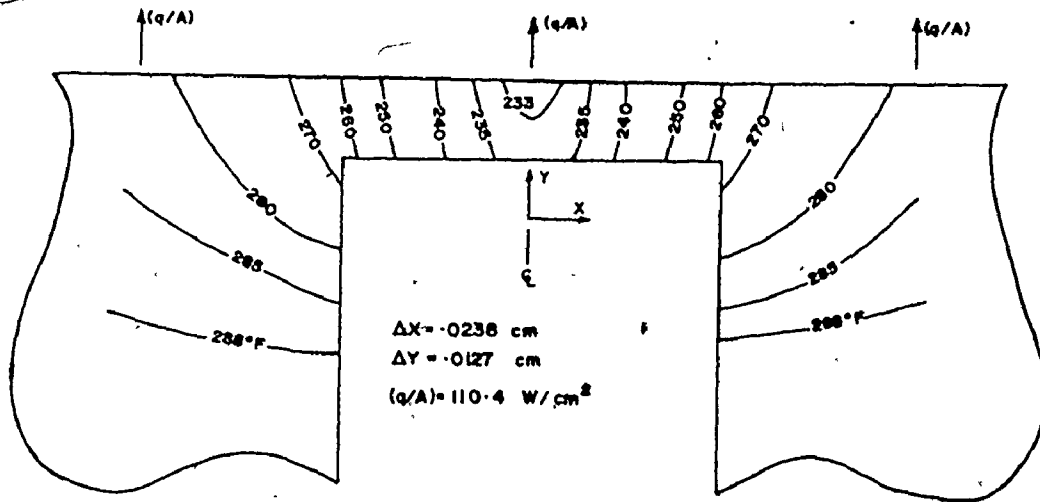


FIGURE G.2 - TEMPERATURE DISTRIBUTION OF A UNIFORM HEAT FLUX METER

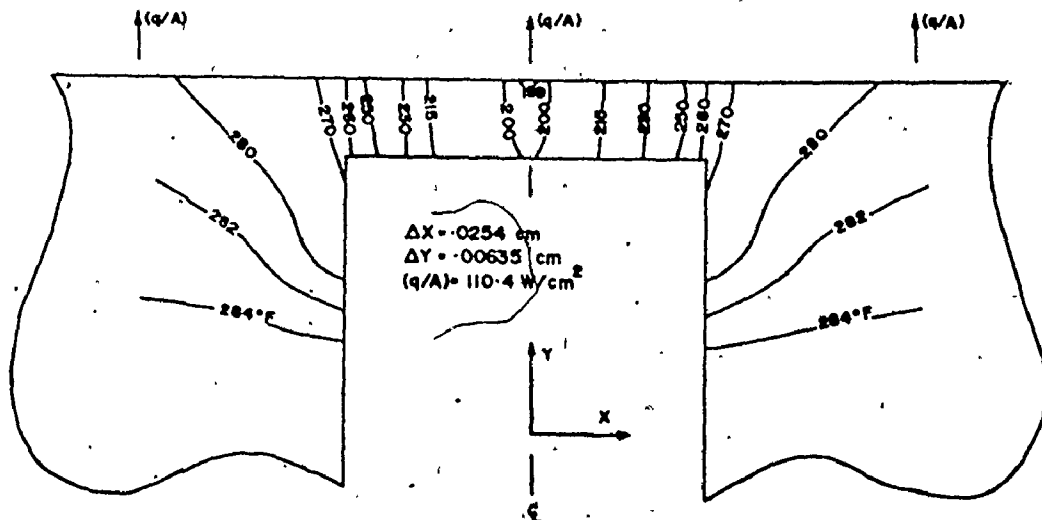


FIGURE G.3 - TEMPERATURE DISTRIBUTION OF A UNIFORM HEAT FLUX METER

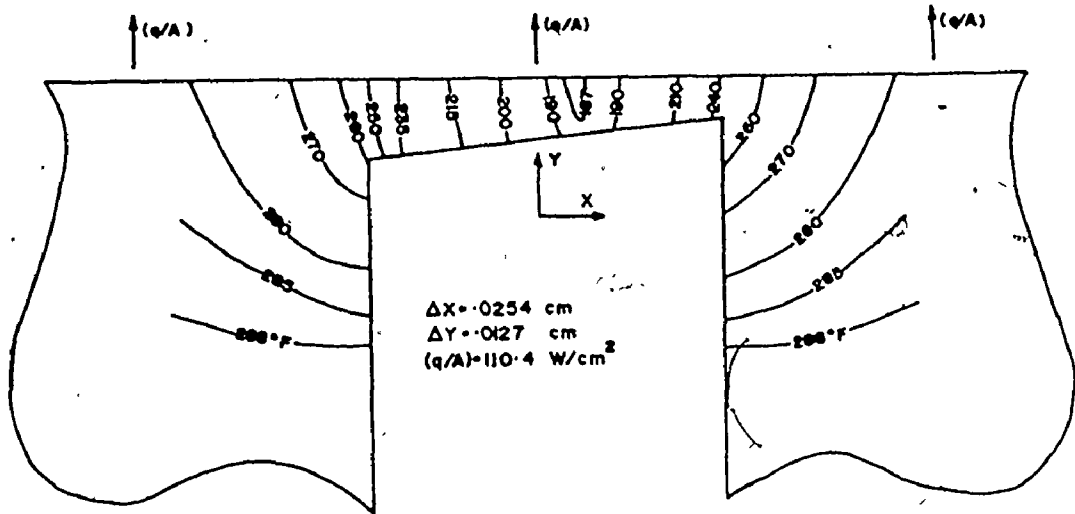


FIGURE G.4 - TEMPERATURE DISTRIBUTION OF A TILTED HEAT FLUX METER

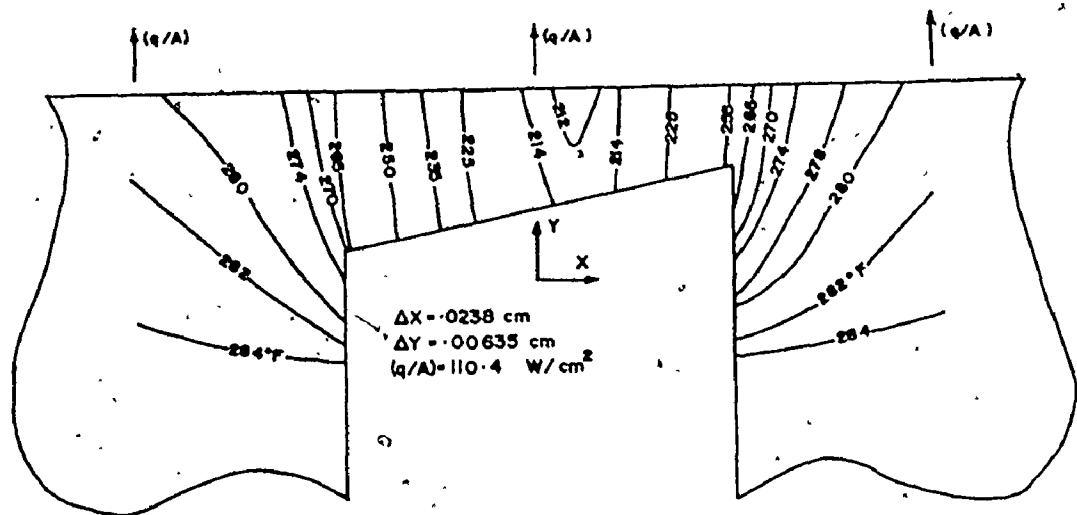


FIGURE G.5 - TEMPERATURE DISTRIBUTION OF A TILTED HEAT FLUX METER

By using the same values as was used in the finite difference method:

$$(q/A) = 110 \text{ W/cm}^2 \text{ (350,000 Btu/hr ft}^2\text{)}$$

$$k = 3.668 \text{ W/cm}^{\circ}\text{C (212 Btu/hr ft}^{\circ}\text{F)}$$

$$t_d = 0.51 \text{ mm (.020 in.)}$$

$$L = 0.476 \text{ cm (.1875 in.)}$$

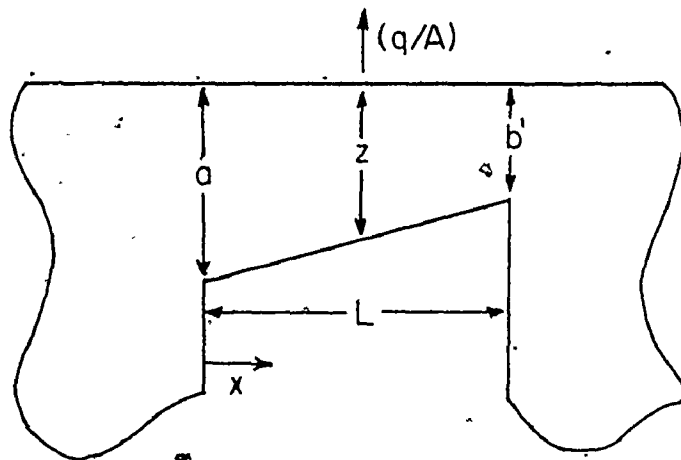
A temperature difference of 30°F (16.6°C) was obtained.

(ii) Tilted Heat Flux Meter

Let

$$b = \frac{a - b'}{L}$$

$$z = a - b \cdot x$$



By performing a heat balance on the heat flux meter, it is relatively easy to derive:

$$k \frac{dT}{dx} = (q/A) \frac{x}{a - bx} + \frac{C_1}{a - bx} \quad (\text{G-3})$$

$$k T = (q/A) \left[-\frac{x}{b} + \frac{a}{b^2} \ln(a - bx) \right] - \frac{C_1}{b} \ln(a - bx) + C_2 \quad (\text{G-4})$$

Assumes the following boundary conditions:

$$\text{At } x=0, T=T_a$$

$$\text{At } x=L, T=T_b$$

$$\therefore C_1 = k b (T_a - T_b) \ln\left(\frac{a}{a-bL}\right) - (q/A) \left[L \ln\left(\frac{a}{a-bL} + \frac{a}{b}\right) \right] \quad (G-5)$$

$$\therefore C_2 = \frac{C_1}{b} \ln(a) + k T_a + (q/A) \left[\frac{a}{b^2} \ln(a) \right] \quad (G-6)$$

Instead of trying to form a general equation, it is better to calculate C_1 and C_2 for a specific case and substitute in Equation G.4 to solve for T .

Example: Solve for $x = L/2$ with

$$a = .51 \text{ mm } (.020 \text{ in.})$$

$$b = .254 \text{ mm } (.010 \text{ in.})$$

$$L = .483 \text{ cm } (.190 \text{ in.})$$

$$k = 3.668 \text{ W/cm}^{\circ}\text{C } (212 \text{ Btu/hr ft}^{\circ}\text{F})$$

$$(q/A) = 110 \text{ W/cm}^2 \text{ } (350,000 \text{ Btu/hr ft}^2)$$

$$T_a = 93.3^{\circ}\text{C } (200^{\circ}\text{F})$$

$$T_b = 87.8^{\circ}\text{C } (190^{\circ}\text{F}) \quad (\text{ie. assume the same end temperature found in numerical method}).$$

The temperature at the centre of the disk was found to be 150°F . This value is exactly the one predicted by the finite-difference method.

G.3 Discussion

For cases number 2 and 4, more mesh points were used to solve the system and therefore it is more accurate. With this particular mesh size, the numerical method predicts exactly the temperature difference calculated with the analytical solution. This implies that for a uniform thickness meter the one-dimensional heat balance represented by Equation G.2 is valid for this system. Moreover, as will be shown in Appendix I, it is valid for the circular heat flux meter as well.

It would be tempting to believe that, due to the one to one correspondence between the analytical solution and the numerical solution, it is not necessary to solve the system numerically. It is in fact true for a uniform thickness heat flux meter and this study was used to prove it. It was thought initially that the isotherm at the edge of the heat flux meter could affect the temperature difference on the disk. This analysis shows that this is not true for a uniform heat flux meter. On the other hand, it is impossible theoretically to predict the two edge temperatures for a tilted heat flux meter so that the two centre-to-edge temperature differences could be predicted. Because of the asymmetric geometry, the thermal centre is shifted toward the edge with the smaller thickness. For a tilt of only 3° on a nominal .51 mm thickness, there is an appreciable difference from the ideal behaviour. And a small tilt can very well play a large role in accounting for the unexpectedly low calibration factor observed in this project.

APPENDIX H

UNSTEADY-STATE CALIBRATION PROCEDURE

Because of the various defects that could be introduced in the construction of a heat flux meter, as discussed in Chapter 4, it was not surprising to find that heat flux meters showed a behaviour different from that expected. Because of these defects, it is imperative to calibrate each heat flux meter individually.

A calibration factor (CF) of a heat flux meter was obtained by comparing the total enthalpy loss from the cylinder, over the duration of the experiment, with that obtained by integrating the measured (apparent) local heat flux density over the total heat transfer area and over the quenching time, viz.:

$$Q = \rho C_p V (T_i - T_f) = \int_A \int_0^t (CF)(q/A)_{app} dA dt \quad (H.1)$$

The apparent heat flux density was calculated by equation 4.1, assuming a uniform average heat flux density over the disk surface. It was assumed also that the calibration factor was constant (independent of heat flux) and unique for a particular heat flux meter. Therefore, Equation H.1 may be rearranged to give the defining equation for the calibration factor:

$$CF = \frac{\rho C_p V (T_i - T_f)}{\int_A \int_0^t (q/A)_{app} dA dt} = \frac{Q}{\int_A \int_0^t (q/A)_{app} dA dt} \quad (H.2)$$

Procedure for Evaluation

The general procedure for calibration required at least one quenching experiment (preferably replicated) with the heat flux meter positioned at each angle (0, 30, 60, 90, 120, 150, 180). It was thus assumed that the measured heat flux density at each of these angles was symmetric and uniform over the length of the cylinder. Because measurements of heat flux versus time were only made at these seven different angles it was necessary to discretize the area integral and assume that the measured heat flux pertained over an angle of $\pm 15^\circ$ from the point in question. The integral over time was easily evaluated by integrating the heat flux density versus time for each quenching experiment by the Trapezoidal Rule.

The evaluation of the sensible heat content of the cylinder posed another problem. Equation H.2 implicitly assumes that the cylinder had a uniform initial temperature of T_i and a uniform final temperature, T_f . This assumption is reasonable because the cylinder was preheated relatively slowly and at the end of the quench (essentially the same temperature for each experiment) the heat flux at the surface was very small. Unfortunately, however, it was impractical to try to quench the copper cylinder from the same initial temperature each time; hence some modification of Equation H.2 was required to allow for the different sensible heat contents of the cylinder for each of these experiments. Note that, with the same final temperature for each experiment, the total quench time, that is the integration limit on the integral was different for each experiment but related to the total

sensible heat content. Equation H.2 was therefore rearranged to

$$CF = \frac{1}{A_0 \frac{\int_0^{t_0} (q/A)_0 dt}{Q_0} + A_{30} \frac{\int_0^{t_{30}} (q/A)_{30} dt}{Q_{30}} + \dots + A_{180} \frac{\int_0^{t_{180}} (q/A)_{180} dt}{Q_{180}}} \quad (H-3)$$

Hence each experiment provides a $\int (q/A) dt / Q$ value, called here the calibration ratio. For replicated runs at a point, these may be averaged. Given the symmetry assumption, and the measuring points used, the areas at each point become some appropriate fraction of the total area and the final expression for CF becomes:

$$CF = \frac{1}{A_T \left\{ \frac{1}{12} \frac{\int_0^{t_0} (q/A)_0 dt}{Q_0} + \frac{1}{6} \frac{\int_0^{t_{30}} (q/A)_{30} dt}{Q_{30}} + \dots + \frac{1}{12} \frac{\int_0^{t_{180}} (q/A)_{180} dt}{Q_{180}} \right\}} \quad (H-4)$$

Hence each of the calibration ratios was weighted according to the area over which it pertained.

Inverse values of the calibration ratio are tabulated in Appendix C. These inverse calibration ratios have the dimensions of area. This calibration procedure, although producing different calibration factors for different meters, did provide excellent reproducibility of the boiling heat flux densities from one test cylinder to another (within 10% in most cases).

H.2 Some Analysis Related to the Calibration Factor

H.2.1 Table of Calibration Factors

Table H.1 presents the different calibration factors obtained for various heat flux meters used throughout this study. Since a large number of quenching experiments were performed under saturation and subcooled conditions, it was possible to calculate the calibration factor for a given heat flux meter by the aforementioned procedure from these experiments. Unfortunately, the calibration factor for any given meter was slightly different (mostly greater by about 20% under large subcoolings) as the level of subcooling increased. Some cylinders showed a difference of only a few percent while others showed a more substantial difference. This suggests that perhaps the calibration factor depended on the level of heat flux and also on something that was unique to the meter. A small contact resistance between the main cylinder and the copper plug insert could explain this phenomena. If the copper plug cooled somewhat faster than the rest of the cylinder, then the integration over time would not pertain exactly to the cylinder whose sensible heat was assumed to be transferred. Since this integral would be smaller for larger heat fluxes, the calibration factor should be larger as the levels of heat are increased. Such an effect was observed. Furthermore, it was that those cylinders which required the largest force to press-fit the insert (and therefore were expected to have the least thermal resistance) had the smallest change in the calibration factor with subcooling. Since these differences in calibration factor were small, it was decided to use the one obtained under

TABLE H.1

CALIBRATION FACTORS

<u>BLOCK NUMBER</u>	<u>CODE[*] NUMBER</u>	<u>DEGREE OF SUBCOOLING (°C)</u>	<u>CALIBRATION FACTOR</u>
2	0	0	.528
2	0	5	.461
2	0	10	.451
2	0	20	.449
5	0	0	.705
5 ⁺	0	0	.942
5	0	5	.691
5	0	10	.735
5	0	20	.800
7	3	0	.906
8	3	0	.746
8	6	0	1.254
8	0	0	.846
8	0	20	1.193
9	0	0	1.008
11	0	0	.279
12	0	0	.483
13	0	0	.946
14	0	0	.508
15	3	0	.631
15	6	0	.701
15	0	0	.762
15	0	20	.873
17	0	0	.644
20	0	0	1.353
22	0	0	.873
22	0	30	1.017
23	0	0	.706
23 ⁺	0	0	.532

* Code Numbers are defined in Appendix C
 + Side Number 2 of the heat flux meter

saturation conditions where the effect of thermal contact resistance would be smallest.

A more disturbing behaviour was observed for Cylinders 8 and 15, for which different calibration factors were obtained for different lengths of these cylinders. An explanation of this behaviour was attempted in Chapter 5. It was decided in that case to use an average calibration factor at saturation.

H.2.2 Sensitivity of the Calibration Factor

The temperature difference on the disk is passed through an amplifier/transmitter and recorded by the minicomputer. It is impractical to perfectly calibrate this transmitter and hence the computer may record a value which is slightly different from the actual one. It is possible to account for this error in calibration by obtaining a correction at the time of doing any given experiment. It can be assumed that the heat flux was so small at the beginning when the cylinder was located in air prior to being quenched and similarly when it was in water at the end of the experiment that the temperature difference on the disk was essentially zero. Usually the recorded values both at the beginning and the end were the same; hence all e.m.f. values over the entire quenching time were corrected for this offset. Note that this offset also accounted for small voltages that were induced by faulty connections or other effects.

It was desired to determine the sensitivity of the calibration factor on this offset. To do this, the experimental data of Cylinders

TABLE H.2

INFLUENCE OF THE TEMPERATURE DIFFERENCE
OFFSET ON THE CALIBRATION FACTOR

	BLOCK 15			BLOCK 23		
	<u>-.02 mV</u>	<u>Normal</u>	<u>+.02 mV</u>	<u>-.02 mV</u>	<u>Normal</u>	<u>+.02 mV</u>
Calibration Factor	.613	.762	.882	.570	.717	.865
% Increase	-19.5	0	+15.7	-20.5	0	+20.6
Overall CHF (W/cm^2)						
Uncalibrated	171.9	166.4	160.9	200.2	194.7	189.4
% Increase	+3.3	0	-3.3	+2.8	0	-2.7
Calibrated	105.4	126.8	141.8	114.1	139.6	163.8
% Increase	-16.9	0	+11.8	-18.3	0	+17.3

15 and 23 were calibrated three times using the normal offset, the normal offset minus 0.02 mV and the normal offset plus 0.02 mV respectively. The findings are summarized in Table H.2. Note that a correction of 0.02 mV to the normal e.m.f. recorded at the critical heat flux, results in less than 5% change in the CHF. On the other hand, since this correction was integrated over the entire quench time, the calibration factor is changed significantly (ca. 20%). Therefore the calibration factor is very sensitive to the offset. It should be added that 0.02 mV is much more than the expected error. On the other hand, the uncalibrated critical heat flux is not very sensitive to the temperature difference offset. This low sensitivity is extremely important here since the comparison of critical heat fluxes at different angles, under different subcooled conditions, in an array, etc. is important.

H.2.3 Variance of the Calibration Factor

At one point during this experiment, it was desired to know how many experiments were necessary to establish an appropriate calibration factor for a particular heat flux meter. A statistical analysis was undertaken in which a calibration factor was determined by considering only a discrete number of calibration ratios at each angle (either 1 or 2 values for each angle). Because there were usually two or more experiments performed at each angle, it was possible to generate a number of calibration factors by using all possible permutations in the calculation. With all the calibration factors so obtained it was possible to take an average value and calculate the variance. This analysis indicates the accuracy of this calibration factor if only 1 or 2

experiments are performed at each angle.

This analysis was performed on some copper cylinders and the results are presented on Table H.3. Even if only one quenching experiment was done at each angle, the calibration factor can be determined with fairly good accuracy (standard deviation about 4%). If two experiments were performed at each angle, the standard deviation is decreased to about 1%. Table H.3 also contains the standard deviation for the overall critical heat flux. The standard deviation of the overall CHF is also significantly reduced when at least two experiments were performed at each angular location (less than 3% for one experiment to about 1% when two experiments were performed).

TABLE H.3

STANDARD DEVIATION OF THE CALIBRATION FACTOR
AND OVERALL CRITICAL HEAT FLUX

BLOCK NUMBER	CODE* NUMBER	AVERAGE	CALIBRATION FACTOR			OVERALL CHF (UNCALIBRATED)					
			USING 1 VALUE STD. DEV.	NO. OF	USING 2 VALUES STD. DEV.	NO. OF	AVERAGE (w/cm ²)	USING 1 VALUE STD. DEV.	NO. OF	USING 2 VALUES STD. DEV.	NO. OF
5	0	.706	.034	1440	.020	112	141.7	4.9	3240	1.9	448
9	0	1.009	.032	3024	.011	512	116.3	3.0	1344	1.4	128
15	3	.634	.026	256	.005	4	190.4	3.8	256	1.0	4
15	6	.702	.023	432	.003	8	165.0	4.6	960	1.3	56
15	0	.763	.020	432	.002	8	167.0	3.6	432	1.5	8
22	0	.898	.063	1440	.032	112	152.4	5.2	1920	3.3	224

* Code numbers are defined in Appendix C.

APPENDIX I

THEORETICAL ANALYSIS OF A HEAT FLUX METER

As mentioned in Chapter 4 and described in Appendix J, the calibration factor of a particular heat flux meter obtained with a steady-state experiment is much too high and is a function of the heat flux density prevailing at the boiling surface. Two reasons are given for the unusually high calibration factors obtained: First, there is an inherent temperature depression on the surface in the vicinity of the heat flux meter and, secondly, there is a thermal contact resistance between the copper plug insert and the copper cylinder. The theoretical analysis which is reported in this appendix was initiated to determine the effect on the calibration factor of the temperature depression in the vicinity of the meter under steady-state boiling conditions. This analysis determines the relative contribution of this local effect on the calibration factor. In essence, the problem is defined as finding the response of the heat flux meter when it is submitted to nucleate boiling, according to a given boiling curve, when a point far away from the heat flux meter is subjected to the critical heat flux. This analysis was then extended to cover other parts of the boiling curves in order to see how well a heat flux meter would follow or predict (from the measured ΔT) the known applied boiling curve. In addition, this analysis would demonstrate whether the calibration factor was a strong function of heat flux.

This appendix is concerned with describing the numerical technique used to solve the problem, presenting and discussing the results and finally presenting some conclusions concerning the calibration factor and the overall operation of the heat flux meter.

I.1 Method of Solution

The temperature field in a heat flux meter and its vicinity must be found in order to determine the boiling heat flux over the surface of the meter and that over the surface surrounding the meter. Unfortunately, this temperature field is a function of the heat flux density; thus an iterative calculation procedure results.

To obtain the temperature field, the Laplace Equation in cylindrical coordinates must be solved, viz.:

$$\frac{\partial^2 T}{\partial r^2} + \frac{1}{r} \frac{\partial T}{\partial r} + \frac{\partial^2 T}{\partial z^2} = 0 \quad (1-1)$$

In solving this problem, the following assumptions are made:

- (i) It is assumed that the heat flux meter is flat, that is, the curvature of the cylinder is negligible.
- (ii) It is assumed that the heat transfer coefficient at any point on the nonisothermal heating surface is the same as would be obtained if the surface surrounding the point was at the same temperature. In other words, if the temperature at a point on the surface is known, the heat transfer coefficient at that point can be obtained from the boiling curve which had been previously determined for an isothermal

surface.

(iii) It is also assumed that the heat flux meter response time is small enough that a pseudo-steady-state may be assumed to prevail within the meter and for the boiling process.

Because Equation I, 1 is a two-dimensional elliptic equation, it must be solved in a closed range of integration. It is therefore necessary to specify all boundary conditions for the system which are:

(i) At the boiling surface, the boundary condition is the heat flux density which is determined by the local (point) temperature prevailing at the surface. The relationship between the heat flux density and the surface temperature is provided through a given boiling curve (at $z=0$,

$$(q/A) = f(T_{\text{wall}}).$$

(ii) At a certain distance away from the edge of the heat flux meter, the temperature is not affected by the presence of the meter (that is, the conduction in the r-direction is negligible). This boundary condition is set by specifying a temperature at the surface and then calculating the temperature at the inside mesh points using Fourier's law of conduction along that line (at $r=R_{\text{far}}$, $T = T_{\text{far}} + \frac{z}{k} (q/A)_{\text{far}}$).

The thermal conductivity k is assumed to be constant.

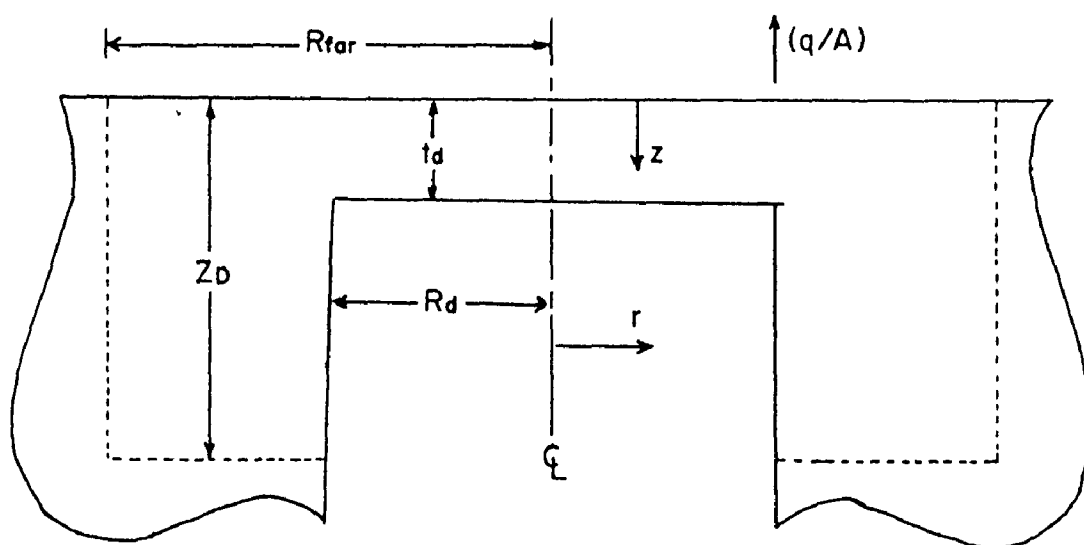
(iii) Similarly, it is assumed that at a certain depth below the boiling surface, the metal recess does not influence the temperature distribution so that a constant temperature line prevails (that is, these mesh points do not "see" or sense the heat flux meter). (at $z=Z_0$,

$$T = T_{\text{far}} + \frac{Z_0}{k} (q/A)_{\text{far}}.$$

(iv) It is assumed that there is a zero heat flow at the internal

boundary of the heat flux meter, that is, the gradient normal to the surface is zero ($\frac{dT}{dz}=0$, at $z=t_d$ and $0 \leq r \leq R_d$; $\frac{dT}{dr}=0$, at $r=R_d$ and $z > t_d$).

(v) Finally, because the heat flux meter is symmetric, it is only necessary to consider half of it. Therefore a symmetry condition prevails at the geometric centre of the meter ($\frac{dT}{dr}=0$ at $r=0$).



Based on these boundary conditions, the finite difference equations were derived for every nodal point in the system. Figure I.1 presents the derivation of all possible equations for the system. For the particular system used in this study, there were 5 mesh points by 10 mesh points in the heat flux meter portion and 9 mesh points in the radial direction and 15 in the z -direction outside the heat flux meter. There were a total of 195 equations which were solved simultaneously using Gauss elimination method. It took approximately 7 seconds (CPU time on a CDC 6400 computer) to get a complete solution using double

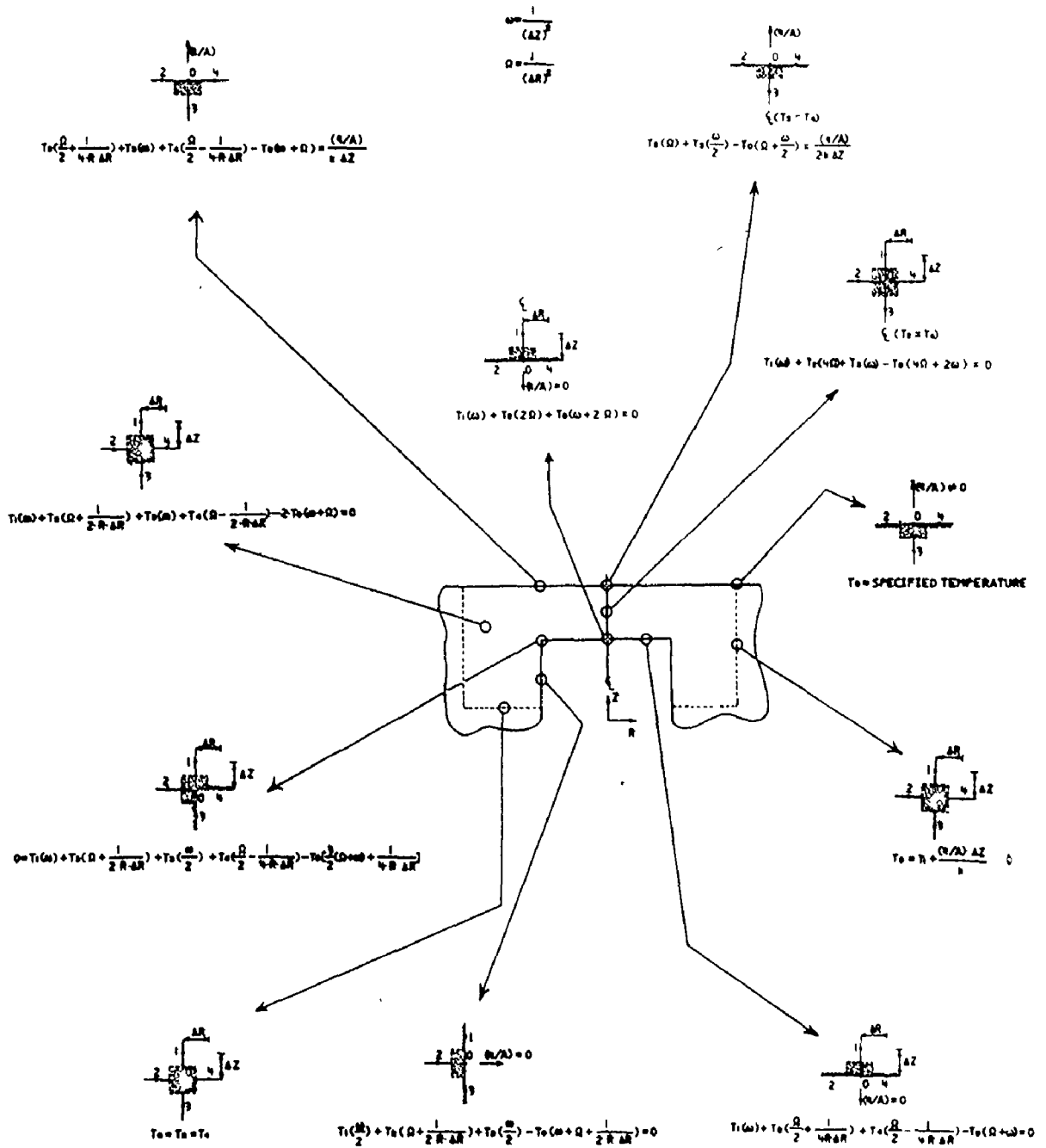


FIGURE I.1 - SYSTEM OF EQUATIONS FOR A HEAT FLUX METER

precision arithmetic. When an uniform heat flux was applied on the surface, only one solution was necessary. On the other hand, when the meter was submitted to a boiling curve, every point on the surface had a different heat flux and it was therefore necessary to iterate until every temperature on the surface agreed from one iteration to the next within a given tolerance.

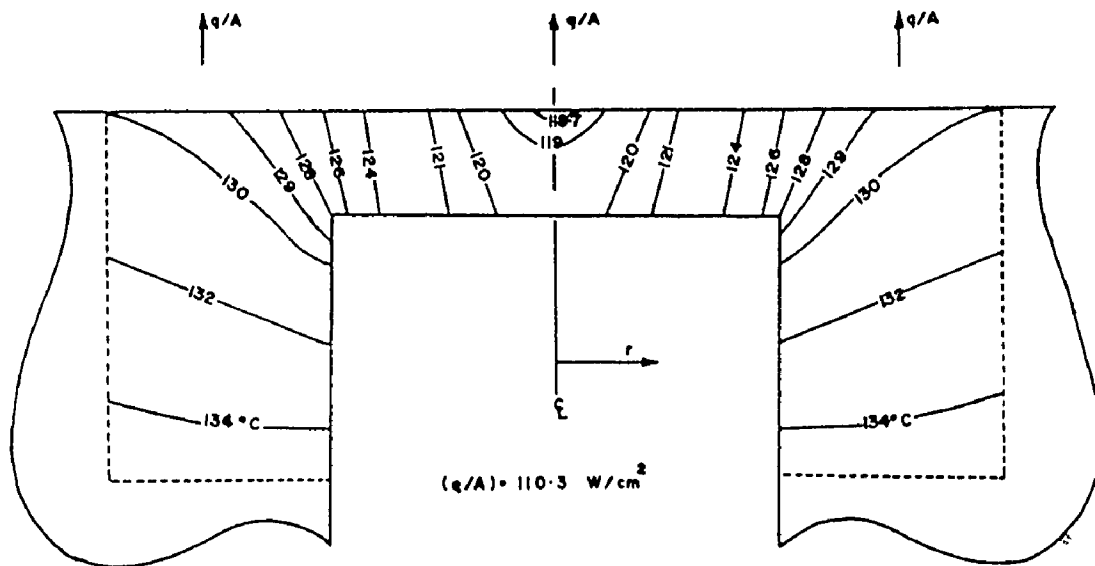
I.2 Results and Discussion

I.2.1 Reliability of the Numerical Method

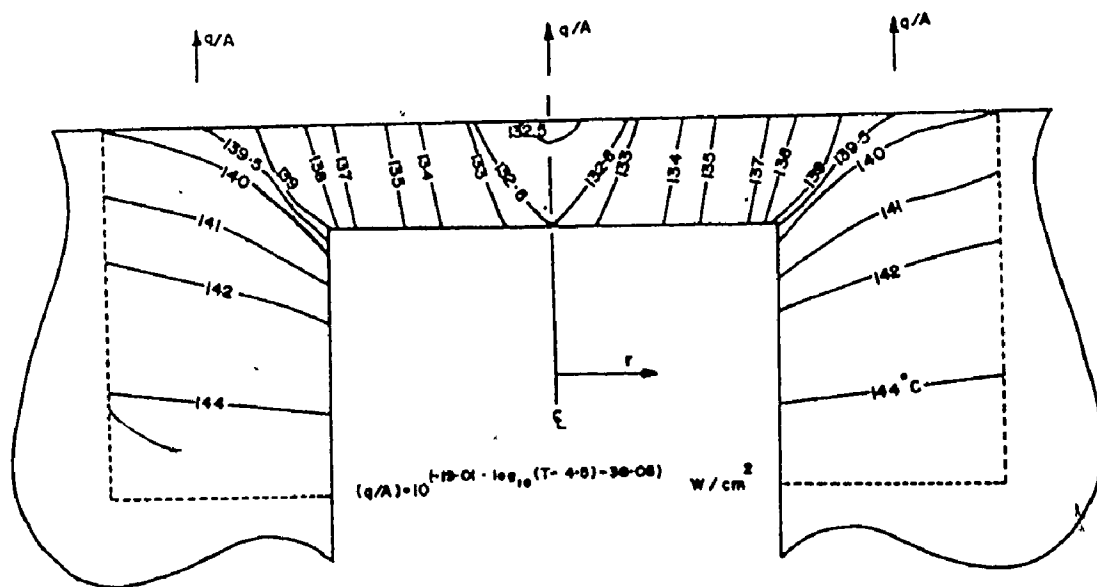
Whenever a numerical method is used to solve an equation, it is imperative that the mesh size be fine enough to provide the true temperature distribution in the system. One way to test the accuracy of the numerical solution is to solve the system using two different mesh sizes. This was done by comparing the results obtained with 37 mesh points and with those using 195 mesh points. A uniform heat flux density was applied at the surface and the same temperature difference on the disk was predicted for both the fine and coarse mesh systems. It was therefore decided that the finer mesh system which involved 195 equations provided sufficient accuracy under all conditions to be tested. A typical calculated temperature profile is presented on Figure I.2(a).

I.2.2 Heat Flux Density as Predicted by the Meter

It was evident from the calculations assuming a uniform heat flux over the entire surface of the meter and cylinder that the heat



(a) UNIFORM SURFACE HEAT FLUX



(b) VARIABLE SURFACE HEAT FLUX

FIGURE 1-2- TEMPERATURE DISTRIBUTION ON A HEAT FLUX METER AND ITS VICINITY

flux meter was predicting a heat flux which was smaller than the one applied. For instance, in the case described by Figure I.2(a), the surface temperature difference is 7.5°C which predicts a surface heat flux of 102.4 W/cm^2 . This value shows a difference of 7.9 W/cm^2 (7.5%) when compared to the applied one. This 7.5% error is consistent throughout this study and for all levels of heat flux. This is not too important because this error is corrected when a particular heat flux meter is calibrated.

The error mentioned here is only an apparent one because the temperature difference is taken at the surface. However if an average temperature is taken both at the edge and the centre of the meter, the same heat flux density as the applied one would be predicted. This shows once more the validity of the one-dimensional equation to predict the surface heat flux. Unfortunately, an average temperature was not taken at each point and therefore a constant percentage error was introduced in this study and should be kept in mind when results are analysed.

I.2.3 Steepness of the Boiling Curve

It is evident that the influence of the temperature depression near the heat flux meter on the calibration factor is greater for a steeper boiling curve. To verify this effect, the heat flux meter was submitted to three different boiling curves where the point far away from the meter was set to the temperature at which the critical heat flux occurs. The results are summarized on Table 1. Table 2 gives the equations used in the various cases. The results of Table 1 clearly show the influence, on the correction factor, of the inherent

temperature depression on a heat flux meter. The assumption of a uniform heat flux density on the whole boiling surface can lead to errors of more than 100% and it is strongly dependent on the shape of the boiling curves. Therefore, at any moment, the heat flux near the heat flux meter is different from that on the rest of the copper cylinder. In a steady-state experiment, this difference will always be seen and therefore would show a correction factor (point value calibration factor) greater than 1 because far away from the heat flux meter, the maximum temperature that can be reached is the one at which CHF occurs. This difference is strongly dependent on the slope of the nucleate boiling regime as shown in Table I.2 and Figure I.3.

This effect imposes severe limitations on the use of this type of heat flux meter in a steady-state experiment. In a transient experiment, there should be no major influence of the temperature depression in the immediate vicinity of the heat flux meter, since the heat flux meter should still follow the boiling curve, that is for each surface temperature a particular heat flux density should exist. The only difference will be that a particular heat flux will occur earlier in this region than on the rest of the cylinder. The whole boiling curve should still be covered. On the other hand, because the heat flux density is highly nonlinear with temperature, the influence of the steepness of the boiling curve on the correction factor suggests that it may be a function of surface heat flux. This supposition led to a full analysis of the heat flux meter as it relates to the prediction of the boiling curve. This will be described in the sections to follow.

TABLE I.1

INFLUENCE OF STEEPNESS IN BOILING CURVES
ON THE STEADY-STATE CALIBRATION FACTOR

CURVE	TFAR	TDENT	TDIFF	DFAR	DPET	DFAR PET
0	115.8	110.7	3.900	135.6	53.2	2.55
1	144.8	138.3	6.399	136.9	57.9	2.40
2	143.6	134.0	6.092	134.3	61.2	1.65

TABLE I.2

BOILING CURVE EQUATIONS

CURVE	EQUATIONS	CONDITIONS
0	$(q/A) = 10 \ln(36.797 \text{ Log}_{10}(T) - 23.8059)$	for all T
1	$(q/A) = 10 \ln(18.939 \text{ Log}_{10}(T) - 38.78)$	$T < 144.8 \text{ }^\circ\text{C}$
	$(q/A) = 10 \ln(-9.350 \text{ Log}_{10}(T) + 22.3464)$	$T > 144.8 \text{ }^\circ\text{C}$
2	$(q/A) = 10 \ln(19.0136 \text{ Log}_{10}(T-4.5) - 38.0539)$	$T < 132.5 \text{ }^\circ\text{C}$
	$(q/A) = 10 \ln(-244.114x^2 + 1053.21xy - 1133.684)$	$132.5 \leq T \leq 150.75$
	$(q/A) = 10 \ln(-10.3354y + 24.7296)$	$T < 150.75 \text{ }^\circ\text{C}$

$y = \text{Log}_{10}(T)$

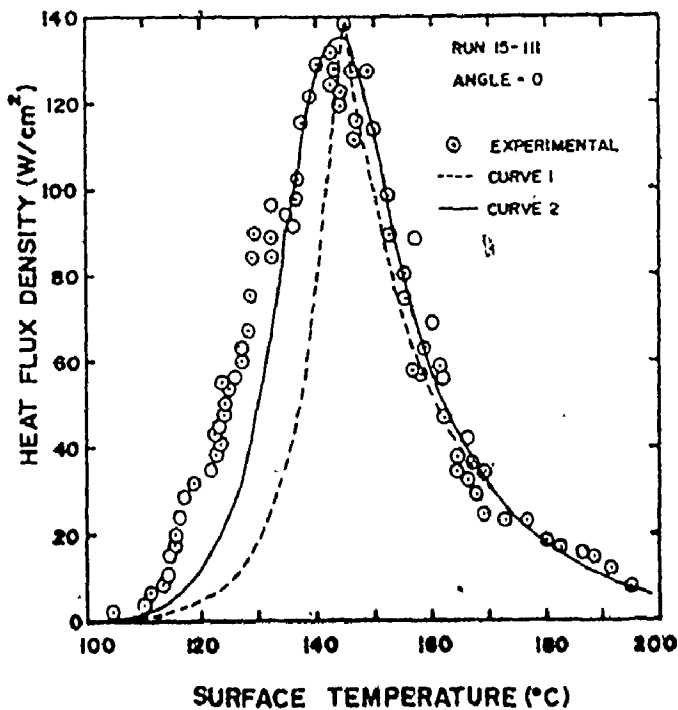


FIGURE I.3 - BOILING CURVES USED IN THIS STUDY

I.2.4 Boiling Curve Prediction by the Meter

It was therefore necessary to determine the influence of the temperature depression on the correction factor of the overall boiling curve and to see how it affects the shape and location of the predicted boiling curve as compared to the one applied.

To achieve this objective, the boiling curve as determined for run 15-111 was chosen as typical; it was obtained in the way described using a calibration factor of 0.65. This experimental curve was used to establish a boiling curve in equation form. Because, it was desired to determine how well the heat flux meter could predict the applied boiling curve, it was not required to have a perfect representation of the experimental data. Curves 1 and 2 were used in this study. The equations of these boiling curves and its diagrammatic representation are given on Table I.2 and Figure I.3 respectively. Curve 2 is a better representation of the experimental data than Curve 1. The results obtained with these two cases will be discussed in turn. The surface temperature of a point away from the edge of the heat flux meter was set to a value varying between 200°C and 100°C and the temperature distribution in the heat flux meter and its vicinity was allowed to converge using one of the two boiling curves. The integrated average of the applied heat flux and the heat flux density predicted from Equation 2.16 using the temperature difference on the surface of the disk were calculated. With this procedure it was then possible to obtain the complete boiling curve as would be predicted from the one-dimensional equation for an ideal heat flux meter and compare it with the original

boiling curve. The results obtained from this analysis are presented in Tables I.4 and I.5 and plotted in Figures I.4 and I.5. Table I.3 defines the variables used.

For the two boiling curves investigated, the critical heat flux density predicted from the temperature difference on the disk was less than the applied one. This low prediction must be attributed to the heat flux variation associated with the temperature variation and the temperature depression on the surface of the disk whereas an average heat flux was assumed in the predicting equation. Moreover, although the shape of the original boiling curve is relatively well followed, the boiling curve predicted with the meter is shifted to higher temperatures by few degrees. This shift in the boiling curve is the major cause of the high calibration factors found during steady-state experiments. This effect produces a heat flux density correction (or a point value calibration factor) which is a function of the surface heat flux. This suggests that for this type of meter to be used in a steady-state experiment would require a knowledge of the heat flux density correction as a function of surface heat flux. It is important to reemphasize that the high correction to be applied in the nucleate boiling regime is a result of a slight shift in the boiling curve so that this type of heat flux meter is quite adequate for a transient experiment. The calibration factor obtained during a set of quenching experiments takes into account any small variation in the predicted boiling curve and possible dependence on heat flux density of the point value calibration factor. Moreover this calibration factor, which is assumed to be constant, accounts for any other effects resulting during its fabrication

TABLE I.3

DEFINITION OF VARIABLES USED IN THIS ANALYSIS

- TFAR - Temperature given on the surface at the nodal point which is furthest from the heat flux meter.
- TCENT - Surface temperature at the centre of the disc.
- TAVG - Weighted average surface temperature on the heat flux meter.
- TDIFF - Surface temperature difference on the heat flux meter.
- QAVG - Weighted average surface heat flux on the heat flux meter surface.
- QFAR - Heat flux corresponding to TFAR, ie. heat flux prevailing on the surface far away from the meter.
- QMET - Heat flux predicted by the heat flux meter.
- QAVT - Heat flux corresponding to the average temperature on the disc.
- QFAR/QMET - Calibration factor for the meter under steady-state condition.
- QFAR/QAVG - Ratio of the heat flux on the surface away from the meter to the average heat flux on the meter.
- FRAC - Fraction which is solution of the following equation:

$$TAVG = FRAC \times T(\text{centre}) + (1-FRAC) \times T(\text{edge})$$

and used to determine the proper surface temperature for the boiling curve.

TABLE I.4

HEAT FLUX METER ANALYSIS

CASE NUMBER 1
CURVE 1

T _{BAR} (°C)	T _{IDENT} (°C)	T _{AUG} (°C)	T _{DIFF} (°C)	Q _{AUG} (W/cm ²)	Q _{BAR} (W/cm ²)	Q _{MET} (W/cm ²)	Q _{AT} (W/cm ²)	Q _{BAR} /Q _{MET}	Q _{BAR} /Q _{AUG}	FRAC
195.0	194.1	194.4	.615	8.88	8.60	7.84	8.86	1.0966	.9686	.4794
185.0	183.4	184.0	1.039	14.87	14.07	13.33	14.83	1.0558	.9463	.4785
175.0	172.2	173.2	1.663	26.22	23.66	24.05	26.12	.9839	.9023	.4768
160.0	163.5	165.1	2.986	41.06	34.65	38.72	40.85	.8949	.8440	.4742
161.0	153.0	155.8	5.343	70.10	51.59	69.67	70.00	.7405	.7360	.4682
158.0	146.6	150.7	7.705	96.13	61.51	100.79	95.67	.6103	.6399	.4622
157.5	144.7	149.4	8.664	105.89	63.36	113.43	104.00	.5586	.5984	.4603
157.3	144.3	149.0	8.716	107.38	64.31	114.14	106.37	.5634	.5989	.4633
157.0	144.0	148.7	8.719	108.66	65.27	114.20	108.60	.5716	.6007	.4671
156.8	143.7	148.3	8.709	110.81	66.25	114.70	111.37	.5807	.5979	.4743
156.5	143.5	148.0	8.631	111.71	67.25	113.09	113.43	.5946	.6020	.4789
156.0	143.0	147.4	8.468	114.12	69.29	111.00	118.05	.6242	.6072	.4896
155.5	142.6	146.8	8.287	115.85	71.40	108.67	122.40	.6571	.6163	.4976
150.0	142.3	146.3	8.055	116.30	73.59	105.66	126.05	.6965	.6327	.5040
154.5	142.3	145.9	7.810	116.56	75.84	102.47	129.81	.7401	.6507	.5090
154.0	141.8	145.3	7.566	116.78	78.18	99.30	133.36	.7873	.6694	.5143
153.5	141.5	145.1	7.320	116.22	80.59	96.09	136.75	.8387	.6933	.5174
152.0	140.8	143.9	6.580	113.75	88.34	86.44	123.78	1.0220	.7766	.5203
150.0	140.0	142.7	5.698	105.75	99.99	74.91	105.63	1.3348	.9455	.5152
144.8	138.3	140.5	4.399	80.72	138.93	57.91	78.60	2.3989	1.7211	.5019
142.0	136.8	138.6	3.430	61.09	95.98	46.00	60.32	2.0864	1.5712	.4969
135.0	132.3	133.2	1.777	28.57	36.85	23.51	28.70	1.5676	1.2897	.4905
130.0	128.5	129.0	1.005	15.50	18.03	13.33	15.58	1.3525	1.1632	.4862
125.0	124.2	124.5	.502	7.84	8.58	6.68	7.93	1.2843	1.0941	.4841
118.0	117.7	117.8	.186	2.78	2.88	2.51	2.79	1.1462	1.0359	.4819
112.0	111.9	111.9	.072	1.05	1.07	.97	1.06	1.1094	1.0208	.4817
102.0	102.0	102.0	.012	.18	.18	.16	.18	1.1243	1.0130	.4802

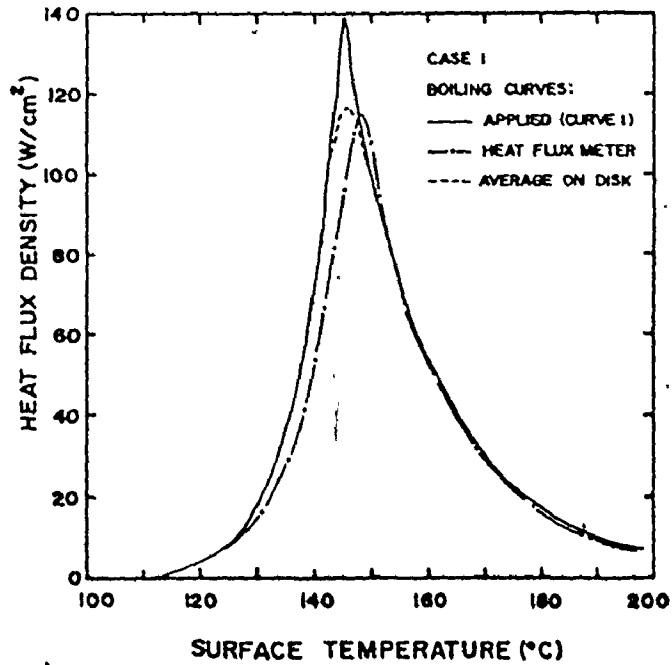


FIGURE I.4 - PREDICTED BOILING CURVE

TABLE I.5

HEAT FLUX METER ANALYSIS

CASE NUMBER 2
CURVE 2

T _{FAH} (°F)	T _{CELS} (°C)	T _{AVG} (°C)	T _{DIFF} (°F)	Q _{AVG} (W/cm ²)	Q _{FAH} (W/cm ²)	Q _{MET} (W/cm ²)	Q _{AVT} (W/cm ²)	Q _{FAH/Q_{MET}}	Q _{FAH/Q_{AVG}}	FRAC
175.0	194.4	194.5	.536	7.73	7.50	5.90	7.71	1.0870	.9694	.4795
185.0	183.4	184.1	-.045	13.67	12.92	12.37	13.52	1.0443	.9451	.4785
175.0	177.2	177.2	0.000	25.65	22.94	23.82	25.53	.9628	.8942	.4764
160.0	163.3	164.9	3.124	42.52	34.98	40.90	42.29	.8511	.8219	.4731
162.0	153.7	156.5	5.571	72.08	50.94	72.61	72.15	.7015	.7057	.4665
158.0	144.8	149.4	8.104	111.99	65.95	116.12	113.63	.5680	.5889	.4701
157.0	143.2	147.9	9.086	134.88	70.43	120.26	122.39	.5856	.5924	.4752
156.5	142.5	147.2	9.161	121.86	72.79	121.28	125.80	.6032	.5973	.4781
156.0	141.8	146.6	9.184	124.34	75.24	121.64	128.53	.6185	.6051	.4807
155.5	141.3	145.0	9.181	125.67	77.77	121.64	130.49	.6394	.6189	.4829
155.0	140.7	145.4	9.136	127.25	80.41	121.09	132.11	.6640	.6319	.4852
154.0	139.8	144.4	8.977	129.09	85.97	119.06	133.90	.7221	.6660	.4891
153.5	139.4	143.9	8.873	129.49	88.91	117.72	134.23	.7512	.6666	.4908
153.0	138.9	143.4	8.783	129.63	91.96	116.56	134.26	.7889	.7094	.4919
152.5	138.6	143.0	8.558	129.54	95.12	114.93	134.02	.8277	.7343	.4933
152.0	138.3	142.5	8.527	129.22	98.41	113.22	133.55	.8691	.7615	.4943
150.0	137.0	141.0	7.946	126.41	109.90	104.15	129.64	1.0353	.8694	.4983
147.0	135.6	139.1	7.106	116.21	126.79	94.55	120.52	1.3410	1.0726	.5012
143.6	134.0	137.0	6.092	105.17	134.28	81.19	106.28	1.6539	1.2769	.5021
140.0	132.3	134.8	4.965	87.63	125.32	66.26	87.79	1.8914	1.4301	.5024
135.0	129.9	131.6	3.354	59.18	99.47	44.84	58.35	1.9966	1.5118	.4987
130.0	126.9	128.0	2.049	33.70	45.89	27.48	33.63	1.6702	1.3620	.4924
120.0	119.5	119.4	5.11	8.53	9.45	7.39	8.63	1.2466	1.1094	.4846
110.0	109.0	109.9	1.12	1.65	1.69	1.32	1.66	1.1150	1.0270	.4814
105.0	104.9	104.9	0.045	0.66	0.67	0.61	0.67	1.0957	1.1065	.4810

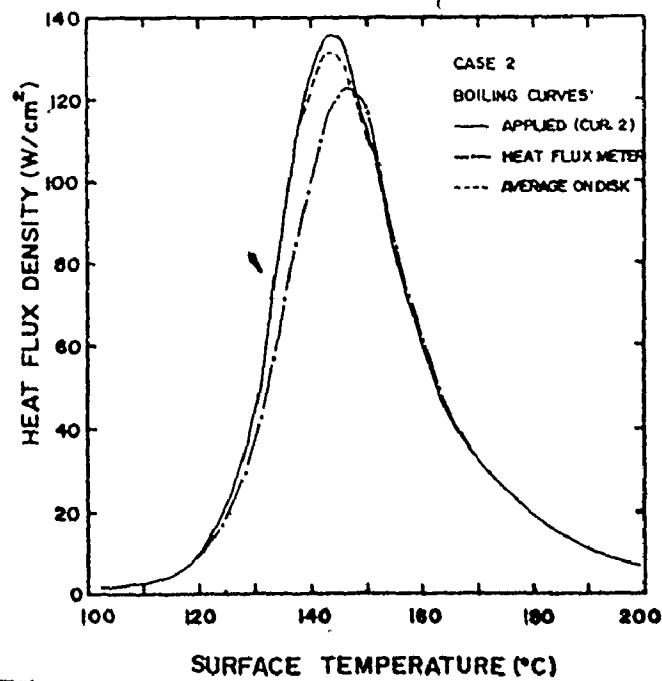


FIGURE I.5 - PREDICTED BOILING CURVE

(see Appendix E).

I.2.5 Average Surface Temperature

Throughout the experimental program, an average temperature between the edge and the centre temperatures was used as the average wall temperature against which the heat flux density was plotted to give a representative boiling curve for the surface. Therefore, it was natural to choose an intermediate temperature which would be a good representation of the surface temperature at which the indicated heat flux density should occur for this surface. It is important to note that the average temperature assumption was used strictly to plot experimental boiling curves; in this analysis, the integrated average temperature was used to plot the predicted boiling curve. To verify this average temperature assumption the difference between the temperature at the edge of the disk and the average surface temperature on the disk was compared with the predicted temperature difference on the disk. This comparison can be expressed by the following equation:

$$\text{FRAC} = \frac{T_{\text{EDGE}} - T_{\text{AVERAGE}}}{T_{\text{EDGE}} - T_{\text{CENTRE}}} \quad (1-2)$$

The results of this analysis are presented in the right column of Tables I.4 and I.5. For the above assumption to be valid, the calculated ratio should be 0.5. In all cases, the tabulated values are roughly 0.5; this analysis therefore validates the 0.5 value used.

I.3 Conclusion

By solving the Laplace equation to obtain the temperature distribution in the heat flux meter and its vicinity, explanations were provided for the relatively high calibration factors that were obtained during the steady-state experiments. Darnedde(D1), who used a similar heat flux meter, was also perplexed as to why the calibration factor he required for steady-state experiments was greater than 1. He suggested that it was possibly caused by conduction along the thermocouple wire. In this appendix, it was shown that this effect was chiefly caused by a small shift of the predicted boiling curve to higher temperatures. As a result, it imposes a severe restriction on the use of this type of heat flux meter for steady-state experiments. On the other hand, the shape of the boiling curve is well reproduced and this heat flux meter can be used efficiently to provide pool boiling data from a transient experiment.

APPENDIX J

STEADY-STATE CALIBRATION

As a check of the unsteady-state calibration procedure, a steady-state experiment was designed to determine the calibration factor of a particular heat flux meter. The particular heat flux meter had been calibrated via the indirect method involving the multiple quenching experiments as described in Appendix H. Hence a direct comparison is possible.

A detailed description of the apparatus has been reported previously in Chapter 3 along with the experimental procedure. In essence, it consists of mounting a copper chamber on part of the cylindrical surface which contains the heat flux meter. The copper cylinder was drilled to accept fourteen, 500 W, 230 V cylindrical heaters. The power input was controlled by powerstat transformers. The evaporation rate on the boiling surface was then related to the average heat flux density over the active boiling surface. This heat flux density could then be compared to the apparent one indicated by the heat flux meter and a direct calibration factor could be obtained for any given heat flux density.

This work was done with Cylinders 14 and 15 and the results obtained in both cases will be discussed in turn.

J.1 Discussion of Results of Cylinder 14

J.1.1 Unsteady-State Calibration

A series of experiments were performed on Cylinder 14 to determine its calibration factor under unsteady-state boiling. The critical heat flux results obtained at different angular locations are presented in Appendix C. Unfortunately, the critical heat flux results are atypical of those usually obtained as the corrected critical heat flux values are smaller by about 20% of those usually obtained. Moreover, the severe depression in the critical heat flux value at the 30° angle was not observed with this cylinder. Unfortunately these anomalous results were not detected until after the cylinder had been modified and installed for the steady-state calibration experiments. This was the only cylinder that showed such behaviour.

J.1.2 Steady-State Experiments

A series of steady-state experiments were run on different days following the procedure described earlier. Table J.1 presents the results obtained. Also included in the table is a calibration factor given by the ratio of the heat flux obtained from the condensation rate to the heat flux measured with the meter.

Run 22 to run 28 were done in a similar fashion but every time more care was devoted to try and reach a higher heat flux density as indicated by the meter. However, it was impossible to obtain a temperature difference on the disk which would approach the one obtained in

TEMPERATURE (°C)	TEMP. DIFF. (mV)	% POWER	TIME (s)	COND 1 (ml)	COND 2 (ml)	HEAT FLUX		CAL. FACTOR
						METER (W/cm ²)	STEAM (W/cm ²)	
Run 14-22 July 13, 1976								
102.0	.035	25	1260.0	120	196	10.20	12.85	1.260
103.5	.042	25	660.0	48	119	12.35	14.90	1.206
104.2	.070	35	540.0	72	198	22.79	30.30	1.330
105.3	.134	45	540.0	114	324	38.84	49.58	1.275
106.9	.181	50	540.0	118	424	52.24	64.88	1.242
110.1	.224	55	570.0	136	534	64.24	77.41	1.205
111.3	.279	56	540.0	146	533	79.53	81.56	1.026
113.7	.343	59	480.0	132	534	98.52	91.93	0.933
Run 14-23 July 15, 1976								
103.3	.040	25	810.0	98	106	13.95	10.81	0.775
103.4	.120	40	600.0	114	279	34.53	38.42	1.113
107.9	.168	50	600.0	150	454	48.10	62.52	1.300
112.4	.206	53	480.0	125	418	58.81	71.98	1.224
114.1	.265	59	480.0	158	532	75.39	91.58	1.215
115.0	.316	64	540.0	185	674	90.13	103.10	1.144
115.0	.354	65	360.0	130	520	100.20	119.40	1.192
Run 14-24 July 20, 1976								
109.2	.075	35	690.0	116	220	21.55	26.35	1.223
111.3	.142	45	540.0	145	313	40.62	47.89	1.179
Run 14-25 August 6, 1976								
110.1	.093	35	690.0	120	222	26.57	26.59	0.997
111.0	.173	50	570.0	176	390	49.45	56.54	1.143
111.3	.220	56	720.0	266	630	62.94	72.30	1.149
111.6	.256	58	600.0	226	582	73.20	80.15	1.095
111.9	.289	60	600.0	236	616	82.54	84.83	1.027
111.9	.324	63	600.0	242	710	92.65	97.78	1.055
112.4	.358	65	600.0	255	758	102.20	104.40	1.021
113.4	.343	61	660.0	250	730	97.71	91.39	0.935
114.3	.382	64	600.0	235	742	108.60	102.20	0.941
115.2	.408	66	480.0	227	700	115.80	120.50	1.040
116.6	.425	68	420.0	206	646	120.30	127.10	1.056
117.2	.457	71	420.0	225	748	129.20	147.20	1.139
Run 14-26 August 16, 1976								
111.8	.096	40	660.0	150	260	27.58	32.55	1.180
114.5	.180	50	540.0	198	444	51.17	67.94	1.328
113.4	.193	55	600.0	208	495	54.84	68.17	1.243
Run 14-27 August 20, 1976								
106.3	.019	20	1110.0	82	92	54.91	68.49	1.247
111.3	.090	40	600.0	133	250	25.75	34.43	1.337
112.6	.147	50	480.0	145	330	41.95	56.81	1.354
113.1	.185	55	420.0	145	356	52.74	70.04	1.328
113.2	.210	58	360.0	135	341	59.85	78.27	1.308
114.7	.243	65	360.0	151	411	69.05	94.34	1.366
116.2	.261	67	300.0	139	377	73.95	103.80	1.404
116.6	.296	69	144.0	69	206	83.79	118.20	1.411
116.8	.304	70	117.0	55	170	86.06	120.10	1.396
116.2	.276	68	330.0	152	443	70.20	110.90	1.419
116.6	.303	69	270.0	133	386	85.77	118.10	1.377
Run 14-28 September 15, 1976								
111.6	.112	45	480.0	92	202	32.03	34.77	1.086
111.8	.125	45	570.0	131	290	35.73	42.02	1.177
113.2	.203	55	360.0	115	301	57.85	69.09	1.194
114.1	.245	62	360.0	153	394	69.70	90.43	1.297
111.6	.113	42	480.0	111	226	32.31	38.96	1.204
109.0	.050	25	600.0	66	83	14.37	11.43	0.795
112.0	.186	55	360.0	124	310	53.05	71.15	1.341
111.5	.110	45	420.0	96	201	31.45	39.54	1.257
113.1	.212	60	360.0	132	342	60.44	78.90	1.299
113.9	.265	67	330.0	169	431	75.43	107.90	1.431
114.5	.298	70	270.0	146	350	84.71	107.10	1.264
115.2	.335	73	210.0	132	302	95.11	118.00	1.247
114.9	.338	73	210.0	118	305	95.00	120.00	1.250
115.0	.370	76	240.0	141	345	105.00	132.00	1.263
111.0	.110	45	420.0	72	153	33.73	30.10	0.893
112.0	.140	45	420.0	80	177	34.26	34.82	1.014

TABLE J.1 (cont.)

TEMPERATURE (°C)	TEMP. DIFF. (mV)	% POWER	TIME (s)	COND 1 (ml)	COND 2 (ml)	HEAT FLUX		CAL. FACTOR
						METER (W/cm ²)	STEAM (W/cm ²)	
Run 14-43 ^a								
September 29, 1976								
112.8	.155	50	616.1	184	465	44.21	62.36	1.411
113.2	.168	50	572.6	182	463	47.88	66.81	1.396
114.9	.240	65	394.0	166	455	68.17	97.52	1.431
110.3	.070	40	906.1	110	225	20.07	20.52	1.022
114.3	.105	60	552.5	173	444	52.61	69.39	1.319
114.3	.195	60	521.8	168	457	55.46	72.37	1.305
112.4	.118	45	610.8	134	300	33.69	40.58	1.205
113.7	.175	55	519.1	162	417	49.83	66.38	1.332
113.7	.100	55	468.8	146	384	51.25	67.68	1.321
115.3	.240	65	403.1	168	472	68.11	96.75	1.421
115.3	.240	65	412.6	174	486	68.11	97.33	1.429
113.0	.255	67	348.4	158	450	72.28	106.70	1.477
106.9	.045	30	1421.2	122	125	12.99	7.27	0.560
113.7	.215	65	488.2	153	455	61.22	77.01	1.258
114.1	.223	65	488.8	153	477	63.45	80.63	1.271
114.1	.230	65	450.4	148	445	65.44	87.64	1.248
114.1	.235	65	475.5	160	477	66.86	82.89	1.240
113.9	.235	65	477.5	161	480	66.89	83.06	1.242
113.9	.240	65	480.5	162	477	68.31	82.03	1.201
114.3	.290	70	396.0	157	490	82.47	102.20	1.240

^a This run was done with York packing in the upper section of the inside boiling chamber to eliminate possible liquid entrainment directly into the condenser.

Run 14-44
October 14, 1976

108.4	.055	35	1818.8	194	315	15.83	14.31	0.964
101.4	.063	35	1458.3	186	314	18.13	17.79	0.981
107.1	.028	25	1908.1	168	181	8.09	7.84	0.970
103.2	.043	30	1237.4	136	216	12.38	14.42	1.165
107.9	.045	30	1498.8	183	254	12.96	14.00	1.080
104.8	.026	20	2396.7	173	141	7.54	4.85	0.645
109.2	.090	40	908.5	182	346	28.56	31.47	1.217
103.2	.055	30	1126.7	152	230	15.83	16.87	1.065
107.1	.037	25	1501.8	150	181	10.68	9.96	0.933

an unsteady-state experiment even though the evaporation rate on the surface suggested that a much higher heat flux density was obtained. This phenomena suggested possible liquid entrainment directly into the condenser. Run 43 was then done by placing York packing in the upper section of the inside boiling chamber to eliminate possible liquid entrainment. The same results were obtained. Moreover, when the power input to the cylinder was too high, the temperature of the cylinder increased very rapidly as the boiling proceeded to the transition regime. It was possible during a temperature runaway to visually observe temperature differences which were in the order of magnitude to those observed during the unsteady-state experiment. It was then decided to observe directly the boiling phenomena on the cylinder. This direct observation indicated that boiling in the immediate region of the meter at steady-state was quite different (less violent) than the rest of the surface. These observations led to the conduction analysis which is presented in Appendix I and to the evaluation of the effect of a thermal contact resistance between the plug and the rest of the cylinder. It is shown in Appendix I that the inherent temperature depression on the disk and its vicinity can account for the large calibration factor encountered in this study. Therefore this direct method of calibrating a heat flux meter fails.

The effects of the thermal resistance at the boundaries of the copper insert and the inherent temperature depression are negligible when the heat flux density from the surface is near zero; therefore it should be possible to evaluate the calibration factor in the following

way. Experiments like run 44 were performed under conditions of decreasing heat flux. Unfortunately, the accuracy at very low heat fluxes was poor because the condensate rate was low and the temperature difference on the disk was small and oscillated slightly. Nevertheless, about 14 observations of calibration factor were made using low heat inputs. These calibration factor data were assumed to vary linearly with heat flux density and were regressed accordingly. This regression equation then provided a calibration factor at zero heat flux where the confounding effects were absent. Table J.2 presents the values used for the linear regression and gives the equation of the best line passing through these points. A calibration factor of 0.67 with a standard deviation of .13 was found for this meter. This value is higher than the 0.51 obtained in an unsteady-state experiment. However, using a value of 0.67, the CHF so obtained are closer to those observed on other cylinders.

It was possible in some instances to record quite high heat fluxes before the temperature of the cylinder ran away. The highest heat flux obtained (Run 25) was 147 W/cm^2 as calculated with the vapour condensation rate. This value is approximately equal to the critical heat flux value usually obtained from the unsteady-state experiments. This observation demonstrates the equivalence between the CHF values under steady-state and unsteady-state experiments.

J.1.3 Unsteady-State Experiments with a Temperature Runaway

Based on the hypothesis that if steady-state and unsteady-state behaviours are different, the rate of the transient should affect the

TABLE J.2

EVALUATION OF THE CALIBRATION FACTOR FOR
BLOCK 14 WITH STEADY-STATE EXPERIMENTS

RUN	CAL. FACTOR	(q/A) STEAM (W/cm ²)
23	.775	10.81
23	.997	26.59
28	.795	11.43
43	.560	7.27
44	.904	14.31
44	.981	17.79
44	.970	7.84
44	1.155	14.42
44	1.080	14.00
44	.645	4.86
44	1.217	31.47
44	1.065	16.87
44	.933	8.96

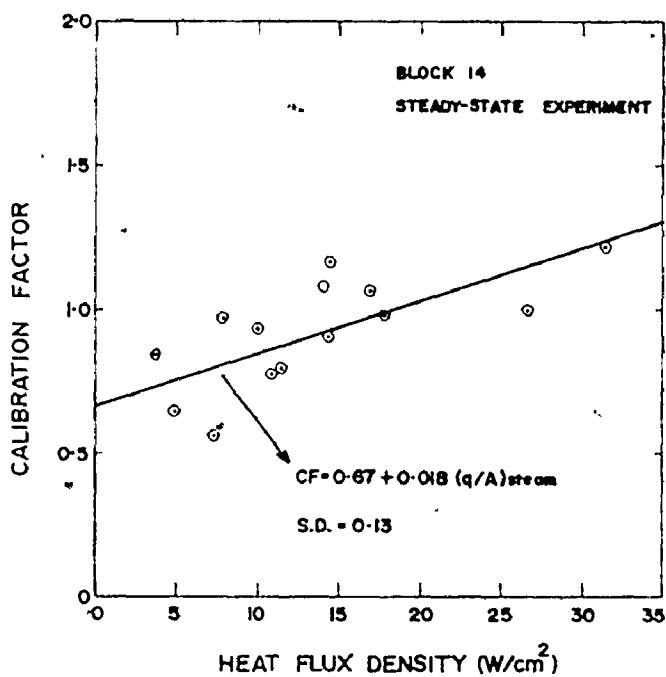


FIGURE J.1 - PLOT OF THE STEADY-STATE CALIBRATION
FACTOR VERSUS HEAT FLUX AT THE SURFACE.

TABLE J.3

CRITICAL HEAT FLUX VALUES OBTAINED WITH
BLOCK 14 DURING TEMPERATURE RUNAWAY

ANGLE	RUN	CHF (W/cm ²)	AVER. CHF (W/cm ²)
(a) Going up	37	116.1	118.1
	38	129.5	
	39	125.9	
	41	101.1	
(b) Going down	40	113.1	115.2
	42	117.3	

boiling curve and the critical heat flux value. With the experimental set-up, it was possible to regulate the rate at which the cylinder was cooling when CHF occurred at the meter. This was achieved by controlling the power input to the copper cylinder while it was going through the CHF either starting in the nucleate boiling regime (low temperature) and increasing the temperature or starting in the transition regime and allowing the cylinder to cool. The copper cylinder was therefore allowed to go through a temperature runaway and allowed to cool at different rates while the results were being recorded with a minicomputer. Table J.3 presents the results obtained with this set of experiments. No difference in the CHF was observed as a function of cooling rate and the value of CHF obtained compares very well with a value of 115 W/cm^2 obtained in the quenching sets of experiments performed earlier.

This set of experiments provides more valuable information regarding possible hysteresis in the boiling curve whether CHF is approached from the nucleate boiling regime. In both cases, the CHF is the same and the temperature at which it occurs is also approximately the same.

J.2 Discussion of Results of Cylinder 15

Steady-state experiments were also performed on Cylinder 15 which was considered to be an extremely good one. More than 178 runs were performed on this cylinder before it was drilled. The raw data for the three runs performed are presented on Table J.4. The calibration factor was again observed to be a function of heat flux on the

TABLE J.4

STEADY-STATE CALIBRATION RESULTS FOR BLOCK 15

TEMP. (°C)	TEMP. DIFF. (mV)	% POWER	TIME (s)	COND. 1 (mJ)	COND. 2 (mJ)	HEAT FLUX DENSITY		CALIBRATION FACTOR
						METER (W/cm ²)	STEAM (W/cm ²)	
Run 15-179								
May 7, 1977								
108.2	.030	20	1037.4	73	92	8.64	7.33	.848
110.5	.042	37	700.1	82	162	12.04	19.12	1.589
112.0	.046	35	761.1	120	240	13.14	27.14	2.265
112.8	.090	40	699.2	131	327	14.27	17.87	2.652
113.9	.057	45	442.6	98	263	16.22	49.10	1.026
104.6	.005	10	1512.5	38	17	1.45	.91	.641
106.7	.012	15	1430.3	88	41	3.47	2.37	.684
114.5	.087	52	400.3	109	321	23.31	66.25	2.843
115.3	.100	55	333.4	102	302	28.38	74.85	2.637
117.2	.117	60	260.9	70	280	33.08	88.68	2.681
118.1	.127	62	261.7	98	310	35.85	97.88	2.730
111.3	.032	25	1087.5	120	160	9.15	12.16	1.328
112.8	.047	35	660.3	100	232	13.41	29.03	2.166
Run 15-180								
May 10, 1977								
108.8	.019	66	870.7	69	66	5.46	6.26	1.146
107.6	.013	15	2845.7	154	91	3.75	2.64	.704
104.6	.003	10	1927.4	52	13	.87	.56	.641
110.3	.032	25	1202.3	121	181	9.17	12.44	1.354
Run 15-181								
May 17, 1977								
112.4	.102	40	500.1	103	220	29.12	36.35	1.248
114.3	.137	50	306.4	83	221	36.96	59.69	1.530
116.0	.157	60	225.1	78	236	44.50	86.63	1.947
108.8	.077	20	1621.4	126	132	4.89	6.73	1.376
103.1	.002	10	2023.3	55	15	.58	.61	1.053
108.6	.077	20	703.7	57	48	4.89	5.64	1.153
106.5	.012	15	903.8	50	28	3.47	2.57	.740
110.9	.025	25	1160.8	128	156	7.16	11.10	1.551
107.6	.015	18	1356.5	91	78	4.32	4.75	1.099
107.2	.165	65	175.8	73	255	65.71	119.90	2.622

TABLE J.5

EVALUATION OF THE CALIBRATION FACTOR FOR
BLOCK 15 WITH STEADY-STATE EXPERIMENTS

RUN	CAL. RATIO	TEMP. DIFF (mV)
179	.848	.030
179	1.589	.042
179	.641	.005
177	.684	.012
179	1.328	.032
180	1.146	.019
180	.775	.013
180	.641	.003
180	1.354	.032
181	1.376	.017
181	1.053	.003
181	1.153	.017
181	.740	.012
181	1.551	.025
181	1.099	.015
C		T _d

A straight line was fitted using a least square and the following equation was obtained:

$$C = -.76 + 20.6 * T_d$$

with a standard deviation of .23 based on 15 observations.

surface. It has been shown in Appendix I that the inherent temperature depression in the heat flux meter and its vicinity can account for most of the observed calibration factor variation with surface heat flux. The relatively high calibration factor was shown to be mainly due to the shift of the predicted boiling curve relative to the actual one.

A steady-state calibration factor can still be found by eliminating the effect of the thermal contact resistance and the temperature depression as mentioned above. Therefore, with a set of experiments performed at low heat fluxes, it is possible to extrapolate the calibration factor to zero heat flux. The result of this extrapolation is presented on Table J.5. A calibration factor of 0.68 was obtained with an appreciable variance. This value is nevertheless very close to the value 0.70 obtained by the indirect calibration with the quenching experiments.

J.3 Conclusion

These experiments showed the effect of the inherent temperature depression on and in the immediate vicinity of the disk. As a result, the average heat flux density over the meter is considerably different from that over the main surface and the steady-state calibration method failed. On the other hand, this effect becomes less severe as the average heat flux density over the surface becomes less and should disappear at zero heat flux. Therefore, the apparent calibration factor at each measured heat flux was extrapolated to zero heat flux. This extrapolated calibration factor was then compared with that obtained by the unsteady-state method and excellent agreement was found.

In conclusion, it should be emphasized that the effect observed during these steady-state experiments will in no way invalidate the use of the heat flux meter during the quenching experiments since the area surrounding the heat flux meter will register a lower average temperature just before the rest of the cylinder. It will nevertheless go through the critical heat flux.

APPENDIX K

COOLING AND BOILING CURVES PREDICTION

This experimental program relies heavily on the performance of the heat flux meter and even more so on the ability to find an appropriate calibration factor. As was seen earlier the uncalibrated results were quite insensitive to any offset required to correct the temperature difference on the disk but the calibrated heat flux is very sensitive to any error in this offset because the calibration factor is sensitive to it. For any particular cylinder, very good relative results were obtained for the change in CHF with angle or subcooling. The calibration factor is required to put these heat flux densities on an absolute scale, hence the importance of trying to obtain it by different experimental or calculation techniques. Since the steady-state calibration method failed to provide an accurate check (although it suggested that the calibration obtained by the unsteady-state method was reasonable), it was imperative to find some other method to generate confidence in the calibration factor which was used. This was done through two different but related calculation schemes:

- (1) To predict the cooling curves at points on the cylinder, using the experimentally measured heat flux densities (via the calibrated heat flux meter) at each of the seven points as a boundary condition. The predicted cooling curves are then compared with the experimental ones.

(ii) To predict the boiling curves at each point on the cylinder by making the experimental and predicted cooling curves coincide at the seven points. The resulting boiling curves are then compared with those generated by the calibrated heat flux meter.

These two calculation schemes are really different solutions to the "inverse problem" already discussed in Section 2.2.1. In addition, this analysis allowed the assumption concerning the uniform heat flux density over the length of the cylinder at any angular position to be checked. Since this assumption was made in deriving the equation for evaluating the calibration factor, proving its validity adds credence to the method used to obtain the calibration factor.

In the first phase, this analysis only considered a two-dimensional system. It served two purposes: to generate the desired information and evaluate whether the calculation would serve the desired purpose. In the second phase of this analysis, the method of superposition was used to extend the solution to a three-dimensional one and thus include the angular variation of heat flux.

It is the purpose of this appendix to outline these calculation procedures and present the results. The two-dimensional and three-dimensional analysis are presented in turn.

K.1 Two-Dimensional Analysis

K.1.1 Description of the Numerical Technique

The problem can be formulated in the following terms: Consider a finite cylinder ($0 \leq r \leq R$ and $-L \leq z \leq +L$) having a constant thermal

diffusivity α and initially at a uniform temperature, T_0 . At time $t > 0$, the cylinder is allowed to lose heat at the surface. In this case the heat flux at the surface is determined by the surface temperature through a prescribed boiling curve. The temperature distribution within the cylinder as a function of time is calculated.

It is therefore necessary to solve the unsteady heat diffusion equation:

$$\frac{1}{\alpha} \frac{\partial T}{\partial t} = \frac{\partial^2 T}{\partial r^2} + \frac{1}{r} \frac{\partial T}{\partial r} + \frac{\partial^2 T}{\partial z^2} \quad (\text{K-1})$$

The boundary conditions, taking symmetry into account are:

$$t=0, T=T_0 \text{ for } 0 \leq r \leq R \text{ and } 0 \leq z \leq L \quad (\text{K-2})$$

$$t>0, \left. \frac{\partial T}{\partial r} \right|_{r=0} = 0 \quad (\text{K-3})$$

$$\left. \frac{\partial T}{\partial z} \right|_{z=0} = 0 \quad (\text{K-4})$$

$$\left. \frac{\partial T}{\partial r} \right|_{r=R} = f(T_{R,z}) \quad (\text{K-5})$$

$$\left. \frac{\partial T}{\partial z} \right|_{z=L} = f(T_{r,L}) \quad (\text{K-6})$$

These boundary conditions indicate that it is only necessary to consider one quarter of the cylinder.

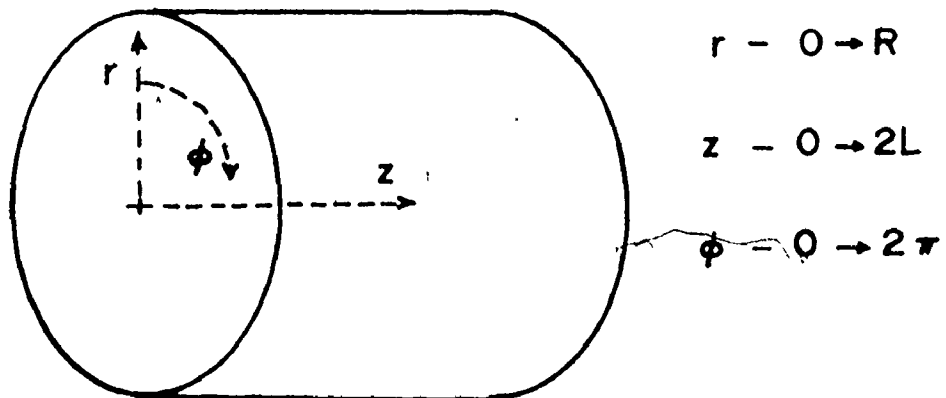
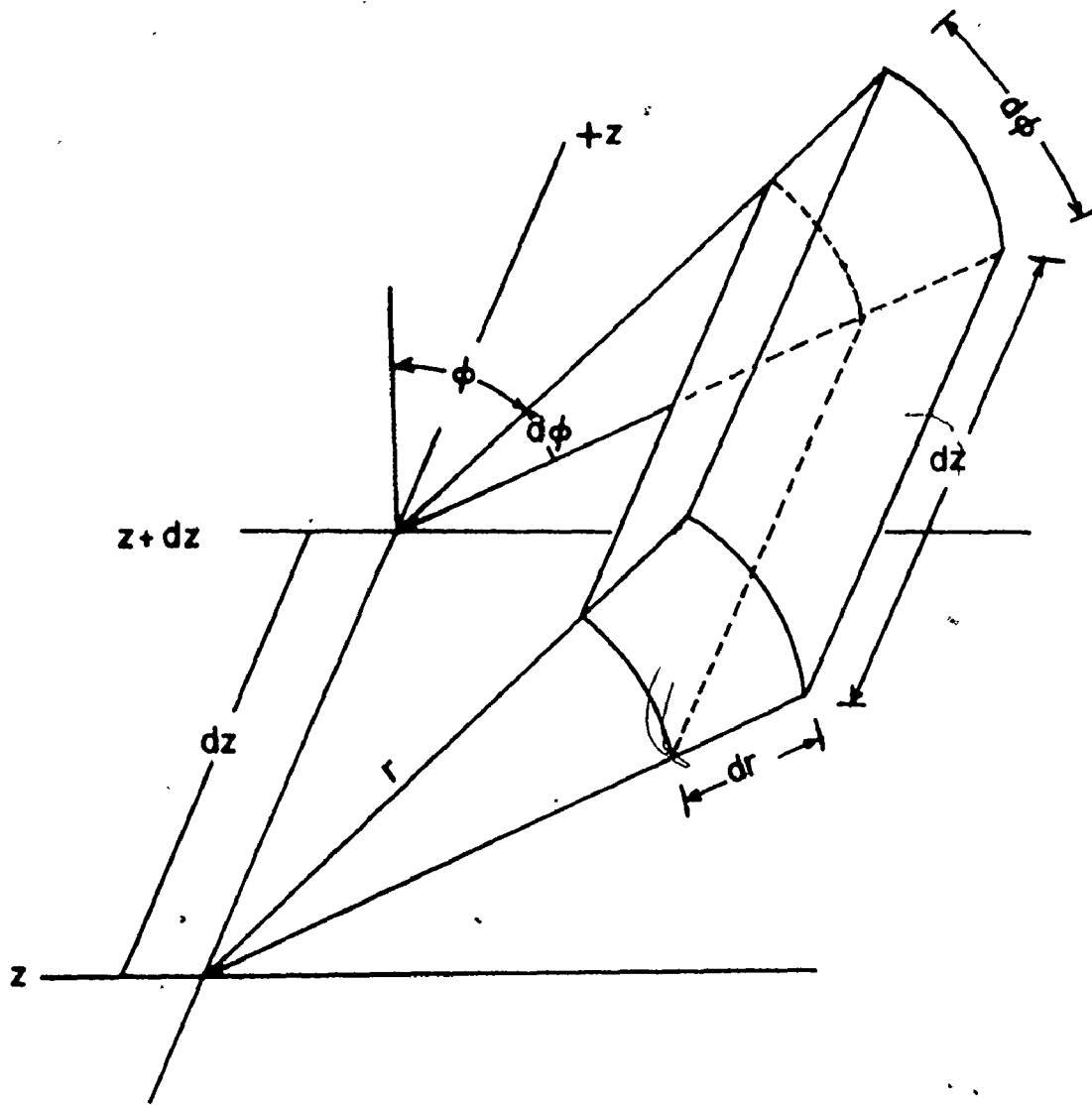


FIGURE K-1- CYLINDRICAL COORDINATE SYSTEM

Because of the non-linear character of the surface boundary condition, it is necessary to solve Equation K.1 using numerical methods. In this case, the Alternating-Direction Implicit (ADI) method was used (C1). Its main advantage is that resulting matrix of coefficients in the system of finite difference equations is tridiagonal and hence can be solved easily and rapidly.

In this formulation, T_{ij} , is defined as the temperature prevailing at the point (i, j) ($i = 1, 2, \dots, NR$ in the radial direction, $j = 1, 2, \dots, NZ$ in the z -direction). The radial and axial diffusion terms are expressed by:

$$\frac{\partial^2 T}{\partial r^2} + \frac{1}{r} \frac{\partial T}{\partial r} = \frac{T_{i+1,j} - 2T_{i,j} + T_{i-1,j}}{\Delta r^2} + \frac{1}{(i-1)\Delta r} \frac{T_{i+1,j} - T_{i-1,j}}{2\Delta r} \quad (K-7)$$

$$\frac{\partial^2 T}{\partial z^2} = \frac{T_{i,j+1} - 2T_{i,j} + T_{i,j-1}}{\Delta z^2} \quad (K-8)$$

It is extremely important to formulate the boundary conditions correctly in finite difference form to minimize the discretization error (T4). Each is discussed in turn below:

$$(i) \quad \text{At } r = 0 \text{ (} i = 1\text{), } \frac{\partial T}{\partial r} = 0 \quad (K-9)$$

Therefore by L'Hopital's rule, the term

$$\frac{1}{r} \frac{\partial T}{\partial r} = \frac{\partial^2 T}{\partial r^2} \quad \text{as } r \rightarrow 0 \quad (K-10)$$

and the diffusion equation becomes

$$\frac{1}{\alpha} \frac{\partial T}{\partial t} = 2 \frac{\partial^2 T}{\partial r^2} + \frac{\partial^2 T}{\partial z^2} \quad (\text{K}\cdot\text{11})$$

and because of symmetry

$$\frac{\partial^2 T}{\partial r^2} = \frac{2(T_{2,j} - T_{1,j})}{\Delta r^2} \quad (\text{K}\cdot\text{12})$$

(ii) At $z = 0$ ($j = 1$), $\frac{\partial T}{\partial z} = 0$ and the axial diffusion equation becomes:

$$\frac{\partial^2 T}{\partial z^2} = \frac{2(T_{i,2} - T_{i,1})}{\Delta z^2} \quad (\text{K}\cdot\text{13})$$

(iii) At the outer surface of the cylinder ($i = NR$ or $j = NZ$), there is a heat flow out of the surface determined by the local temperature and the assumed boiling curve. This heat flux density is expressed by:

$$-k \frac{\partial T}{\partial n} = (q/A) \quad (\text{K}\cdot\text{14})$$

where n is the normal to the surface (either r or z). In finite difference form, Equation K.14 has been found to be best represented by the central difference form (T4), viz.:

$$-k \frac{(T_{M+1} - T_{M-1}))}{2\Delta n} = (q/A) \quad (\text{K}\cdot\text{15})$$

where T_{M+1} is a fictitious point located at Δn beyond the boundary.

This formulation allows, T_{M+1} , in the diffusional Equation (K.7 or K.8) to be replaced by:

$$T_{M+1} = T_{M-1} - (q/A) \rho \cdot \left[\frac{2\Delta n}{K} \right] \quad (K.16)$$

In this particular study, the ends of the cylinder were assumed to be perfectly insulated by the transite holders. Also the holders extended over a portion of the metal cylinder and effectively insulated this circumferential surface area. These insulated surfaces caused axial temperature gradients to exist within the cylinder.

The solution of Equation K.1 was effected by solving Equation K.9 for all of the implicit temperatures in the r-direction after a time interval, $\Delta t/2$ (Δt being the time interval after which a solution is sought); the temperatures in the z-direction had been previously evaluated at time t and therefore known. Equation K.1 was then solved (Equation K.8) for the temperatures in the z-direction after a time $\Delta t/2$ using the updated temperatures in the r-direction.

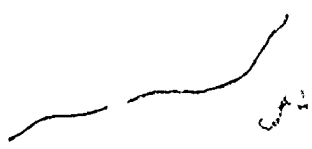
In this solution, a time interval of .1 s, 10 mesh point in the r-direction and 10 mesh points in the z-direction were employed; doubling the number of mesh points or halving the time interval did not change the temperature at any point by more than 0.1%. Moreover, the numerical technique was compared with a numerical solution based on superposition and an analytical solution (employing a constant heat flux with time) and very good agreement was obtained (T4).

K.1.2 Results and Discussion

The edge thermocouple of the heat flux meter traces out a cooling curve for that particular point on the cylinder. If as a first approximation it was assumed that the heat flux density was uniform around the cylinder and corresponds to that from the boiling curve generated by the calibration heat flux meter at the instantaneous temperature condition, it was possible through a finite difference formulation of the unsteady-state conduction equation for the cylinder, described in the previous section, to predict the temperature-time history of the surface temperature. Account was taken of the insulation provided by the transite end pieces and the circumferential area covered by them.

The predicted cooling curve was then compared directly with the measured one to indicate whether the assumed boiling curve was reasonable or not. The difficulty was that the measured heat flux density was observed to be nonuniform around the cylinder (this variation was indicated in Figure 5.4); consequently some deviation between the predicted and observed cooling curve was to be expected. Graphs on Figure K.1 show typical results: The least deviation occurs at 120° and the greatest at 30° . This result is to be expected, however, since the boiling curve which was used corresponded closely to that observed at 120° ; the boiling curve at 30° was observed to be much lower.

It was also possible through this analysis to predict what the boiling curve would have to be to generate the measured cooling curve. In this case, the analysis started with the initial temperature and, with an assumed boiling heat flux density, predicted what the temperature



at the point should be after a small time interval (the interval between measured temperatures). If the predicted temperature was more than 0.05°C different from that measured, the boiling heat flux density, which again was assumed uniform around the cylinder, was adjusted appropriately until this temperature condition was met. The procedure was repeated for each measured temperature in turn. In this way, a boiling flux density curve was generated. This direct iterative procedure was efficient and effective since the experimental cooling curve represented the lowest surface temperature of the whole cylinder at any time and hence the boundary conditions for all other points were determined in advance from it. Figure K.2 indicates the heat flux density curve generated by this procedure. The severe variations in it arise by virtue of the sensitivity of it relative to the errors in measured temperature. If a cubic spline smoothing technique was used (R3) to smooth the temperature data, this variation was minimized, as indicated by the dashed boiling curves in Figure K.2. In any event, the required boiling curve is of the same magnitude as the one generated by the calibrated heat flux meter. There does seem to be an effect of wall temperature (the predicted curve is shifted to lower wall temperatures), but this can be accounted for by the averaging procedure used to assign an appropriate wall temperature to the average heat flux recorded by the heat flux meter. It may also result from the assumption of constant heat flux density around the cylinder. Obviously since the heat flux density does vary around the cylinder, conduction in the ϕ -direction does occur; hence, for a more accurate prediction, a three-dimensional analysis is required in which account of the varying heat flux is

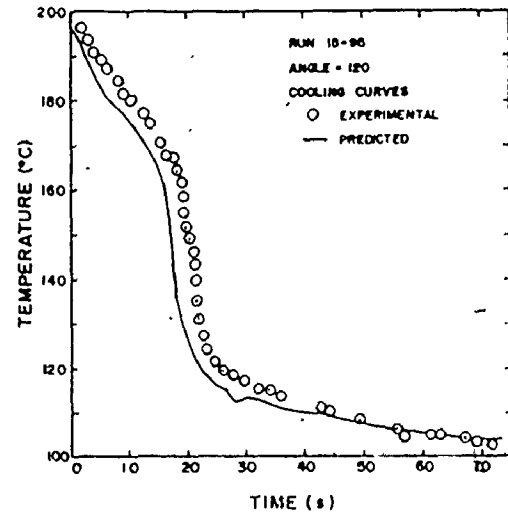
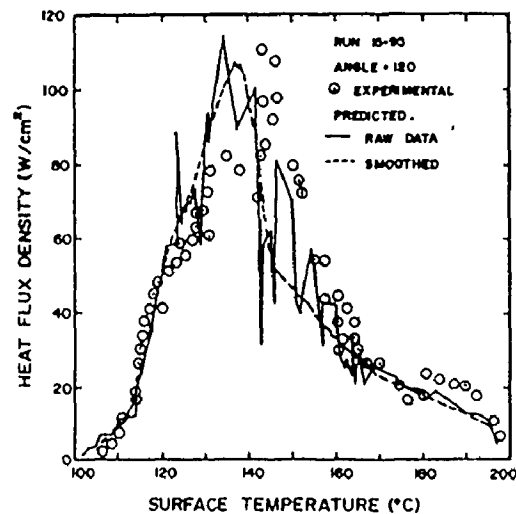
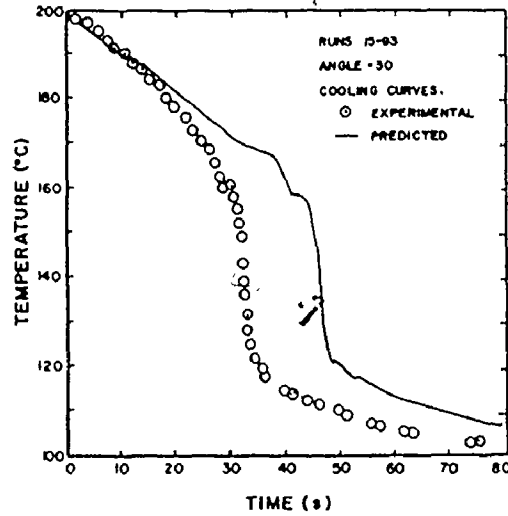
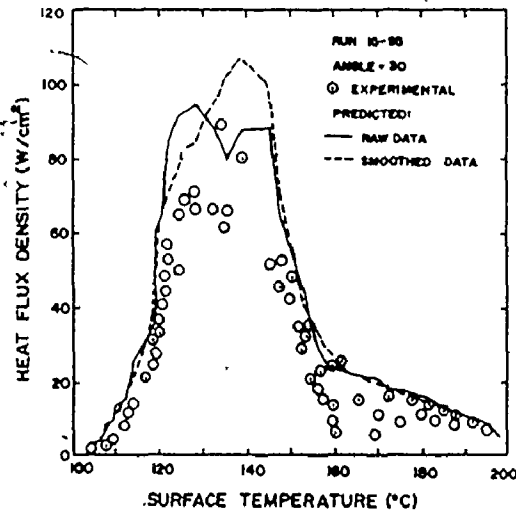
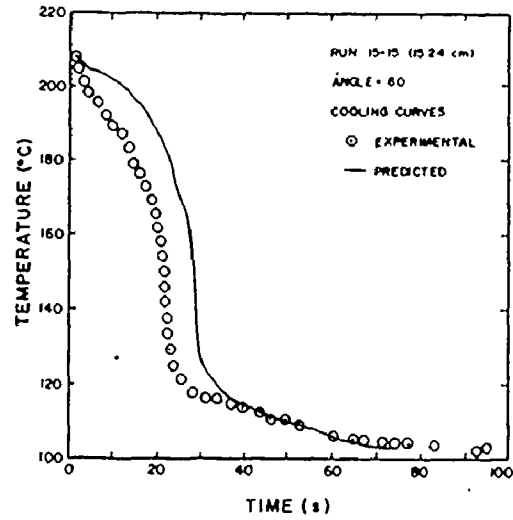
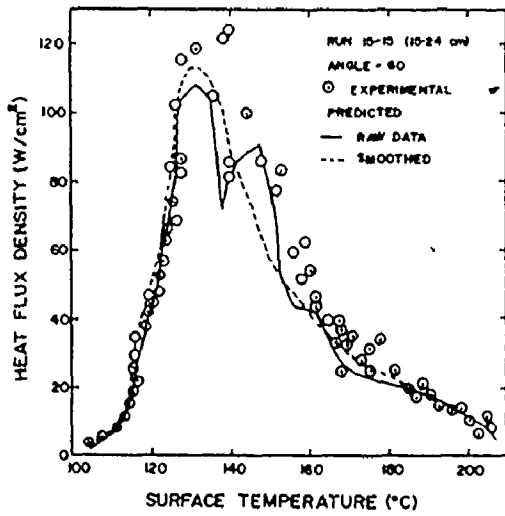


FIGURE K.2 - BOILING AND COOLING CURVES PREDICTION(2-D SYSTEM)

included. This three-dimensional analysis is covered in the sections to follow.

K.2 Three-Dimensional Analysis

The use of an ADI numerical method for a three-dimensional system would necessitate a large amount of programming and excessive computer time. Instead, a simpler scheme, based on the principle of superposition, was used. This new scheme appears to have been used for the first time by Archambault and Chevrier(A1). A direct comparison with an analytical method and an ADI numerical method showed that this new scheme gave the same results as long as the boundary conditions were specified correctly(T4). In addition to being easier to program, it required 20% less computer time for a two-dimensional system(T4). The description of this numerical method for a three-dimensional system will now be derived followed by a discussion of the results obtained with this method.

K.2.1 Method of Solution

The problem can be formulated in the same manner as was done in Section K.1.1. However, now the problem necessitates including the angular conduction term of the unsteady heat diffusion equation:

$$\frac{1}{\alpha} \frac{\partial T}{\partial t} = \frac{\partial^2 T}{\partial r^2} + \frac{1}{r} \frac{\partial T}{\partial r} + \frac{\partial^2 T}{\partial z^2} + \frac{1}{r^2} \frac{\partial^2 T}{\partial \phi^2} \quad (K-17)$$

The boundary conditions, taking symmetry into account, are:

$$t=0, T=T_0 \text{ for } 0 \leq r \leq R \text{ and } 0 \leq z \leq L \quad (\text{K-18})$$

$$t > 0, \left. \frac{\partial T}{\partial r} \right|_{r=0} \neq 0. \quad (\text{K-19})$$

$$\left. \frac{\partial T}{\partial r} \right|_{r=R} = f(T_{R,z,\theta}) \quad (\text{Boiling curves}) \quad (\text{K-20})$$

$$\left. \frac{\partial T}{\partial z} \right|_{z=0} = 0 \quad (\text{Axial symmetry}) \quad (\text{K-21})$$

$$\left. \frac{\partial T}{\partial z} \right|_{z=L} = f(T_{r,L,\theta}) \quad (\text{Heat loss from the ends}) \quad (\text{K-22})$$

$$\left. \frac{\partial T}{\partial \phi} \right|_{\phi=0} = 0 \quad (\text{K-23})$$

$$\left. \frac{\partial T}{\partial \phi} \right|_{\phi=\pi} = 0 \quad (\text{K-24})$$

} (Each vertical half of the cylinder
is the same)

These boundary conditions indicate that it is only necessary to consider two quadrants of a half length of the cylinder.

Because of the non-linear character of the surface boundary conditions, it is necessary to solve numerically Equation K.17. In the numerical technique formulation, $T_{i,j,k}$, is defined the temperature prevailing at point (i,j,k) (where $i = 1, 2, \dots, NR$ in the radial direction, $j = 1, 2, \dots, NZ$ in the axial direction and $k = 1, 2, \dots, NA$ in the angular

direction). The radial, axial and angular diffusion terms are expressed by:

$$\frac{\partial^2 T}{\partial r^2} + \frac{1}{r} \frac{\partial T}{\partial r} = \frac{T_{i+1,j,k} - 2T_{i,j,k} + T_{i-1,j,k}}{\Delta r^2} + \frac{1}{(i-1)\Delta r} \frac{T_{i+1,j,k} - T_{i-1,j,k}}{2\Delta r} \quad (K.25)$$

$$\frac{\partial^2 T}{\partial z^2} = \frac{T_{i,j+1,k} - 2T_{i,j,k} + T_{i,j-1,k}}{\Delta z^2} \quad (K.26)$$

$$\frac{1}{r^2} \frac{\partial^2 T}{\partial \phi^2} = \frac{T_{i,j,k+1} - 2T_{i,j,k} + T_{i,j,k-1}}{[(i-1)\Delta r \Delta \phi]^2} \quad (K.27)$$

It is extremely important to formulate the boundary conditions correctly in finite difference form to minimize the discretization error (T4). Each is discussed in turn below:

(1) At $r = 0$ ($i = 1$), $\frac{\partial T}{\partial r} \neq 0$

This nonequality arises because the thermal centre does not coincide with the geometric centre as a result of the high angular variation of the surface heat flux. This implies that to obtain the temperature at the geometric centre with greatest accuracy would require simultaneous solution of all mesh points in the cylinder. However, this is virtually impossible due to the size of the system involved and the large computer time that would be required to obtain a complete solution. Instead, the system was solved from one surface point to its antipode. It is felt that this procedure gives an accurate solution because the centre point reacts fairly slowly to heat flux changes at the surface. This procedure

provides many solutions for the centre point and an average of these temperatures should provide a good representation of the centre temperature.

$$(ii) \quad \text{At } z = 0 \text{ (j. = 0), } \frac{\partial T}{\partial z} = 0$$

and the axial diffusion term becomes

$$\frac{\partial^2 T}{\partial z^2} = \frac{2(T_{i,2,k} - T_{i,1,k})}{\Delta z^2} \quad (K.28)$$

(iii) At the outer surface of the cylinder ($i = NR$ or $j = NZ$), there is a heat flow out of the surface determined by the local temperature and the assumed boiling curve. The formulation of these points was presented in Section K.1.1.

(iv) In the angular direction, the system is solved for only one half of the cylinder because of the symmetry conditions at

$$\left. \begin{array}{l} \phi = 0 \text{ (k=1)} \\ \text{and } \phi = \pi \text{ (k=NA)} \end{array} \right\} \frac{\partial T}{\partial \phi} = 0 \quad (K.29)$$

Similarly to (ii) the symmetric point lying outside of the domain of solution is replaced by its symmetric point within the domain of solution.

$$(v) \quad \text{At } z = L \text{ (j = NZ), } -k \frac{\partial T}{\partial z} = 0$$

In this particular study, the ends of the cylinder were assumed to be perfectly insulated by the transite holders. Also the holders extended over a portion of the metal cylinder and effectively insulated this

circumferential surface area. These insulated surfaces caused axial temperature gradients to exist within the cylinder. The method of superposition is used to solve Equation K.17 by solving implicitly each of Equations K.25, K.26 and K.27 in the three respective directions while, in each case, the interaction of conduction in the other two directions is neglected. These three independent unidirectional temperature distributions, $U_{i,j,k}$, $V_{i,j,k}$ and $W_{i,j,k}$ for the radial, axial and angular directions respectively, provide three solutions for all the points in the system. The three-dimensional temperature distribution at time $(t + \Delta t)$ is obtained by algebraically summing the recorded temperature differences $(U_{i,j,k,t+\Delta t} - T_{i,j,k,t})$, $(V_{i,j,k,t+\Delta t} - T_{i,j,k,t})$ and $(W_{i,j,k,t+\Delta t} - T_{i,j,k,t})$ to the temperature $T_{i,j,k,t}$ at each point at time t giving the following equation:

$$T_{i,j,k,t+\Delta t} = U_{i,j,k,t+\Delta t} + V_{i,j,k,t+\Delta t} + W_{i,j,k,t+\Delta t} - 2T_{i,j,k,t} \quad (K-30)$$

for $2 \leq i \leq NR$

$1 \leq j \leq NZ$

$1 \leq k \leq NA$

Because a three-dimensional system is used to solve this problem, it is not necessary to solve in all dimensions in some instances for the centre point. At the centre there is no angular variation and therefore when solving Equation K.27, it is only solved from $i = 2$ to NR . Similarly when the axial temperature distribution at the centre is sought it is not necessary to do it for all angular mesh points but only for one as it is a unique point. To complete the full temperature

distribution at the centre point an average temperature is first calculated from all the radial one-dimensional solutions and then added to the one calculated with the axial one-dimensional solution at the centre point to give:

$$T_{i,j,k,t+\Delta t} = \frac{1}{NA} \sum_{k=1}^{NA} V_{i,j,k,t+\Delta t} + U_{i,j,l,t+\Delta t} - T_{i,j,k,t} \quad (K-31)$$

for $i = 1$
 $1 \leq j \leq NZ$
 $1 \leq k \leq NA$

This method of solution was used in the same way as the ADI numerical method was used for the two-dimensional system to predict cooling curves for each of the seven experimental points or the boiling curve from the experimentally measured (smoothed) cooling curves. A listing of the computer program for the three-dimensional situation is presented in Appendix Z. The results obtained with this system will now be discussed.

K.2.2 Results and Discussion

Three different runs, two at saturation and one at 20°C subcooling, were investigated. Cylinder 15 was chosen for this analysis because it was a cylinder on which a great number of experiments were performed under various conditions; it was used to investigate the effect of length, partial axial insulation, subcooling and partial

circumferential insulation under saturated and subcooled conditions. Finally it was used in the steady-state calibration experiment. The analysis in three-dimensions essentially comprises choosing one experiment at each of the seven angles investigated (0, 30, 60, 90, 120, 150 and 180⁰) and using the measured cooling curves or the boiling curves as boundary conditions in the solution of the problem. It should be noted that the seven boiling and cooling curves used in any one analysis originate from seven different experiments. Because the initial quenching temperature for each experiment was different, some alignment of temperature at time zero was necessary. This procedure induces some errors in the prediction as some temperature gradients may exist at the chosen starting temperature. Since the heat flux at these high temperatures is relatively small initially, these gradients should not be severe. The results for the three cases investigated are presented on Figures K.3, K.4 and K.5. The agreement with the experimental curves is quite good and now the prediction at a 30⁰ angle is very good as it follows very closely the very low heat fluxes usually encountered in the transition regime.

The resulting boiling curves for selected points are shown to be in quite good agreement with those generated by the indirectly calibrated heat flux meter, thus suggesting again that the meter calibration procedure is reasonable and that reliable heat transfer rates can be measured in this way.

K.3 Influence of Transite

In this experimental program, the ends of the copper cylinder

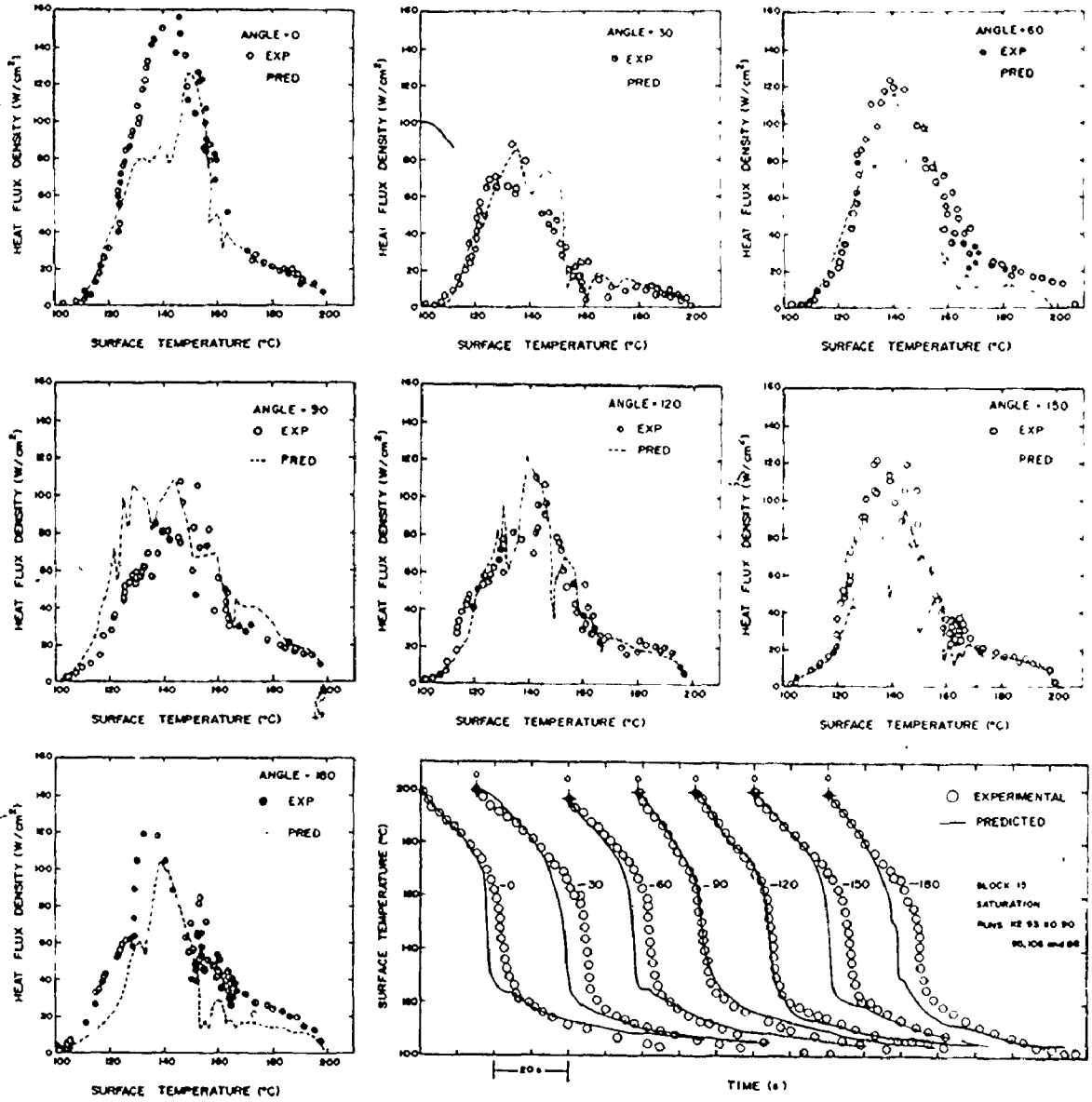


FIGURE K.3 - BOILING AND COOLING CURVES PREDICTION(3-D SYSTEM)

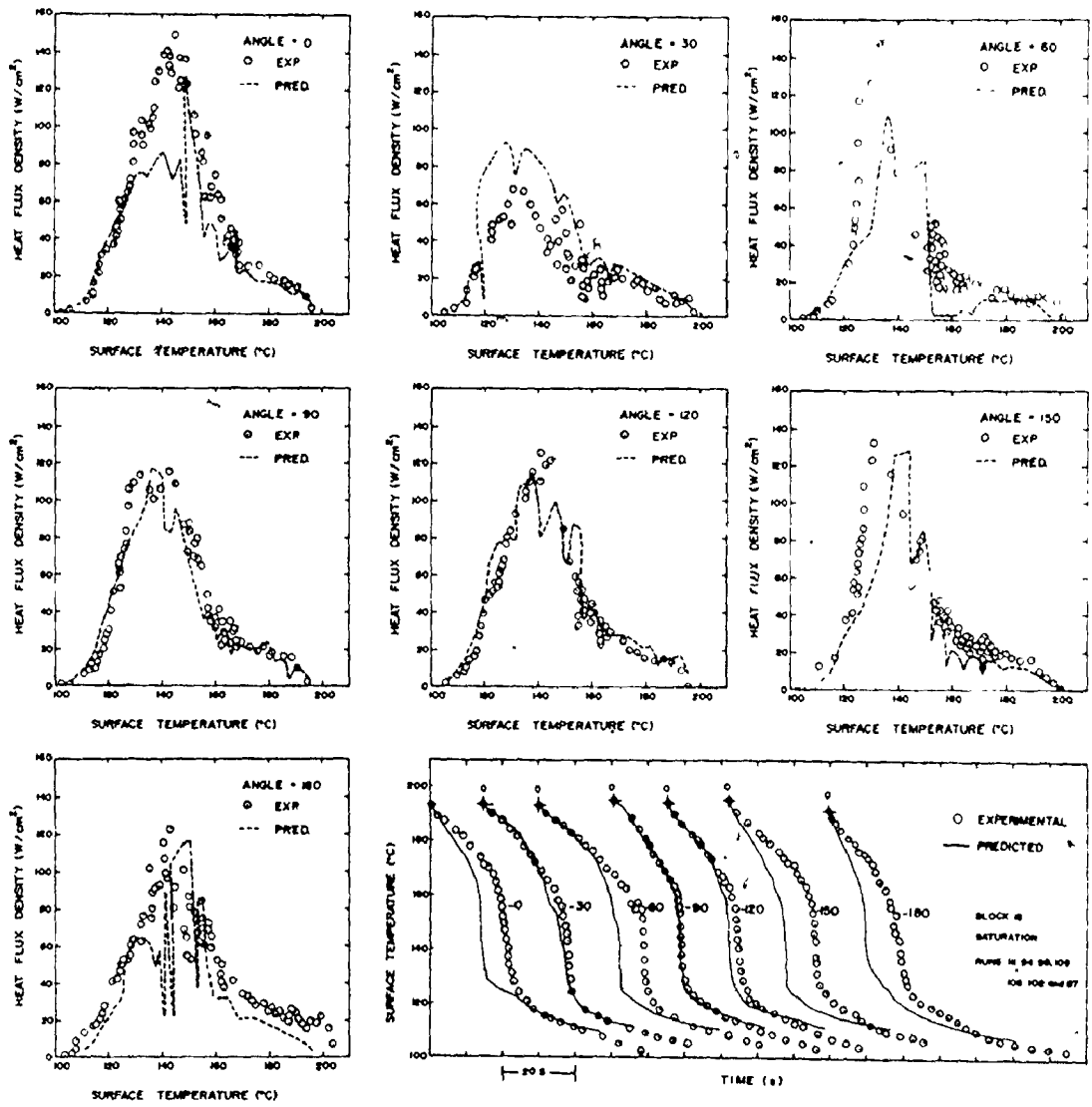


FIGURE K.4 - BOILING AND COOLING CURVES PREDICTION(3-D SYSTEM)

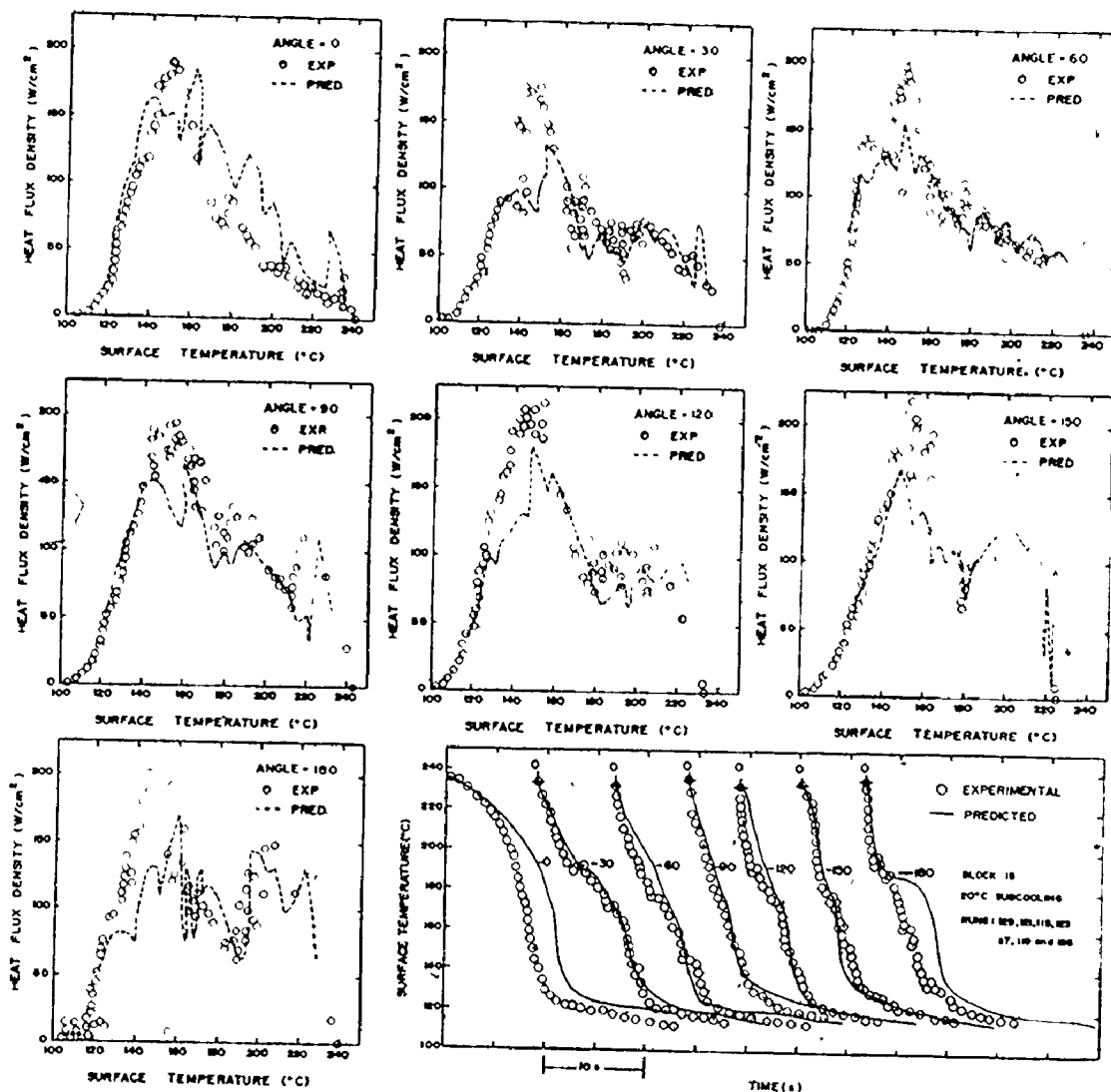


FIGURE K.5 - BOILING AND COOLING CURVES PREDICTION(3-D SYSTEM)

were assumed to be perfectly insulated by the transite holders. Also the holders extended over a portion of the metal cylinder and thus effectively insulated this circumferential surface area. These insulated surfaces could cause axial temperature gradients to exist within the cylinder and on the surface of the cylinder. The unsteady-state calibration procedure assumed, however, that the surface heat flux at any angle was uniform over the cylinder length. This assumption is reasonable because copper has such a high thermal conductivity. With the numerical method at hand it was possible to verify the validity of this assumption. To do this, the cooling curve was predicted for a 15.24 cm, 11.43 cm and 7.62 cm long copper cylinders with an insulated 0.635 cm width on both sides of the cylinder. Results for most of the cases studied are presented in Table K.1. The integrated average heat flux for all mesh points on the surface was divided by the integrated average heat flux for all points at $z = 0$ (centre of the cylinder). The results indicated in Table K.1 clearly show that the assumption of a uniform axial surface heat flux is valid since a maximum error of only 3% is introduced with this assumption. The error is smaller for a longer cylinder because of the smaller temperature gradient induced. These results were obtained with the two-dimensional study because it required less computer time and more cases could be studied. For a 7.62 cm cylinder, similar results were obtained with the three-dimensional system.




TABLE K.1

INFLUENCE OF TRANSITE

MESH POINT	<u>15-15</u>	<u>15-15</u>	<u>15-15</u>	<u>15-76</u>	<u>15-87</u>	<u>15-93</u>	<u>15-95</u>	<u>15-95</u>	<u>15-95</u>
1	1.0000	1.0000	1.0000	1.0000	1.0000	1.0000	1.0000	1.0000	1.0000
2	.9991	1.0029	.9997	.9991	1.0012	1.0000	1.0001	.9986	1.0032
3	.9995	1.0037	1.0002	1.0066	1.0016	1.0025	.9984	.9986	1.0053
4	1.0010	1.0012	.9973	1.0083	1.0078	1.0074	1.0000	1.0004	1.0003
5	1.0007	1.0035	.9997	1.0086	1.0133	1.0149	1.0063	1.0082	1.0149
6	1.0053	1.0000	.9975	1.0121	1.0303	1.0302	1.0172	1.0184	1.0281
7	1.0092	1.0019	.9978	1.0234	1.0537	1.0567	1.0296	1.0314	1.0554
8	1.0251	1.0022	1.0029	1.0653	1.1135	1.1168	1.0552	1.0680	1.1089
9	.8306	1.0076	1.0056	.6083	0.	0.	.8512	.5882	0.
10	0.	1.0067	1.0086	0.	0.	0.	0.	0.	0.
11		1.0123	1.0228	1.0626					
12		1.0256	1.0475	1.1195					
13		1.0682	1.0576	.2057					
14		.4026	0.	0.					
15		0.	0.	0.					
Assumed Length(cm)	15.24	15.24	11.43	11.43	7.62	7.62	15.24	11.43	7.62
Total (area weight)	16.741	26.077	25.274	16.463	15.443	15.457	16.916	16.424	15.448
Error (%)	1.46	1.60	1.56	2.90	2.95	3.05	2.52	2.65	2.99

APPENDIX L

CORRECTION OF SUBCOOLING LEVEL AT THE CRITICAL HEAT FLUX

A series of experiments were performed on copper cylinders at various water temperature of the quenching bath to determine the influence of subcooling on the critical heat flux density. Although the level of subcooling was preset at the beginning of the experiment, by the time the cylinder actually went through the critical heat flux, the quenching bath temperature had increased. Furthermore, since higher initial cylinder temperatures were required (because the CHF occurred at higher temperatures) and since higher heat flux densities were observed at higher subcoolings, more enthalpy was transferred to the water prior to the CHF at higher subcoolings. Hence the actual subcooled condition at the time when the critical heat flux occurred was different from the initial condition and the correction to account for the enthalpy transfer from cylinder to water was different for each initial subcooling. Since it was desired to compare the present experimental CHF data with that predicted from available correlations in the current literature, the subcooling which actually existed at the time the critical heat flux occurred should be known. A heat balance based on the measured heat flux and the average temperature increase of the quenching bath provided the necessary correction to the initial subcooling; this balance is shown below.

It was impossible to perform a direct ~~heat~~ balance, whereby

the average temperature of the water at any time could be calculated by integrating the heat flux density over the appropriate areas and with time, because the steel frame and the transite disks also contributed to reduce the subcooling level of the quenching bath. Instead, it was decided to calculate the fraction of the total heat content of the block which was transferred up to the time of the critical heat flux point and to assume that the complete copper cylinder assembly lost the same fraction of its heat content. This was accomplished by the integration procedure mentioned above; the results for the two highest subcoolings investigated are presented in Table L.1. These results show that roughly one third of the total heat content left the cylinder at the CHF point. Moreover, it was possible to measure the average increase in temperature of the quenching bath at the end of the experiment. The overall increases in the quenching bath temperature were approximately 1°C , 2°C , 4°C and 7°C for 5°C , 10°C , 20°C and 30°C subcooling respectively. These values provide a measure, in terms of temperature, of the overall enthalpy increase of the water and, also, of the total enthalpy loss of the copper cylinder assembly. With the assumption of a lumped copper cylinder assembly and a completely mixed water tank, it is possible to calculate corrections of 1.4°C and 2.1°C for 20°C and 30°C subcooling, respectively.

However, over the duration of the quench, there is a region of higher temperature in the vicinity of the copper cylinder which could be measured. Temperatures in excess of 80°C were recorded at the top of the cylinder at CHF for a 30°C initial subcooling. The assumption of the completely mixed system is therefore inadequate. To compensate

for this effect, it was deemed necessary to use a slightly higher correction for the initial subcooling. It was decided that a value corresponding to no more than half the measured average increase in temperature would provide a more realistic correction although this correction was still believed to be conservative. The result of applying this correction was that the level of subcooling which existed at the time of CHF was about 90 percent of the initial value.

TABLE L.1

HEAT BALANCE UP TO CRITICAL HEAT FLUX

ANGLE	RUN NUMBER	HEAT LOSS RATIO ^a	AVERAGE RATIO	TIME AT CHF
BLOCK 15				
20°C Subcooling				
0	113	.368	.363	10.24
	114	.360		10.71
	129	.400		9.48
30	121	.527	.464	10.59
	122	.401		9.05
60	115	.633	.365	7.86
	116	.337		6.43
90	123	.372	.341	5.30
	124	.310		5.24
120	117	.313	.329	5.75
	118	.344		4.74
150	119	.295	.276	3.94
	120	.257		4.15
180	125	.311	.354	5.24
	126	.373		6.01
	127	.380		6.88
	128	.353		5.44
			<u>.361</u>	
BLOCK 22				
30°C Subcooling				
0	45	.185	.231	7.05
	46	.157		6.12
	53	.361		6.89
30	39	.279	.289	3.87
	40	.300		4.05
60	47	.366	.278	3.29
	58	.190		2.64
90	41	.312	.309	3.22
	42	.280		3.52
	59	.335		3.75
120	51	.305	.309	3.00
	52	.312		3.11
150	43	.352	.337	3.46
	44	.321		4.11
180	49	.357	.338	4.26
	50	.319		3.79
			<u>.301</u>	

^a Ratio of the heat content loss up to CHF over the total heat content of the block.

APPENDIX M

CALCULATION OF SONIC ORIFICE VAPOUR FLOW RATE

Using an orifice which has been sized to operate with the sonic velocity at its throat (a sonic orifice) is a very easy way to control the flow rate of a gas or vapour under pressure. This ease of control arises because as long as the ratio of the downstream to upstream pressure is smaller than some predictable critical value the velocity in the throat is sonic and the mass flow rate depends only on the upstream pressure.

In this experimental program, vapour was injected underneath a single copper cylinder as well as underneath the multiple array of cylinder. The available pressure of the steam supply system was 100 psig and therefore it was possible to use a sonic orifice for this purpose. The size of the sonic orifice used in this study was 0.635 cm in diameter. Therefore to control the steam flow rate across the orifice it suffices to control the upstream pressure of the orifice. The objective of this appendix is to present the calculation procedure for determining the mass vapour flow rate corresponding to the four upstream pressures used throughout this study.

Brodkey(813) gives the equation for a sonic orifice, viz.:

$$W = A \sqrt{\frac{\gamma M_w}{R} \left[\frac{2}{\gamma+1} \right]^{\frac{\gamma+1}{\gamma-1}} \frac{P_0}{\sqrt{T_0}}} \quad (M-1)$$

where $\gamma = C_p/C_v$. Brodkey also gives the equation for calculating the sonic velocity for an ideal gas, viz.:

$$C = \sqrt{\frac{\gamma RT}{M_w}} \quad (M.2)$$

from which the value of γ can be extracted because the velocity of sound for steam at 134°C (407.2°K) is given as 494 m/s (R9). The value of γ was calculated as 1.14 and assumed to be constant for the pressure range considered (R value used is $83.13 \times 10^6 \text{ dyne-cm/gmole}^\circ\text{K}$).

The condition of operation for the sonic orifice requires that(B13)

$$\frac{P_0}{P} \geq \left[\frac{\gamma+1}{2} \right]^{\frac{\gamma}{\gamma-1}} = 1.74 \quad (M.3)$$

$$\therefore P_0 \geq 1.74 P$$

This condition stipulates that the upstream pressure should be greater than 26 psia for the present situation. In this study the minimum pressure used was 35 psia and therefore well above the lower limit. The 0.635 cm diameter orifice was designed according to the ASME specifications(F3). Careful machining and polishing of the orifice contour was done in an attempt to obtain a discharge coefficient close to 1 over the whole range. This orifice was calibrated previously by Khosla(K3) who found that the mass flow rate was predicted by Equation M.1.

It is now possible to calculate the mass vapour flow rates

corresponding to 100, 60, 40 and 20 psig. To do so it is necessary to have the temperature of the steam at each pressure. By assuming a constant enthalpy expansion from saturated steam at 100 psig, the temperatures at each downstream pressure can be calculated; these are given in Table M.1. With Equation M.1 it is possible to calculate the mass flow rate of vapour going through the orifice and compare it to the amount of vapour generated by a single cylinder undergoing CHF at saturation (110 W/cm^2 , 12.4 g/s). The results of this calculation are presented in Table M.1.



TABLE M.1

VAPOUR VOLUMETRIC FLOW RATE
CORRESPONDING TO UPSTREAM PRESSURE

<u>UPSTREAM PRESSURE</u> (psig)	<u>STEAM TEMP.</u> (°K)	<u>MASS FLOW RATE</u> (g/s)	<u>FRACTION OF CHF AT SAT.</u>
100	443	39.3	3.17
60	434	25.9	2.09
40	429	19.1	1.54
20	426	12.2	.98

APPENDIX Y

MAIN MINICOMPUTER PROGRAMS USED IN THIS STUDY

METER IS A PROGRAM WHICH HAS BEEN DONE TO HANDLE DATA ACQUISITION FOR A MAXIMUM OF 3 HEAT FLUX METERS AND A MAXIMUM OF 6 INDIVIDUAL TEMPERATURES. METER OPERATES UNDER MODS. IT IS LOADED BY CALLING METER AND IS ACTIVATED BY PRESSING CTRL E ASCII CHARACTER FOLLOWED BY ONE OF THESE LETTERS :

- C - FOR CONTACT SENSE HISTORY PRINTOUT
- F - OPERATIONS ARE FINISHED AND CONTROL IS PASSED TO THE CLI
- L - CHANGE IN THE OUTPUT DEVICE
- O - OUTPUT RESULTS ALREADY OBTAINED
- M - RUN WITHOUT ANY PARAMETER CHANGE
- S - CHANGE THE RUN PARAMETERS AND RUN
- T - OUTPUT INDIVIDUAL TEMPERATURES

BY PRESSING CTRL E ALL THE CHANNELS ARE CLOSED, ALL THE JOBS ARE KILLED, ALL OUTPUTS ARE CANCELLED AND THE PROGRAM WAITS ONE OF THE ABOVE LETTERS TO BE RECEIVED. EVERY OPTION ASSOCIATED WITH THE DIFFERENT LETTERS WILL BE EXPLAINED IN THE SECTIONS TO FOLLOW.

A - LETTER 'C'

WHEN THE LETTER 'M' OR 'S' IS PRESSED, THE PROGRAM DOES NOT START TO TAKE READINGS IMMEDIATELY BUT WAITER WAITS THAT THE CONTACT SENSE '0' BE CLOSED. THIS ALLOWS TO START THE DATA ACQUISITION AT THE EXPERIMENT LOCATION WHENEVER IT IS READY. THE PROGRAM CAN BE STOPPED AND RESTARTED AT ANY TIME DURING A RUN BY OPENING CONTACT SENSE '0' AND RE-CLOSING IT.

THE A/D CHANNELS ARE READ EVERY .01 SECOND AND AVERAGE AFTER A CERTAIN TIME PERIOD WHICH IS DETERMINED BY CONTACT SENSES '1' AND '2' PATTERN AND THE FOURTH PARAMETER SPECIFIED WHEN THE LETTER 'S' IS PRESSED. THE FOLLOWING TABLE GIVES A DESCRIPTION OF THE TIME AVERAGING AS A FUNCTION OF THE MODE CHOSEN AND THE CONTACT SENSES PATTERN.

 * AVERAGING TABLE *

CONTACT SENSES		MODE	
1	2	0	2
0	1	50	100
0	0	20	50
1	0	10	20
1	1	5	10

THE VALUES ARE IN CYCLES (ONE CYCLE IS 0.01 SECOND) WHICH MEANS THAT THE AVERAGES ARE TAKEN EVERY 200 CYCLES (IE 2 SECONDS) FOR THE CASE WHEN CONTACT SENSE 2 IS CLOSED ONLY AND MODE 2 IS CHOSEN AS AN INPUT PARAMETER AT THE INITIATION OF THE PROGRAM.

CONTACT SENSES '1' AND '2' ALLOW TO VARY THE RATE OF AVERAGING DURING ANY EXPERIMENT. LOW AVERAGING PERIODS ARE TAKEN WHEN THE CYLINDER IS GOING THROUGH THE CRITICAL HEAT FLUX AND HIGHER AVERAGING PERIODS ARE USED WHEN TEMPERATURE IS CHANGING SLOWLY AS IN THE CASE OF FILM AND LOW TRANSITION REGIME AS WELL AS AT LOW NUCLEATE BOILING REGIME. THE MODE IS SPECIFIED WHEN THE PROGRAM IS LOADED. CONTACT SENSES ARE CHANGED DURING THE EXPERIMENT BY VISUAL OBSERVATION OF THE BOILING PHENOMENA.

THEREFORE THE LETTER 'C' IS USED AT THE END OF AN EXPERIMENT TO OUTPUT THE TIME HISTORY OF THE CONTACT SENSES. IT GIVES THE TIME OF THE CHANGE AND THE NUMBER OF CYCLES WHICH PREVAILS TILL THE NEXT CHANGE. THE OUTPUT IS MADE TO THE TELETYPE.

B - LETTER 'F'

WHEN THE DATA HAVE BEEN OBTAINED AND ALL THE INFORMATION NEEDED HAVE BEEN RETRIEVED, THE COMMAND IS PASSED BACK TO THE CLI. THIS IS DONE BY PRESSING THE LETTER 'F' (STANDING FOR FINISH). IT IS THE ONLY WAY TO RETURN TO THE CLI AS THE CTRL A ACTION OF MODS HAS BEEN DISABLED.

C - LETTER 'L'

THIS OPTION PROVIDES THE POSSIBILITY TO CHANGE THE OUTPUT DEVICE FOR ANY SUBSEQUENT OUTPUT REQUEST. BY PRESSING THE LETTER 'L', A QUESTION WILL BE ASKED AND THE ANSWER IS :

- 0 - IF YOU WANT THE OUTPUT TO THE TELETYPE
- 1 - IF YOU WANT THE OUTPUT TO THE LINE PRINTER
- 2 - IF YOU WANT THE OUTPUT TO A DISK FILE (IE APPENDED TO INFO.JT)

ALL OUTPUT IS DONE IN ASCII.

IF OUTPUT TO THE DISK IS DESIRED, A SECOND QUESTION WILL BE ASKED: "INFO ON THE DISK, UP TO WHAT TIME?". A TIME IN CYCLES MUST BE INPUT AND THE CARRIAGE RETURN PRESSED. THE DATA WILL BE TRANSFERRED TO THE DISK FILE IN ASCII FORM UP TO THE TIME SPECIFIED IN THE INPUT. AFTER THE COMPLETION OF THIS LETTER, ONLY THE OUTPUT DEVICE IS CHANGED AND NO OUTPUT IS PERFORMED. WHEN LETTER 'O' OR 'T' IS PRESSED THE OUTPUT WILL BE TO THE DEVICE JUST SPECIFIED. BY DEFAULT IT IS TO THE TELETYPE.

D - LETTER 'O'

WHEN LETTER 'O' IS PRESSED, THE DATA WHICH HAS JUST BEEN OBTAINED WITH THE HEAT FLUX METER IN THE EXPERIMENT ARE OUTPUT TO THE CHOSEN OUTPUT DEVICE. BY DEFAULT, THE OUTPUT WILL BE TO THE TELETYPE. WHEN THE DATA ARE TAKEN, THE DATA IS ALSO OUTPUT TO THE SPECIFIED DEVICE, HOWEVER IT IS POSSIBLE THAT AN ERROR WAS INTRODUCED IN THE OUTPUT AND THEREFORE THIS OPTION GIVES A CHANCE TO OUTPUT THE RESULTS AND NOT LOSE AN EXPERIMENT. MOREOVER, THIS OPTION ALSO ALLOWS THE OPERATOR TO STORE THE DATA ON DISK. THE DATA PLACED ON DISK ARE IN ASCII AND ARE APPENDED TO A LOG FILE NAMED "INFO.JT". WHEN THE TRANSFER IS COMPLETED, AN ASCII 'E' IS PRINTED.

F - LETTER 'R'

THERE ARE FOUR PARAMETERS WHICH ARE USUALLY SPECIFIED WHEN THE PROGRAM IS INITIATED. THESE ARE :

- NFLUX - # OF HEAT FLUX METERS
- NTEMP - # OF INDIVIDUAL TEMPERATURES
- DTMOV - CONVERSION BLOCK FROM A/D UNITS TO ENGINEERING UNITS
- MODE - MODE OF CONTACT SENSE

AFTER THESE PARAMETERS HAVE BEEN SPECIFIED, THE PROGRAM WAITS THAT CONTACT SENSE '0' BE CLOSED TO START. HOWEVER, WHEN THE LETTER 'R' IS PRESSED THE PARAMETERS ARE NOT CHANGED AND THE PROGRAM IS INITIATED WITH :

- NFLUX - 1
- NTEMP - 0
- DTMOV - 0 (OTHIG. RANGE -0.2 TO 2 MV)
- MODE - 0

G - LETTER 'S'

THIS LETTER GIVES THE OPTION TO CHANGE THE RUN PARAMETERS WHEN THE PROGRAM IS INITIATED. THE PROGRAM CAN HANDLE UP TO 3 HEAT FLUX METERS AND 6 INDIVIDUAL TEMPERATURES. ALL FOUR PARAMETERS WILL BE EXPLAINED IN TURN.

(1) NFLUX - IS THE NUMBER OF HEAT FLUX METERS WHICH ARE USED DURING THE EXPERIMENT. EVERY HEAT FLUX METER TAKES TWO A/D CHANNELS, ONE FOR THE TEMPERATURE DIFFERENCE ON THE DISK AND ONE FOR THE BLOCK TEMPERATURE. THE FIRST 10 A/D CHANNELS ARE RESERVED FOR HEAT FLUX METERS ONLY, EVEN IF THERE IS ONLY ONE METER INVOLVED. A/D CHANNELS 11 TO 16 ARE RESERVED TO INDIVIDUAL TEMPERATURES.

(2) NTEMP - IS THE NUMBER OF INDIVIDUAL TEMPERATURES WHICH ARE DESIRED TO BE RECORDED AS A FUNCTION OF TIME. IT CAN BE CYLINDER TEMPERATURES ON THE SIDE COLUMN OR IT CAN BE WATER TEMPERATURE DURING SUBCOOLED BOILING ACROSS THE CENTRE COLUMN.

(3) DTMOV - THE TEMPERATURE DIFFERENCE ENGINEERING CONVERSION UNIT IS DEPENDENT ON THE CALIBRATION OF THE THERMOCOUPLE TRANSMITTERS. THERE ARE TWO POSSIBLE OPTIONS. IF THE TRANSMITTERS FOR THE TEMPERATURE DIFFERENCE IS CALIBRATED BETWEEN -0.2 TO 2 MV (OTHIG) THE INPUT IS 0 AND IF CALIBRATED BETWEEN -0.2 TO 1 MV (DTLOW) THE INPUT IS 1.

(4) MODE - THE CONTACT SENSE MODE IS DETERMINED BY THE TYPE OF EXPERIMENT WHICH IS MADE. FOR INSTANCE, IF THE EXPERIMENT IS PERFORMED WITH A PARTLY INSULATED CYLINDER, IT WILL COOL RELATIVELY SLOW AT SATURATION BOILING SO THAT MODE 2 WILL BE CHOSEN HERE.

H - LETTER 'T'

THIS LETTER ALLOWS TO OUTPUT THE INDIVIDUAL TEMPERATURES TO THE DESIRED DEVICE. THE OUTPUT FORMAT IS DETERMINED BY THE NUMBER OF INDIVIDUAL TEMPERATURES.

A GENERAL COMMENT MUST BE ADDED AT THIS POINT. THIS PROGRAM IS NOT FOOLPROOF WHICH IS TO SAY THAT THE RIGHT NUMBER MUST BE ENTERED. THE PROGRAM DOES NOT CHECK IF IT IS AN ASCII CHARACTER BETWEEN 60 AND 69. INSTEAD IT ASSUMES IT CORRECT AND USES THE LAST THREE BINARY DIGITS OF THE INPUT CHARACTER. FOR INSTANCE A '0' WOULD BE INTERPRETED AS A '4'. THERE IS ALSO AN RTOS TAPE WHICH IS AVAILABLE SO THAT THE OPERATOR CAN OPERATE ON A SOS SYSTEM WHEN THE DISK SYSTEM IS NOT FUNCTIONING PROPERLY.

I WOULD LIKE TO EXPRESS MY APPRECIATION TO JEAN-PIERRE TREMBLAY FOR ALLOWING ME TO USE SOME OF HIS PROGRAM AND SUGGESTING ME METHODS OF INCREASING THE EFFICIENCY OF THE PROGRAM. THIS PROGRAM COULD BE USED FOR OTHER EXPERIMENT WITH ONLY MINOR CHANGES.

JULES THIBAUT

```

0001 BOSS
01 ENT BOSS DTNOM DATA TSTOR BPTRI
02 ENT LINE OPENI OPENI SLASH ECHO APPEN
03 EITH METER ERROR AFLAG OUT NPLUX TASH
04 EITH BPTR ECRIT PRI TPUT DTLOW DTHIO
05 EITH CNTE CNPT LPTER NTEMP WORSF TOUT
06 EITH KEYED DBIN LINER LOCAT BDEC DATIN
07
08
09
10
11
12 00000-000261 PZERO LIN
13 00001-000311 OPNO
14 00002-000344 OPNI
15 00003-000390 SLSH
16 00004-000270 ECH
17 00005-000404 APPN
18
19 004000-LINE= JSR @PZERO
20 006001-APPEN= JSR @PZERO+1
21 006002-APPEN= JSR @PZERO+2
22 006003-SLASH= JSR @PZERO+3
23 006004-ECHO= JSR @PZERO+4
24 006005-APPEN= JSR @PZERO+5
25
26 006001 TITH 1
27
28
29
30 00000 000075 BLOC BPTRI
31 00001 077777 WORSF
32
33
34
35 00002 000017 MEM SYSTM
36 00003 001000 MEM
37 00004 077777 ERROR
38 00005 125400 INC I 1
39 00006 044417 STA 1 DATA
40 00007 020420 LDA 0 C5500
41 00010 123000 ADD I 0
42 00011 040415 STA 0 TSTOR
43 00012 020416 LDA 0 C4900
44 00013 000017 SYSTM
45 00014 011000 MEMI
46 00015 000004 ERROR
47
48 000000 IFE RTOSP
49 00016 000017 SYSTM
50 00017 021027 ODIS
51 00020 000015 ERROR
52 ENDC
53
54 00021 020551 LDA 0 C75
55 00022 024757 LDA 2 BLOC+1
56 00023 054014 STA 1 USP
57 00024 000416 JMP BOSS+1
58
59 00025 000000 DATA 0

```

```

0002 BOSS
01 00026 000000 TSTOR 0
02 00027 012574 C7500 3500
03 00030 015364 L4900 6900
04 00031 000005 CTRL 5
05 00032 000100 POS 103
06 00035 000106 POS 106
07 00034 000117 POS 117
08 00035 000122 POS 122
09 00036 000123 POS 123
10 00037 000114 POS 114
11 00040 000124 POS 124
12
13 MAIN ROUTINE WHICH CONTROLS ALL THE PROGRAMS
14 IT IS ACTIVATED BY PRESSING CTRL E
15
16 00041 000741 BOSS JMP MEM
17 00042 077777 PRI
18 00043 006017 SYSTM
19 00044 007400 CLRCHR
20 00045 000020 ERROR
21 00046 024762 LDA 1 CTRL E
22 00047 106404 SUB 0 1 SZR
23 00050 000773 JMP BOSS+2
24 00051 126520 SUBIL 1 1
25 00052 046570 STA 1 @POINT+1
26 00053 022570 LDA 0 @POINT+2
27 00054 006017 SYSTM
28 00055 021011 SPVL
29 00056 000045 ERROR
30 00057 022721 LDA 0 RLOC
31 00060 006017 SYSTM
32 00061 021011 SPVL
33 00062 000056 ERROR
34 00063 024507 LDA 1 C75
35 00064 006017 SYSTM
36 00065 010400 DELAY
37 00066 000042 ERROR
38 00067 006017 SYSTM
39 00070 000000 ECRIT
40 00071 000046 ERROR
41 00072 000000 A LINE
42 00073 000004 ECHO
43 00074 024736 LDA 1 POS
44 00075 106405 SUB 0 1 SZR
45 00076 000426 JMP LETC
46 00077 024734 LDA 1 POS+1
47 00100 106405 SUB 0 1 SZR
48 00101 000459 JMP LETE
49 00102 024732 LDA 1 POS+2
50 00103 106405 SUB 0 1 SZR
51 00104 006455 JMP LETO
52 00105 024730 LDA 1 POS+1
53 00106 106405 SUB 0 1 SZR
54 00107 000522 JMP LETR
55 00110 024726 LDA 1 POS+4
56 00111 106405 SUB 0 1 SZR
57 00112 000441 JMP LETS
58 00113 024724 LDA 1 POS+5
59 00114 106405 SUB 0 1 SZR

```

```

0003 BOSS
01 00115 002405 JMP AL
02 00116 024722 LDA 1 POS+4
03 00117 106408 SUB 0 1 SZR
04 00120 002403 JMP AL+1
05 00121 000781 JMP A
06
07 00122 000330 L LETL
08 00123 000428 LETT
09
10
11
12
13 00124 024961 LETC LDA 1 C12
14 00125 044557 STA 1 CNTR
15 00126 006000- LINE
16 00127 024515 LDA 1 POINT+3
17 00128 044560 STA 1 STOR
18 00131 006001- OPNO
19 00132 034014 LDA 2 USP
20 00133 032512 LDA 2 @POINT+4
21 00134 051402 STA 2 BYTEP 3
22 00135 026553 LDA 1 B5TOR
23 00136 077777 BDEC
24 00137 010551 IST STOR
25 00140 026550 LDA 1 B5TOR
26 00141 125005 MOV 1 1 SZR
27 00142 000701 JMP BOSS+2
28 00143 000136 BDEC
29 00144 010544 IST STOR
30 00145 020541 LDA 0 C15
31 00146 077777 LOCAT
32 00147 022476 LDA 0 @POINT+4
33 00150 006017 SYSTM
34 00151 017000 URL 0
35 00152 000071 ERROR
36 00153 014531 DSJ CNTR
37 00154 000756 JMP C
38 00155 000466 JMP BOSS+2
39
40
41
42
43 00156 006017 LETF SYSTM
44 00157 004400 RTN
45 00160 083077 HALT
46
47
48
49
50 00161 102400 LETO SUB 0 0
51 00162 042460 STA 0 @POINT+1
52 00163 020643 LDA 0 TSTOR
53 00164 042472 STA 0 BAIDE+3
54 00165 020533 LDA 0 IDOUT
55 00167 077777 TASH
56 00170 000132 ERROR
57 00171 000652 JMP BOSS+2
58
59

```

```

0004 BOSS
01 00172 000075 C75 75
02
03
04
05
06
07
08
09
10 00173 006001-LETS OPNO
11 00174 020527 LDA 0 01
12 00175 006017 SYSTM
13 00176 017000 URL 0
14 00177 000170 ERROR
15 00200 006000- LINE
16 00201 006004- ECHO
17 00202 024454 LDA 1 C40
18 00203 122400 SUB 1 0
19 00204 042442 STA 0 @POINT+5
20 00205 006003- SLASH
21 00207 024451 LDA 1 C40
22 00210 122400 SUB 1 0
23 00211 042444 STA 0 BAIDE+2
24 00212 006001- SLASH
25 00213 006004- ECHO
26 00214 101202 MOV 0 0 SZC
27 00215 000403 JMP +3
28 00216 024432 LDA 1 POINT+7
29 00217 000402 JMP +2
30 00220 024427 LDA 1 POINT+6
31 00221 044501 STA 1 DTNOM
32 00222 006003- SLASH
33 00223 006004- ECHO
34 00224 024434 LDA 1 C40
35 00225 122400 SUB 1 0
36 00226 024423 LDA 1 POINT+10
37 00227 107000 ADD 0 1
38 00230 046422 STA 1 @POINT+11
39 00231 102400 LETR SUB 0 0
40 00232 042410 STA 0 @POINT+1
41 00233 020473 LDA 0 IDNET
42 00234 024473 LDA 1 IDNET+1
43 00235 000167 TASH
44 00236 000177 ERROR
45 00237 002415 JMP BAIDE+1
46
47 00240 000040 C40
48 00241 077777 POINT OUT
49 00242 077777 AFLAG
50 00243 077777 BPTR
51 00244 077777 ECRIT
52 00245 077777 LINER
53 00246 077777 NPLUX
54 00247 077777 DTLOW
55 00250 077777 DTHIO
56 00251 077777 CNTE
57 00252 077777 CNPT
58 00253 077777 LPTER
59 00254 000043 BOSS+2

```

```

0005 BOSS
01 00235 077777 NTEMP
02 00234 077777 DATIN
03
04 00237 000003 C3 3
05 00240 000040 C60 40
06 00241 054406 LTN STA 3 ACC
07 00242 020424 LDA 0 C15 .SAVE RETURN ADDRESS
08 00243 004734 JSR @POINT .CR
09 00244 030421 LDA 0 C12 .OUTPUT IT
10 00245 004734 JSR @POINT .LF
11 00246 001401 JMP @ACC3
12 00247 000000 ACC3 0
13
14 .SUBROUTINE TO OBTAIN AND ECHO A CHARACTER
15
16
17 00270 054777 E+H STA 3 ACC
18 00271 00A017 SYSTM
19 00272 007400 @CHAR .GET A CHARACTER
20 00273 000000 ERROR
21 00274 00A017 SYSTM
22 00275 010000 @CHAR ECHO IT
23 00276 000027 ERROR
24 00277 002770 JMP @ACC3
25
26 .SUBROUTINE TO OUTPUT A SLASH
27
28 00300 054767 SLASH STA 3 ACC
29 00301 000406 LDA 0 F57
30 00302 006737 JSR @POINT .OUTPUT A SLASH
31 00303 002764 JMP @ACC3
32
33 00304 000000 ENTR 0
34 00305 000011 L 1
35 00306 000015 C15 15
36 00307 000037 F57 37
37 00310 000000 STOR 0
38
39 00311 054756 @FMO STA 3 ACC
40 00312 022731 LDA 0 @POINT+2 .GET @TTO BPTR
41 00313 126400 SUB 1 1
42 00314 006017 SYSTM
43 00315 014000 @FMO .OPEN CHANNEL 0
44 00316 004527 JSR INUSE
45 00317 002730 JMP @ACC3
46
47 00320 001500 IDOUT 1500
48 00321 077777 TR@JT
49 00322 000250 @T@M DTM@
50 00323 001122 @1 AA@2
51 00324 001176 @2 BB@2
52 00325 001236 @4 DD@2
53 00326 000406 @IDMET ID=1, PRI=6
54 00327 077777 METER
55
56 .ROUTINE TO CHANGE THE OUTPUT DEVICE
57 @TTO - 0
58 @LPT - 1
59 @DISA - 2 .APPEND TO INFO JT

```

```

0007 BOSS
00402 027112
00403 052000
01 00404 054663 APPN STA 3 ACC
02 00405 020772 LDA 0 FILE
03 00406 00A017 SYSTM
04 00407 000000 .CREATE A FILE
05 00410 004411 JSR EXIST .CHECK IF ALREADY EXISTENT
06 00411 020766 LDA 0 FILE .GET FILE DPTA
07 00412 126400 SUB 1 1
08 00413 00A017 SYSTM
09 00414 012403 .APPEND 2
10 00415 004430 JSR INUSE
11 00416 002651 JMP @ACC3 .ENDC
12 .ENDC .END OF CONDITIONAL
13
14 00417 000002 C2 2
15 00420 000003 C5A 5
16
17 .SUBROUTINE TO CHECK IF CREATE ERROR IS OTHER THAN
18 .ALREADY EXISTENT FILE
19
20 00421 024404 EXIST LDA 0 C11 .CHECK IF FILE ALREADY EXIST
21 00422 146414 SUB# 2 1 SZR
22 00423 000731 ERROR .OTHER ERROR GO TO @DISA
23 00424 001400 JMP 0 .RETURN
24
25
26 00425 000011 C11 11
27 00426 000000 DSTOP 0
28 00427 000430 BUF
29 000003 BUF .BLK 3
30
31 00433 003477 IDTOT 3477
32 00434 077777 TOUT .ID=7 PRI=77
33 .TEMPERATURE
34
35 .SUBROUTINE TO OUTPUT INDIVIDUALS TEMPERATURES
36
37 00435 102440 LETT SUBO 0 0
38 00436 042604 STA 0 @POINT+1 .CLEAR KILL FLAG
39 00437 020774 LDA 0 IDTOT
40 00440 024774 LDA 1 IDTOT+1
41 00441 000235 T@S
42 00442 000423 ERROR
43 00443 002611 JMP @AIDE+1
44
45 .CHECK IF CHANNEL ALREADY IN USE
46
47 00444 000021 C21 21
48 00445 024777 INUSE LDA 1 C21
49 00446 146414 SUB# 2 1 SZR
50 00447 000442 ERROR
51 00448 001400 JMP 0 3 .RETURN
52
53 00451 047106 AA .TXT @INFLUX / NTEMP / T.H(0) L(1) / AVER(0 1 2)
54 00452 046125
55 00453 054040
56 00454 027440
57 00455 047124

```

```

0006 BOSS
01
02 00330 006001-LETL @FEMO
03 00331 020774 LDA 0 04
04 00332 006017 SYSTM
05 00333 017000 @LPT 0
06 00334 000276 ERROR
07 00335 006004- @LPT
08 00336 024722 LDA 1 C5A
09 00337 122400 SUB 1 0
10 00340 042711 STA 0 @AIDE
11 00341 024456 LDA 1 C2
12 00342 122414 SUB# 1 0 SZR .IS IT A 2 (IE DISK)
13 00343 002711 JMP @AIDE+1 .NO, RETURN
14 00344 006001- @FEMO
15 00345 006000- @LINE
16 00346 020756 LDA 0 02
17 00347 006017 SYSTM
18 00350 017000 @LPT 0
19 00351 000324 ERROR
20 00352 020457 LDA 0 @BUF-1 .GET BUFFER ADDRESS
21 00353 024445 LDA 1 C5A .GET MAXIMUM # OF CHARACTERS
22 00354 077777 @EYED
23 00355 000401 JMP +1
24 00356 010451 LDA 2 @BUF-1
25 00357 051462 STA 2 BYT@ 3
26 00360 077777 @BIN .DECIMAL TO BINARY
27 00361 000764 JMP -14
28 00362 040444 STA 0 DSTOP .STORE NUMBER
29 00363 002671 JMP @AIDE+1 .RETURN TO BOSS
30
31 00364 054703 @FNI STA 3 ACC .SAVE RETURN ADDR
32 00365 000406 LDA 0 @BPTR1 .GET @LPT BPTR
33 00366 126400 SUB 1 1
34 00367 006017 SYSTM
35 00370 014001 @FNI .OPEN 1
36 00371 004454 JSR INUSE
37 00372 002675 JMP @ACC3 .GO BACK
38
39 +1+2
40 .TXT @BLPTE
41
42 00374 022114
43 00375 000124
44 00376 000000
45
46 .APPN
47 IFN RTOSP
48 STA 3 DSTOP
49 @FNI
50 SUB# 2 1 1 .CREATE A 1
51 STA 1 @AIDE .CHANGE LPT@R VALUE FOR @LPT
52 JMP @DSTOP
53 .ENDC
54
55 .IFE RTOSP
56 .FOR OUTPUT ON DISK FILE
57
58 +1+2
59 .TXT @INFO JT
60
61 00400 044314
62 00401 043117

```

```

0008 BOSS
00456 042513
00457 050040
00460 027440
00461 052054
00462 044050
00463 050051
00464 026114
00465 024061
00466 024440
00467 027440
00470 040526
00471 042522
00472 024060
00473 026061
00474 026062
00475 024440
00476 000000
01 BB .TXT @INFO @A DISK @F TO WHAT TIME? @USE
00477 044516
00500 043117
00501 020117
00502 047040
00503 042111
00504 051513
00505 026125
00506 050040
00507 052117
00510 020127
00511 044101
00512 052040
00513 052111
00514 046505
00515 037440
00516 000000
02 DD .TXT @TTO(0) .LPT(1) .DISA(2) .@DB
00517 052124
00520 047450
00521 000051
00522 020054
00523 020114
00524 050124
00525 024061
00526 024440
00527 026040
00530 042111
00531 051513
00532 024062
00533 024440
00534 000000
03
04 000041 .ENDC BOSS

```

0001 METER

```

01 00012 125203
02 00013 000772
03 00014 102440
04 00015 042743
05 00016 102520
06 00017 024736
07 00018 000017
08 00019 021101
09 00020 000110
10 00021 020724
11 00022 024724
12 00023 000103
13 00024 000102
14 00025 020512
15 00026 101005
16 00027 000405
17 00028 020721
18 00029 024721
19 00030 000125
20 00031 000126
21 00032 024570
22 00033 044556
23 00034 052705
24 00035 050547
25
26 00036 024555 LOOP0
27 00037 044554
28 00038 044552
29 00039 026701
30 00040 125203
31 00041 000501
32 00042 024542
33 00043 125202
34 00044 000520
35 00045 026705
36 00046 044534
37 00047 010553
38
39 00048 024462 LOOP1
40 00049 044554
41 00050 024532
42 00051 044547
43 00052 024451
44 00053 044546
45 00054 024462
46 00055 044545
47
48 00056 026542 LOOP2
49 00057 052542
50 00058 022542
51 00059 133022
52 00060 101400
53 00061 042537
54 00062 052535
55 00063 010533
56 00064 010533
57 00065 010533
58 00066 014513
59 00067

```

TITL METER

```

ENT AVER NFLUX METER WORKSP KFLAG BPTR DATUM
ENT TC0N DTLOW DTHIG DATIN CYCLE NTEMP TOET
EXTN KILL TASK DIVID ROUND DATA
EXTN ERROR CONTACT TIDK BIT BPTR1 OUT
EXTN HEURE ADC SCAN TPOUT TIME TSTOR

TXTH 1
MREL
BLK 10
BLK 16 .A/D STORAGE BLOCK
ADDI
BLK 10 .SUM OF A/D STORAGE BLOCK
BIT
1500 .ID=3 AND PRI=100
TPOUT .OUTPUT ROUTINE
1004 .ID=2, PRI=4
ATOD .A/D CHANNELS JOB
3010 .ID=6, PRI=10
TOET .TEMPERATURE ACQUISITION
HEURE .TIMER JOB
2003 .ID=4, PRI=3
COTAC .CONTACT SENSE JOB
TIME
WORKSP

METER IS A TASK TO COLLECT DATA FROM A HEAT FLUX
METER AND STORE THE AVERAGE IN A BLOCK WHICH WILL BE
SUBSEQUENTLY CONVERTED TO ENGINEERING UNITS AND
OUTPUT TO A TELETYPE, LPT OR DISK

LDA 3 WORKSP
STA 3 USP
LDA 0 NFLUX .GET THE # OF HEAT FLUX METERS
MOVZL 0 0 .MULTIPLY IT BY 2
STA 0 NFLUX+1 .STORE IT
LDA 1 NTEMP .GET THE # OF INDIVIDUAL TEMPERATURES
MOV 1 1 SNR .IS IT ZERO
JMP +3
LDA 0 C10
ADD 1 0
STA 0 NATD .STORE #A/D CHANNELS
LDA 0 IDADC
LDA 1 IDADS+1
TASK
ERRR
LDA 0 IDCON
LDA 1 IDCON+1
TASJ .INITIATE CONTACT SENSE JOB
ERRR
R SUBJL 1 1 .CREATE 1
SYSTM
DELAY
ERRR
LDA 1 RBITE .CHECK IF CONTACT SENSE #0 IS CLOSED

```

0003 METER

```

01 00202 126520
02 00203 006017
03 00204 010400
04 00205 000135
05 00206 014503
06 00207 000747
07 00208 024430
08 00209 044503
09 00210 024621
10 00211 044516
11 00212 024432
12 00213 044515
13
14 00214 022514 LOOP3
15 00217 030477
16 00220 026511
17 00221 077777
18 00222 077777
19 00223 044465
20 00224 010464
21 00225 102440
22 00226 042505
23 00227 042503
24 00230 010501
25 00231 010501
26 00232 014442
27 00233 000743
28 00234 014441
29 00235 000705
30 00236 000434
31
32 00237 000001 NFLUX 1
33 00240 000000 0
34 00241 000000 NTEMP 0
35 00242 000000 NATD 0
36 00243 077777 AIDE DATA
37 00244 000013 DATUM
38 00245 000034 ADDI
39 00246 000000 ADDO
40 00247 077777 BPTR1
41
42 00250 006017 RESET SYSTM
43 00251 021002 RUCKL .REMOVE USER CLOCK
44 00252 000205 ERROR
45 00253 024450 LDA 1 C3
46 00254 077777 TIDA .KILL THE OUTPUT JOB
47 00255 000252 ERROR
48 00256 020426 LDA 0 BPTR .GET BYTE POINTER TO OUTPUT DEVI
49 00257 006017 SYSTM
50 00260 021011 SPAL .KILL SPOOLING
51 00261 000255 ERROR
52 00262 020436 LDA 0 C40 .GET A SPACE
53 00263 006442 JSR BOUTP .FORCE $TTO
54 00264 022763 LDA 0 @AIDE+4 .KILL SPOOLING ON $LPT
55 00265 006017 SYSTM
56 00266 021011 SPAL
57 00267 000261 ERROR
58 00270 000615 JMP R .GO BACK
59

```

SUBJL 1 1

```

8181
8182
8183
8184
8185
8186
8187
8188
8189
8190
8191
8192
8193
8194
8195
8196
8197
8198
8199
8200
8201
8202
8203
8204
8205
8206
8207
8208
8209
8210
8211
8212
8213
8214
8215
8216
8217
8218
8219
8220
8221
8222
8223
8224
8225
8226
8227
8228
8229
8230
8231
8232
8233
8234
8235
8236
8237
8238
8239
8240
8241
8242
8243
8244
8245
8246
8247
8248
8249
8250
8251
8252
8253
8254
8255
8256
8257
8258
8259
8260
8261
8262
8263
8264
8265
8266
8267
8268
8269
8270
8271
8272
8273
8274
8275
8276
8277
8278
8279
8280
8281
8282
8283
8284
8285
8286
8287
8288
8289
8290
8291
8292
8293
8294
8295
8296
8297
8298
8299
8300
8301
8302
8303
8304
8305
8306
8307
8308
8309
8310
8311
8312
8313
8314
8315
8316
8317
8318
8319
8320
8321
8322
8323
8324
8325
8326
8327
8328
8329
8330
8331
8332
8333
8334
8335
8336
8337
8338
8339
8340
8341
8342
8343
8344
8345
8346
8347
8348
8349
8350
8351
8352
8353
8354
8355
8356
8357
8358
8359
8360
8361
8362
8363
8364
8365
8366
8367
8368
8369
8370
8371
8372
8373
8374
8375
8376
8377
8378
8379
8380
8381
8382
8383
8384
8385
8386
8387
8388
8389
8390
8391
8392
8393
8394
8395
8396
8397
8398
8399
8400
8401
8402
8403
8404
8405
8406
8407
8408
8409
8410
8411
8412
8413
8414
8415
8416
8417
8418
8419
8420
8421
8422
8423
8424
8425
8426
8427
8428
8429
8430
8431
8432
8433
8434
8435
8436
8437
8438
8439
8440
8441
8442
8443
8444
8445
8446
8447
8448
8449
8450
8451
8452
8453
8454
8455
8456
8457
8458
8459
8460
8461
8462
8463
8464
8465
8466
8467
8468
8469
8470
8471
8472
8473
8474
8475
8476
8477
8478
8479
8480
8481
8482
8483
8484
8485
8486
8487
8488
8489
8490
8491
8492
8493
8494
8495
8496
8497
8498
8499
8500
8501
8502
8503
8504
8505
8506
8507
8508
8509
8510
8511
8512
8513
8514
8515
8516
8517
8518
8519
8520
8521
8522
8523
8524
8525
8526
8527
8528
8529
8530
8531
8532
8533
8534
8535
8536
8537
8538
8539
8540
8541
8542
8543
8544
8545
8546
8547
8548
8549
8550
8551
8552
8553
8554
8555
8556
8557
8558
8559
8560
8561
8562
8563
8564
8565
8566
8567
8568
8569
8570
8571
8572
8573
8574
8575
8576
8577
8578
8579
8580
8581
8582
8583
8584
8585
8586
8587
8588
8589
8590
8591
8592
8593
8594
8595
8596
8597
8598
8599
8600
8601
8602
8603
8604
8605
8606
8607
8608
8609
8610
8611
8612
8613
8614
8615
8616
8617
8618
8619
8620
8621
8622
8623
8624
8625
8626
8627
8628
8629
8630
8631
8632
8633
8634
8635
8636
8637
8638
8639
8640
8641
8642
8643
8644
8645
8646
8647
8648
8649
8650
8651
8652
8653
8654
8655
8656
8657
8658
8659
8660
8661
8662
8663
8664
8665
8666
8667
8668
8669
8670
8671
8672
8673
8674
8675
8676
8677
8678
8679
8680
8681
8682
8683
8684
8685
8686
8687
8688
8689
8690
8691
8692
8693
8694
8695
8696
8697
8698
8699
8700
8701
8702
8703
8704
8705
8706
8707
8708
8709
8710
8711
8712
8713
8714
8715
8716
8717
8718
8719
8720
8721
8722
8723
8724
8725
8726
8727
8728
8729
8730
8731
8732
8733
8734
8735
8736
8737
8738
8739
8740
8741
8742
8743
8744
8745
8746
8747
8748
8749
8750
8751
8752
8753
8754
8755
8756
8757
8758
8759
8760
8761
8762
8763
8764
8765
8766
8767
8768
8769
8770
8771
8772
8773
8774
8775
8776
8777
8778
8779
8780
8781
8782
8783
8784
8785
8786
8787
8788
8789
8790
8791
8792
8793
8794
8795
8796
8797
8798
8799
8800
8801
8802
8803
8804
8805
8806
8807
8808
8809
8810
8811
8812
8813
8814
8815
8816
8817
8818
8819
8820
8821
8822
8823
8824
8825
8826
8827
8828
8829
8830
8831
8832
8833
8834
8835
8836
8837
8838
8839
8840
8841
8842
8843
8844
8845
8846
8847
8848
8849
8850
8851
8852
8853
8854
8855
8856
8857
8858
8859
8860
8861
8862
8863
8864
8865
8866
8867
8868
8869
8870
8871
8872
8873
8874
8875
8876
8877
8878
8879
8880
8881
8882
8883
8884
8885
8886
8887
8888
8889
8890
8891
8892
8893
8894
8895
8896
8897
8898
8899
8900
8901
8902
8903
8904
8905
8906
8907
8908
8909
8910
8911
8912
8913
8914
8915
8916
8917
8918
8919
8920
8921
8922
8923
8924
8925
8926
8927
8928
8929
8930
8931
8932
8933
8934
8935
8936
8937
8938
8939
8940
8941
8942
8943
8944
8945
8946
8947
8948
8949
8950
8951
8952
8953
8954
8955
8956
8957
8958
8959
8960
8961
8962
8963
8964
8965
8966
8967
8968
8969
8970
8971
8972
8973
8974
8975
8976
8977
8978
8979
8980
8981
8982
8983
8984
8985
8986
8987
8988
8989
8990
8991
8992
8993
8994
8995
8996
8997
8998
8999
9000
9001
9002
9003
9004
9005
9006
9007
9008
9009
9010
9011
9012
9013
9014
9015
9016
9017
9018
9019
9020
9021
9022
9023
9024
9025
9026
9027
9028
9029
9030
9031
9032
9033
9034
9035
9036
9037
9038
9039
9040
9041
9042
9043
9044
9045
9046
9047
9048
9049
9050
9051
9052
9053
9054
9055
9056
9057
9058
9059
9060
9061
9062
9063
9064
9065
9066
9067
9068
9069
9070
9071
9072
9073
9074
9075
9076
9077
9078
9079
9080
9081
9082
9083
9084
9085
9086
9087
9088
9089
9090
9091
9092
9093
9094
9095
9096
9097
9098
9099
9100
9101
9102
9103
9104
9105
9106
9107
9108
9109
9110
9111
9112
9113
9114
9115
9116
9117
9118
9119
9120
9121
9122
9123
9124
9125
9126
9127
9128
9129
9130
9131
9132
9133
9134
9135
9136
9137
9138
9139
9140
9141
9142
9143
9144
9145
9146
9147
9148
9149
9150
9151
9152
9153
9154
9155
9156
9157
9158
9159
9160
9161
9162
9163
9164
9165
9166
9167
9168
9169
9170
9171
9172
9173
9174
9175
9176
9177
9178
9179
9180
9181
9182
9183
9184
9185
9186
9187
9188
9189
9190
9191
9192
9193
9194
9195
9196
9197
9198
9199
9200
9201
9202
9203
9204
9205
9206
9207
9208
9209
9210
9211
9212
9213
9214
9215
9216
9217
9218
9219
9220
9221
9222
9223
9224
9225
9226
9227
9228
9229
9230
9231
9232
9233
9234
9235
9236
9237
9238
9239
9240
9241
9242
9243
9244
9245
9246
9247
9248
9249
9250
9251
9252
9253
9254
9255
9256
9257
9258
9259
9260
9261
9262
9263
9264
9265
9266
9267
9268
9269
9270
9271
9272
9273
9274
9275
9276
9277
9278
9279
9280
9281
9282
9283
9284
9285
9286
9287
9288
9289
9290
9291
9292
9293
9294
9295
9296
9297
9298
9299
9300
9301
9302
9303
9304
9305
9306
9307
9308
9309
9310
9311
9312
9313
9314
9315
9316
9317
9318
9319
9320
9321
9322
9323
9324
9325
9326
9327
9328
9329
9330
9331
9332
9333
9334
9335
9336
9337
9338
9339
9340
9341
9342
9343
9344
9345
9346
9347
9348
9349
9350
9351
9352
9353
9354
9355
9356
9357
9358
9359
9360
9361
9362
9363
9364
9365
9366
9367
9368
9369
9370
9371
9372
9373
9374
9375
9376
9377
9378
9379
9380
9381
9382
9383
9384
9385
9386
9387
9388
9389
9390
9391
9392
9393
9394
9395
9396
9397
9398
9399
9400
9401
9402
9403
9404
9405
9406
9407
9408
9409
9410
9411
9412
9413
9414
9415
9416
9417
9418
9419
9420
9421
9422
9423
9424
9425
9426
9427
9428
9429
9430
9431
9432
9433
9434
9435
9436
9437
9438
9439
9440
9441
9442
9443
9444
9445
9446
9447
9448
9449
9450
9451
9452
9453
9454
9455
9456
9457
9458
9459
9460
9461
9462
9463
9464
9465
9466
9467
9468
9469
9470
9471
9472
9473
9474
9475
9476
9477
9478
9479
9480
9481
9482
9483
9484
9485
9486
9487
9488
9489
9490
9491
9492
9493
9494
9495
9496
9497
9498
9499
9500
9501
9502
9503
9504
9505
9506
9507
9508
9509
9510
9511
9512
9513
9514
9515
9516
9517
9518
9519
9520
9521
9522
9523
9524
9525
9526
9527
9528
9529
9530
9531
9532
9533
9534
9535
9536
9537
9538
9539
9540
9541
9542
9543
9544
9545
9546
9547
9548
9549
9550
9551
9552
9553
9554
9555
9556
9557
9558
9559
9560
9561
9562
9563
9564
9565
9566
9567
9568
9569
9570
9571
9572
9573
9574
9575
9576
9577
9578
9579
9580
9581
9582
9583
9584
9585
9586
9587
9588
9589
9590
9591
9592
9593
9594
9595
9596
9597
9598
9599
9600
9601
9602
9603
9604
9605
9606
9607
9608
9609
9610
9611
9612
9613
9614
9615
9616
9617
9618
9619
9620
9621
9622
9623
9624
9625
9626
9627
9628
9629
9630
9631
9632
9633
9634
9635
9636
9637
9638
9639
9640
9641
9642
9643
9644
9645
9646
9647
9648
9649
9650
9651
9652
9653
9654
9655
9656
9657
9658
9659
9660
9661
9662
9663
9664
9665
9666
9667
9668
9669
9670
9671
9672
9673
9674
9675
9676
9677
9678
9679
9680
9681
9682
9683
9684
9685
9686
9687
9688
9689
9690
9691
9692
9693
9694
9695
9696
9697
9698
9699
9700
9701
9702
9703
9704
9705
9706
9707
9708
9709
9710
9711
9712
9713
9714
9715
9716
9717
9718
9719
9720
9721
9722
9723
9724
9725
9726
9727
9728
9729
9730
9731
9732
9733
9734
9735
9736
9737
9738
9739
9740
9741
9742
9743
9744
9745
9746
9747
9748
9749
9750
9751
9752
9753
9754
9755
9756
9757
9758
9759
9760
9761
9762
9763
9764
9765
9766
9767
9768
9769
9770
9771
9772
9773
9774
9775
9776
9777
9778
9779
9780
9781
9782
9783
9784
9785
9786
9787
9788
9789
9790
9791
9792
9793
9794
9795
9796
9797
9798
9799
9800
9801
9802
9803
9804
9805
9806
9807
9808
9809
9810
9811
9812
9813
9814
9815
9816
9817
9818
9819
9820
9821
9822
9823
9824
9825
9826
9827
9828
9829
9830
9831
9832
9833
9834
9835
9836
9837
9838
9839
9840
9841
9842
9843
9844
9845
9846
9847
9848
9849
9850
9851
9852
9853
9854
9855
9856
9857
9858
9859
9860
9861
9862
9863
9864
9865
9866
9867
9868
9869
9870
9871
9872
9873
9874
9875
9876
9877
9878
9879
9880
9881
9882
9883
9884
9885
9886
9887
9888
9889
9890
9891
9892
9893
9894
9895
9896
9897
9898
9899
9900
9901
9902
9903
9904
9905
9906
9907
9908
9909
9910
9911
9912
9913
9914
9915
9916
9917
9918
9919
9920
9921
9922
9923
9924
9925
9926
9927
9928
9929
9930
9931
9932
9933
9934
9935
9936
9937
9938
9939
9940
9941
9942
9943
9944
9945
9946
9947
9948
9949
9950
9951
9952
9953
9954
9955
9956
9957
9958
9959
9960
9961
9962
9963
9964
9965
9966
9967
9968
9969
9970
9971
9972
9973
9974
9975
9976
9977
9978
9979
9980
9981
9982
9983
9984
9985
9986
9987
9988
9989
9990
9991
9992
9993
9994
9995
9996
9997
9998
9999

```

0002 METER

```

01 00112 125203
02 00113 000772
03 00114 102440
04 00115 042743
05 00116 102520
06 00117 024736
07 00118 000017
08 00119 021101
09 00120 000110
10 00121 020724
11 00122 024724
12 00123 000103
13 00124 000102
14 00125 020512
15 00126 101005
16 00127 000405
17 00128 020721
18 00129 024721
19 00130 000125
20 00131 000126
21 00132 024570
22 00133 044556
23 00134 052705
24 00135 050547
25
26 00136 024555 LOOP0
27 00137 044554
28 00138 044552
29 00139 026701
30 00140
```



```

0031 LUTIL
-TITLE UTILITY
-ENT COMAP, BIT ECRIT
-ENT MFCOR TIME CNTS CHG*
-ENT REC AVER
-ENT CMOR, IXMT, UIEX, UCER
-NPXL
ROUTINE TO ACT UPON A CHANGE OF THE CONTACT SENSE
TO - START(1) OR STOP(2) THE PROGRAM
AND -2 DETERMINING THE AVERAGING TIME
14 00308+040000 RYTL1 181
15 00021+000024 25 ;CONTACT SENSE DEVICE CODE
16 00022+000012 JMC 0 ;MFCOR OF CONTACT SENSE OCT
17 00023+000024 ;MFCOR OF SAVE STATE AREA
18 00024+000024 ;DEVICE MASK-TTO(1), RYC, PFM, LPT
19 00025+000024 ;ADDRESS OF INTERRUPT MANAGER
20 00026+000024 ;CONTACT SENSE IOEF FLAG
21 00027+000024 ;GET THE IOEF FLAG
22 00028+000024 ;IS IT SET
23 00029+000024 ;GET CONTACT SENSE DEVICE CODE
24 00030+000024 ;GET DEVICE OCT ADDRESS
25 00031+000024 ;DECLARE CONTACT SENSE TO ROOS/RTOS
26 00032+000024 ;SET THE IOEF FLAG
27 00033+000024 ;START DEVICE
28 00034+000024 ;GET ADDRESS OF RECEIVING WORD
29 00035+000024 ;LOAD THE BIT MASK
30 00036+000024 ;CHECK IF IT IS CLOSED OR OPENED
31 00037+000024 ;IS IT 0 OR 2
32 00038+000024 ;INC. IT IS 1
33 00039+000024
34 00040+000024
35 00041+000024
36 00042+000024
37 00043+000024
38 00044+000024
39 00045+000024
40 00046+000024
41 00047+000024
42 00048+000024
43 00049+000024
44 00050+000024
45 00051+000024
46 00052+000024
47 00053+000024
48 00054+000024
49 00055+000024
50 00056+000024
51 00057+000024
52 00058+000024
53 00059+000024
54 00060+000024
55 00061+000024
56 00062+000024
57 00063+000024
58 00064+000024
59 00065+000024
60 00066+000024
61 00067+000024
62 00068+000024
63 00069+000024
64 00070+000024
65 00071+000024
66 00072+000024
67 00073+000024
68 00074+000024
69 00075+000024
70 00076+000024
71 00077+000024
72 00078+000024
73 00079+000024
74 00080+000024
75 00081+000024
76 00082+000024
77 00083+000024
78 00084+000024
79 00085+000024
80 00086+000024
81 00087+000024
82 00088+000024
83 00089+000024
84 00090+000024
85 00091+000024
86 00092+000024
87 00093+000024
88 00094+000024
89 00095+000024
90 00096+000024
91 00097+000024
92 00098+000024
93 00099+000024
94 00100+000024
95 00101+000024
96 00102+000024
97 00103+000024
98 00104+000024
99 00105+000024
100 00106+000024
101 00107+000024
102 00108+000024
103 00109+000024
104 00110+000024
105 00111+000024
106 00112+000024
107 00113+000024
108 00114+000024
109 00115+000024
110 00116+000024
111 00117+000024
112 00118+000024
113 00119+000024
114 00120+000024
115 00121+000024
116 00122+000024
117 00123+000024
118 00124+000024
119 00125+000024
120 00126+000024
121 00127+000024
122 00128+000024
123 00129+000024
124 00130+000024
125 00131+000024
126 00132+000024
127 00133+000024
128 00134+000024
129 00135+000024
130 00136+000024
131 00137+000024
132 00138+000024
133 00139+000024
134 00140+000024
135 00141+000024
136 00142+000024
137 00143+000024
138 00144+000024
139 00145+000024
140 00146+000024
141 00147+000024
142 00148+000024
143 00149+000024
144 00150+000024
145 00151+000024
146 00152+000024
147 00153+000024
148 00154+000024
149 00155+000024
150 00156+000024
151 00157+000024
152 00158+000024
153 00159+000024
154 00160+000024
155 00161+000024
156 00162+000024
157 00163+000024
158 00164+000024
159 00165+000024
160 00166+000024
161 00167+000024
162 00168+000024
163 00169+000024
164 00170+000024
165 00171+000024
166 00172+000024
167 00173+000024
168 00174+000024
169 00175+000024
170 00176+000024
171 00177+000024
172 00178+000024
173 00179+000024
174 00180+000024
175 00181+000024
176 00182+000024
177 00183+000024
178 00184+000024
179 00185+000024
180 00186+000024
181 00187+000024
182 00188+000024
183 00189+000024
184 00190+000024
185 00191+000024
186 00192+000024
187 00193+000024
188 00194+000024
189 00195+000024
190 00196+000024
191 00197+000024
192 00198+000024
193 00199+000024
194 00200+000024
195 00201+000024
196 00202+000024
197 00203+000024
198 00204+000024
199 00205+000024
200 00206+000024
201 00207+000024
202 00208+000024
203 00209+000024
204 00210+000024
205 00211+000024
206 00212+000024
207 00213+000024
208 00214+000024
209 00215+000024
210 00216+000024
211 00217+000024
212 00218+000024
213 00219+000024
214 00220+000024
215 00221+000024
216 00222+000024
217 00223+000024
218 00224+000024
219 00225+000024
220 00226+000024
221 00227+000024
222 00228+000024
223 00229+000024
224 00230+000024
225 00231+000024
226 00232+000024
227 00233+000024
228 00234+000024
229 00235+000024
230 00236+000024
231 00237+000024
232 00238+000024
233 00239+000024
234 00240+000024
235 00241+000024
236 00242+000024
237 00243+000024
238 00244+000024
239 00245+000024
240 00246+000024
241 00247+000024
242 00248+000024
243 00249+000024
244 00250+000024
245 00251+000024
246 00252+000024
247 00253+000024
248 00254+000024
249 00255+000024
250 00256+000024
251 00257+000024
252 00258+000024
253 00259+000024
254 00260+000024
255 00261+000024
256 00262+000024
257 00263+000024
258 00264+000024
259 00265+000024
260 00266+000024
261 00267+000024
262 00268+000024
263 00269+000024
264 00270+000024
265 00271+000024
266 00272+000024
267 00273+000024
268 00274+000024
269 00275+000024
270 00276+000024
271 00277+000024
272 00278+000024
273 00279+000024
274 00280+000024
275 00281+000024
276 00282+000024
277 00283+000024
278 00284+000024
279 00285+000024
280 00286+000024
281 00287+000024
282 00288+000024
283 00289+000024
284 00290+000024
285 00291+000024
286 00292+000024
287 00293+000024
288 00294+000024
289 00295+000024
290 00296+000024
291 00297+000024
292 00298+000024
293 00299+000024
294 00300+000024
295 00301+000024
296 00302+000024
297 00303+000024
298 00304+000024
299 00305+000024
300 00306+000024
301 00307+000024
302 00308+000024
303 00309+000024
304 00310+000024
305 00311+000024
306 00312+000024
307 00313+000024
308 00314+000024
309 00315+000024
310 00316+000024
311 00317+000024
312 00318+000024
313 00319+000024
314 00320+000024
315 00321+000024
316 00322+000024
317 00323+000024
318 00324+000024
319 00325+000024
320 00326+000024
321 00327+000024
322 00328+000024
323 00329+000024
324 00330+000024
325 00331+000024
326 00332+000024
327 00333+000024
328 00334+000024
329 00335+000024
330 00336+000024
331 00337+000024
332 00338+000024
333 00339+000024
334 00340+000024
335 00341+000024
336 00342+000024
337 00343+000024
338 00344+000024
339 00345+000024
340 00346+000024
341 00347+000024
342 00348+000024
343 00349+000024
344 00350+000024
345 00351+000024
346 00352+000024
347 00353+000024
348 00354+000024
349 00355+000024
350 00356+000024
351 00357+000024
352 00358+000024
353 00359+000024
354 00360+000024
355 00361+000024
356 00362+000024
357 00363+000024
358 00364+000024
359 00365+000024
360 00366+000024
361 00367+000024
362 00368+000024
363 00369+000024
364 00370+000024
365 00371+000024
366 00372+000024
367 00373+000024
368 00374+000024
369 00375+000024
370 00376+000024
371 00377+000024
372 00378+000024
373 00379+000024
374 00380+000024
375 00381+000024
376 00382+000024
377 00383+000024
378 00384+000024
379 00385+000024
380 00386+000024
381 00387+000024
382 00388+000024
383 00389+000024
384 00390+000024
385 00391+000024
386 00392+000024
387 00393+000024
388 00394+000024
389 00395+000024
390 00396+000024
391 00397+000024
392 00398+000024
393 00399+000024
394 00400+000024
395 00401+000024
396 00402+000024
397 00403+000024
398 00404+000024
399 00405+000024
400 00406+000024
401 00407+000024
402 00408+000024
403 00409+000024
404 00410+000024
405 00411+000024
406 00412+000024
407 00413+000024
408 00414+000024
409 00415+000024
410 00416+000024
411 00417+000024
412 00418+000024
413 00419+000024
414 00420+000024
415 00421+000024
416 00422+000024
417 00423+000024
418 00424+000024
419 00425+000024
420 00426+000024
421 00427+000024
422 00428+000024
423 00429+000024
424 00430+000024
425 00431+000024
426 00432+000024
427 00433+000024
428 00434+000024
429 00435+000024
430 00436+000024
431 00437+000024
432 00438+000024
433 00439+000024
434 00440+000024
435 00441+000024
436 00442+000024
437 00443+000024
438 00444+000024
439 00445+000024
440 00446+000024
441 00447+000024
442 00448+000024
443 00449+000024
444 00450+000024
445 00451+000024
446 00452+000024
447 00453+000024
448 00454+000024
449 00455+000024
450 00456+000024
451 00457+000024
452 00458+000024
453 00459+000024
454 00460+000024
455 00461+000024
456 00462+000024
457 00463+000024
458 00464+000024
459 00465+000024
460 00466+000024
461 00467+000024
462 00468+000024
463 00469+000024
464 00470+000024
465 00471+000024
466 00472+000024
467 00473+000024
468 00474+000024
469 00475+000024
470 00476+000024
471 00477+000024
472 00478+000024
473 00479+000024
474 00480+000024
475 00481+000024
476 00482+000024
477 00483+000024
478 00484+000024
479 00485+000024
480 00486+000024
481 00487+000024
482 00488+000024
483 00489+000024
484 00490+000024
485 00491+000024
486 00492+000024
487 00493+000024
488 00494+000024
489 00495+000024
490 00496+000024
491 00497+000024
492 00498+000024
493 00499+000024
494 00500+000024
495 00501+000024
496 00502+000024
497 00503+000024
498 00504+000024
499 00505+000024
500 00506+000024
501 00507+000024
502 00508+000024
503 00509+000024
504 00510+000024
505 00511+000024
506 00512+000024
507 00513+000024
508 00514+000024
509 00515+000024
510 00516+000024
511 00517+000024
512 00518+000024
513 00519+000024
514 00520+000024
515 00521+000024
516 00522+000024
517 00523+000024
518 00524+000024
519 00525+000024
520 00526+000024
521 00527+000024
522 00528+000024
523 00529+000024
524 00530+000024
525 00531+000024
526 00532+000024
527 00533+000024
528 00534+000024
529 00535+000024
530 00536+000024
531 00537+000024
532 00538+000024
533 00539+000024
534 00540+000024
535 00541+000024
536 00542+000024
537 00543+000024
538 00544+000024
539 00545+000024
540 00546+000024
541 00547+000024
542 00548+000024
543 00549+000024
544 00550+000024
545 00551+000024
546 00552+000024
547 00553+000024
548 00554+000024
549 00555+000024
550 00556+000024
551 00557+000024
552 00558+000024
553 00559+000024
554 00560+000024
555 00561+000024
556 00562+000024
557 00563+000024
558 00564+000024
559 00565+000024
560 00566+000024
561 00567+000024
562 00568+000024
563 00569+000024
564 00570+000024
565 00571+000024
566 00572+000024
567 00573+000024
568 00574+000024
569 00575+000024
570 00576+000024
571 00577+000024
572 00578+000024
573 00579+000024
574 00580+000024
575 00581+000024
576 00582+000024
577 00583+000024
578 00584+000024
579 00585+000024
580 00586+000024
581 00587+000024
582 00588+000024
583 00589+000024
584 00590+000024
585 00591+000024
586 00592+000024
587 00593+000024
588 00594+000024
589 00595+000024
590 00596+000024
591 00597+000024
592 00598+000024
593 00599+000024
594 00600+000024
595 00601+000024
596 00602+000024
597 00603+000024
598 00604+000024
599 00605+000024
600 00606+000024
601 00607+000024
602 00608+000024
603 00609+000024
604 00610+000024
605 00611+000024
606 00612+000024
607 00613+000024
608 00614+000024
609 00615+000024
610 00616+000024
611 00617+000024
612 00618+000024
613 00619+000024
614 00620+000024
615 00621+000024
616 00622+000024
617 00623+000024
618 00624+000024
619 00625+000024
620 00626+000024
621 00627+000024
622 00628+000024
623 00629+000024
624 00630+000024
625 00631+000024
626 00632+000024
627 00633+000024
628 00634+000024
629 00635+000024
630 00636+000024
631 00637+000024
632 00638+000024
633 00639+000024
634 00640+000024
635 00641+000024
636 00642+000024
637 00643+000024
638 00644+000024
639 00645+000024
640 00646+000024
641 00647+000024
642 00648+000024
643 00649+000024
644 00650+000024
645 00651+000024
646 00652+000024
647 00653+000024
648 00654+000024
649 00655+000024
650 00656+000024
651 00657+000024
652 00658+000024
653 00659+000024
654 00660+000024
655 00661+000024
656 00662+000024
657 00663+000024
658 00664+000024
659 00665+000024
660 00666+000024
661 00667+000024
662 00668+000024
663 00669+000024
664 00670+000024
665 00671+000024
666 00672+000024
667 00673+000024
668 00674+000024
669 00675+000024
670 00676+000024
671 00677+000024
672 00678+000024
673 00679+000024
674 00680+000024
675 00681+000024
676 00682+000024
677 00683+000024
678 00684+000024
679 00685+000024
680 00686+000024
681 00687+000024
682 00688+000024
683 00689+000024
684 00690+000024
685 00691+000024
686 00692+000024
687 00693+000024
688 00694+000024
689 00695+000024
690 00696+000024
691 00697+000024
692 00698+000024
693 00699+000024
694 00700+000024
695 00701+000024
696 00702+000024
697 00703+000024
698 00704+000024
699 00705+000024
700 00706+000024
701 00707+000024
702 00708+000024
703 00709+000024
704 00710+000024
705 00711+000024
706 00712+000024
707 00713+000024
708 00714+000024
709 00715+000024
710 00716+000024
711 00717+000024
712 00718+000024
713 00719+000024
714 00720+000024
715 00721+000024
716 00722+000024
717 00723+000024
718 00724+000024
719 00725+000024
720 00726+000024
721 00727+000024
722 00728+000024
723 00729+000024
724 00730+000024
725 00731+000024
726 00732+000024
727 00733+000024
728 00734+00
```


APPENDIX Z - MAIN FORTRAN PROGRAMS USED IN THIS STUDY

```

PROGRAM MAIN (INPUT,OUTPUT,PUNCH,TAPES=INPUT,TAPE6=OUTPUT,TAPE7=PU
INCH,TAPE18)
DIMENSION TEMP(588,5),QFLOW(588,5),TIME(588,5),NT(5)
DIMENSION NHET(5),DTOP(5),T(18),TIC(18),XL(5),OT(18),MT(5)
DIMENSION XLHOR(5),XUMOR(5),THIC(5),AQ(5)
DIMENSION X(500),Y(588)
.....
THIS PROGRAM READS IN THE INFORMATION OUTPUT ON THE
MINI-COMPUTER AND CALCULATES THE HEAT FLUX DENSITY
CURVE AND PLOTS IT IF REQUIRED
.....
      NOT = NUMBER OF RUNS
      NPLUX = NUMBER OF HEAT FLUX METERS
      DTOFF = OFFSET OF THE TEMPERATURE DIFFERENCE ON THE DISC
      TOFF = OFFSET OF THE COGE TEMPERATURE
.....
      A=0.00F03
      VPPC2F=
      FLAG=1
.....
      READ(5,6) NOT,IPLOT
      6,FORMAT(2I5)
.....
      DO 38 ILL=1,NOT
      READ(5,*) NALOG,NRUN,NPLUX,TIIG
      READ(5,*) NHET(I),DTOP(I),T(1),TIC(I),XL(I),OT(I),MT(I),
      1 NPLUX),X(I),Y(I),XUMOR(I),THIC(I),AQ(I)
.....
      DO 48 I=1,NPLUX
      48 READ(5,11) XHOR(I),XUMOR(I),THIC(I),AQ(I)
      11,FORMAT(2F10,2F10,3)
.....
      READ THE CONTACT SENSE HISTORY TABLE
.....
      I=1
      45 READ(5,*) TIME(I)
      IF (TIME(I) .EQ. 500.) GO TO 46
      READ(5,*) DT(I)
      I=I+1
      GO TO 45
      46 CONTINUE
.....
      READ THE PAM DATA
.....
      CALL READIN (NPLUX,TIME,QFLOW,TEMP,NHET,DTOP,TOFF,NT,XL,OT,TIME)
.....
      DO 38 N=1,NPLUX
      IF (NHET(N) .EQ. 0) GO TO 38
      WRITE(5,1) NALOG,NRUN,NHET(N),XUMOR(N)
      IAX=8
      OMAX=8
      NH=NT(N)
.....
      DO 29 I=1,NH
      IT=TEMP(I,N)
      TT=35.05968+IT/100.*41.96882-0.40647*(IT/100)**2
      T=(TT-32.)/1.8
      TEMP(I,N)=TEMP(I,N)-QFLOW(I,N)/20.
      TEMP(I,N)=38.05968+TEMP(I,N)/100.*41.96882-0.40647*(TEMP(I,N)/100.
      1 **2)
      CFAC=0.928+TEMP(I,N)
      QFLOW(I,N)=0.5K6*THIC(N)*QFLOW(I,N)/(90(N)**2*1088.*CFAC)
      QLT=TEMP(I,N)-TL(I)
      IF (QLT .LT. 0) QLT=0
      TEMP(I,N)=TEMP(I,N)+QLT/100.
      QMET=3.5374*QFLOW(I,N)/1000.
      TEMET=(TEMP(I,N)-32.)/5.79.
      Y(I)=ALOG10(QFLOW(I,N))
      Y(I)=ALOG10(QMET)
      PUNCH(7) TIME(I,N),TEMET,QMET,TT
      7,FORMAT(LE19,8)
.....
      WRITE(5,3) TIME(I,N),TEMP(I,N),QFLOW(I,N),TEMET,QMET
      3,FORMAT(19X,6(EL19,4,1X))
.....
      IF (QFLOW(I,N) .LT. OMAX) GO TO 29
      IAX=QFLOW(I,N)
      OMAX=QFLOW(I,N)
      29 CONTINUE
      OMAX=MAX(3,1337/1088.
      IAX=ITEMP(IMAX,N)-32.)/1.8
.....
      WRITE(5,2) TIME(IAX,N),OMAX,IAX
      2,FORMAT(19X,6(EL19,4,1X),2(19X,4,1X),2(19X,4,1X))
.....
      CALCULATE THE CALIBRATION RATIO
.....
      QLOS=0
      NH=NT-1
      DO 15 I=1,NH
      QLOS=QLOS+QFLOW(I,N)*QFLOW(I+1,N)/(TIME(I+1,N)-TIME(I,N))/(2.*
      1 3688.)
      15 CONTINUE
      HEAT=QLOS*0.001*3.1416*(5./24.1)**2*(3./32.)*(TEMP(1,N)-TEMP(NT,N))
      1 NH)
      RATIO=HEAT/QLOS
.....
      WRITE(6,4) HEAT,QLOS,RATIO
      4,FORMAT(19X,6(EL19,4,1X),2(19X,4,1X),2(19X,4,1X))
      IF (IPLOT .NE. 0) GO TO 38
.....
      CALL PLOT(X,Y,XUMOR(N),XLHOR(N),FLAG,MT(N))
      38 CONTINUE
      1,FORMAT(19X,6(EL19,4,1X),2(19X,4,1X),2(19X,4,1X),2(19X,4,1X))
      I=1
      3,12X,HEAT FLUX,7)
      CALL PLOT(8,0.,999)
      STOP
      ENO
.....
      SUSPOUTINE READIN(NPLUX,TIME,QFLOW,TEMP,NHET,DTOP,TOFF,NT,XL,OT,
      1 TIME)
      DIMENSION TEMP(588,5),QFLOW(588,5),TIME(588,5),NT(5)
      DIMENSION NHET(5),DTOP(5),T(18),TIC(18),XL(5),OT(18),MT(5)
      DIMENSION X(500),Y(588)
      GO TO (2,3,3,3) NPLUX
.....
      FOR 1 HEAT FLUX METER
      1 CONTINUE
.....
      N=3 OR 4 WHICH IS THE WIDTH OF THE DATA ON THE CARD
      NH=N-1
      NHM=N-1
      IF (TIME(188) .EQ. 99999.) GO TO 11
      NHM=NH
      GO TO 1
      11 NH=1
      NHM=1
      DO 21 I=1,L,N

```

```

35 I=1
IF (TIME(I) .LT. TI ) GO TO 36
GO TO 35
36 DELT=OT(I)-1
TIME(I)=TIME(I)+DELT
IF (TIME(I) .EQ. 99999.) GO TO DELT
IF (TIME(I) .EQ. 99999.) GO TO DELT
TIME(I)=TIME(I)+DELT
21 CONTINUE
IF (NH .EQ. 1) GO TO 22
TIME(N)=TIME(N)-DELT
23 CONTINUE
TIME(N)=TIME(N)+DELT
TIME(N)=TIME(N)+DELT
GO TO 50
.....
FOR 2 HEAT FLUX METERS
2 NHM=1
READ(5,108) TIME(N), (QFLOW(J,I),TEMP(J,I) ,J=1,2),J,M,NH)
IF (TIME(N) .EQ. 99999.) GO TO 12
NHM=2
GO TO 2
12 NHM=1
L=M-1
DO 22 I=1,L,2
I=TIME(I)+100.
IF (TIME(I) .LT. TI ) GO TO 46
GO TO 45
46 DELT=OT(I)-1
22 TIME(I)=TIME(I)+DELT
TIME(N)=TIME(N)+DELT
GO TO 50
.....
FOR 3 OR 4 HEAT FLUX METERS
3 READ(5,108) TIME(N), (QFLOW(M,J),TEMP(M,J) ,J=1,NPLUX)
IF (TIME(N) .EQ. 99999.) GO TO 13
NHM=1
GO TO 3
13 NHM=1
GO TO 50
.....
FOR 5 HEAT FLUX METERS
5 CONTINUE
.....
N=1 OR 2 FOR THE NUMBER OF CARDS FOR 5 DATA
N=1
IF (NH .EQ. 1) GO TO 70
71 CONTINUE
READ(5,188) TIME(N), (QFLOW(N,J),TEMP(N,J)),J=1,3)
IF (TIME(N) .EQ. 99999.) GO TO 15
READ(5,181) (QFLOW(N,J),TEMP(N,J)),J=4,5)
NHM=1
GO TO 71
70 CONTINUE
READ(5,188) TIME(N), (QFLOW(N,J),TEMP(N,J)),J=1,5)
IF (TIME(N) .EQ. 99999.) GO TO 15
NHM=1
GO TO 70
15 NHM=1
.....
THIS PART OF THE PROGRAM CORRECTS FOR OFFSET ON THE TEMPERATURE
AND TEMPERATURE DIFFERENCE ON A HEAT FLUX METER DUE TO IMPROPER
CALIBRATION. IT ALSO CORRECTS FOR REVERSED PLUGS (ICIT MTL CHAN.)
THE SIGN AND CORRECT THE DATA). IT NEGLECTS A BAD RUN AMONGST
GOOD ONES.
NHET(I) = RUN IS CORRECTED FOR OFFSET
NHET(I) = DATA IS IMPERCTED AND CORRECTED
NHET(I) = 0 RUN IS NEGLECTED
.....
58 DO 68 J=1,NPLUX
IF (NHET(J) .GT. 0) GO TO 68
IF (NHET(J) .GT. 0) GO TO 61
DO 62 I=1,M
62 QFLOW(I,J)=-QFLOW(I,J)
61 CONTINUE
DO 63 I=1,M
IF (TEMP(I,J) .GT. 1499. .OR. TEMP(I,J) .LT. 438.) TEMP(I,J)=700.
63 QFLOW(I,J)=QFLOW(I,J)-DTOP(I,J)
.....
4 KK=1
IF (QFLOW(K,J) .LT. 1.) GO TO 4
I=TEMP(I,J)
TIME(I,J)=TIME(K)
TEMP(I,J)=I
QFLOW(I,J)=QFLOW(K,J)
KK=1
DO 44 I=K,M
IF (ABS(I-TEMP(I,J)) .LT. 15. .AND. ABS(Q1-QFLOW(I,J)) .LT. XL
1 (J)) GO TO 64
IF (QFLOW(I,J) .LT. 1.) GO TO 64
KK=I
TEMP(K,J)=TEMP(I,J)
QFLOW(K,J)=QFLOW(I,J)
TIME(K,J)=TIME(I)
I=TEMP(I,J)
Q1=QFLOW(I,J)
64 CONTINUE
NT(J)=KK
.....
IF THE LAST POINT HAS NOT TAKEN, TAKE IT
IF (TIME(KK,J) .EQ. TIME(N)) GO TO 60
IF (QFLOW(KK,J) .LT. 1.) GO TO 60
KK=KK+1
TIME(KK,J)=TIME(N)
TEMP(KK,J)=TEMP(N)
QFLOW(KK,J)=QFLOW(N)
NT(J)=KK
60 CONTINUE
188 FORMAT(19X,2(19X,4,1X))
181 FORMAT(7X,6(19X,4,1X))
RETURN
ENO

```



```

1000  RUNCHEAT(20), TAVG, QAVG, QNET, QAVT
1001  FORMAT(1X, 1P, 2P, 3P, 4P, 5P, 6P, 7P, 8P, 9P, 10P, 11P, 12P, 13P, 14P)
1002  FORMAT(1X, 1P, 2P, 3P, 4P, 5P, 6P, 7P, 8P, 9P, 10P, 11P, 12P, 13P, 14P)
1003  FORMAT(1X, 1P, 2P, 3P, 4P, 5P, 6P, 7P, 8P, 9P, 10P, 11P, 12P, 13P, 14P)
1004  FORMAT(1X, 1P, 2P, 3P, 4P, 5P, 6P, 7P, 8P, 9P, 10P, 11P, 12P, 13P, 14P)
1005  FORMAT(1X, 1P, 2P, 3P, 4P, 5P, 6P, 7P, 8P, 9P, 10P, 11P, 12P, 13P, 14P)
1006  FORMAT(1X, 1P, 2P, 3P, 4P, 5P, 6P, 7P, 8P, 9P, 10P, 11P, 12P, 13P, 14P)
1007  FORMAT(1X, 1P, 2P, 3P, 4P, 5P, 6P, 7P, 8P, 9P, 10P, 11P, 12P, 13P, 14P)
1008  FORMAT(1X, 1P, 2P, 3P, 4P, 5P, 6P, 7P, 8P, 9P, 10P, 11P, 12P, 13P, 14P)
1009  FORMAT(1X, 1P, 2P, 3P, 4P, 5P, 6P, 7P, 8P, 9P, 10P, 11P, 12P, 13P, 14P)
1010  FORMAT(1X, 1P, 2P, 3P, 4P, 5P, 6P, 7P, 8P, 9P, 10P, 11P, 12P, 13P, 14P)

```

```

C
100 CONTINUE
END

```

```

SUBROUTINE HEATF (T, Q)
C MACH /HEAT/ IX, BX, AV, BY, CY, AZ, BZ, TXY, TVZ
C L=0.5
A=ALCG10(T)
IF (T < .01) GO TO 10
IF (T < .01) GO TO 20
Q=1.0*(AV*9T+BY*CY+AZ*BZ)*CAL
RETURN
10 Q=1.0*(AV*9T+BY*CY+AZ*BZ)*CAL
RETURN
20 Q=1.0*(AV*9T+BY*CY+AZ*BZ)*CAL
RETURN
END

```

```

SUBROUTINE PLACE(M,N,I,A,JCOL,IRW,MEM,QLOSS,IPAD)
DIMENSION A(1),JCOL(1),IRW(1)
COMMON DR,RR,RZ
DOUBLE PRECISION A
GO TO (1,2,3,4,5,6,7),M

```

AT THE BOILING SURFACE WHERE THE HEAT FLUX IS KNOWN IN THE Z DIRECTION

```

1 A(MEM)=0.5*R-0.25/(DR*DR*FLOAT(IRA0-1))
JCOL(MEM)=1-1
IRW(MEM)=1
MEM=MEM+1
A(MEM)=AZ
JCOL(MEM)=1
IRW(MEM)=1
MEM=MEM+1
A(MEM)=0.5*R+0.25/(DR*DR*FLOAT(IRA0-1))
JCOL(MEM)=1+1
IRW(MEM)=1
MEM=MEM+1
A(MEM)=1
JCOL(MEM)=1+M
IRW(MEM)=1
MEM=MEM+1
A(MEM)=QLOSS*(T, Q) RETURN
JCOL(MEM)=0
IRW(MEM)=1
MEM=MEM+1
RETURN

```

SYMMETRY LINE ON THE SURFACE

```

2 A(MEM)=-(0.5*R+0.25*Z)
JCOL(MEM)=1
IRW(MEM)=1
MEM=MEM+1
A(MEM)=0.5*R
JCOL(MEM)=1+1
IRW(MEM)=1
MEM=MEM+1
A(MEM)=0.25*Z
JCOL(MEM)=1+M
IRW(MEM)=1
MEM=MEM+1
IF (QLOSS < 0.) (. ) RETURN
A(MEM)=QLOSS
JCOL(MEM)=0
IRW(MEM)=1
MEM=MEM+1
RETURN

```

AN INTERIOR POINT ON THE LINE OF SYMMETRY

```

3 A(MEM)=Z
JCOL(MEM)=1+M
IRW(MEM)=1
MEM=MEM+1
A(MEM)=-(1.0*P+2.*Z)
JCOL(MEM)=1
IRW(MEM)=1
MEM=MEM+1
A(MEM)=L.*R
JCOL(MEM)=1+1
IRW(MEM)=1
MEM=MEM+1
A(MEM)=Z
JCOL(MEM)=1+M
IRW(MEM)=1
MEM=MEM+1
RETURN

```

AN INTERIOR POINT

```

4 A(MEM)=Z
JCOL(MEM)=1+M
IRW(MEM)=1
MEM=MEM+1
A(MEM)=P-0.5/(DR*DR*FLOAT(IRA0-1))
JCOL(MEM)=1-1
IRW(MEM)=1
MEM=MEM+1
A(MEM)=Z.*RZ
JCOL(MEM)=1
IRW(MEM)=1
MEM=MEM+1
A(MEM)=0.5/(DR*DR*FLCAT(IPAD-1))
JCOL(MEM)=1+1
IRW(MEM)=1
MEM=MEM+1
A(MEM)=Z
JCOL(MEM)=1+M
IRW(MEM)=1
MEM=MEM+1
RETURN

```

POINT IN THE CYLINDER HOLE BELOW THE HEAT FLUX METER

```

5 A(MEM)=0.5*Z
JCOL(MEM)=1+M
IRW(MEM)=1
MEM=MEM+1
A(MEM)=RZ+0.5/(DR*DR*FLOAT(IRA0-1))
JCOL(MEM)=1
IRW(MEM)=1
MEM=MEM+1
A(MEM)=0.5/(DR*DR*FLCAT(IRA0-1))
JCOL(MEM)=1
IRW(MEM)=1
MEM=MEM+1
A(MEM)=0.5*Z
JCOL(MEM)=1+M
IRW(MEM)=1
MEM=MEM+1
RETURN

```

```

RETURN
POINT ON THE SURFACE FARTHEST FROM THE HEAT FLUX METER CENTRE (MEM)
NOT FIXED IN THIS PROGRAM. IT IS ASSUMED THAT PASSED THIS POINT
THE TEMPERATURE ONT SURFACE REMAINS CONSTANT

```

```

6 A(MEM)=0.5*R-0.25*P/FLCAT(IRA0-1)
JCOL(MEM)=1-1
IRW(MEM)=1
MEM=MEM+1
A(MEM)=-(0.5*R-0.25*P/FLCAT(IRA0-1)+Z)
JCOL(MEM)=1
IRW(MEM)=1
MEM=MEM+1
A(MEM)=Z
JCOL(MEM)=1+M
IRW(MEM)=1
MEM=MEM+1
A(MEM)=4.*QLOSS
JCOL(MEM)=1
IRW(MEM)=1
MEM=MEM+1
RETURN

```

POINT ON THE SURFACE WHERE THE TEMPERATURE IS FIXED

```

7 A(MEM)=QLOSS
GROSS=T*P*PI*MEM FROM THE MAIN PROGRAM
IRW(MEM)=1
JCOL(MEM)=0
MEM=MEM+1
A(MEM)=1
IRW(MEM)=JCOL(MEM)+1
MEM=MEM+1
RETURN
END

```

```

SUBROUTINE TRGB (NOP, NW, VAL, ICL, IRM, NVAR, NEO, MEM, XMIN)

```

```

THIS SUBROUTINE SOLVES A SET OF SIMULTANEOUS EQUATIONS
WHEN THE MATRIX IS VERY SPARSE. THE NON-ZERO ELEMENT OF THE
MATRIX ARE SUPPLIED WITH THREE VECTORS -
VAL(I) - THE NON-ZERO VALUE
JCOL(I) - COLUMN NUMBER OF THE ELEMENT
IRW(I) - ROW NUMBER OF THE ELEMENT
WHERE I VARIES FROM 1 TO MEM
NVAR - NO. OF INDEPENDENT VARIABLES
NEO - NO. OF EQUATIONS
MEM - LENGTH OF VECTOR VAL, ICL, IRM
NEM - LENGTH OF VECTOR VAL, ICL AND IRM WHICH ARE DEFINED
XMIN - BELOW THIS LIMIT THE ELEMENT IS SET TO ZERO
NM - WORKING VECTOR
NM(I) TO MNINE(I) - EQUATION STATUS
NOP - OPERATION VECTOR
NOP(1) - MEM
NOP(2) - LENGTH OF NOP VECTOR REQUIRED IF TAGB1 AND TRGB2
ARE TO BE USED
NOP(3) - RESULTS ARE CONTAINED IN VAL (NOP(3)+1) TO VAL (NOP(3)+NW)
MEM - NO. OF EQUATIONS
THE VECTOR OF COEFFICIENTS OF THE RIGHT HAND SIDE EQUATION IS
ENTERED IN VAL(I) WITH ICL(I)=0
DIMENSION NOP(6), VAL(4000), NM(8000), ICL(3000), IRW(2000)
DOUBLE PRECISION VAL

```

EXAMINE THE PROGRAM FROM SYMMETRY LINE TO THE HOLE

```

PROGRAM MAIN (INPUT,OUTPUT,PUNCH,TAPES=INPUT,TAPES=OUTPUT,
1 TAPES=PUNCH)
.....
THIS PROGRAM CALCULATES THE COOLING CURVES FOR LOCATIONS
AROUND THE CYLINDER. THE BOUNDARY CONDITIONS AT THE SURFACE
OF THE CYLINDER ARE: HEAT FLUX DENSITY OBTAINED EXPERIMENTALLY.
IT USES A 3-DIMENSIONAL FINITE DIFFERENCE ANALYSIS BASED ON
THE PRINCIPLE OF SUPERPOSITION. THE VARIABLES ARE DEFINED IN
THE PROGRAM USED TO EVALUATE THE BOILING CURVES.
.....
COMMON NR,NZ,NA,OT,OR,OZ,OA,COMO,XLONG,DIA,TINIT,TIME
COMMON NHO,CA,MCASE,ITER,ITER,IT
COMMON T(10,10,13),PHIR(10,13),PHIZ(10,13),TIM(500),TEMP(500,13)
READ IN THE INFORMATION
READ(5,*) NR,NZ,NA,OT,OR,OZ,OA,COMO,XLONG,DIA,RHO,CP,IMAX,MCASE,ITER,
1 IREQ,ILIN,IPR1
DR=DIA/(2*FLOAT(NR-1))
OZ=XLONG/(2*FLOAT(NZ-1))
OA=3.1416/FLOAT(NA-1)
READ IN THE BOILING CURVES
IF (MCASE.EQ. 1) GO TO 5
CALL HEAT (K)
5 CONTINUE
CALL THE OUTPUT SUBROUTINE
M=1
CALL OUTPT(M)
SET THE INITIAL TEMPERATURE DISTRIBUTION
IF (IREQ.NE. 0) GO TO 25
TIME=0.
DO 100 I=1,NR
DO 100 J=1,NZ
DO 100 K=1,NA
100 T(I,J,K)=TINIT
25 CONTINUE
READ(5,*) TIME
DO 101 I=1,NA
DO 101 K=1,NA
101 READ(5,*) T(I,J,K),J=1,NZ
21 FORMAT(10(IX,F6.2))
26 CONTINUE
START THE SOLUTION
IPRINT=IPR1
I=0
ITE=1
DO 200 ITER=1,IMAX
K=1
CALL HEAT (K)
CALL TIMES
K=1
CALL BALAN (K)
CALL SOLVE
TIME=TIME+OT
IPRINT=IPRINT+1.
IF (IPRINT.NE. 0) GO TO 40
IPRINT=IPR1
M=3
CALL OUTPT(M)
40 CONTINUE
ITE=ITE+1
IF (ITE.NE. 0 .AND. ITER.NE. IMAX) GO TO 80
ITE=ITER
TIME=TIME+OT
DO 20 K=1,NA
20 TEMP(T,K)=T(NR,K)
IF (IT.GE. 500) ITE=IMAX
DO 85 K=1,NA
85 T(TNR,K) .LE. 100.) GO TO 15
60 CALL SECONDDIFNM
X=YLIN-5.
IF (X.LT. TNDM) GO TO 80
80 CONTINUE
M=4
CALL OUTPT(M)
15 CONTINUE
K=0
CALL BALAN (K)
M=2
CALL OUTPT(M)
STOP
END
.....
SUBROUTINE SOLVE
DIMENSION A(120),B(120),C(20),D(20),E(20),V(10,10,13)
DIMENSION U(10,10,13),W(10,10,13)
COMMON NR,NZ,NA,OT,OR,OZ,OA,COMO,XLONG,DIA,TINIT,TIME
COMMON NHO,CA,MCASE,ITER,ITER,IT
COMMON T(10,10,13),PHIR(10,13),PHIZ(10,13),TIM(500),TEMP(500,13)
AR=OT*COMO/(RHO*CP*DR**2)
AZ=OT*COMO/(RHO*CP*OZ**2)
AA=OT*COMO/(RHO*CP*OA**2)
NUMERICAL METHOD BASED ON THE SUPERPOSITION PRINCIPLE USED BY
CHWAZER AND ANANDASUBRAMANIAN, TRANSFER, JAN., 1977.
ADAPTED FOR 3-D SYSTEM (R,Z AND PHI COORDINATES)
.....
FIRST IMPLICITLY IN THE R-DIRECTION FOR EVERY Z AND A SLICES
DO 100 J=1,NZ
M=(NA+1)/2
DO 100 L=1,M
N=(NR-2)+1
DO 101 M=1,MM
IF (M.EQ. 1) GO TO 102
IF (M.EQ. NN) GO TO 103
IF (M.EQ. NN) GO TO 104
FOR AN INTERIOR POINT
IF (M.GT. NR) GO TO 105
IN THE UPPER QUADRANT, WE ARE OPPOSING THE R-DIRECTION (IE INWARD)
I=NR-M+1
K=L
A(I)=-AR*(1.5/(FLOAT(I)-1.))
B(I)=1.2*AR
C(I)=1.2*AR*(1.5/(FLOAT(I)-1.))
D(I)=T(I,J,K)
GO TO 101
IN THE LOWER QUADRANT WE ARE GOING OUTWARD
105 I=M-NR+1
K=M-L+1
A(I)=-AR*(1.5/(FLOAT(I)-1.))
B(I)=1.2*AR
C(I)=-AR*(1.5/(FLOAT(I)-1.))
D(I)=

```

```

102 K=L
A(I)=PHIR(I,J,K)*2*OR/COMO
B(I)=1.2*AR
C(I)=1.2*AR*(1.5/(FLOAT(I)-1.))
D(I)=T(I,J,K)-AR*X*(1.5/(FLOAT(I)-1.))
.....
AT THE SURFACE IN THE LOWER QUADRANT
103 K=NA+1-L
I=NR
A(I)=PHIR(I,J,K)*2*OR/COMO
B(I)=1.2*AR
C(I)=1.2*AR*(1.5/(FLOAT(I)-1.))
D(I)=T(I,J,K)-AR*X*(1.5/(FLOAT(I)-1.))
.....
AT THE MATERIAL CENTRE
104 I=1
K=L
A(I)=-2*AR
B(I)=1.2*AR
C(I)=1.2*AR*(1.5/(FLOAT(I)-1.))
D(I)=T(I,J,K)
101 CONTINUE
CALL SOLUTION ROUTINE
M=1
CALL TRIDAG(N,NA,A,B,C,D,E)
DO 106 K=1,NA
M=M+1
K=L
U(I,J,K)=E(M)
M=M+1
K=L
U(I,J,K)=E(M)
106 CONTINUE
108 CONTINUE
.....
IN THE Z-DIRECTION
DO 200 I=1,NR
DO 108 K=1,NA
DO 201 J=1,NZ
IF (J.EQ. 1) GO TO 202
IF (J.EQ. NZ) GO TO 203
.....
INTERIOR POINT
A(J)=AZ
B(J)=1.2*AZ
C(J)=1.2*AZ*(1.5/(FLOAT(J)-1.))
D(J)=T(I,J,K)
GO TO 101
.....
AT THE LINE OF SYMMETRY (J=1)
202 A(J)=0.
B(J)=1.2*AZ
C(J)=1.2*AZ*(1.5/(FLOAT(J)-1.))
D(J)=T(I,J,K)
GO TO 201
.....
AT THE FACE OF THE CYLINDER (J=NZ)
203 A(J)=2*PHIZ(I,K)*OE/COMO
B(J)=1.2*AZ
C(J)=1.2*AZ*(1.5/(FLOAT(J)-1.))
D(J)=T(I,J,K)-AZ*X
201 CONTINUE
CALL SOLUTION ROUTINE
L=1
CALL TRIDAG(L,NZ,A,B,C,D,E)
DO 204 J=1,NZ
204 V(I,J,K)=E(L)
200 CONTINUE
.....
IN THE PHI-DIRECTION
DO 300 I=1,NR
DO 108 J=1,NA
DO 301 K=1,NA
IF (K.EQ. 1) GO TO 302
IF (K.EQ. NA) GO TO 303
.....
AN INTERIOR POINT
A(K)=-AA*Y
B(K)=1.2*AA*Y
C(K)=-AA*Y
D(K)=T(I,J,K)
GO TO 101
.....
AT THE TOP
302 A(K)=0.
B(K)=1.2*AA*Y
C(K)=1.2*AA*Y*(1.5/(FLOAT(K)-1.))
D(K)=T(I,J,K)
GO TO 301
.....
AT THE BOTTOM
303 A(K)=-2*AA*Y
B(K)=1.2*AA*Y
C(K)=1.2*AA*Y*(1.5/(FLOAT(K)-1.))
D(K)=T(I,J,K)
301 CONTINUE
CALL THE SOLUTION ROUTINE
M=1
CALL TRIDAG(M,NA,A,B,C,D,E)
DO 306 K=1,NA
M=M+1
K=L
U(I,J,K)=E(M)
306 CONTINUE
308 CONTINUE
.....
DO 400 I=1,NR
DO 400 J=1,NA
DO 400 K=1,NA
T(I,J,K)=U(I,J,K)+V(I,J,K)-2*T(I,J,K)
400 CONTINUE
FOR THE CENTRE POINTS
I=1
DO 402 J=1,NZ
U=0.
DO 403 K=1,NA
UU=UU+U(I,J,K)
U=UU/FLOAT(NA)
T(I,J,K)=U
DO 400 K=1,NA
401 T(I,J,K)=UU+V(I,J,K)-TT
402 CONTINUE
RETURN
END

```



```

SUBROUTINE OUTPT(M)
COMMON NR, NA, NAZ, DR, OZ, OA, CONO, XLONG, DIA, TINIT, TIME
COMMON RHO, CP, NCASE, IREDA, IREDAE, IREDAE, IREDAE
COMMON T(10,10,13), PHIR(10,13), PHIZ(10,13), TIM(500), TEMP(500,13)
DIMENSION N(1,1,1), M(1,1,1)
GO TO (1,2,3,4),M
1 CONTINUE
WRITE(1,18) XLONG, DIA, DR, NR, OZ, NA, NAZ, OA, CONO, RHO, CP
18 FORMAT(1,18) X, THE PROBLEM IS SOLVED FOR THE FOLLOWING CASE **//,
1 101 = LENGTH **F6.2// CM **//
2 102 = DIAMETER **F6.2// CM **//
3 103 = DR **F6.2// CM (USING **F6.2// STEPS) **//
4 104 = T(101) **F6.2// DEG. C **//
5 105 = T(102) **F6.2// DEG. C **//
6 106 = T(103) **F6.2// DEG. C **//
7 107 = THER. COND. **F6.2// W/CM DEG. C **//
8 108 = DENSITY **F6.2// G/CM**3 **//
9 109 = THER. CAP. **F6.2// U.SEC./DEG.C GM**//)
RETURN
2 CONTINUE
WRITE(6,22) (I,I=1,NA)
DO 24 L=1,IT
WRITE(6,21) TIM(L), (TEMP(L,K),K=1,NA)
20 CONTINUE
DO 26 I=1,13) GO TO 23
26 PUNCH(7,21) TIM(L), (TEMP(L,K),K=1,NA)
RETURN
23 CONTINUE
DO 24 L=1,IT
DO 25 K=1,NA
M(K)=2
IF (M .EQ. K) GO TO 25
41 KNOWN ANGLES ONLY(0,30,60,90,120,150,180)
M(K/2)=
MELP(N)=TEMP(L,K)
25 CONTINUE
PUNCH(7,21) TIM(L), (MELP(N),N=1,7)
26 CONTINUE
DO 27 I=1,13) F6.2)
27 FORMAT(1,13) X, TIME*, 2X, 14(2X, IZ, 3X), //)
RETURN
3 CONTINUE
OUTPUT THE TEMPERATURE DISTRIBUTION WITHIN THE CYLINDER
AT ONE PARTICULAR TIME
WRITE(1,30) TIME
31 FORMAT(1,13) F6.2)
32 FORMAT(1,13) F6.2) SECONDS*)
33 FORMAT(1,13) F6.2)
DO 102 K=1,NA
WRITE(1,31) K
DO 103 I=1,13)
102 WRITE(1,31) (T(I, J, K), J=1, NZ)
RETURN
4 CONTINUE
PUNCH THE TEMPERATURE DISTRIBUTION AT THE DESIRED TIME
PUNCH(7,32) TIME
DO 103 K=1,NA
DO 104 I=1,13)
103 PUNCH(7,31) (T(I, J, K), J=1, NZ)
RETURN
END

```

PROGRAM BOILING (INPUT, OUTPUT, PUNCH, TAPES=INPUT, TAPES=OUTPUT, 1 TAPE=PUNCH)

THIS PROGRAM EVALUATES THE BOILING CURVES AT SEVEN LOCATIONS AROUND A CYLINDER IN ORDER TO FIT THE EXPERIMENTAL COOLING CURVES TO WITHIN 0.05 OR 0.05 DEG. C) PROVIDED AT THESE SEVEN LOCATIONS. THE PROGRAM TO DO SO IT SOLVES THE 3-DIMENSIONAL UNSTEADY-STATE HEAT DIFFUSION EQUATION USING THE PRINCIPLE OF SUPERPOSITION.

WHERE =

- NR - NUMBER OF MESH POINTS IN THE R-DIRECTION
- NZ - NUMBER OF MESH POINTS IN THE Z-DIRECTION
- NA - NUMBER OF MESH POINTS IN THE PHI-DIRECTION
- TINIT - INITIAL UNIFORM TEMPERATURE (DEG. C)
- CCO - THERMAL CONDUCTIVITY (W/CM DEG. C)
- TLONG - LENGTH OF THE CYLINDER (CM)
- DIA - DIAMETER OF THE CYLINDER (CM)
- RHO - MATERIAL DENSITY (G/CM**3)
- CP - HEAT CAPACITY (J/G DEG. C)
- IMAX - MAXIMUM NUMBER OF ITERATION
- I(1, J, K) - PRESENT TEMPERATURE DISTRIBUTION (DEG. C)
- I - R-DIRECTION
- J - Z-DIRECTION
- K - PHI-DIRECTION

```

COMMON NR, NZ, NA, DR, OZ, OA, CONO, XLONG, DIA, TINIT
COMMON RHO, CP, NCASE
COMMON T(10,10,13), PHIR(10,13), PHIZ(10,13)
COMMON ILOC, NMAX, T(200,7), OA(200,7), TIM(200)
DIMENSION UPOS(7), OMEG(7), TOLD(10,10,13)
READ IN THE INFORMATION
READ(5,*) NR, NZ, NA, TINIT, CONO, XLONG, DIA, RHO, CP, IMAX, NCASE,
1 IRED, LIM
DR=OIA/(2*FLOAT(NR-1))
OZ=XLONG/(2*FLOAT(NZ-1))
OA=3.1416/FLOAT(NA-1)
READ THE COOLING CURVES OR INITIALIZE BOILING CURVES
IF (NCASE .EQ. 1 .OR. IRED .NE. 0) GO TO 5
5 =
CALL HEAT (K)
5 CONTINUE
CALL THE OUTPUT SUBROUTINE
CALL OUTPT (1)
SET THE INITIAL TEMPERATURE DISTRIBUTION
IF (IRED .NE. 0) GO TO 25
ILOC=1
DO 100 I=1, NR
DO 100 J=1, NZ
DO 100 K=1, NA
I(I, J, K)=TINIT
GO TO 26
25 CONTINUE
READ(5,12) ILOC, NMAX
DO 16 L=1, NMAX
READ(5,13) TEM(L), (T(I, J), J=1,7)
16 READ(5,14) (OA(L, J), J=1,7)
12 FORMAT(1,7)
13 FORMAT(8(1X, F6.2))
14 FORMAT(7X, 7(1X, F6.2))
READ(5,31) TIME
DO 101 K=1, NA
DO 102 I=1, NR
DO 103 J=1, NZ
101 FORMAT(1,13) F6.2)
102 CONTINUE
START THE SOLUTION
ITER=0
ILOC=ILOC
28 CONTINUE
ICHAN=0
DO 17 K=1,7
7 POS(K)=OMEG(K)*.
DO 103 J=1, NZ
DO 104 I=1, NR
DO 104 K=1, NA
103 TOLD(I, J, K)=T(I, J, K)
21 CONTINUE
DO 104 I=1, NR
DO 104 J=1, NZ
DO 104 K=1, NA
104 T(I, J, K)=TOLD(I, J, K)
80 CALL SECON(T, H, O)
X=TLIN-1
IF (X .LT. TKNOW) GO TO 200
K=1
CALL HEAT(K)
CALL TIME
RE-EVALUATE THE TIME STEP
X=TEM(ILOC+1)-TEM(ILOC)
T=X/DT
M=X+
DT=X/FLOAT(M)
DO 20 L=1, M
CALCULATE THE SURFACE HEAT FLUX
K=1
CALL HEAT(K)
CALL THE SOLUTION
CALL SOLVE
28 CONTINUE
IFLG=0
DO 18 K=1,7
M=K
IF (NA .EQ. 13) M=K*2-1
T=(NR+1, NI)-(ILOC+1, K)
IF (ABS(X) .LT. 0.05) GO TO 10
CONVERGENCE SECTION
IF (X) / 0.05)
71 POS(K)=QA(ILOC, K)
DO 102 J=1, NZ
70 HREC(K)=QA(ILOC, K)
72 CONTINUE
IF (OMEG(K) .EQ. 0) OR OMEG(K) .EQ. 0.1) GO TO 73
QA(ILOC, K)=10*POS(K)+OMEG(K)/2.
GO TO 8
73 CONTINUE
QA(ILOC, K)=QA(ILOC, K)+X*.3/(TEM(ILOC+1)-TEM(ILOC))
6 CONTINUE
IFLG=IFLG+1
ICHAN=ICHAN+1
IF (ICHAN .GT. 70) GO TO 27
WRITE(6,*) IX, QA(ILOC, K), ICHAN, K
18 CON
GO
27
R=M

```

```

IF (ILOC .GT. ILOC2) GO TO 7
7 GO TO 8
8 Q=Q(ILOC,K)=QA(ILOC-1,K)
CONTINUE
200 GO TO 23
CONTINUE
WRITE(1,*) ILOC,MMAX
PUNCH(1,*) ILOC,MMAX
DO 201 J=1,MMAX
WRITE(1,*) T(ILOC,J),T(1,1),J=1,7)
PUNCH(1,*) T(ILOC,J),T(1,1),J=1,7)
201 CONTINUE
80 CONTINUE
IF (ILOC .EQ. MMAX) GO TO 189
PUNCH(1,*) TIME
DO 188 J=1,MMAX
WRITE(1,*) J,MMAX
PUNCH(1,*) J,MMAX
188 CONTINUE
189 CALL BALAN(8)
END

SUBROUTINE HEAT (K)
COMMON NR,NZ,NA,DT,DR,OZ,OA,COND,XLONG,DIA,TINIT
COMMON RHO,C,P,MELISE
COMMON ILOC,MMAX,T(1(200,7),Q(1(200,7),TEM(200)
THE SUBROUTINE EVALUATES THE HEAT FLUX AT THE SURFACE
THE FIRST PART READS THE SEVEN EXPERIMENTAL COOLING CURVES
K=1
IF (K .EQ. 8) GO TO 20
20 READ(5,*) TEMINI,(TAIN,K),K=1,7)
FORMAT(1(1X,F0.1))
IF (TAIN(1,1) .EQ. 0) GO TO 21
WRITE(16,*) TEMINI,(TAIN,K),K=1,7)
K=K+1
GO TO 20
21 INITIAL GUESS
DO 22 J=1,MMAX
Q(J)=0.1
22 RETURN
20 CONTINUE
EVALUATE THE HEAT FLUX AT THE SURFACE
GO TO (5,6,8,9), NCASE
.....
NCASE=1
3 CONTINUE
IMPOSSIBLE FOR BOILING CURVES PREDICTION
WRITE(16,*) NCASE
.....
NCASE=2
THE HEAT FLUX AT THE SURFACE IS IN THE R-DIRECTION ONLY
AND EVALUATED WITH THE SET OF BOILING CURVES
8 CONTINUE
NO HEAT LOSS THROUGH THE ENDS
DO 50 I=1,MR
DO 50 J=1,MR
50 PHIZ(I,K)=0
IF (TAIN(1,1) .EQ. 0) STOP
60 DO 61 K=1,MMAX
PHIR(I,K)=Q(ILOC,K)
61 CALL LOOKUP(K,T(INR,J,K),PHIR(J,K))
GO TO 62
62 DO 63 J=1,MMAX
N=NR/2
IF (N .EQ. K) GO TO 63
63 AN ODD NUMBER
PHIR(J,K)=
CALL LOOKUP(N,T(INR,J,K),PHIR(J,K))
IF (J .EQ. 1) PHIR(J,K)=Q(ILOC,K)
GO TO 61
64 AN EVEN NUMBER
PHIR(J,K)=
CALL LOOKUP(N,T(INR,J,K),PHIR(J,K))
N=NR/2
PHIR(J,K)=PHIR(J,K)+PHIR(J,K)/2
IF (J .EQ. 1) PHIR(J,K)=Q(ILOC,K)+Q(ILOC,K-N)/2
65 CONTINUE
IF (NCASE .EQ. 3) GO TO 7
RETURN
7 CONTINUE
NCASE=3, MZ MUST BE 10 AND THERE ARE TRANSITE ENO SUPPORTS
70 DO 70 K=1,MMAX
T(INR,K)=PHIR(1,K)*0.8
RETURN
8 CONTINUE
END

```

```

SUBROUTINE BALAN(8)
COMMON NR,NZ,NA,DT,DR,OZ,OA,COND,XLONG,DIA,TINIT
COMMON RHO,C,P,MELISE
COMMON ILOC,MMAX,T(1(200,7),Q(1(200,7),TEM(200)
FIND THE WEIGHTING FACTOR IN THREE DIRECTION
CALCULATE THE WEIGHTING FACTOR AS A FUNCTION OF AREA ON
THE RADIUS LINE
V(1)=1.414*(DIA/2)**2
V(2)=1
V(3)=1
V(1)=1.414*((FLOAT(1)-0.5)*DR)**2-(FLOAT(1)-0.5)*DR)**2
V(2)=1.414*((FLOAT(INR)-1)*DR)**2-(FLOAT(INR)-1)*DR)**2
V(3)=1
V(1)=V(1)/V(1+V(2)+V(3))
V(2)=V(2)/V(1+V(2)+V(3))
V(3)=V(3)/V(1+V(2)+V(3))
60 DO 60 J=1,MMAX
V(1)=V(1)+V(1)*V(1)/(DIA/2)**2
IN THE Z-DIRECTION
N(1)=M(INZ)=0.5/FLOAT(MZ-1)
N(2)=1
DO 61 J=2,MMAX
N(1)=1./FLOAT(MZ-1)
61 N(2)=1./FLOAT(MZ-1)
IN THE PHI-DIRECTION
U(1)=U(INA)=0.5/FLOAT(INA-1)
U(2)=1
DO 62 J=2,MMAX
U(1)=1./FLOAT(INA-1)
62 U(2)=1./FLOAT(INA-1)
NOW CALCULATE THE FINAL OVERALL AVERAGE TEMPERATURE
TSUM=0
DO 50 J=1,MMAX
TSUM=TSUM+T(I,J,1)*V(1)
DO 50 J=2,MMAX
TSUM=TSUM+T(I,J,1)*V(2)
50 TSUM=TSUM+T(I,J,1)*V(3)*U(K)
WRITE(1,*) TSUM
1 FORMAT(1X, 'AVERAGE TEMPERATURE=',F10.5)
RETURN
END

SUBROUTINE LOOKUP(K,R)
COMMON NR,NZ,NA,DT,DR,OZ,OA,COND,XLONG,DIA,TINIT
COMMON RHO,C,P,MELISE
COMMON ILOC,MMAX,T(1(200,7),Q(1(200,7),TEM(200)
TABLE LOOKUP
MMAX=1
IF (R .GT. TAIN(K)) GO TO 3
CONTINUE
Q=Q(I,K)
RETURN
SEARCH
3 IF (TAIN(K) .LT. R) GO TO 7
IF (TAIN(K) .EQ. R) GO TO 7
4 GO TO 6
7 Q=Q(I,K)
RETURN
END

```